

DEVELOPMENT OF A FLEXIBLE AND MODULAR METROLOGY SYSTEM  
FOR MEASURING COMPLEX SURFACES

FLORIAN RICHARD SCHNEIDER

A thesis submitted in partial fulfilment of the requirements of the University  
of the West of England, Bristol for the degree of  
Doctor of Philosophy

This research programme was carried out in collaboration with the  
Deggendorf Institute of Technology

Bristol Institute of Technology, University of the West of England, Bristol

December 2019

This page intentionally left blank.

---

## Abstract

The demand for customised optical devices is increasing tremendously. Such optical devices do not employ traditional designs like planar, spherical, or even aspherical shapes. Instead, modern lenses exhibit free-form surfaces with a large variety of gradients in all directions.

Therefore, a central problem appeared. The existing metrology solutions cannot be longer used as stand-alone measurement systems. Modern optical workshops are forced to employ at least two different metrology systems. Coordinate measurement machines used for strong aspheres, free-form shaped specimen and for non-reflective surfaces in general; Interferometers can be used for highly accurate measurements of reflective surfaces with a substantial limitation regarding the shape of the specimen.

However, research was performed to investigate, define, and create a metrology solution that can be operated at any stage of the production chain of the optical industry. The presented metrology system has the goal to combine the advantages of interferometers and coordinate measurement systems in order to increase the productivity of modern optical workshops.

To ensure that the theoretical assumptions lead to a real product, a new methodology approach, based on Montgomery's scientific method, was created.

Following that new methodology approach, the two independent theoretical models and one final, physical, prototype were created. Cross-comparison processes

and verification stages ensured that the assumptions are correct and that they can be used to design a fully functional physical demonstrator.

However, the findings obtained during this research showed clearly that the new metrology device fulfils the individual requirements of any stage of the production chain of the optical industry. Especially the advanced axes design, comparable to a spherical coordinate system, enables fast and highly accurate measurements. The combination of a multi-sensor feature and an advanced user interface employing several pre-defined operation modes ensure the usability on the shop floor.

During this research, some unique processes and devices were created. Especially the fully integrated axes alignment process and the 3D Scale are noticeable.

However, the high potential of the final prototypes was proven by performing many test series for external customers and other international research projects.

---

## Acknowledgements

I want to express my special appreciation and thanks to my director of studies Professor Dr Lyndon Smith. Furthermore, I want to thank Marisa Downham and the Faculty BIT of the University of the West of England for their great support. In addition, I want to express my appreciation to my retired director of studies, Professor Dr Richard Stamp, for his help and expertise.

Additionally, I want to thank the Deggendorf Institute of Technology for their support and hospitality. Furthermore, I want to thank the Laboratory of Optical Engineering at the Deggendorf Institute of Technology and especially Dr Markus Schinhärl for hospitality, knowledge, and support.

In regards to the Federal Ministry of Education and Research (BMBF), they enabled to perform the initial project EMMA with their financial support.

A special thanks to my parents Richard and Dagmar Schneider for all their love, support, and encouragement over the last years.

In the end, I would like to express appreciation to my beloved wife Cindy who spent love and patience. She was always my support in the wearing moments when there was no one to answer my queries.

This thesis is dedicated to all the people who never stop believing in me.

Thank you.

## Table of publications

### Publications in journals (peer-reviewed)

Almost finished, upload end of 2019. (Design of a spherical coordinate measurement system)

Almost finished, upload end of 2019. (3D-scale - a new device to detect and compensate axial-, and radial run-out of rotational axes)

### Publications in proceedings of international conferences, reviewed.

M. Schinhaerl, F. R. Schneider, R. Rascher, C. Vogt, P. Sperber

*The relationship between influence function accuracy and polishing quality in magnetorheological finishing*

In 5th International Symposium on Advanced Optical Manufacturing and Testing Technologies: Advanced Optical Manufacturing Technologies, volume 7655, page 76550Y ff. SPIE, Dalian, PR China, 2010

F. R. Schneider, M. Schinhaerl, C. Vogt, R. Maurer, P. Sperber, R. Rascher, R. Stamp, G. Smith

*Effects of mechanical inaccuracies on the measurement result in metrology systems*

In 5th International Symposium on Advanced Optical Manufacturing and Testing Technologies: Optical Test and Measurement Technology and Equipment, volume 7656, page 765611 ff. SPIE, Dalian, PR China, 2010

---

C. Vogt, M. Schinhaerl, F. R. Schneider, P. Sperber, R. Rascher

*Investigations on Grinding Tools for Silicon Carbide Based Advanced Materials*

In Optical Fabrication and Testing on CD-ROM, page OWD2 ff. Optical Society of America, Washington, D.C., USA, 2010

M. Schinhaerl, C. Vogt, F. R. Schneider, P. Sperber, R. Rascher

*Investigations on Magnetorheological Finishing of High-Quality Optical Surfaces with Varying Influence Function*

In Optical Fabrication and Testing on CD-ROM, page OWD3 ff. Optical Society of America, Washington, D.C., USA, 2010

R. Maurer, F. R. Schneider, C. Vogt, M. Schinhaerl, P. Sperber, R. Rascher

*Physical marker based stitching process of circular and non-circular interferograms*

Proceedings of SPIE - The International Society for Optical Engineering 05/2011;  
DOI:10.1117/12.889491, San Diego, USA, 2013

C. Vogt, S. Sinzinger, H. Adelsberger, R. Maurer, F. R. Schneider, R. Mandler, L. Kuepper, R. Rascher, P. Sperber

*An Experimental Study on a Flexible Grinding Tool*

44th CIRP Conference on Manufacturing Systems, 08/2011; 325:91-96.

DOI:10.4028/www.scientific.net/AMR.325.91, Madison, Wisconsin, USA, 2011

R. Maurer, F. R. Schneider, C. Wünsche, R. Rascher

*Calculation of the reference surface error by analysing a multiple set of sub-measurements*

Proceedings of SPIE - The International Society for Optical Engineering 09/2013;

DOI:10.1117/12.2024003, San Diego, USA, 2013

F. R. Schneider, R. Maurer, R. Rascher, R. Stamp, G. Smith

*Analysis of three different measurement strategies carried out with the TII-3D coordinate measurement system*

Proceedings of SPIE - The International Society for Optical Engineering 09/2013;

DOI:10.1117/12.2024001, San Diego, USA, 2013



---

F. R. Schneider, R. Rascher, R. Stamp, G. Smith

*A simple procedure to include a free-form measurement capability to standard coordinate measurement machines*

SPIE - Optifab 2013, Rochester, New York, USA, 2013

F. R. Schneider, R. Rascher, C. Wünsche

*Measurement of a freeform object with the TII-3D measurement system*

OSA - Freeform Optics, Houston Texas, USA, 2013

R. Maurer, F. R. Schneider

*Tactile and contactless measurement of an optical surface*

Symposium of Freeform technologies, The National Metrology Institute of Germany (PTB), Braunschweig, Germany, 2014

**Publications in national magazines and Journals (not peer-reviewed)**

F. R. Schneider

*Topographische Koordinatenmessmaschine TII-3D*

*[Topographical coordinate measurement machine TII-3D]*

Untertitel, Hrsg. Technische Hochschule Deggendorf, Deggendorf, Germany, 2013

**Presentations / Speeches at international conferences**

F. R. Schneider, R. Rascher

*Effects of mechanical inaccuracies on the Measurement result in metrology systems*

5th SPIE International Symposium on Advanced Optical Manufacturing and Testing Technologies, Dalian, PR China, 2010

F. R. Schneider, C. Vogt, R. Maurer

*Vibration errors caused by tactile measurements (Awarded with the third price)*

1st International Euspen Challenge, Bremen, Germany, 2010

---

F. R. Schneider

*Topographic measurement system TII-3D, Design and thermal effects*

2. International Workshop “Novel Developments and Applications in Sensor Technology”, Coburg, Germany, 2010

F. R. Schneider

*Presentation of a tactile sensing unit*

3. International Workshop “Novel Developments and Applications in Sensor Technology”, Coburg, Germany, 2012

F. R. Schneider

*Analysis of three different measurement strategies carried out with the TII-3D coordinate measurement system*

Spie SPIE Optics + Photonics, San Diego, USA, 2013

F. R. Schneider, C. Vogt

*A simple procedure to include a free-form measurement capability to standard coordinate measurement machines*

SPIE - Optifab 2013, Rochester, New York, USA, 2013

F. R. Schneider, R. Rascher

*Measurement of a freeform object with the TII-3D measurement system*

OSA - Freeform Optics, Houston Texas, USA, 2013

R. Maurer, F. R. Schneider

*Tactile and contactless measurement of an optical surface*

Symposium of Freeform technologies, The National Metrology Institute of Germany (PTB), Braunschweig, Germany, 2014

F. R. Schneider

*Presentation of a tactile sensing unit*

3. International Workshop “Novel Developments and Applications in Sensor Technology”, Coburg, Germany, 2012

F. R. Schneider

*Analysis of three different measurement strategies carried out with the TII-3D coordinate measurement system*

Spie SPIE Optics + Photonics, San Diego, USA, 2013

---

F. R. Schneider, C. Vogt

*A simple procedure to include a free-form measurement capability to standard coordinate measurement machines*

SPIE - Optifab 2013, Rochester, New York, USA, 2013

F. R. Schneider, R. Rascher

*Measurement of a freeform object with the TII-3D measurement system*

OSA - Freeform Optics, Houston Texas, USA, 2013

R. Maurer, F. R. Schneider

*Tactile and contactless measurement of an optical surface*

Symposium of Freeform technologies, The National Metrology Institute of Germany (PTB), Braunschweig, Germany, 2014

## **Presentation / Speech at national conferences**

F. R. Schneider

*Topographisches Messgerät TII-3D*

*[Topographical measurement device TII-3D]*

4. Optikseminar, Technologie Campus Teisnach, Germany, 2010

F. R. Schneider

*Topographisches Messgerät TII-3D und im Detail Temperatureffekte bei  
Langzeitmessungen*

*[Topographical measurement device TII-3D and, in detail, temperature caused effects  
during long term measurements]*

3. Optikseminar, Technologie Campus Teisnach, Teisnach, Germany, 2010

F. R. Schneider

*Formvermessung mit der Koordinatenmessmaschine TII-3D*

*[Shape measurements performed with the coordinate measurement machine TII-3D]*

5. Optikseminar, Technologie Campus Teisnach, Teisnach, Germany, 2011

---

F. R. Schneider

*Einfluss von Fehlern auf die Messtechnik*

*[Influence of errors regarding metrology systems]*

1. Forum Wirtschaft und Hochschule 2011, Munich, Germany, 2011

F. R. Schneider

*Optische 3D-Messtechnik in der industriellen Produktion*

*[Optical 3D measurements in the industrial production]*

Clusterworkshop Forum Mechatronik 2013, Nuremberg, Germany, 2013

### **Poster at international and national meetings**

F. R. Schneider

*Project EMMA*

Permanent exhibition, Deggendorf Institute of Technology, Deggendorf, Germany

F. R. Schneider

*Presentation of four projects, Ifaso, Optasense, Wipovi and EMMA*

Various exhibitions at conferences

F. R. Schneider

*Aktueller Stand TII-3D*

*[Latest status of the TII-3D]*

1. Internes Optikseminar TC Teisnach, Teisnach, Germany, 2013



---

## Table of contents

Abstract .....	iii
Acknowledgements .....	v
List of publications .....	vi
Table of contents.....	xvii
Table of figures.....	xxii
List of tables .....	xxviii
List of equations .....	xxx
List of nomenclatures .....	xxxiii
List of abbreviations .....	xxxv

### CHAPTER 1

#### INTRODUCTION

1.1 State of the art .....	1
1.2 Lens manufacturing processes .....	4
1.3 Thesis statement .....	5

### CHAPTER 2

#### LITERATURE REVIEW

2.1 Commonly used optical elements .....	9
2.1.1 Materials and material properties .....	11
2.2 Production chain in the optical industry .....	13
2.3 Metrology systems .....	16
2.3.1 Interferometer-based systems.....	17

2.3.2 Coordinate measurement machines.....	19
2.4 Related research - SCMM .....	23
2.5 Summary .....	25

**CHAPTER 3**

**AIMS OF THE WORK**

3.1 Motivation .....	30
3.2 Objective.....	33

**CHAPTER 4**

**METHODOLOGY AND APPROACH**

4.1 Research Methodology.....	36
4.1.1 Application of the methodology .....	39
4.2 System approach.....	42
4.2.1 Applied software tools .....	44
4.2.2 Matlab™ model of the SCMM .....	46
4.2.3 CREO™ model of the SCMM.....	48
4.2.4 SCMM test carrier .....	49
4.3 Summary.....	50

**CHAPTER 5**

**DEVELOPMENT OF THE SCMM**

5.1 Mathematical models of the SCMM .....	52
5.1.1 Design of the SCMM.....	53
5.1.2 Planar operation mode .....	56

---

5.1.3 Best-fit operation mode.....	67
5.2 The Centre-search process.....	84
5.3 The 3D-scale .....	88
5.4 Software packages.....	89
5.5 Measurement strategies .....	91

## **CHAPTER 6**

### **UNCERTAINTY ESTIMATION OF THE SCMM**

6.1 Environment .....	93
6.2 Specimen .....	94
6.3 Operator .....	95
6.4 The accuracy of the SCMM .....	96
6.4.1 Tolerance of the air bearings .....	96
6.4.2 The temperature variations .....	99

## **CHAPTER 7**

### **EXPERIMENTAL VALIDATION OF THE SYSTEM**

7.1 Test series test carrier .....	101
7.1.1 Test series verification of the function .....	101
7.1.2 Test series Measurement modes .....	105
7.1.3 Test series free-form mode.....	113
7.1.4 Test series thermal influence .....	116
7.1.5 Test series repeatability .....	124
7.1.6 Summary .....	127

7.2	Centre search process .....	129
7.2.1	Setup of the experiments.....	130
7.2.2	Results of the Centre search tests .....	132
7.2.3	Summary .....	135
7.3	3D-scale .....	136
7.3.1	Setup of the experiments.....	136
7.3.2	Experimental results .....	138
7.3.3	Summary .....	140

## **CHAPTER 8**

### **DISCUSSION OF THE RESULTS**

8.1	Analysis of repeatability and accuracy .....	142
8.2	Reliability of the SCMM.....	146
8.3	Discussion of the experimental results.....	147
8.4	Advantages and limitations .....	151
8.5	Application of the SCMM .....	154
8.6	Summary and reflection .....	154

## **CHAPTER 9**

### **CONCLUSIONS**

9.1	Conclusions .....	156
9.2	Differences to the initial PhD roadmap .....	160

---

**CHAPTER 10**

**SUGGESTIONS FOR FUTURE WORK**

10.1 3D-scale ..... 164

10.2 Centre Search 3D V2 ..... 166

10.3 The new tactile sensing unit ..... 169

10.4 Full 3D Cross-section-mode ..... 171

**CHAPTER 11 REFERENCES**

Appendix A ..... 186

## Table of figures

Figure 1: Free-form shapes replace traditional shapes .....	9
Figure 2: Production chain in the optical industry.....	13
Figure 3: Concept of the Michaelson Interferometer.....	17
Figure 4: Common designs of coordinate measurement machines.....	21
Figure 5: 3D sketch of a spherical CMM .....	22
Figure 6: Engineering method by Montgomery.....	36
Figure 7:Schneider’s engineering and scientific method.....	37
Figure 8: Identification of essential factors .....	39
Figure 9: Spherical coordinate system.....	54
Figure 10: Sketch of the planar operation mode.....	56
Figure 11: Top view planar operation mode.....	57
Figure 12: Examples of misalignment .....	58
Figure 13: Cylindrical coordinate system.....	59
Figure 14: Top view planar operation mode.....	61
Figure 15: Cartesian coordinates in the planar mode .....	62
Figure 16: B-axis correction angle.....	64
Figure 17: Corrected measurement points.....	65
Figure 18: Best-fit mode – concave .....	67
Figure 19: Best-fit mode – convex .....	68
Figure 20: Sensor plane in the best-fit mode .....	69
Figure 21: Side view including the sensor plane.....	70
Figure 22: Angle alpha at convex setup .....	71

---

Figure 23: A-axis angle $\alpha$ verification.....	73
Figure 24: A-axis angle $\alpha$ verification with Creo™ .....	74
Figure 25: Elliptical coherences SCMM .....	75
Figure 26: Conversion circle to an ellipse .....	77
Figure 27: XYZ verification with Matlab™ (M2010a) .....	80
Figure 28: XYZ verification with Creo™ .....	82
Figure 29: Examples misalignment 3D .....	83
Figure 30: Centre search approach .....	84
Figure 31: Expected signal of the sensing unit.....	85
Figure 32: Y-axis alignment .....	86
Figure 33: Sensor signal Y-axis .....	87
Figure 34: 3D-Scale schematic sketch.....	88
Figure 35: Setup for the general function verification .....	102
Figure 36: Measurement result SCMM.....	103
Figure 37: Measurement result interferometer .....	104
Figure 38: Setup of the test series Track-mode.....	106
Figure 39: Details of the test series.....	106
Figure 40: Results of the Track-mode measurements.....	108
Figure 41: Results of the Spiral-mode measurements.....	110
Figure 42: The Cross-section-mode measurements .....	112
Figure 43: Setup free-form test series .....	113
Figure 44: Free-form shaped demonstrator .....	114
Figure 45: 3D sketch of the free-form specimen .....	114
Figure 46: Werth-Video-Check-UA™ measurement .....	115

Figure 47: Interferometer measurement result .....	116
Figure 48: Setup temperature influence test series .....	117
Figure 49: 1 <sup>st</sup> result of temperature influence test .....	117
Figure 50: 2 <sup>nd</sup> result of temperature influence test.....	118
Figure 51: Foil covered SCMM .....	119
Figure 52: 3 <sup>rd</sup> result of temperature influence test .....	120
Figure 53: Housing of the SCMM .....	121
Figure 54: Housing of the sensing unit .....	122
Figure 55: Interferometer measurement to verify the temperature influence .....	123
Figure 56: 4 <sup>th</sup> result of temperature influence test .....	123
Figure 57: Measurement of the reference surface.....	124
Figure 58: Result of 100 SCMM measurements .....	126
Figure 59: Centre Search test series setup in detail .....	131
Figure 60: Centre Search test setup.....	132
Figure 61: Result of the C-axis positioning process .....	133
Figure 62: Corrected C-axis position .....	134
Figure 63: Y-axis alignment .....	135
Figure 64: 3D-scale demonstrator .....	137
Figure 65: Result 3D-scale test series .....	139
Figure 66: Histogram of the repeatability test series .....	145
Figure 67: 3D-scale prototype.....	164
Figure 68: 3D-scale sketch .....	165
Figure 69: Concept of Centre Search 3D .....	167
Figure 70: Centre of rotating devices detection .....	168



---

Figure 71: Prototype of a new tactile sensing unit .....	170
Figure 72: Michelson interferometer.....	191
Figure 73: A Twyman-Green interferometer .....	191
Figure 74: Fizeau interferometer .....	192
Figure 75: Stitching Interferometry .....	193
Figure 76: 3D sketch of the CMM cantilever design .....	195
Figure 77: 3D sketch of the CMM bridge design.....	197
Figure 78: 3D sketch of the CMM portal design .....	198
Figure 79: 3D sketch of the CMM gantry design .....	199
Figure 80: Cylindrical coordinate system .....	203
Figure 81: Concave spherical surface.....	206
Figure 82: Convex spherical surface .....	207
Figure 83: Spherical coordinate system .....	208
Figure 84: Optical aberration .....	211
Figure 85: Luphos™ sensing unit in SCMM .....	221
Figure 86: Sios™ sensing unit .....	223
Figure 87: MicroEpsilon™ Confocal chromatic sensor.....	224
Figure 88: ME/LOE sensing unit .....	225
Figure 89: LOE sensing unit II .....	226
Figure 90: Specimen on a brass block .....	231
Figure 91: Influences on the measurement result.....	238
Figure 92: Temperature documentation .....	241
Figure 93: Examples of different CMM designs .....	251
Figure 94: Radial and axial runout of the SCMM .....	256

Figure 95: Tolerance analysis B-axis and C-axis .....	257
Figure 96: Test setup radial and axial runout .....	261
Figure 97: Resulting interferometer measurement.....	262
Figure 98: Result of radial and axial measurement .....	263
Figure 99: Geometric relations for thermal drift .....	266
Figure 100: Length variations SCMM at 1K.....	271
Figure 101: Length variations SCMM at 0.15K.....	272
Figure 102: CREO3™ (M100) 3D sketch of the 3D-scale system.....	273
Figure 103: 3D-Scale schematic sketch.....	276
Figure 104: SCS design of the 3D-scale device.....	277
Figure 105: Spherical coordinate system .....	279
Figure 106: Calculated plane 3D-Scale.....	280
Figure 107: Two examples of planes with different centres .....	283
Figure 108: Centre search process – 1 <sup>st</sup> step .....	287
Figure 109: Sensor signal C-axis alignment.....	288
Figure 110: Result of the 1 <sup>st</sup> step centre search .....	289
Figure 111: Centre search process – 2 <sup>nd</sup> step part 1.....	290
Figure 112: Centre search process – 2 <sup>nd</sup> step part 2.....	291
Figure 113: Result of the 2 <sup>nd</sup> step centre search part 1.....	292
Figure 114: Result of the 2 <sup>nd</sup> step centre search part 2.....	292
Figure 115: Scheme of the Y coordinate calculation .....	293
Figure 116: Calculation procedure of Y0.....	294
Figure 117: Illustration of the Track-mode .....	299
Figure 118: Simulation Track-mode.....	302

---

Figure 119: Illustration of the Spiral-mode.....	304
Figure 120: Simulation Spiral-mode.....	307
Figure 121: Illustration of the Cross-Section mode .....	310
Figure 122: GUI- manual user mode .....	320
Figure 123: GUI - Centre Search.....	321
Figure 124: GUI - Automatic mode .....	322
Figure 125: GUI - Measurement modes in detail.....	323
Figure 126: GUI - I/O settings.....	325
Figure 127: GUI - Settings of the SCMM .....	327
Figure 128: GUI – Data analysis software .....	329
Figure 129: SCMM measurement file .....	330
Figure 130: Process of data analysis .....	333
Figure 131: XYZ transformation .....	335
Figure 132: Zernike polynomials .....	336
Figure 133: Surface with removed piston and XY-tilt .....	338
Figure 134: Cross-correlation of the measurement.....	339
Figure 135: Final result of the data analysis .....	341
Figure 136: Data analysation in the Track-mode.....	342
Figure 137: Result screen of the data analysis software .....	344
Figure 138: Computation of the Cross-section-mode .....	346
Figure 139: Cross-section-mode result screen .....	348

## Table of tables

Table 1: Different surface types.....	10
Table 2: Used verification parameters.....	47
Table 3: A-axis angle $\alpha$ result by CREO3™ (M100) and Matlab™ (M2010a) .....	73
Table 4: XYZ verification by CREO3™ (M100) and Matlab™ (M2010a) .....	81
Table 5: Technical data of the used air bearings .....	97
Table 6: Combined error in Z-direction.....	98
Table 7: Combined error in Y- direction.....	98
Table 8: Results thermal expansion prediction .....	99
Table 9: Predicted temperature influence.....	100
Table 10: Statistical average and standard deviation .....	144
Table 11: Common materials for optical elements .....	200
Table 12: Conic coefficients .....	213
Table 13: Joining technologies .....	248
Table 14: Sources of uncertainties.....	250
Table 15: Tolerance field of the B-axis.....	257
Table 16: C-axis axial error (ar_C) in Z-direction.....	259
Table 17: C-axis axial error (ar_C) in Y-direction.....	259
Table 18: C-axis radial error (rr_C) in Z- direction .....	259
Table 19: C-axis radial error (rr_C) in Y- direction .....	260
Table 20: Combined error in Z-direction.....	260
Table 21: Combined error in Y- direction.....	260
Table 22: Thermal expansion coefficients .....	266

---

Table 23: Dimensions and materials of the SCMM.....	267
Table 24: Results of thermal expansion prediction .....	269
Table 25: Predicted temperature influence.....	270
Table 26: Test setup Track-mode.....	303
Table 27: Setup of Spiral-mode.....	308
Table 28: Setup of the Cross-section-mode.....	311

## Table of equations

Equation 1: Polar X-coordinate .....	60
Equation 2: Polar Y-coordinate .....	60
Equation 3: Polar Z-coordinate .....	60
Equation 4: Calculation of chord $rp$ .....	63
Equation 5: Calculation of coordinate $Xp$ .....	63
Equation 6: Calculation of coordinate $Yp$ .....	63
Equation 7: Beta correction angle .....	65
Equation 8: Beta corrected X-coordinate .....	65
Equation 9: Beta corrected Y-coordinate .....	66
Equation 10: Calculation of the angle $\alpha$ .....	72
Equation 11: Calculation of the minor axis $d$ .....	78
Equation 12: Calculation of the major axis $f$ .....	78
Equation 13: X value of the projection .....	79
Equation 14: Y value of the projection .....	79
Equation 15: Angle $\varepsilon$ of the projection .....	80
Equation 16: Z value of the projection .....	80
Equation 17: Cylindrical coordinate system vector $r$ .....	204
Equation 18: Cylindrical coordinate system angle $\varphi$ .....	204
Equation 19: Cylindrical coordinate system X .....	204
Equation 20: Cylindrical coordinate system Y.....	204
Equation 21: Cylindrical coordinate system Z.....	204
Equation 22: Spherical coordinate system vector $r$ .....	209

---

Equation 23: Spherical coordinate system angle $\theta$ .....	209
Equation 24: Spherical coordinate system angle $\varphi$ .....	209
Equation 25: Cartesian coordinate system X .....	209
Equation 26: Cartesian coordinate system Y .....	209
Equation 27: Cartesian coordinate system Z .....	209
Equation 28: Equitation of an aspherical object .....	212
Equation 29: Z-component of the C-axis axial runout .....	258
Equation 30: Y-component of the C-axis axial runout .....	258
Equation 31: Z-component of the C-axis radial runout .....	258
Equation 32: Y-component of the C-axis radial runout .....	258
Equation 33: Temperature indicated length error .....	268
Equation 34: Temperature indicated error Z-direction .....	268
Equation 35: Temperature indicated error Y- direction .....	269
Equation 36: Cartesian X component 3D-Scale .....	278
Equation 37: Cartesian Y component 3D-Scale .....	278
Equation 38: Cartesian Z component 3D-Scale.....	278
Equation 39: Matrix notation of cross-product .....	281
Equation 40: The cardan tilt angle alpha .....	281
Equation 41: The cardan tilt angle beta .....	281
Equation 42: The cardan tilt angle gamma .....	281
Equation 43: The radius r of a circle ABC .....	282
Equation 44: The centre point CP of a circle.....	283
Equation 45: Sum of Sin fit.....	288
Equation 46: Calculation of the angle $\omega$ .....	295

Equation 47: Calculation of the Y0 position.....	295
Equation 48: Spacing factor calculation.....	300
Equation 49: Spacing array .....	301
Equation 50: Final array with C-axis positions .....	301
Equation 51: Archimedean spiral.....	305
Equation 52: Calculation no. of windings .....	305
Equation 53: Calculation of angular array phi .....	306
Equation 54: Calculation of spiral constant a .....	306
Equation 55: Final function of the arithmetic spiral .....	307
Equation 56: First Zernike polynomial z0.....	337
Equation 57: Second Zernike polynomial z1.....	337
Equation 58: Third Zernike polynomial z2 .....	337
Equation 59: Cross-correlation equation .....	340



---

## Table of nomenclatures

$\Delta Y_{tot\ 0.15}$	.....	Length variation in Y at 0.15 Kelvin
$\Delta Z_{tot\ 0.15}$	.....	Length variation in Z at 0.15 Kelvin
$\Delta Y_{tot}$	.....	Total length variation in Y at 1 Kelvin
$\Delta Z_{tot}$	.....	Total length variation in Z at 1 Kelvin
$arr_{BC\_Y}$	.....	Axial and radial runout of B-, and C-axis in Y
$arr_{BC\_Z}$	.....	Axial and radial runout of B-, and C-axis in Z
$arr_{C\_Y}$	.....	Axial and radial runout of C-axis in Y
$arr_{C\_Z}$	.....	Axial and radial runout of C-axis in Z
$c\_p$	.....	Length of the cantilever
$d$	.....	Length of the elliptical minor axis in the top view
$e$	.....	Length of the elliptical major axis in the side view and top view
$f$	.....	Length of the elliptical minor axis in the side view
$r\_p$	.....	Chord between $\gamma = 0^\circ$ and the maximum $\gamma$ angle of the C-axis
$R$	.....	Radius of curvature of the specimen
$S$	.....	Physical length of the sensing unit
$X\_p$	.....	Cartesian coordinate in X-direction
$X$	.....	Cartesian coordinate in X-direction
$Y\_p$	.....	Cartesian coordinate in Y-direction
$Y$	.....	Cartesian coordinate in Y-direction
$Z$	.....	Sensor value
$\beta_{corr}$	.....	Correction angle of the B-axis

$\beta$ .....Turning angle of the B-axis  
 $\gamma$ .....Turning angle of the C-axis  
 $\varepsilon$ ..... Angle Epsilon, the projection of angle  $\gamma$   
 $\varphi$ .....Rotation angle in the XY-plane

---

## Table of abbreviations

2,5D .....	<i>Two and a half dimension</i>
2D .....	<i>Two-dimensional</i>
3D .....	<i>Three Dimensional</i>
AFJP .....	<i>Active Fluid Jet Polishing</i>
B4, B6, B8 .....	<i>4<sup>th</sup>, 6<sup>th</sup>, 8<sup>th</sup> ... order aspheric terms</i>
CAD .....	<i>Computer Aided Design</i>
CAM .....	<i>Computer Aided Manufacturing</i>
CCD .....	<i>Charge-Coupled Device</i>
CGH .....	<i>Computer Generated Hologram</i>
CMM .....	<i>Coordinate Measurement Machine</i>
CMMs .....	<i>Coordinate Measurement Machine</i>
CNC .....	<i>Computer numerical control</i>
cos .....	<i>Cosinus</i>
DIN .....	<i>Deutsche Industrie Norm. German industry standard</i>
DIT .....	<i>Deggendorf Institute of Technology</i>
e.g. ....	<i>Exempli gratia</i>
EN .....	<i>Europaeische Norm, European Standards</i>
ENV .....	<i>European Prestandard</i>
GUI .....	<i>Graphical User Interface</i>
h .....	<i>Hour</i>
HD .....	<i>High Definition</i>

Hz.....*Herz*

ISO .....*International Organization for Standardization*

k..... *Conic constant*

L1..... *Length L1*

L2..... *Length L2*

L3..... *Length L3*

L4..... *Length L4*

LOE ..... *Laboratory of Optical Engineering*

m<sup>2</sup> ..... *Square-metres*

MHz ..... *Mega Herz*

mm ..... *Millimetre*

MRF ..... *Magnetorheological finishing*

N-BK7..... *Borosilicate-crown glass from SCHOTT*

NC.....*Numeric Control*

nm .....*Nanometre*

No .....*Number*

OK.....*Okay*

P1.....*Point P1*

PTC ..... *Parametric Technology Corporation*

PV ..... *Peak to Valley*

QED..... *QED Technologies, a CMC Company*

QS ..... *Quality Control*

---

$r$  ..... *Radial coordinate of the polar coordinate system*  
 $R_0$ ..... *Curvature, inverse of radius*  
 ref. .... *Refere (to)*  
 RMS ..... *Root Mean Square*  
 SI..... *International System of Units*  
 SiC..... *Silicon Carbide*  
 SSD..... *Sub Surface Damages*  
 SSI ..... *Subaperture Stitching Interferometer*  
 UA..... *Ultra Accuracy*  
 V2 ..... *Version 2*  
 VLT..... *Very Large Telescope*  
 X..... *Cartesian Coordinate System X-direction*  
 XYZ..... *Cartesian Coordinate System*  
 Y..... *Cartesian Coordinate System Y-direction*  
 Z..... *Cartesian Coordinate System Z-direction*  
 $\varphi$  ... .. *Angular coordinate of polthe ar coordinate system*

# Chapter 1

## Introduction

### 1.1 State of the art

The history of metrology science is closely linked with human history. In the mediaeval times, a measurement task consisted of counting things. However, modern metrology science can measure distances or geometrical deviations in the nanometre range.

Since ancient times, man discovered many different tools to measure masses, distances or even time. Nevertheless, with improvements in the production processes, improvements of the metrology systems became necessary. The major problem with such metrology solutions had been their natural origin. The people used natural standards such as feet, span, or hand. Since most of such scales had their background in the body dimensions of the reigning leader, the scales had no extended validity or got lost during wars or other serious events. On the other hand, a consolidated look at the

brilliant engineering performance of the old Egyptians, Romans, Greeks, or other famous ancient cultures shows us that their technologies worked very accurately and reliably.

The introduction of the modern physical metrology systems began with the development of the first Interferometer in 1881 by Michelson. Another significant milestone was the development of the first 2-axis coordinate measurement machine in the 1950s by the Ferranti Company. The first 3-axis machine appeared in the 1960s in the market.

Together with the introduction of the International System of Units (SI), these first developments of physical metrology systems led to the development of modern metrology science.

Today, modern metrology workshops are equipped with a wide range of different metrology solutions. Depending on the field of application, the developed metrology solutions vary in the necessary accuracy. Some measurement tasks require a lower accuracy but a broad measuring range; other tasks require very accurate metrology solutions.

A specific branch requiring highly accurate measurements is the optical industry. The progress of modern electronic devices, such as smartphones, requires more and more complicated optical systems. Current NC controlled production processes initially developed for machining metal parts, found their way into all stages of the production chain of the optical industry. However, the traditional metrology solutions, such as coordinate measurement machines and interferometers, are limited regarding the

measurement speed or the ability to operate on free-form shaped objects. Therefore, the optical industry usually applies different measurement solutions in order to fulfil the needs of each specific stage of the production chain. This determining factor requires research about a measurement solution that can be used at any stage of the production process in the optical industry.

The typical production chain in the optical industry combines specific processes to produce highly accurate optical elements. The production chain starts with the preparation of the raw material, for instance, with the application of water jets or diamond saw blades. In the next step, rough grinding processes generate the basic shape of the object, such as planar, spherical, aspherical or free form shaped. These processes usually meet the final shape of the object within less than a millimetre shape deviation. Such rough grinding processes produce non-reflective and mostly very rough surfaces. The next step is commonly a smoother grinding process, in order to meet the shape of the specimen within a shape deviation of a few microns. The machined surfaces are mostly partially reflective. In the last stages, polishing processes are applied. Depending on the required accuracy of the optical element, global polishing processes and zonal-polishing processes are applied. The polishing processes enable the production of elements with a shape deviation between a few hundred and less than 20 nanometres.

Consequently, a PhD research with the goal “DEVELOPMENT OF A FLEXIBLE AND MODULAR METROLOGY SYSTEM FOR MEASURING COMPLEX SURFACES” was performed.



## 1.2 Lens manufacturing processes

The development of metrology equipment and production machines goes hand in hand. Each step forward in the science of production processes requires new developments in metrology science. The following sub-chapter provides a brief description of lens manufacturing processes. Details about the different production processes may be found in Chapter 2.2 and A.6.

The most commonly used production processes in the optical industry are cutting, milling, grinding and polishing. Each production process has its own characteristic production marks on top of the surface of the specimen. Rough production processes, such as cutting and grinding, produce rough and structured surfaces. Such surfaces are mostly opaque and not very reflective. Since contactless measurement systems mostly require reflective surfaces, the first production processes are verified by the application of tactile measurement tools, such as coordinate measurement machines or profilometers. During traveling along the production chain, the accuracy and quality of the specimen usually increases, for instance, by the application of zonal grinding or polishing principles. Such highly accurate surfaces are highly reflective and can be measured with contactless techniques and tactile metrology machines. Since the emitted rays of contactless sensor systems have to be reflected on the surface of the specimen, the only limitation for contactless measurement systems is the slope gradient of the reflecting surface and therefore the general shape of the specimen. Interferometers, for example, are physically limited to planar and spherical

shapes. Aspherical or even free-form shaped surfaces are naturally very difficult to measure with contactless system.

Therefore, with the increasing demand for aspherical and free-form shaped optical surfaces, the demand for a universal metrology solution, usable at any stage of the production chain, is growing.

### 1.3 Thesis statement

The primary goal of this PhD thesis is to present an approach for the development of a particular type of coordinate-measurement-machine that can be used at any stage of the production chain of the optical industry. This specific approach is based on the concept of a spherical coordinate measurement machine that operates by the employment of a combination of linear and rotational axes. The following Chapters present the research process of the metrology system.

The motivation for this research was a project named EMMA<sup>1</sup>. This BMBF<sup>2</sup> funded research project had the goal to investigate and redesign the prototype of a non-working prototype of a spherical coordinate measurement machine. The project had been conducted at the Deggendorf Institute of Technology at the Laboratory of Optical Engineering under the supervision of Prof. Dr.-Ing. Rolf Rascher and Prof. Dr.rer.nat. Peter Sperber. Dipl.-Ing.(FH) Markus Schinhaerl, PhD, MEng assisted with help and

---

<sup>1</sup> EMMA - Acronym "Entwicklung eines modularen Messgerätes für Asphären" / "Development of a modular metrology for aspheres".

<sup>2</sup> BMBF – Bundesministerium für Bildung und Forschung / Federal ministry of education and research.

advice to build the hardware. Details about the project EMMA can be found in Chapter A.1.

However, a qualified literature review is the base of a successful research project. The literature review revealed detailed information about related research, especially in the area of metrology machines, optical elements, and design of machines in general. The literature review is published in Chapter 2.

The third Chapter combines the results of the literature review and the knowledge gained in the project EMMA to define the aims of this thesis. Chapter 3 is presenting a detailed summary of the author's motivation and the objectives of the work there.

However, a qualified research project has to be carried out by the application of a reliable methodology. Chapter 4 presents the specific procedures and techniques used to identify the necessary information in order to define and understand the research problem. Furthermore, this Chapter reflects the methods of collecting and analysing obtained data.

The bases for this research are the particular mathematical models describing the presented measurement machine. Chapter 5 publishes the developed algorithms for all essential features of the spherical measurement machine. Therefore, algorithms for the alignment strategy, the basic setup, and the tool path generation are presented.

Compared with a theoretical approach, a real built machine is generally subject to errors. The origin of such errors is complex. There are many different sources of errors

influencing a machine. Depending on the grade of accuracy of the designed machine, some of the errors are more critical than others are. Chapter 6 presents the uncertainty estimation of the introduced metrology machine. Among others, environmental caused errors, mechanical errors, or even the application of not ideal measurement strategies are considered.

The combination of the gained results, taken from the theoretical approach, the development of the test carrier and the error compensation led to the experimental validation of the plan. This validation contains both computer simulations to test the reliability and efficacy of the developed algorithms and furthermore physical comparative tests, including the application of state of the art metrology machines. Significant experimental validations are presented in Chapter 7.

Chapter 8 presents the discussion of the results of the experimental validation in consideration of the knowledge obtained from the literature review and the development of the mathematical relationships.

The conclusion of the discussion and the results are printed in Chapter 9.

The thesis is completed with Chapter 10, the suggestions for future work. This thesis presents a sophisticated measurement system with some generic features. The presented approaches and developments still enable enough leeway for future research.

## Chapter 2

### Literature review

The second Chapter provides a consolidated view of the recently published literature about topics related to this PhD research. The introduced research about an innovative measurement system enabling usability at any stage of the production chain in the optical industry requires knowledge of state of the art in four significant areas.

The first area is related to commonly used optical elements, especially regarding their surface descriptions, the used materials, and the employed production processes.

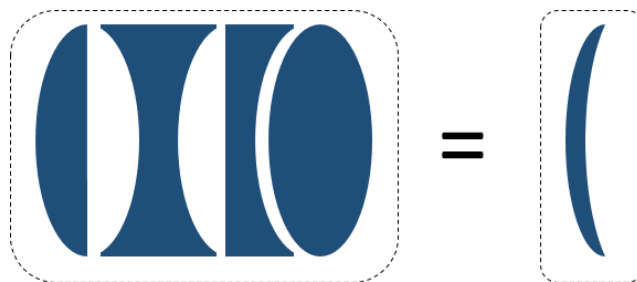
The second part presents the modern production chain in the optical industry.

The third part of the literature review focuses on existing and commonly used metrology systems to reveal their limitations and advantages.

With respect to this thesis, the last part of the literature review investigates performed research in the field of spherical coordinate or swing arm metrology machines in detail.

## 2.1 Commonly used optical elements

The demand for high-quality optical devices is significantly increasing. Many modern industrial products need optical devices [1, 2]. The prime mover of most modern consumer electronics is miniaturisation. For optical systems used in new products, it is therefore essential to reduce the size and weight of the optical assembly. A few aspheric or free-form shaped refractors can replace an array employing many large and heavy lenses. The replacement helps to reduce the overall dimensions of the system and enables manufacturers to decrease product dimensions. Figure 1 depicts the reduction of a traditional lens array into one free-form shaped lens.



*Figure 1: Free-form shapes replace traditional shapes. A stack of conventional optical elements can be replaced by one free-form shaped optical element*

The literature knows three different traditional types of optical surfaces in the optical industry and in addition, modern free-form shaped objects. Manufacturers made significant efforts to develop new processes to produce smart objects<sup>3</sup>, especially free-form shaped parts. A selection of commonly used optical elements is presented in Chapter A.4. The Laboratory of Optical Engineering (LOE) performed significant research

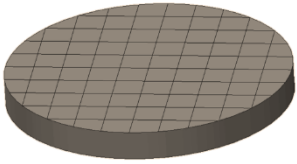

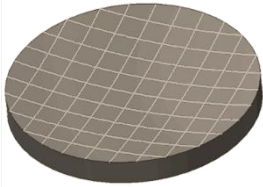
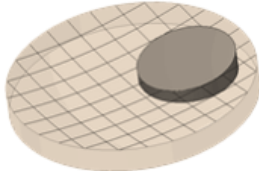
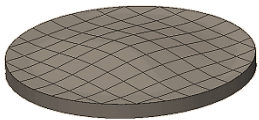
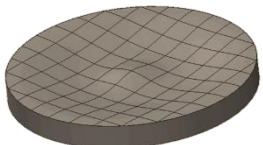
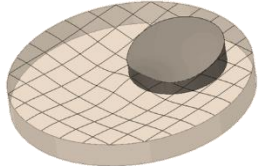

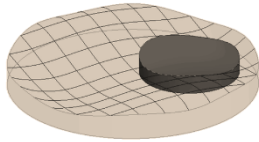
---

<sup>3</sup> In the context of this thesis, smart objects are defined as optical elements combining more than one feature, for example, focusing and filtering of light.

related to all stages of a modern production chain, including machining, grinding, and polishing [3–9].

Table 1 depicts a brief selection of commonly used optical objects.

*Table 1: Different surface types. The optical industry knows four general surface types in three different variations. Round objects represent the dominant design of optical elements, but there is a widespread of different structures available in the market. The mesh on top of the surface is only for better visualisation of the shape and curvature of the objects.*

Surface type	Convex type	Concave type	Off-axis type
Planar surface			
Spherical surface			
Aspherical surface			
Free-form surface	No distinction between convex and concave shapes		

Planar and spherical optical surfaces are relatively easy to produce, even with an accuracy of  $\lambda/20^4$  or better. However, the market situation for planar and spherical

<sup>4</sup> $\lambda/20 - \lambda$  represents the wavelength of a He Ne Laser (red) with a wavelength of 632.816 nanometre.  $\rightarrow \lambda/20 = 31.6408$  nanometre

optical objects changed. While planar and spherical objects are still prevalent in the design of domestic and semi-professional devices, such as telescopes, the need for such items in the professional market is declining. Aspherical and free-form shaped objects are going to dominate the market [10–21].

Detailed information about the mathematical surface definition of planar, spherical, aspherical, and free-form shaped optical elements are presented in Chapter A.4.

### 2.1.1 Materials and material properties

In the optical industry, a broad range of different materials is employed. The leading group of used materials are transparent and non-transparent ceramics. Metal and specific plastic types are typically used for thin-layer coatings rather than for optical precision elements.

While transparent optical elements are commonly used for filtering, focusing or dispersing purposes, the optical industry needs non-transparent elements as well, for example, silicon carbide (SiC<sup>5</sup>) mirrors. This brittle-hard material can be used at high temperatures but is very difficult to grind, to polish and especially to measure. The LOE<sup>6</sup> conducted research regarding the production and measurement of SiC-mirrors [4, 6]

---

<sup>5</sup> SiC - Silicon carbide, also known as carborundum. It is a sinter ceramics, often used in hot environments.

<sup>6</sup> LOE – Laboratory of Optical Engineering. A research group at the Deggendorf Institute of Technology, Germany.



Specimens have general physical properties, but for production and measurement purposes, some specific properties are essential:

- Suitability for abrasive production processes such as grinding or polishing
- Suitability for coat processes
- Resistance to cutting fluid
- Resistance against subsurface damages (SSD) caused by production processes
- Scratch resistance for the use as a finished product (And tactile measurements)
- Temperature stability (Use in hot conditions and during a production process)

Concluding, the optical industry uses widespread materials for the production of elements. Each material requires a specific treatment regarding the manufacturing and the measurement process. Specific information about commonly used materials is published in Appendix A.3. Details about the production processes are presented in Appendix A.6.

Furthermore, optical elements do not only exhibit traditional shapes. Advanced aspherical and free-form shaped designs are increasing. Appendix A.4 illustrates the mathematical approaches and models for the surface definitions.

## 2.2 Production chain in the optical industry

Before the launch of the ray-tracing software ZEMAX™<sup>7</sup> in 1990, the product development process and the measurement process had been separate. The product development and product design created a new product by creating some 2D drawings for the following processes, such as milling, grinding and polishing.

What is new is that a streamlined production process in the optical industry operates mostly paperless. Usually, the product design creates a 3D drawing by using a CAD<sup>8</sup> system or optical design software [22, 23]. The resulting 3D model contains all geometric information of the target object.

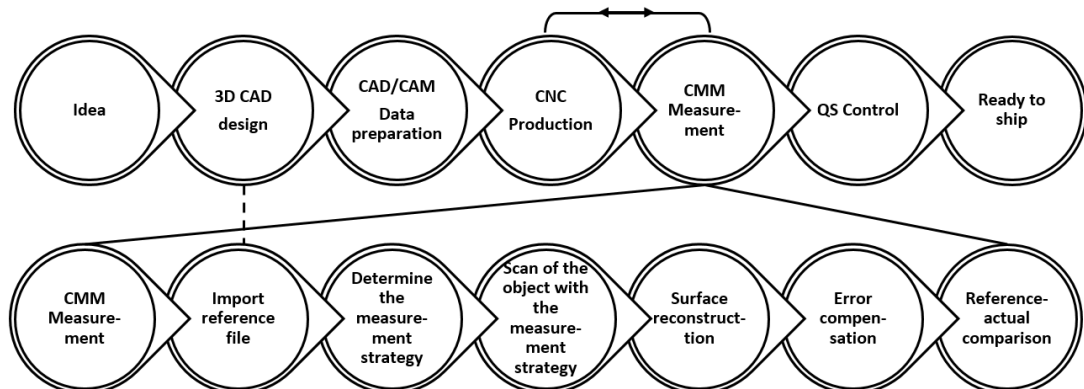


Figure 2: Production chain in the optical industry . Comparable to other industry branches, the processes in the optical industry follow a production process chain. The complete process begins with an idea followed by the design, the production, the measurements, the quality control, and ends with the shipment to the customer. A consolidated view on the measurement process reveals a second process chain, the measurement process chain, depicted in the second row.

Figure 2 presents the production process chain in the modern optical industry. The first start of the process chain is the product idea, followed by the 3D design of the

<sup>7</sup> Zemax™ was the first commonly available ray tracing software for Microsoft™ Windows™. [www.zemax.com](http://www.zemax.com)

<sup>8</sup> CAD: Computer Aided Design; A software tool to design 2D/3D objects in a computer system.

required object. The Laboratory of Optical Engineering (LOE)<sup>9</sup> uses two Software solutions to design the required elements. The first software tool is a classical optical design software named Zemax<sup>TM10</sup>. This software is specialised on ray tracing in optical systems. The second software tool is CREO<sup>TM11</sup>; that is initially a mechanical engineering CAD software. Next, to the underlying 3D and 2D capability, CREO<sup>TM</sup> comes with a professional FEM tool that enables structural and thermal analyses [24].

The next step in the process chain is the CAD/CAM<sup>12</sup> transformation of the 3D object into a machine compatible NC code. This technology enables the user to create the machine tool path directly by analysing the 3D model. The result is a generated NC code that is directly submitted to the CNC production machine.

After uploading the NC code into the CNC machine, the actual production of the object starts. Modern optical CNC machines, such as grinding and polishing machines, can produce objects with a quality better than  $\lambda/40$ <sup>13</sup> peak to valley (PV) at a diameter of 100 millimetres [3, 5, 6].

The measurement process and the manufacturing process are closely linked and interact together. At the beginning of the grinding process, the specimen is typically very rough and does not have a smooth surface. This requires a first tactile measurement with a CMM after the first grinding process to check the shape to make sure that the grinding process is successful. Right after the grinding process, the polishing process

---

<sup>9</sup> LOE: Laboratory of Optical Engineering; A research group of the Deggendorf Institute of Technology (DIT)

<sup>10</sup> Zemax<sup>TM</sup>: A software product of a US company named: Radiant Zemax<sup>TM</sup>

<sup>11</sup> CREO<sup>TM</sup>: A software product of a US company named: Parametric Technology Corporation (PTC)<sup>TM</sup>

<sup>12</sup> CAM: Computer Aided Manufacturing; CAD/CAM; A technique to generate a tool path in the CAD

<sup>13</sup>  $\lambda/40 - \lambda$ . represents the wavelength of a He Ne Laser (red) with a wavelength of 632.816 nanometre.  $\rightarrow \lambda/40 = 15.8204$  nanometre

starts sequentially. The result of the polishing process is a specimen with a very smooth surface. The measurements on polished surfaces are carried out with contactless sensing units such as confocal sensors to avoid damages.

The measurement process itself can be segmented into six parts.

The first sequence includes the import of reference or target geometry. This reference file can be provided by the Ray-tracing or CAD software and be imported by the measurement system.

The second process is the analysis of the target geometry regarding the best possible measurement strategy. Some examples of reasonable measurement strategies can be seen in Chapter A.10.

In the third step, is the measurement process itself. The measurement system operates according to the defined measurement strategy and scans the complete specimen.

After the point-by-point scan of the object under test, the result is a point cloud that looks irregular and not well assorted. In this fourth step, the points are going to be transformed into a surface by employing a surface reconstruction algorithm. The final result is called measurement-matrix as well. The computed surface contains many errors, for example, mechanical inaccuracies of the measurement system, thermal issues, and dynamic effects. These error profiles are saved in error matrices that are computed with the measurement matrix to get an error corrected measurement matrix. The most recent errors are discussed in Chapter 6.

In the final step, the reference-actual comparison happens. The error-compensated measurement matrix and the imported reference file are computed to one final measurement file.

The complete measurement process iterates with the CNC production process until the required product quality and accuracy is reached.

The last step is the QC control, where the complete order is checked and certified. After this critical step, the order is ready to be shipped to the customer.

### 2.3 Metrology systems

Surface measurement is an essential step in the manufacturing process of optical components. The modern optical industry knows two significant categories of measurement systems. Until the development of interferometers, coordinate measurement machines (CMMs) [25–29], especially profilometers, had been prevalent. After the development of interferometers, the situation changed, and the interferometer [30] became the standard measurement device in the optical industry.

Both systems, CMMS and interferometers in different forms, are a significant part of the production chain of optical elements. Each of the systems has some unique advantages and disadvantage. The following sub-Chapters provide a brief discussion about both systems [25, 31–35].

### 2.3.1 Interferometer-based systems

Probably, one of the best-known contactless measurement technique is interferometry. It is based on the superposition of coherent laser light waves. Interference pattern analysis provides information about surface error-profiles [36–38]. Interferometry is fast, enables resolution in the nanometre range, causes no damage to the surface, and is even capable of measuring metre-sized surfaces, for instance, space telescopes, when stitching is employed [39].

Chapter A.2 shows a selection of the most recent interferometer setups that are common in the optical industry. Figure 3 depicts the concept of a Michelson interferometer. That particular type is the base for most of the commonly used interferometer.

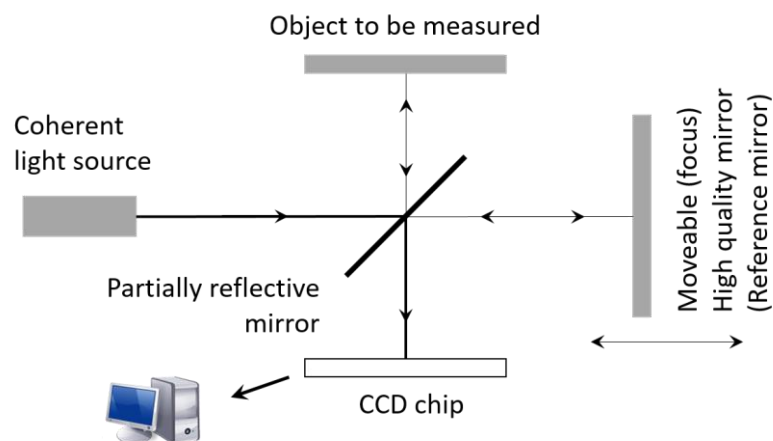


Figure 3: Concept of the Michaelson Interferometer

With respect to the production chain, the main disadvantages of interferometers are their physical limitations regarding the shape of the specimen and that interferometers require reflective surfaces [36–38]. Therefore, research was performed and enabled to reduce the physical limitations by the application of computer-generated holograms (CGH) or by the employment of stitching technology [39, 40]. However, interferometers still require at least partially reflective surfaces; therefore, they are not usable at any stage of the production chain.

### 2.3.2 Coordinate measurement machines

Engineers design coordinate measurement machines mostly with a multi-axis framework that enables the machine to cover the complete workspace with the sensing unit. A further characteristic of a CMM is the measurement process itself. CMMs scan the specimen in a defined manner and record measurement point by measurement point. Once the scan is completed, a software computes all measurement points into a final measurement file.

In general, CMMs consist of three main assembly groups [41]:

- The main structure

This primary assembly contains the complete machine body and the multi-axis framework. One of the primary goals of the measurement system design is to reduce the resonant frequency by using robust and heavy materials. Most of the manufacturers still use a combination of massive granite and steel for the frame design. Furthermore, most of the manufacturers use finite element methods (FEM) to optimise their machine structures. This new method enables the manufacturers to use, for example, polymer, concrete, and aluminium. In combination with modern materials like ceramics (including piezo technology) or silicon carbide, it is possible to design metrology systems with the same or even better characteristics than traditional machines, while being more light, resource-efficient, and cost-efficient.



The advantages of such modern materials are their consistent quality and their immutable characteristics. Natural granite, for example, cannot guarantee the same quality level in each batch, and it interacts with the environment. Since granite is hydrophilic, it has to be treated with impregnation.

- The sensing unit

Sensing units enhance CMMs to become universal measurement systems. Modern CMMs can use a significant number of sensor systems in addition to the traditional tactile systems that interact directly with the surface and maybe damage the object under test. During the last few years, contactless systems like confocal and interferometer-based systems found their way into CMMs.

- Numeric control and data analysis software

Since the improvements in computer science, the control and analysis components became small and more efficient. Most of the CMMs need only a small programmable logic controller to control the machine as well as a desktop computer to run the data analysis software tools [28].

The DIN EN ISO 10360-1:2003-07 [41] presents four main design principles of CMMs. Information about the four traditional designs can be found in Appendix A.2, and Figure 4 illustrates the four commonly used designs of coordinate measurement machines.

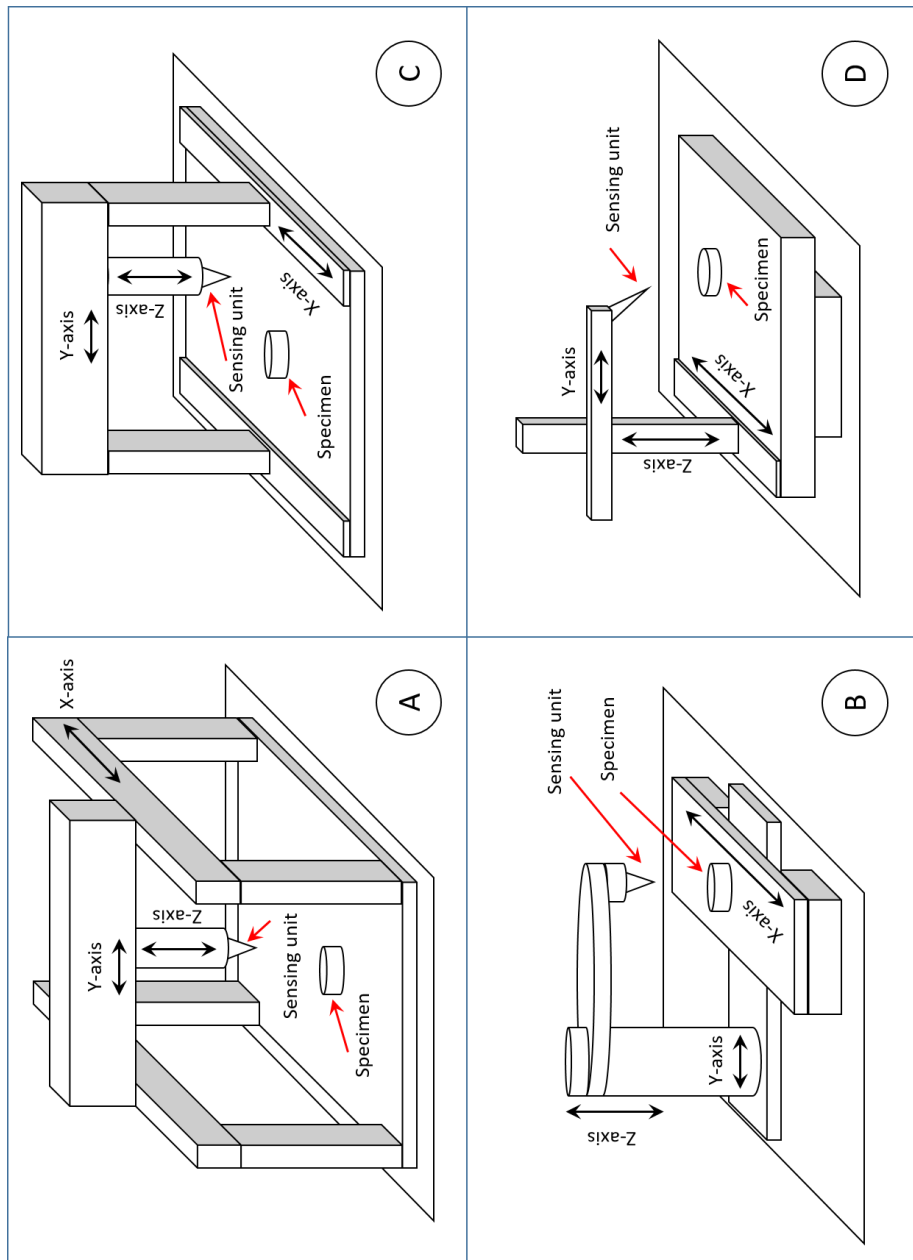


Figure 4: Common designs of coordinate measurement machines.

- A: Portal design
- B: Cantilever design
- C: Bridge design
- D: Gantry design

Besides these standard designs, the spherical-coordinate-system-design is a not very common design. Such devices are mostly used in the manufacturing process of huge objects (diameter > 1000 millimetres) [42, 43]. Figure 5 illustrates an exemplary 3D sketch of a spherical coordinate measurement machine.

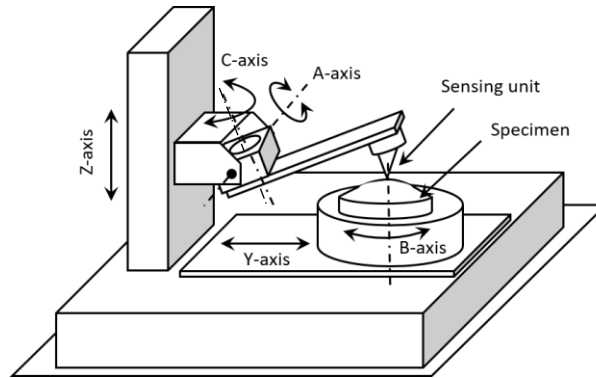


Figure 5: 3D sketch of a spherical CMM. Coordinate measuring machines are known in different designs. The presented CMM design operates by simulating a spherical coordinate system. The significant feature of an SCMM is the application of rotational axes instead of linear axes compared with regular CMMs in the portal design. This design is beneficial for round and high accurate specimen.

A spherical CMM operates by simulating a spherical coordinate system. The primary benefit of this concept is that there are only two rotational axes employed during the measurement process. While the B-axis rotates the specimen continuously under the sensing unit, the C-axis moves across the specimen. This arrangement of axes allows a complete scan of the object without using linear axes.

However, a Z-axis and a Y-axis are necessary to position the specimen right below the sensing unit. After the positioning process, the Z- and Y-axis are locked and secured.

The employment of high-quality air bearings for the B- and C-axis is not very cost-efficient [42]. This circumstance might be the reason why this design is not very common in the optical industry. On the other hand, the accuracy is very high -it is possible to operate to within 200 nanometres [10].

## 2.4 Related research - SCMM

The University of Arizona and its optical laboratories are well known and experienced research institutes in optical sciences. In the year 1990, David S. Anderson, Robert E Parks and Lian-Zhen Shao published the initial publication in the area of spherical coordinate measurement machines [43]. They described a metrology device operating according to the principle of a sphere generator, as published by Angel et al. 1982 [44]. The research team challenged the task to measure large non-planar and non-spherical objects with dimensions greater than one metre in diameter. Such broad and heavy objects are challenging to handle. Therefore, the measurement should take place in situ in the manufacturing machine [42]. The presented approach fulfils the research goals with a sensitivity of 0.1 microns and an accuracy of about one micron [43]. Another important goal of the research had been to design the metrology device by using commercially available components to build an inexpensive aspherical profilometer.

The rapid demand for aspherical surfaces required innovations in the production processes of optical elements. Aspheric departures of 100 microns and more require to ground the aspheric departure into the surface and not to polish due to its low removal rate. Large aspheric objects like mirrors are commonly measured with interferometers applying a holographic test plate [42]. As may be seen in Chapter 2.3.1, interferometers are physically limited by the roughness grade of the surface. Therefore, ground objects are complicated to measure. Anderson and Burge suggested 1995 the use of the swing arm profilometer to enable in situ measurements of the rough surface during the production process [42].

A swing arm, or spherical coordinate, measurement machine consists of a set of linear and rotational axes. Therefore, the correct alignment of the axes is an essential process. Su et al. [45–49] presented a solution by applying an external laser tracker. The laser tracker is used to measure different positions of the sensing unit mount during the movement of the coordinate system of the specimen. The procedure may be repeated several times until the path of the sensor unit mount crosses the vertex or central axis of the specimen. In a second step, iterative measurements of the surface are performed with the goal to find the best-fit sphere adjustment of the SCMM. This setup is reached when the sensing unit delivers the lowest stable values [45, 48].

Jing et al. [48, 49] published a workflow to adjust the rotational table [48]. The workflow starts with the adjustment of the rotary table carrying the specimen. The sensing unit is moved above the rotating object under test in the outer area, close to the edge of the specimen. The rotary table has to be adjusted as long as the sensor signal has a peak to valley value lower than 0.5 microns per full rotation of the specimen. In the next step, the rotation table is stopped, and the sensing unit is moved across the surface of the specimen. The sensing unit has to be moved across the entire surface of the object under test. The adjustment of the rotary table has to be carried out until the signal of the sensing unit shows a peak to valley value lower than 0.5 micrometres.

Another critical factor for highly accurate measurements is the treatment of errors. Jing et al. [48] presented an approach where the possible uncertainties are summed up in all three Cartesian directions XYZ. The dimensions of the analysed component determine the coordinates in the X and Y directions. They measured the

length of the sensor unit carrying arm with a laser tracker. Concerning temperature variation, they measured the uncertainty of 0.05 microns. The arm may swing from the centre point toward the outer edge of the test plate. Therefore, the maximum angle is defined. Depending on the value of the angle, it may be possible to calculate the maximum uncertainty in X and Y direction by applying the presented equation. However, the same procedure had been used to analyse all relevant components of the metrology device, such as the bearings of the rotational axes. Uncertainties of the sensing unit are summed up in the Z-direction [48].

## 2.5 Summary

The presented literature review analysed reasonable publications in the four major research areas related to this thesis. Chapter 2.1 presents publications related to the design and production of commonly used optical elements. The research papers analysed during the literature review showed a significant rise of researchers working with aspherical and free-form shaped elements. Further literature revealed the growing demand for such elements, especially for modern consumer electronics and astronomical telescopes.

Therefore, one research goal of this thesis may be defined by developing a metrology device that can work with most of the commonly used optical elements, such as aspherical and free-form shaped objects. Since the grade of roughness is a crucial factor in selecting the best fitting sensing system, the metrology machine should be able to operate with different types of sensing units. The Laboratory of Optical Engineering

is specialised on research regarding manufacturing and measurement of optical devices. Therefore, a typical optical production chain was established. This production chain, presented in Chapter 2.2, is the reference scheme for this PhD research.

Chapter 2.3 of the literature review had a consolidated view of the existing metrology equipment. The metrology science may be divided into two main categories - Interferometer and coordinate measurement machines. The significant benefits of interferometer-based systems are the speed and high accuracy. Various new approaches such as stitching interferometry enable these devices to operate, in a limited way, even on aspherical or free-form shaped surfaces. The primary disadvantage of interferometers is their need for reflective surfaces. This physical limitation cannot be eliminated.

The second group, coordinate measurement machines, are defined as a device moving a sensing unit by employing a set of axes. The most well-known examples are portal-shaped CMMs and profilometer. While portal CMMs may reach all points to be measured by moving the sensing unit in a defined manner across the specimen, profilometers are mostly designed to create cross-sections. Since profilometers are limited in their degrees of freedom, they are mostly 2D or 2.5D measurement devices. This limitation is their benefit regarding accuracy. Each axis causes errors, and rotational axes are more accurate than linear axes.

The literature review revealed the concept of spherical coordinate measurement machines. This principle is taken as reference for this PhD research. Furthermore, employment at any stage of the production chain requires the application of different

sensing units. The use of tactile sensing units for rough and non-reflective surface should be possible as well as interferometer based sensing units to operate on reflective, polished surfaces.

Chapter 2.4 of the literature review focused on related research about SCMMs. In early 1990, Anderson presented the approach of a swing-arm-metrology-machine. The researchers took the essential function of a sphere generator and designed a very accurate metrology machine used for in-situ measurements of large mirror segments for telescopes. The presented design applies rotational axes instead of linear axes and needs fewer degrees of freedom to operate in 3D.

Furthermore, the axes alignment process of an SCMM is one of the critical factors for an accurate measurement machine. Publications presented different methods to align the system. The usage of an external laser tracker had been presented. Another method showed a set of individual measurements and a manual readjustment of the corresponding tilt angle.

In consequence of the findings of the literature review about related research, some goals for this PhD thesis may be defined. Since the new metrology device may be used in the entire production chain rather than for in-situ measurements, a coordinate transformation has to be developed. These algorithms translate the axes information of the rotational axes directly into Cartesian XYZ coordinates. This procedure enables a simple usage of the measurement results in CNC production machines. Further, an online compensation of encountered errors has to be implemented. This compensation feature includes errors caused by temperature drifts, alignment inaccuracies and axial



and radial runout errors. The alignment process of the axes is a crucial factor. Therefore, research has to be undertaken to develop a novel method to avoid the use of external devices and manual adjustments.

## Chapter 3

### Aims of the work

The measurement process is a crucial factor in the production chain of high-quality products. The best product idea and the most efficient production process cannot grant a satisfying result without a proper metrology process. Especially in the optical industry is the measurement process fundamental. The application of a metrology device at any stage of the production chain is a challenging task.

This PhD research presents a reasonable approach that combines different existing technologies, newly developed methods, and tools into a modern, flexible and highly accurate metrology system. The presented approach provides examples for a reliable machine design as well as for quick adjustment and measurement strategies.

*“It seems that perfection is attained not when there is nothing more to add, but when there is nothing more to remove.”*  
*Antoine de Saint-Exupery*

This citation guided me through my research. Furthermore, it is the fundamental factor in the motivation to write this PhD research.

### 3.1 Motivation

High accuracy measurement devices are a substantial part of the production process of each product. The extensive range of different measurement tasks in the market led to many different types of metrology systems. The metrology industry mostly designed measurement machines for individual needs. Interferometers and coordinate measurement machines represent the two essential groups of metrology systems.

Interferometers are very accurate and quick - but physically limited to only a few surface types. The latest generation of interferometer-based systems is called stitching interferometers. The primary feature of such devices is their capability to cover the object under test with a certain number of small measurements and reconstruct the entire surface in a completing step. Further information about interferometers may be found in Chapter 2.3.1.

Coordinate measurement machines are designed to operate on a large number of surface types - but they are limited in their accuracy and operation speed. One example of a particular type of CMM used in the optical industry is the swing arm CMM [42, 43]. This device belongs to the group of spherical coordinate measurement machines, and it is used to measure large aspherical objects with high accuracy. Some examples of coordinate measurement machines may be found in Chapter 2.3.2.

However, neither of both significant groups may be used during the complete production cycle of high accurate objects. A consolidated view of the particular area of optical applications shows the demand for a suitable metrology system. Coordinate

measurement machines are mostly used at the beginning of the production process. At these stages, rough processes such as cutting or milling generate rough and structured surfaces. CMMs can operate on structured surfaces due to the variable employment of tactile sensing units. High accuracy is not needed at these stages.

When the product reaches the end of the production process, smoother production processes such as grinding or polishing are used. These processes produce smooth and very even surfaces. Such surfaces may be measured by the application of high accurate interferometer based solutions.

The research presented in this PhD thesis provides a new approach to a generation of metrology systems, including the benefits of both systems – CMM and interferometer technology. The primary criteria for a metrology system that was used during the complete product production cycle may be defined with the following characteristics:

- Provide a high measurement accuracy and repeatability
- Multi-sensory
- Shop floor size, less than 3m<sup>2</sup>
- Operate on objects smaller than 300 millimetres in diameter
- To operate on objects with a significant variation of roughness grades, from rough to polished.

- To operate on objects with a significant variety of geometrical shapes, including free-formed<sup>14</sup> objects
- To reduce the general influence of inaccuracies caused by the geometrical design of the machine
- To reduce the influence of user indicated inaccuracies
- To be faster than regular coordinate measurement machines
- To be not sensitive to environmental influences
- To be price sensitive

This set of essential specifications is the reference for the research project. Research has to be performed to combine all requirements into a new approach for a metrology system.

A mechanical device needs a reliable and robust design to reach a high accuracy level. The science knows that rotational axes provide higher accuracy than linear axes [50–52]. This fact is justified in the production process of guiding elements. Milling machines have to move at least three linear axes to produce a linear-motion bearing. Turning machines need only one rotational axis and one linear axis. Therefore, the production process of a linear-motion bearing is complicated and more subject to the influence of errors.

---

<sup>14</sup> In the context of this thesis, free-form shaped objects do not follow any of the regular designs, such as planar, spherical or aspherical.

The example of swing arm CMMs may be taken as reference for the design of the spherical coordinate measurement device. Such devices follow a comparable kinematic design.

## 3.2 Objective

The objective of this research is to develop a suitable metrology solution for optical devices by designing and creating a multi-sensor coordinate measurement machine. The optical industry requires a flexible, highly accurate, and reliable metrology solution usable in all stages of the production process. Within the project EMMA (see Section A.1), the Deggendorf Institute of Technology (DIT), Deggendorf, Germany, bought two old and defect prototypes of a metrology system. The concept of these metrology machines is based on a spherical coordinate measurement machine that operates by simulating a spherical coordinate system [44]. This system had been developed to measure small aspherical shaped objects with a diameter of fewer than 200 millimetres. Unfortunately, the developing company stopped the project several years ago, and there are only a few non-functional prototypes in laboratories left. The DIT started the project EMMA to fix the system and to integrate it into the laboratories production facility. This project was the initial spark of this PhD research.

This thesis shows the further development of the primary machine and its components as well as the development of two new and generic components. The first component, an axes alignment procedure (see Chapter 5.2), allows to aligning the axes very accurately without the application of expensive laser tracking devices [48]. The

second device, a three-dimensional scale (see Chapter 5.3) [53], allows compensating the motion errors of the applied rotational axes. Finally, the metrology system had been equipped with a user interface to reduce the user indicated errors and a general data analysis software.

The thesis includes the following objectives:

- The development of an enhanced swing-arm-coordinate-measurement-machine, useable at any stage of the production chain in the optical industry.
- To develop algorithms to transfer the axes positions into Cartesian coordinates.
- To develop a reliable, accurate and generic axes alignment system for SCMMs.
- To develop a reliable, accurate and generic measurement device related to a measurement frame.
- To design and develop measurement strategies to reduce disturbing influences.
- To present a user interface to reduce user indicated errors.
- Visualise the structure of a data analysis tool for coordinate measurement machines, including planar, spherical, aspherical and free-form measurements.

There are only four measurement principles known which can operate on aspherical or free-form shaped objects.

- Interferometry by employing a CGH or stitching technology (with strong limitation to the slope gradient, “weak aspheres,” and limited in free-formed shapes) [30, 54, 55]

- 2D and 2,5D<sup>15</sup> profilometers [56–59]
- Coordinate measurement machines [27, 28, 60]
- Swing-arm or spherical coordinate measurement machine [42, 43]

Since the market of free-form shaped objects is increasing and the interferometry is physically limited to operate on free-formed surfaces, coordinate measurement machines and Profilometers are the only measurement instruments to aid the demand of the optical industry. Therefore this research had been undertaken to aid the demand and may present an alternative metrology device.

---

<sup>15</sup> 2,5D may be understood as the mathematical composition of several 2D measurement results to a 3D surface



## Chapter 4

### Methodology and Approach

#### 4.1 Research Methodology

This PhD research has the principal goal to present a suitable approach to a highly accurate and modular metrology device. To be able to reach that goal and undertake such sophisticated research, the application of an appropriate research method is required. Montgomery et al. presented an approach designed for engineering tasks [61].

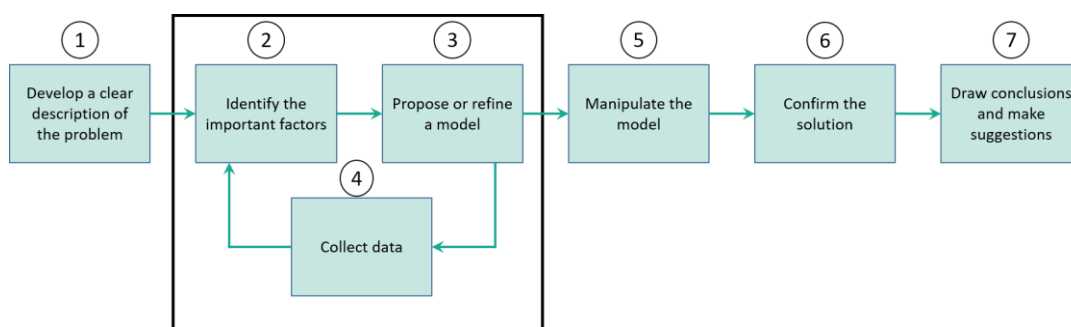


Figure 6: Engineering method by Montgomery. With the publication of the engineering or scientific method, Montgomery presented a procedure to solve engineering problems. The method is based on the interaction of a model of the problem, the influencing factors, and experiments to verify the model. This procedure contains three steps that iterate until the final solution is obtained.

In “Engineering or scientific method”, he presented an approach for engineers to solve problems of interest to society by the useful application of scientific principles. The seven steps of this approach are depicted in Figure 6.

With respect to the presented PhD research, some modifications of Montgomery’s method have to be applied. The result is a new and generic process, specially designed for performing large research projects, as presented in this thesis.

Figure 7 illustrates Schneider’s engineering and scientific method.

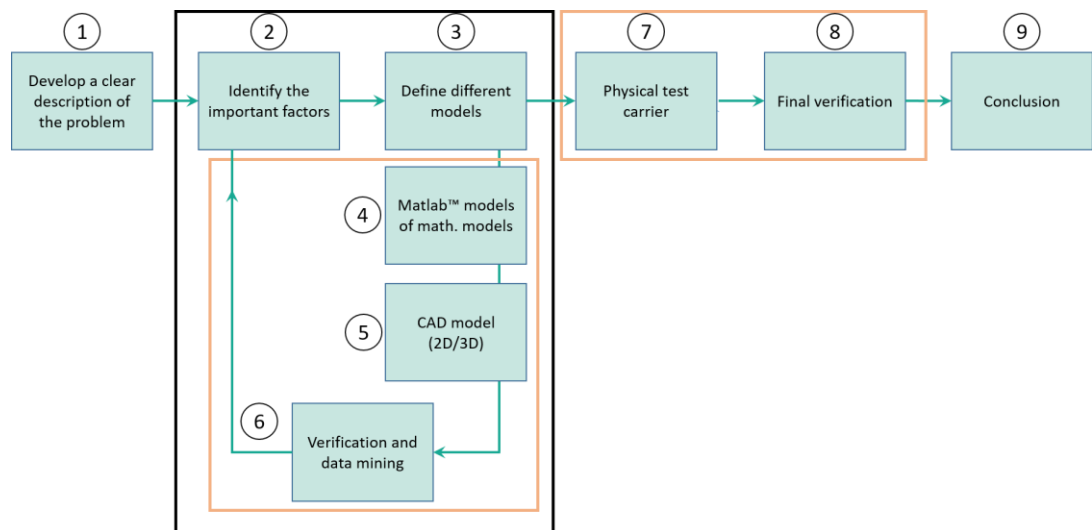


Figure 7: Schneider’s engineering and scientific method – a consistent further development of Montgomery’s scientific and engineering method

The first two stages, **(1)** and **(2)** are similar to Montgomery’s method. The main difference to the original method is the application and combination of three independent verification stages **(3-8)**. First, independent and different models have to be defined **(3)**. In the next stage, **(4)**, all mathematical models, formulas, and equations are computed by the application of a mathematical software tool. Matlab™ (M2010a)

was used during this thesis, but there are other comparable software tools, for instance, Maple™, Scilab™, Mathematica™, or Mathcad™.

In stage **(5)**, CAD models of the geometric relationship are designed. Creo3™ (M100) was used during this PhD thesis, but any other proper CAD software that includes a reliable measurement and data export feature may be used. As other examples, Solidworks™, Catia™, or Siemens™ NX™ are commonly known CAD software solutions that may provide similar functionality.

Step **(6)** verifies the results obtained in step **(4)** and **(5)** by comparing critically. Furthermore, the described process generates a tremendous amount of data. Therefore, data mining and the computation of the obtained results is a critical factor.

As introduced, the new methodology approach consists of three independent verification stages. The third stage is represented by the physical test carrier **(7)**. This feature enables to check and verify all assumptions and results obtained in the previous stages by a final comparative verification process **(8)**. The presented methodology process closes with the last stage, the conclusion.

In the context of this PhD research, the following sub-Chapter presents the application of the presented Schneider's engineering methodology with respect to the presented PhD thesis.

### 4.1.1 Application of the methodology

In compliance with Figure 7, the first step is to develop a clear and concise description of the problem **(1)**. In the context of this thesis, this first step is elaborated in three chapters of this thesis (Chapter 1, Chapter 2, and Chapter 3). An overview of this thesis is presented in Chapter 1.2, the thesis overview. Furthermore, the literature review revealed different problems in the context of the topic of this research. The results are stated in Chapter 2.5, the summary of the literature review. However, the key milestones and goals of this research are published in Chapter 3, aims of the work. The second step requires identifying the essential factors that affect the goals of the research **(2)**.

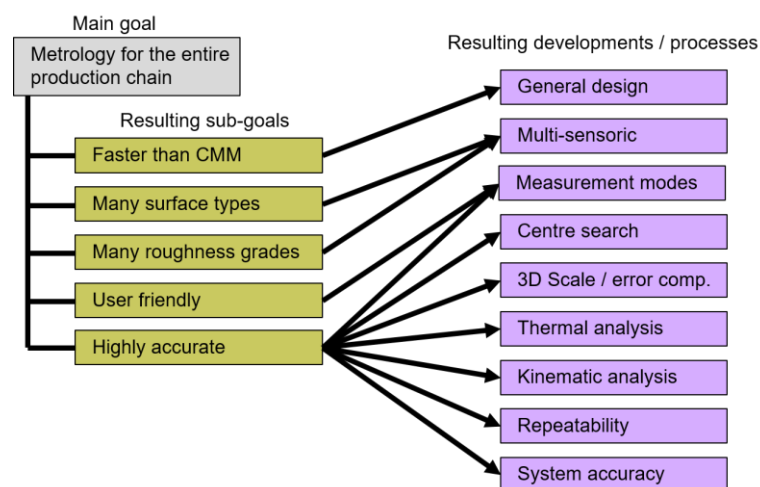


Figure 8: Identification of essential factors. The initial goal leads to different sub-goals and furthermore to resulting development or processes.

Figure 8 illustrates the relationship between the initial goal, the resulting sub-goals and the processes or developments that became necessary to fulfil the initial goal of this thesis. Therefore, the literature review, presented in Chapter 2, focused on the expected sub-goals as presented in Figure 8.

According to the initial goal of this thesis is to present a metrology solution that can operate on many different surface types and roughness grades. Chapter 2.1 presents the latest research about commonly used optical elements, their benefits, and their challenges. Especially the ability to measure aspherical and free-form shaped objects is a crucial factor.

Furthermore, the structure of the surface is a limiting element. Another aspect is inefficient alignment techniques, presented in Section 2.4 and Section A.11.1. The correct alignment of the employed axes is a critical factor for successful measurements.

The literature review revealed that usability is an essential factor. On the first hand, it is necessary to ensure proper handling of the metrology system; on the other hand, proper usability helps to reduce user indicated errors.

Along with the alignment process, named centre search, the compensation of errors is an essential factor, exceptionally repeatable errors from the rotational axes. The errors, an approach to monitor and to compensate them are published in Chapter A.8, the 3D-Scale. Errors caused by the environment, the user and the measurement machine are presented in Chapter 6.

Furthermore, most of the problems concerning the shape and structure of the specimen may be solved by the implementation of a multi-sensor interface and the use of different probe technologies as proposed in Chapter A.5. Another aspect concerning the general shape of the specimen is the use of a suitable machine design, published in Chapter 2.4 and A.2. Regarding the alignment situation, a new strategy had been

developed and implemented; it may be studied in Section A.9. The compensation of repeatable errors generated by the rotational axes may be solved by the application of a newly developed device named 3D-scale. Details can be found in Chapter A.8. Mathematical models regarding the structure of the metrology device and models for the data analysis may be found in Section 5.1.3.1.

In the third step **(3)**, different and independent models are defined to prove the assumptions. Since a physical test carrier had not been available at the beginning of this thesis, all models had been tested with software tools. According to the described methodology, Matlab™ and Creo™ was used to create these models **(4+5)**. Descriptions of the methods can be found in Chapter 4.2.2 and 4.2.3. The verification stage **(6)** includes the systematic comparison and verification of the results of both virtual models.

After designing and creating the physical test carrier, experiments had been performed to collect data for step seven **(7)**. The setups and results of the experiments are depicted in Chapter 7. While performing the experiments, the models and the developed software tools had been refined by using the observed data. Step eight **(8)** of the used problem-solving method defines to verify the models and to conduct an appropriate experiment to confirm that the proposed solutions to the problem are both efficient and effective. Both had been demonstrated in Chapter 7.3.2 and finally, in Chapter 8, the discussion.

Finally, conclusions **(9)** and suggestions for future work had been made in Chapter 9 and Chapter 10.

## 4.2 System approach

Numerous experiments verified the presented methods and the theoretical considerations of this thesis. The detailed information about the different test series can be found in the corresponding Chapter 7.

However, this section provides a consolidated overview of the tools, the equipment, and the techniques to solve the task formulated in this thesis. To be able to verify the theoretical approach, it was necessary to employ advanced software tools and to design a physical demonstrator. The mixture of software-based simulations and performed practical test series are consistent with the methodology, presented in Chapter 4.

The research started during the project EMMA (see Section A.1). The reached goals, the progress, and the gained knowledge of the project had been the base of the idea of driving this PhD research. The BMBF funded project EMMA delivered some reasonable publications, presented in the Appendix, including a final report containing the complete knowledge gained [62]. The second column of the definition of the research question had been the analysis of the results of the literature review, published in Chapter 2.

The literature review had been firstly performed at the beginning of the PhD research in 2009. The essential keywords had been “CMM, coordinate measurement machine, interferometry, spherical coordinate system, and optics”. This research revealed several publications in the field of metrology. Anderson and Burge presented

an approach in 1990 and 1995 [42, 43] about a swing arm CMM which may be seen as related research. The research was taken further, and recent publication had been identified in that field [45, 46, 48, 49, 63]. Furthermore, the literature review revealed many documents about interferometry and especially about stitching interferometry. However, the composition of the literature review's results and the results gained in project EMMA led to the research goal "Development of a flexible and modular metrology system for aspheres and free-form shaped objects".

Nevertheless, the consolidated view on the geometrical relations of the planned spherical coordination measurement machine resulted in a set of mathematical models describing the system theoretically. To verify the algorithms, which may be found detailed in Section 5.1, two software packages had been used.

Furthermore, this thesis is based on some national and international publications, presented in the list of publications (page vi). These publications are presenting investigations in different fields related to the thesis. For example, findings in the area of MRF polishing technologies [3, 5], studies related to grinding technologies [6, 8], investigations about stitching interferometry [54, 64] and research about inaccuracies of spherical coordinate measurement machines, measurement strategies, measurement of free-form shaped surfaces and spherical coordinate measurement machines in general [10, 22, 23, 53, 62, 65].



#### 4.2.1 Applied software tools

The basis of this research had been the verification of the developed algorithms with software tools. Functional hardware equipment to carry out the test series had not been available at the beginning of the presented research. Therefore, it was decided to simulate the developed models with appropriate software tools. There are different software packages in the market, designed to support developers by testing their theories and simulating the results by computing the algorithms. It was decided to use two different approaches and to compare the results among each other.

The first software package is Matlab™ from Mathworks™ in version M2010a (32 bit) and finally verified by M2017a (64 bit). This software package is ubiquitous in the academic world; the logical and straightforward language enables researchers to compute their developed algorithms very quick. Matlab's™ (M2010a) reliability and accuracy had been verified and proven in international publications [66, 67].

Furthermore, Matlab™ (M2010a) provides some distinct features that had been used for the presented research. The name Matlab™ (M2010a) is a combination of Matrix and Laboratory. Therefore, the software is specialised on matrix operations. Matrices are a secure method to represent the information obtained by measurements. Each field of a matrix represents one measurement point. Matlab™ (M2010a) enables to create a stack of several matrices in layers. Therefore, it is possible to generate a stack of matrices where the first layer contains the value of the sensing unit and the next three layers the coordinates of the measurement point in X-, Y-, and Z-direction.

Additionally, the software comes with a compelling plot feature that enables the researcher to display the results quick and precise.

All implemented Matlab™ (M2010a) functions and toolboxes are documented, and the references are added. Furthermore, Matlab™ (M2010a) was used to develop significant parts the software suite needed to operate the test carrier. Detailed information about the software packages of the physical test carrier may be found in Section A.12.

The second software package is CREO™ by PTC™ in the version Creo3™ (M030, updated to M100). CREO3™ (M100) is a sophisticated software suite providing a couple of useful features such as CAD, FEM and motion analyses [68]. This software package enables the virtual design of complex geometrical structures. Another essential feature is the measurement tool included in the CAD system. This feature allows the user to measure distances and angles in a very exact manner [3, 68, 69].

This powerful piece of software enables engineers, designer, and researcher to visualise their ideas by creating 3D models of them. Furthermore, the software suite enables to simulate essential effects, such as the influence of temperature, vibrations, production-, and assembling tolerances. Many open questions regarding such effects can be estimated during the design of a machine.

The following subchapters present the different methods applied to the significant parts and research of this PhD thesis.

#### 4.2.2 Matlab™ model of the SCMM

All Matlab™ (M2010a) codes were programmed with essential mathematical functions. The used mathematical models are published in Chapter 5. For the verification, CREO3™ (M100) was used. The results are published in Chapter 5, A.13, and A.14. Matlab™ (M2010a) offers the option to calculate with a double-precision floating-point. All geometric relations had been tested systematically, each in a two dimensional CAD model. The relations had been tested by using different geometries of the specimen. The development process of the developed algorithms is published in Chapter 5. Since the planned metrology system is designed to operate on the best-fit sphere of the specimen, all tests regarding the geometry of the system had been carried out with planar and spherical objects.

To be able to verify the predicted results, test software had been developed. This piece of software calculated all angles and distances according to the developed algorithms. The computation had been realised with defined steps to simulate the complete range of required objects under test. Each diameter had been calculated with each curvature. The step size had been 1 millimetre. Therefore, 59.100 data sets had been computed. The result of the verification had been the necessary input for the creation of the virtual model in CREO™.

The significant variables can be found in the following Table 2.

*Table 2: Used verification parameters.* This table presents the parameters used for the test series performed with the CAD software suite *CREO3™ (M100)* and *Matlab™ (M2010a)*. As a virtual specimen, round objects with a planar, convex-spherical and concave-spherical shape had been generated. Both software packages performed the calculations to obtain the required setup positions of the virtual SCMM. The results had been compared.

Shape of specimen	Objects diameter D [mm]	Objects curvature R [mm]	Remarks
Planar	10 – 200	0	D changed in 1-millimetre steps. 100 iterations per 1-millimetre change in diameter.
Convex sphere	10 – 200	0 - diameter D	D changed in 1-millimetre steps. 100 iterations per 1-millimetre change in curvature.
Concave sphere	10 – 200	0 - diameter D	D changed in 1-millimetre steps. 100 iterations per 1-millimetre change in curvature.

The details and the mathematical derivation of the algorithms may be found in

Chapter 5.1.

### 4.2.3 CREO™ model of the SCMM

CREO3™ (M100) comes with the feature of a 2D sketcher. All 3D objects get their first two dimensions in this sketcher. After finishing the first 2D sketch, the third dimension is extruded into the third dimension (depths). For verifying the geometrical relations of the metrology machine, the 2D sketcher was used in the first instance. The axes were created with simple lines; points were used as connection points. This method resulted in a technically accurate, but simplified 2D model reduced to lines and points without the need of creating virtual 3D elements. CREO3™ (M100) comes with a technical and mathematical correct dimensioning tool that includes the option to connect dimensions according to defined relationships. By the application of this method, all algorithms were verified by adjusting the 2D sketch and read out the required values to compare them with the Matlab™ (M2010a) result.

However, the same method was used with the virtual 3D model of the metrology device. The 3D model was designed with “internal relations”. Creo™ provides the opportunity to combine different design features, such as lines or angles, with mathematical equations. That means that manipulation of one dimension results in an automatic alignment of other related dimensions. For example, the change of the radius of the curvature leads to an automatic change of the tilt angle of the A-axis and a height adjustment of the Z-axis. This procedure simulates the same input as the user can do. The method has two significant advantages. First, the geometrical relations and the interaction of the complete machine may be verified. Secondly, the necessary user input for the user interface of the physical test carrier may be verified as well.

Nevertheless, CREO3™ (M100) provides two further tools used in this research. The first one is the motion tool. The application of this tool allows applying motion into the axes, especially into the rotational axes. With this tool, a complete simulation of a measurement process was created. The virtual tracking of the sensor tip in relation to the spherical coordinate system and the surface of the specimen provides a full set of three-dimensional measurement points. An additional piece of software had been created to export the dataset and translate all measurement points into XYZ values [22, 23]. The verification process had been successfully finished by subtracting a Matlab™ (M2010a) generated spherical curvature in Cartesian XYZ coordinates from the exported file. Ideally, the result of this subtraction is zero.

#### 4.2.4 SCMM test carrier

The presented research methodology requires the functional verification of the obtained theoretical results and models. Therefore, designed experiments are required. The mathematical models presented in Chapter 5.1 describe an SCMM in a logical way. All researched mathematical models were verified by the application of two software packages, Matlab™ (M2010a) and CREO3™ (M100) (ref. Chapter 4.2.2 and 4.2.3). According to the presented methodology, practical tests are necessary to verify the system, including all components. Therefore, a physical test carrier was developed and built.

The test carrier was designed to meet all objectives of this PhD research. The objectives can be found in Chapter 3.2.

### 4.3 Summary

The presented research methodology is based on the “engineering or scientific method”, developed and published by Montgomery [61].

The methods and approaches had been beneficial to cover a vast number of tasks during this thesis. Especially the employment of two different software tools in combination with a physical test carrier had been constructive. The general tests with Matlab™ (M2010a) and CREO3™ (M100) provided a great chance to test and verify the developed algorithms. The simulations with Matlab™ (M2010a) revealed the accuracy and boundary conditions of the algorithms. It had proven beneficial to plot the results and compare with other methods of calculation to adjust and improve the original algorithms.

However, the tools provided by CREO3™ (M100) had an equal impact factor on the presented research. The 2D and 3D modelling of the components and the complete metrology system had a significant influence. It revealed the strengths and weaknesses of the basic concept. Furthermore, the option to measure each angle and length in a very accurate manner had a significant influence to answer the research questions efficiently and sufficiently.

The motion feature of CREO3™ (M100) allowed running complete test series without the need for a physical test carrier. A correct used motion feature is a potent software tool in the design process of mechanical devices. It had been beneficial to develop different measurement modes, such as Track-, Spiral-, and Section-Mode. Even

the influence of alignment errors may be demonstrated. Naturally, it is possible to manipulate only one thing and investigate the simulated measurement result according to the related influence.

Also, the fact that a tested virtual 3D model of the metrology system had been beneficial to create the physical test carrier is remarkable. A 3D model and the corresponding 2D drawings improve the production and the enhancement of the physical test carrier tremendously. Virtual models enable the designer to perform different simulations — for example, structural and thermal analyses or motion and kinematic simulations. Professional software like CREO3™ (M100) helps to find and remove errors in the design and additionally in the case of this PhD research, errors or unwanted effects.



## Chapter 5

### Development of the SCMM

Research has been undertaken to address the needs of high accuracy metrology systems. The literature review and especially the expertise of the Laboratory of Optical Engineering had been beneficial to encircle the requirements of a new metrology device and to define the topic of this PhD research. Swing-arm CMMs are known in the area of large optical devices.

#### 5.1 Mathematical models of the SCMM

The modern manufacturing industry is desirous of reliable, accurate, and modular metrology systems operating with high-speed. These requirements can only be satisfied by the application and combination of different natural sciences. The following Chapters present the different stages of the development process of a modern and flexible spherical coordinate measurement machine.

David S. Anderson presented a “Versatile Profilometer for Aspheric Optics” in 1990 [43]. The basic idea behind his publication was to create a metrology device operating according to the principle of a sphere generator [44]. Such non-CNC-controlled machines had been used for decades to produce spherical objects such as lenses [70]. Furthermore, his publication presents the fundamental equations of such a sphere generator based metrology device.

### 5.1.1 Design of the SCMM

The presented measurement system belongs to the CMM sub-category of spherical coordinate measurement machines or swing arm CMMs. Contrary to a conventional coordinate measurement machine, which operates by simulating a Cartesian coordinate system with linear axes, a spherical coordinate measurement machine uses a spherical coordinate system as the base. A general example of a spherical coordinate system is presented in Figure 9.

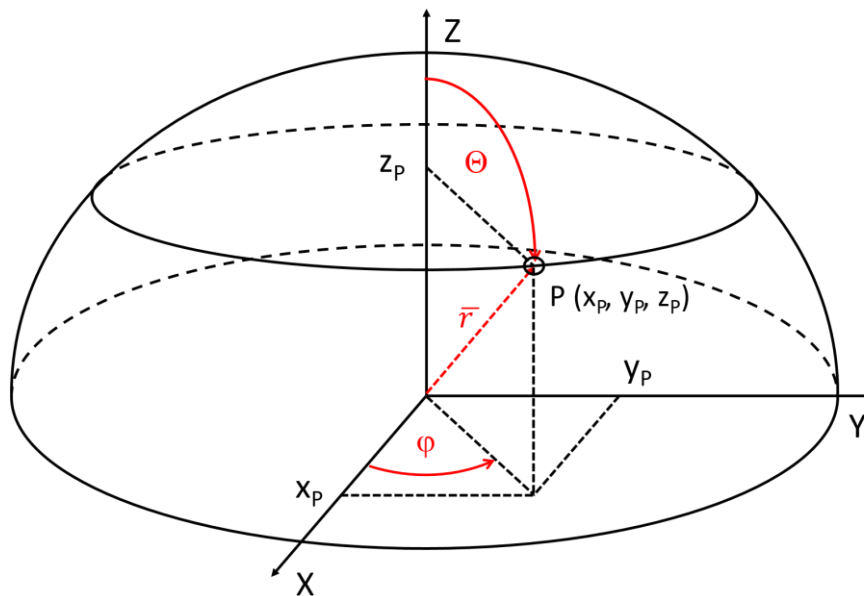


Figure 9: Spherical coordinate system. In a spherical coordinate system (SCS) is a point described with two angles and one vector. The SCS coordinates can be translated into regular Cartesian coordinates.

Figure 9 illustrates the correlations of a spherical coordinate system by the appliance of a point P. Each point in the 3D space can be described with two angles and one vector. The vector  $\vec{r}$  is the shortest distance between the origin of the spherical coordinate system and the point P. The inclination angle  $\varphi$  is the angle between the X-axis and the projection of  $\vec{r}$  in the XY plane. The azimuth angle  $\theta$  is the angle between the Z-axis and the vector  $\vec{r}$ .

A regular CMM operates according to an XYZ Cartesian coordinate system (ref. Section 2.3.2). Therefore, a CMM applies a set of three linear axes, aligned perpendicular to each other. A spherical coordinate measurement machine needs five axes to generate a spherical coordinate system. On the first look, this frame setup is elaborate and requires more axes than a regular CMM. However, a consolidated view on the system shows that there are only two rotational axes applied during

measurement. The other axes are only needed to move the sensing unit and the specimen into the required position, and then they are locked to avoid irregular movements.

Figure 5 presents the sketch of a spherical coordinate measurement machine. In the context of this PhD thesis, the axes are defined as:

- Rotational axes:
  - o A-axis: Mounted on the Z-axis and hosts the C-axis including the cantilever carrying the probe.
  - o B-axis: Mounted on the Y-axis; it is the base for the chuck and the specimen.
  - o C-axis: Mounted on the A-axis and includes the cantilever carrying the probe.
- Linear axes
  - o Y-axis: Embedded on the granite foundation, sustains the B-axis.
  - o Z-axis: Assembled on the granite foundation, carries the A-axis.

The axis framework can be interpreted as two independent modules. The lower module is assembled on the Y-axis and the upper section pillared on the Z-axis. The lower assembly contains the specimen, the hydrodehn chuck system, and the B-axis. The upper section includes the probe, the C-axis, the A-axis and the Z-axis. Both modules have to be adjusted in a defined manner to enable highly accurate measurements — the exact manner as described in Chapters 5.2 in detail. The following sub-Chapters present a consolidated view on the geometric relations of the SCMM.

### 5.1.2 Planar operation mode

The basic concept of this mode is the parallel and vertical alignment of the C-axis, the central axis of the sensing unit and the B-axis. Consequently, the sensing unit travels on a horizontal plane. Therefore, the planar mode may also be used for measurements of objects that have a planar surface or a surface that can be interpreted as planar. In the context of this PhD thesis, the definition of planar refers to the detecting range of the used sensing unit. However, a surface with an expected peak to valley distance smaller than the detection range of the used sensing unit may be seen as planar. Therefore, this definition is not limited to the actual shape of the surface, such as planar, spherical, and aspherical or free-form shaped. Figure 10 illustrates the sketch of the planar operation mode.

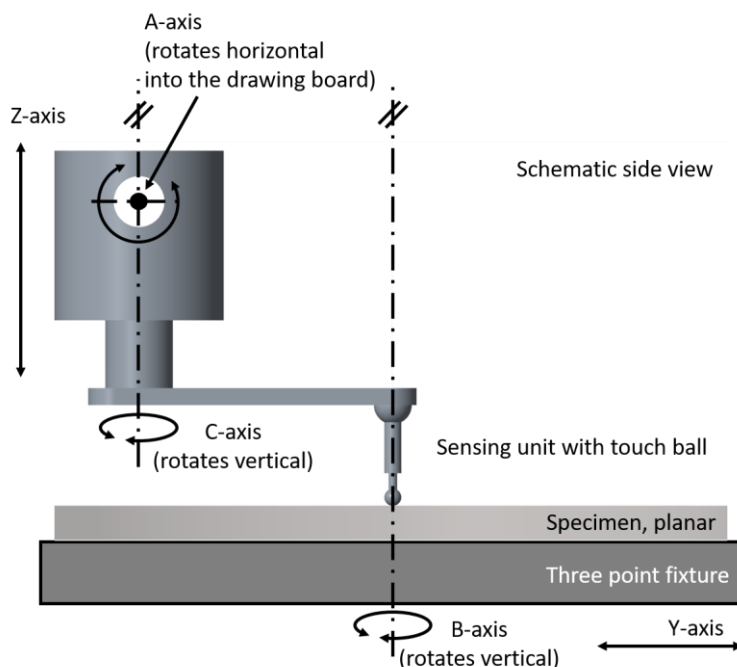


Figure 10: Sketch of the planar operation mode. The CREO3™ (M100) CAD model presents the basic coherencies of the planar operation mode. The central axes of the C-axis, B-axis and of the sensing unit are parallel. In the correct setup, the central axis of the sensing unit is concentrically aligned with the B-axis

The distinctive feature of this setup is the parallelism of the central axes of the B-axis, the C-axis and of the sensing unit. Figure 11 illustrates a typical bow-shaped path of the sensing unit in the top view. The sensing unit travels along a bow-shaped path from the outer edge towards the centre of the specimen.

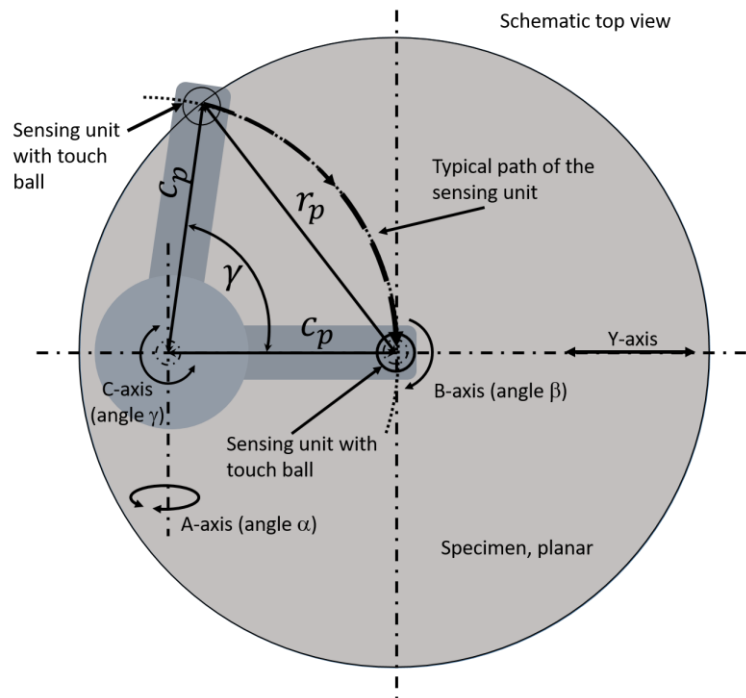


Figure 11: Top view planar operation mode. The top view enables to illustrate the movement of the sensing unit in relation to the specimen. The sensing unit rotates with the distance  $c_p$  around the C-axis. The procedure starts at the edge and ends in the centre of the specimen.

The function of the planar operation mode may be comparable with the function of a turntable. Figure 11 illustrates the importance of the alignment process. For the case of misalignment, it may not be ensured that the measurement covers the entire surface of the specimen. The sensing unit has to cross the centre of the specimen to grant a successful and complete measurement.

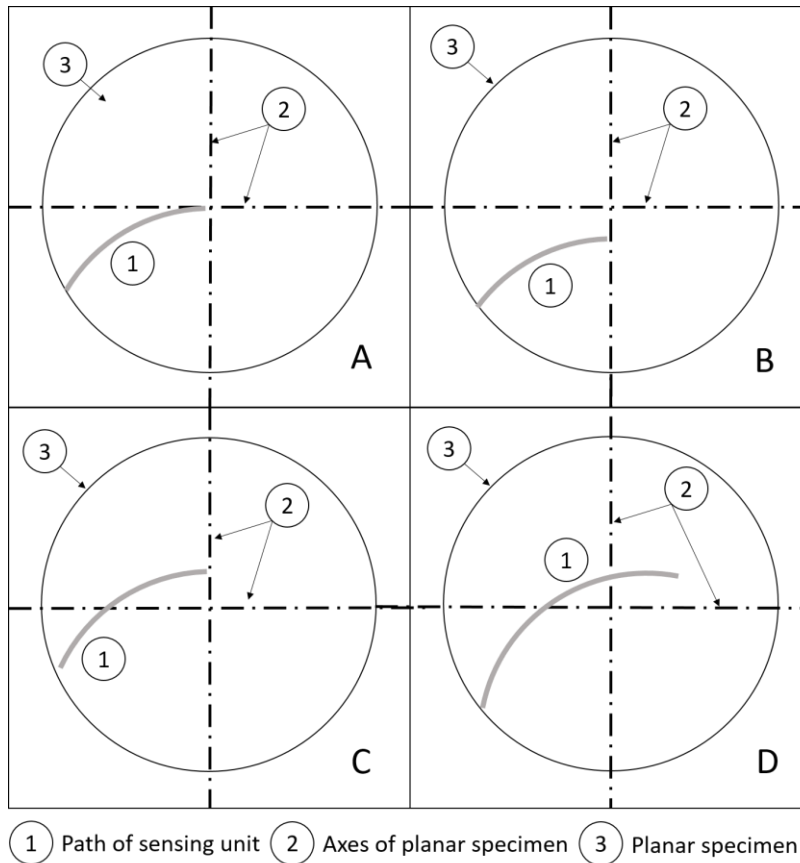


Figure 12: Examples of misalignment in the planar operation mode

Figure 12 shows four examples of a tool path in relation to the axes of a planar specimen. The first picture (A) illustrates a perfect aligned system where the tool path exactly meets the centre of the planar specimen. In that particular case, the sensing unit can scan the entire specimen. In the other three examples (B, C, and D), the tool path does not meet the centre of the specimen. Therefore, the region around the centre of the specimen cannot be entirely scanned by the sensing unit.

Since the sensing unit travels on a horizontal plane, parallel to the rotation plane of the B-axis, the planar setup is an exceptional case regarding the basic design concept

of an SCMM. The axes of the C-axis and the sensing unit do not directly intercept a defined point; they intersect in infinity since they are parallel. However, this setup does not represent a spherical coordinate system. Indeed, the planar operation mode follows a cylindrical coordinate system. A cylindrical coordinate system is a planar polar coordinate system, extended with a third, rectangular height dimension, see Figure 13. Each measured point may be interpreted as a single vector from the centre of the coordinate system towards the sensing unit tip.

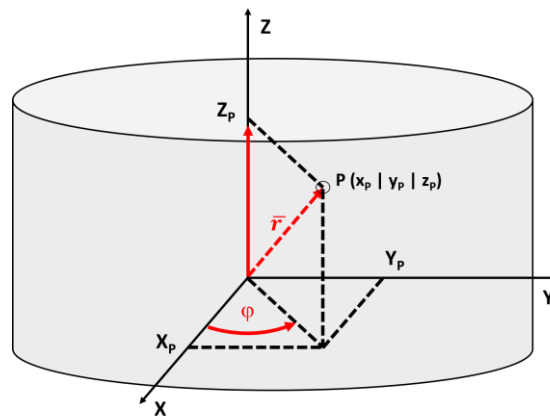


Figure 13: Cylindrical coordinate system. A cylindrical coordinate system is a 2D polar coordinate system with an added component in Z-direction.



### 5.1.2.1 Mathematical correlations of the planar operation mode

Chapter 5.1.2 introduced the planar operation mode. However, the planar operation mode operates in a cylindrical coordinate system (ref. Figure 13).

A cylindrical coordinate system is a three-dimensional construct that describes the X, Y, and Z values of a point with a rotation angle  $\varphi$ , and the origin vector  $r$  as depicted graphically in Figure 13.

$$X = r * \cos(\varphi) \quad (1)$$

$$Y = r * \sin(\varphi) \quad (2)$$

$$Z = \text{sensor value} \quad (3)$$

Where:

X = Cartesian coordinate in X-direction

Y = Cartesian coordinate in Y-direction

Z = "sensor value" = Length measurement result of the sensor; for example in millimetre

r = Vector from origin to the measured point

$\varphi$  = Rotation angle in the XY-plane

Equation 1 and Equation 2 present the calculation of the X and Y component in a polar coordinate system. The X and Y values are extended about Z-component. The probe and the measured distance to the surface of the specimen represent this component.

The transformation of the axes encoder data into polar or cylindrical coordinates needs some prior work. The geometric relations of a spherical coordinate measurement machine in the planar operation mode may be seen in Figure 14 and Figure 15.

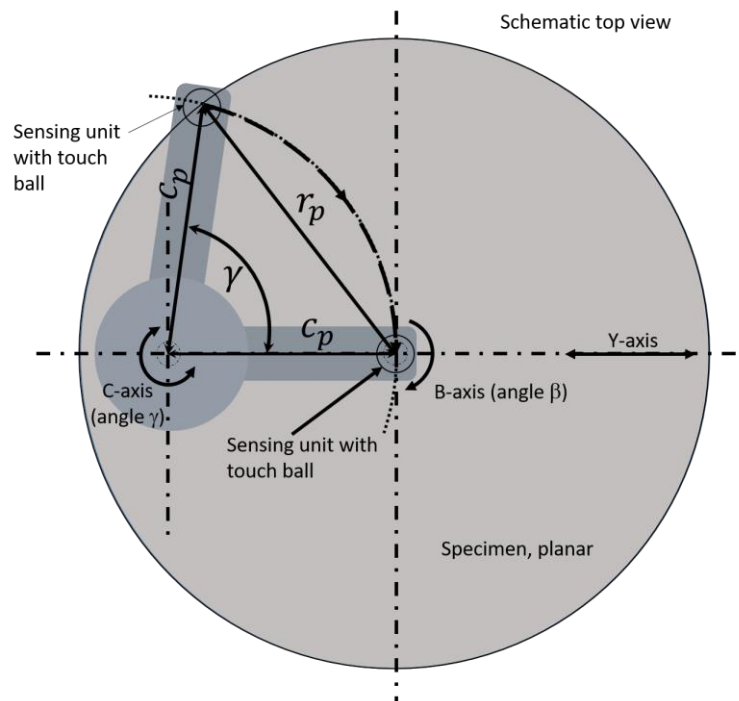


Figure 14: Top view planar operation mode. The sensing unit travels in a bow-shaped path from the edge of the specimen towards the centre. During this movement is the B-axis rotating continuously.

This configuration reveals two significant challenges. The first issue is related to the movement of the probe. The C-axis moves the sensing unit in a bow-shaped curve

from the outer edge towards the centre point of the B-axis. The second challenge is that there are two axes (B-axis and C-axis) rotating simultaneously. Therefore, the commonly used equations for the cylindrical coordinate system have to be expanded.

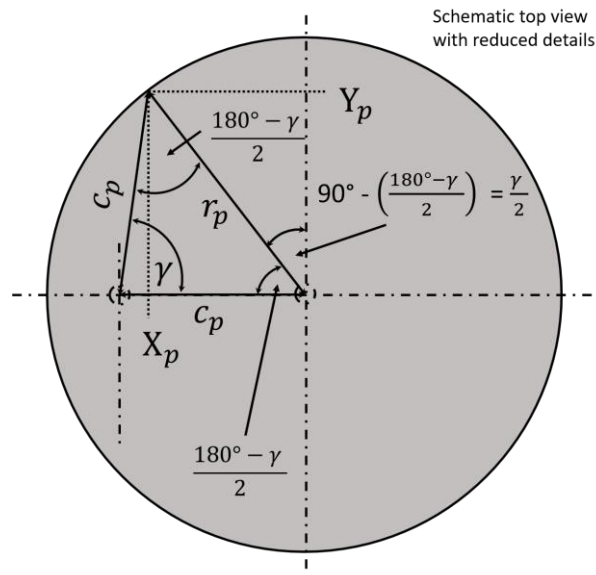


Figure 15: Cartesian coordinates in the planar mode. This illustration shows the mathematical coherencies of the angles during a movement of the sensing unit. The distance  $c_p$  is fixed, the distance  $r_p$  is approaching zero.

Since the basic SCMM design consists of angles and distances, the right choice of the used mathematical procedures is necessary. An appropriate mathematical procedure to describe geometrical issues is trigonometry. The basic calculation scheme of polar coordinates, presented in Equation 1 and Equation 2, is not sufficient to handle two rotational axes. Therefore, some prior calculations have to be performed, and some new parameters have to be defined.

To be able to calculate the length of the chord  $r_p$  some other values are needed. The first parameter is the length  $c_p$  of the swing-arm. This represents the distance between the centre line of the C-axis and the centre line of the sensing unit. With respect

to Equation 1, Equation 2, Equation 4 ( $r_p$ ) and the turning angle  $\gamma$  of the C-axis, the coordinates  $X_p$  and  $Y_p$  can be calculated by using Equation 5 and Equation 6.

$$r_p = 2 * c_p * \sin\left(\frac{\gamma}{2}\right) \quad (4)$$

$$X_p = r_p * \cos\left(\frac{\gamma}{2}\right) \quad (5)$$

$$Y_p = r_p * \sin\left(\frac{\gamma}{2}\right) \quad (6)$$

Where:

$X_p$  = Cartesian coordinate in X-direction

$Y_p$  = Cartesian coordinate in Y-direction

$\gamma$  = Turning angle of the C-axis

$r_p$  = Chord between  $\gamma = 0^\circ$  and the maximum  $\gamma$  angle of the C-axis

$c_p$  = Length of the cantilever between the centre axes of the C-axis and of the sensing unit

The presented equations are valid for the calculation of rotations of the C-axis without a rotating B-axis for the static case, B-axis angle  $\beta = 0^\circ$ .

### 5.1.2.2 Correction of the angle $\beta$ in the planar mode

Figure 14 shows that the sensing unit travels along a bow-shaped tool path with the radius  $c_p$  from the centre axis of the C-axis and intersects with the centre of the B-axis. With the exception of the zero degrees position of the C-axis ( $\gamma = 0^\circ$ ), there is always a gap between the actual position of the sensing unit tip and the X-axis of the specimen. Figure 16 illustrates the deviation between the actual position of the sensing unit and the expected position.

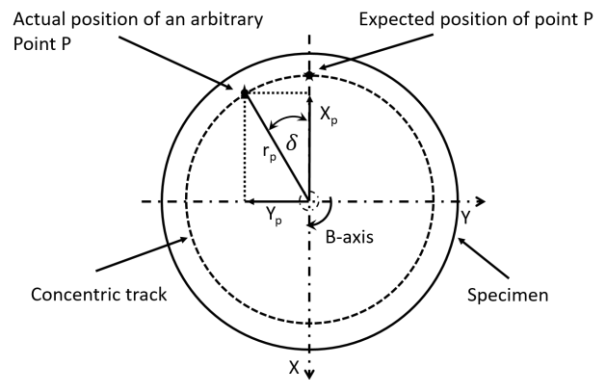


Figure 16: B-axis correction angle . The B-axis encoder has its zero degrees position at  $Y=0$  in the Cartesian coordinate system. The measurement points travel along a bow-shaped path. Therefore, the measurement point at the expected  $B=0^\circ$  position is actually displaced. To compensate that difference, the B-axis correction angle is necessary.

In the example presented, the C-axis is locked in a defined position, and the B-axis is rotating. All recorded measurement points are shifted about the value of the beta correction angle  $\delta$  (Figure 17).

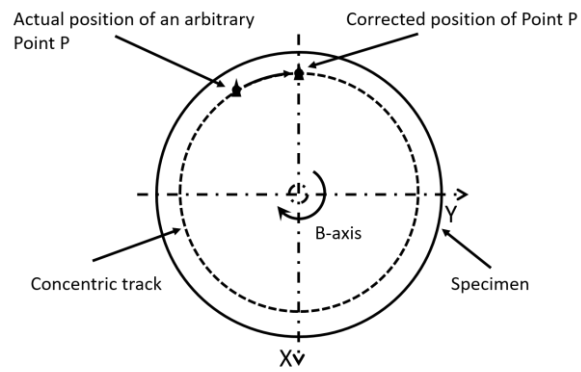


Figure 17: Corrected measurement points . The B-axis correction angle enables to compensate the bow-shaped path of the sensing unit.

Due to the geometric relations of the planar operation mode, the correction angle beta is always half of the rotation angle of the C-axis, as may be seen in Figure 15 and Equation 7. This relationship is also depicted in Figure 15. The equations of the final coordinates  $X_p$  and  $Y_p$  are presented in Equation 8 and Equation 9.

$$\beta_{\text{corr}} = \frac{\gamma}{2} \quad (7)$$

$$X_p = r_p * \cos\left(\beta - \frac{\gamma}{2}\right) \quad (8)$$

$$Y_p = r_p * \sin\left(\beta - \frac{\gamma}{2}\right) \quad (9)$$

Where:

$X_p$  = Cartesian coordinate in X-direction

$Y_p$  = Cartesian coordinate in Y-direction

$r_p$  = Chord between the  $\gamma = 0^\circ$  and the maximum  $\gamma$  angle of the C-axis

$\beta$  = Turning angle of the B-axis

$\beta_{\text{corr}}$  = Correction angle of the B-axis.

$\gamma$  = Turning angle of the C-axis

It may be noted that the correction of the angle beta, as described in this section, is only valid for the theoretical model. Because, as mentioned in Chapter 5.1.2, the theoretical approach requires the parallelism of the central axes of the C-axis to the sensing unit and the B-axis. This circumstance may require a perfectly aligned A-axis. In reality, this requirement is challenging to satisfy. There will always be a divergence of the axes. Therefore, the correction angle beta will not be exactly half of the rotational angle of the C-axis. Especially the wrong tilt angle of the A-axis leads to errors. The precise angle of the A-axis is an essential value for a highly accurate spherical coordinate measurement machine. The best-fit approach fulfils this requirement entirely.

### 5.1.3 Best-fit operation mode

The expression “spherical coordinate measurement machine” indicates that it operates using a spherical coordinate system. Since the first developed operation mode, the planar mode, works by simulating a cylindrical coordinate system, the second operation mode fulfils the requirement to operate according to a spherical coordinate system entirely. The significant difference between both operation modes is the adjustment of the axes. While the planar mode requires the parallelism of the axes, the best-fit operation mode requires the axes to intersect. However, there are two sub-operation modes. One is designed for concavely shaped objects and the other for convexly shaped objects. Both sub-modes may be seen depicted in Figure 18 and Figure 19.

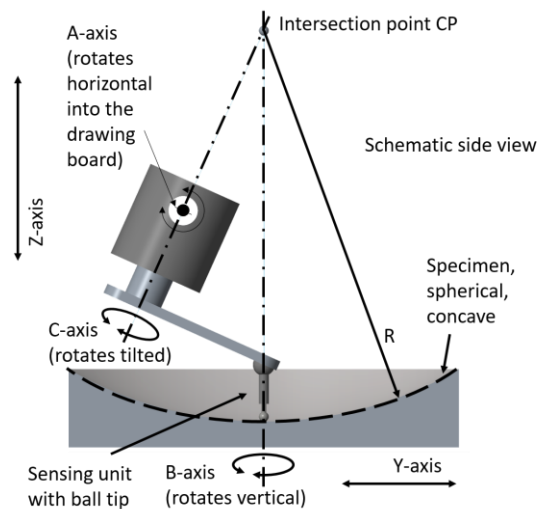


Figure 18: Best-fit mode – concave. The best-fit operation mode can be used in the concave and in the convex setup. In the concave setup is the intersection point of the C-axis, B-axis and sensing unit above the specimen.



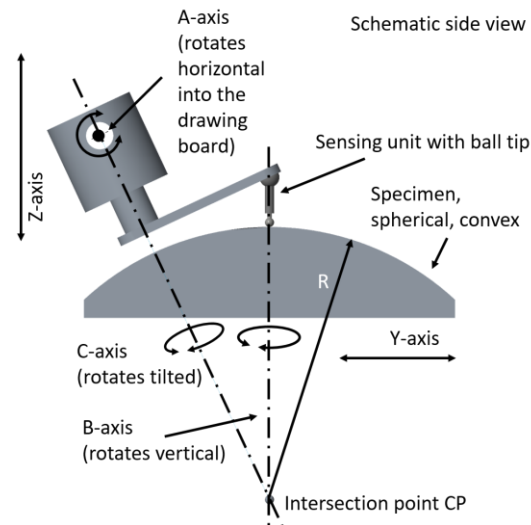


Figure 19: Best-fit mode – convex. In the convex setup is the intersection point of the C-axis, B-axis and sensing unit below the specimen.

Both depicted setups, the concave and the convex setup, look different. However, both setups follow the same theory. As to be seen in Figure 18 and Figure 19, there is an intersection point where the C-axis rotational axis and the B-axis rotational axis intersect. For the case of concave objects, the intersection point is above the specimen; in the convex setup, the intersection point is below the specimen. The mathematical models to calculate the position of all axes is described in Chapter 5.1.3.1.

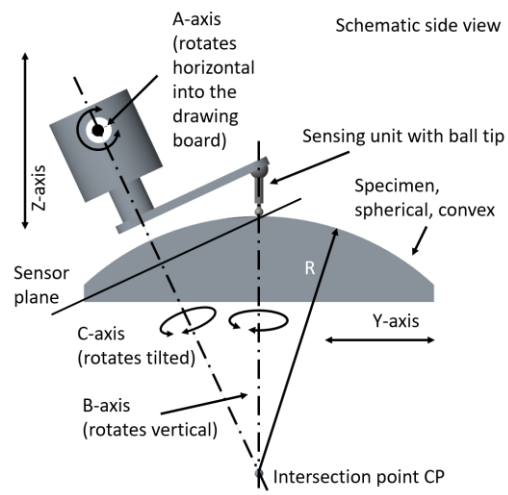


Figure 20: Sensor plane in the best-fit mode. The sensing unit rotates around the central axis of the C-axis. Therefore, the tip of the sensing unit (or focus point) travels on a plane rectangular to the C-axis - the sensor plane.

The probe is assembled on the C-axis. When the C-axis rotates, the tip of the sensing unit draws a circle around the rotational axis of the C-axis. The plane where the circle is drawn is called the sensor plane. Figure 20 shows the sensor plane where the sensing unit travels. The essential feature of the best-fit approach is that the central axis of the sensing unit always stands perpendicular to the best-fit surface.

Unlike the planar operation mode, in the best-fit-mode is the sensor plane always tilted in relation to the rotation plane of the B-axis. When the C-axis rotates, the sensing unit draws a circular path in the sensor plane with the C-axis rotation axis as a central axis. Depending on the tilt angle of the sensor plane, the projection of the resulting circular tool path looks elliptical in the top and side view. The computation method to transform the raw encoder information of the SCMM into Cartesian XYZ coordinates can be found in Section 5.1.3.1.

### 5.1.3.1 Calculation of the A-axis angle $\alpha$

The A-axis angle is the critical factor for a highly accurate spherical coordinate measurement machine. This axis controls the tilt angle between the lower and upper section of the metrology system (ref. Chapter 5.1.1). Figure 21 depicts a sketch of the tilted A-axis and the resulting sensor plane.

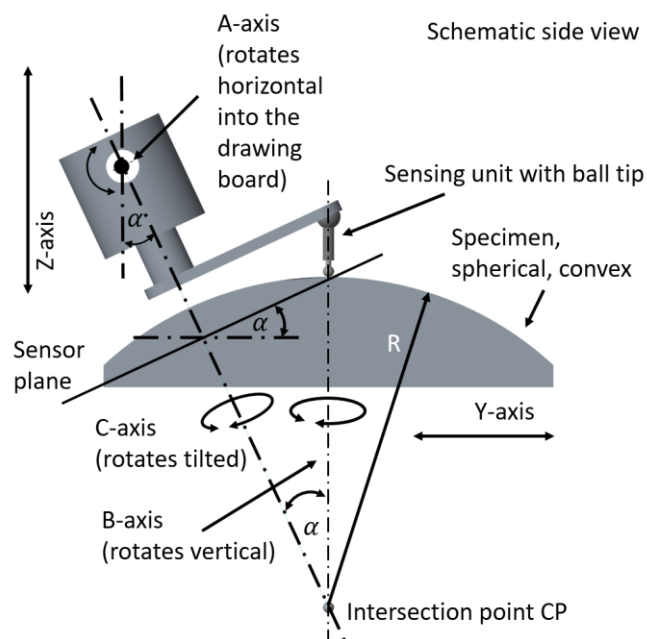


Figure 21: Side view including the sensor plane. The sensing unit rotates around the C-axis. The distance between the central axis of the C-axis and the central axis of the sensing unit is fixed. Therefore, the sensing unit draws a circle in the sensor plane. The sensor plane is always perpendicular to the central axis of the C-axis.

The mathematical model to calculate the correct A-axis angle  $\alpha$  requires different parameters from the specimen and the metrology machine; they are published in Figure 22.

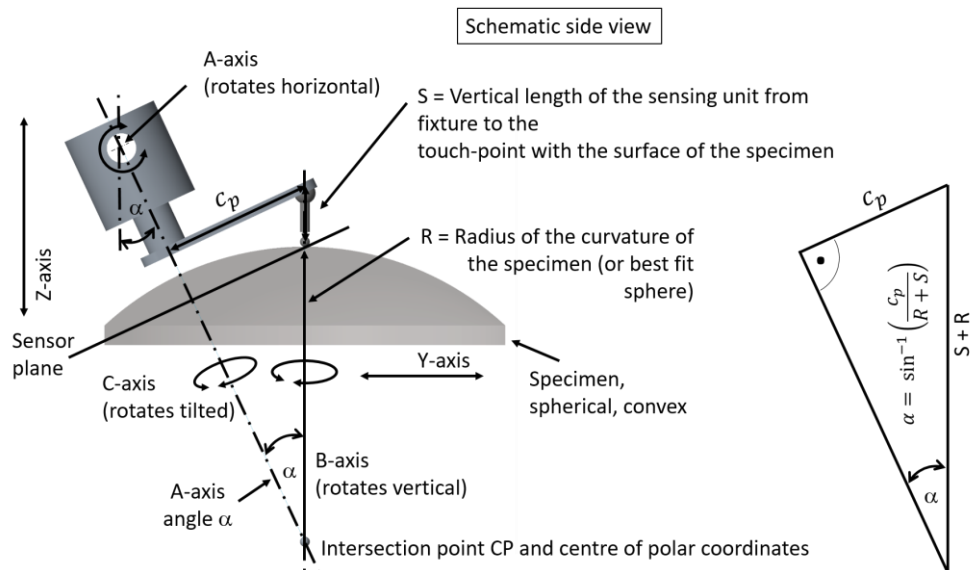


Figure 22: Angle alpha at convex setup. The calculation of the angle  $\alpha$  is the key factor for non-planar measurements. It can be calculated with defined variables. The distance  $c_p$  is set by the user, the radius  $R$  is given by the specimen. The variable  $S$  can be obtained by the addition of the physical length of the sensing unit and its measurement value.

- Parameter  $c_p$ :

This parameter describes the length of the swing arm from the C-axis centre axis to the sensing unit central axis. The parameter is adjustable by the user. The possible length of the swing arm is responsible for the maximum measurable diameter of the specimen.

- Parameter  $S$ :

This parameter combines both the physical length of the sensing unit and the distance measured by the sensing unit. This parameter is determined by moving the Z-axis towards the surface of the specimen until the sensing unit touch the specimen (or until the contact-less sensing unit provides a measurement result). The manufacturer of the sensing unit defines the dimensions of the housing.

- Parameter R:

R is the radius of the curvature of the specimen. For spherical objects, R is the radius of the curvature, for aspherical or free-form shaped objects, R is the best-fit radius provided by the optical design software (e.g. CAD).

Figure 22 depicts the required values and their position in the metrology system. Equation 10 represents the formula for the application of trigonometry. The presented sketch may be seen as a side view of the SCMM with reduced information to highlight the essential relations.

A consolidated view of the geometric relations reveals that angle  $\alpha$  may be calculated by using the following Equation 10.

$$\alpha = \sin^{-1}\left(\frac{c_p}{S + R}\right) \quad (10)$$

Where:

$\alpha$  = Angle of the A-axis

$c_p$  = length of the cantilever from the central axes of the C-axis to the sensing unit

$S$  = Physical length of the sensing unit from the centre of the mount to the tip (or focus point) of the sensing unit

$R$  = Radius of curvature of the specimen

The verification of Equation 10 was performed with Matlab™ (M2010a) and CREO™. The verification was performed with the setup depicted in Figure 23. The presented parameters were used for the Matlab™ (M2010a) and the CREO3™ (M100) verification process. The Matlab™ (M2010a) code of the A-axis angle alpha verification is published in Appendix A.14.

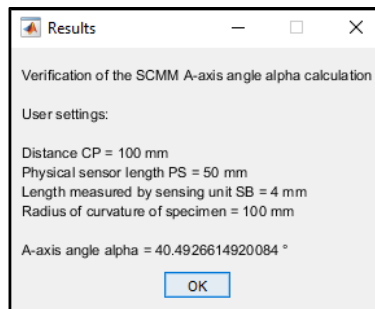


Figure 23: A-axis angle  $\alpha$  verification. This Matlab™ (M2010a) result-window presents a result of the A-axis angle  $\alpha$  verification. The verification process of Equation 10 is performed with Matlab™ (M2010a) and the CAD software Creo™. The presented parameters have been used for both software packages.

The presented Equation 10 enables the calculation of the A-axis angle  $\alpha$  with an accuracy correct to eleven decimal places. Table 3 compares the results of the CREO3™ (M100) and Matlab™ (M2010a) computation. The result of the CREO3™ (M100) calculation is depicted in Figure 24.

Table 3: A-axis angle  $\alpha$  result by CREO3™ (M100) and Matlab™ (M2010a). Both software packages have been used to verify the Equation 10 independently. Both calculations have been performed with the same parameters, presented in Figure 23.

	Creo3™ (M100)	Matlab™ (M2010a)
$\alpha$	40.492661492008 °	40.4926614920084 °

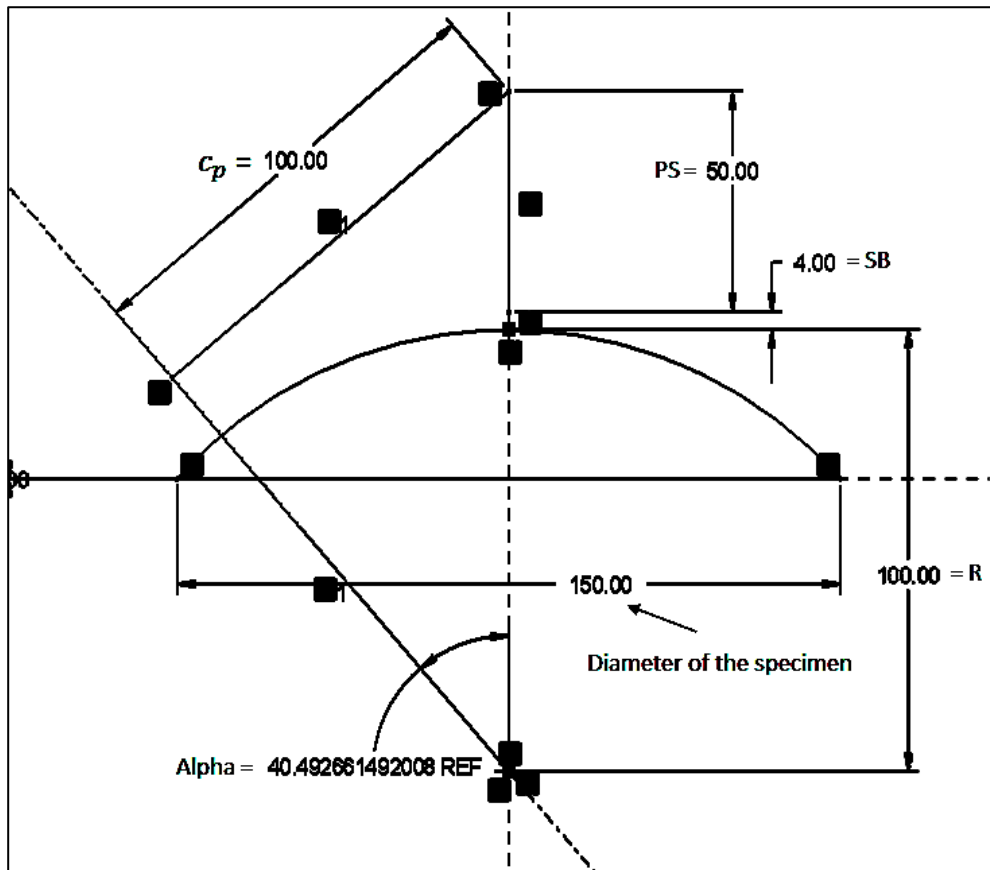


Figure 24: A-axis angle  $\alpha$  verification with Creo™. The CAD software suite CREO3™ (M100) has the feature of a 2D sketcher. This tool allows to draw sketches and to compute required values such as a length or an angle. The expression "REF" is a CREO3™ (M100) marker for "reference value".

### 5.1.3.2 Mathematical correlations in the best-fit operation mode

The best-fit-mode is the primary operating mode of a spherical coordinate measurement machine. It requires the employment of all five available axes to operate. After moving into the correct position, the measurement process may start by driving only the B-axis and the C-axis. The tilt of the A-axis enables the SCMM to move the sensing unit on a best-fit sphere.

Figure 25 illustrates the path of a sensing unit on top of a spherical specimen and illustrates the projection of the path in the top and side view.

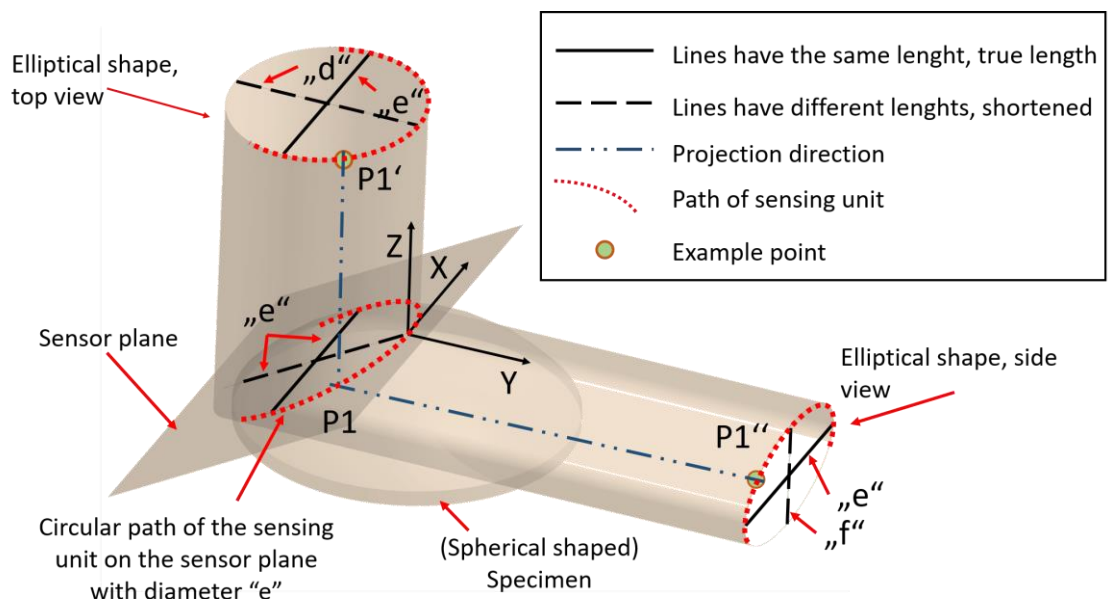


Figure 25: Elliptical coherences SCMM. The sensing unit draws a circle on the sensor plane. The sensor plane is tilted about the A-axis angle  $\alpha$ . Therefore, the circle on the sensor plane becomes elliptical in the top- and side-view.

The probe scans the specimen by travelling on the tilted sensor plane in concentric rings or a spiral-shaped tool path. For a better understanding of the relationship between circle and ellipse, the tool path may be given as one circular path.



However, in the top view or side view, the projection of a circularly shaped toolpath embedded in a tilted plane becomes an elliptical shape. This effect may be seen by tilting a wristwatch.

The tip of the sensing unit travels on a tilted plane. In this plane, the tool path is a circle with the diameter “ $e$ ”. A look from the top view reveals an ellipse with the major axis “ $e$ ” and the perspective foreshortened minor axis “ $d$ ”. The same result may be observed in the side view. In this case, the major axis of the ellipse is “ $e$ ” and the perspective foreshortened minor axis is named “ $f$ ”. Figure 25 illustrates the projection guidelines for the presented SCMM.

The presented mathematical model uses the projection guidelines for circles. The significant advantage of the presented mathematical model is that it contains the A-axis angle  $\alpha$  and the C-axis angle  $\gamma$  directly. This benefit allows the model to be generically used for all operation modes of the spherical coordinate measurement machine, even for the planar operation mode. The use of the true A-axis encoder information instead of a theoretical A-axis angle is a benefit and improves the accuracy of the measurement machine.

A measurement machine has to document the measurement result. The presented approach records the measurement results in raw data from all axes encoders for each measurement point. Since the spherical description is not very common, it has to be translated into a commonly used format. Cartesian XYZ coordinates are a universal format. Contrary to a planar measurement and the application of commonly used

cylindrical coordinate system equations, the best-fit-mode requires the development of equations and a projection scheme.

Figure 26 graphically depicts the relationship between the circle and the ellipse in the top view. It presents the transformation of one example point P1. This point P1 is located on a circle on the sensor plane as may be seen in Figure 25. By the application of the presented projection guidelines for circles, the example point P1 is projected into the top view (P1'). The application of the same method may realise a projection of P1 into P1'' in the side view.

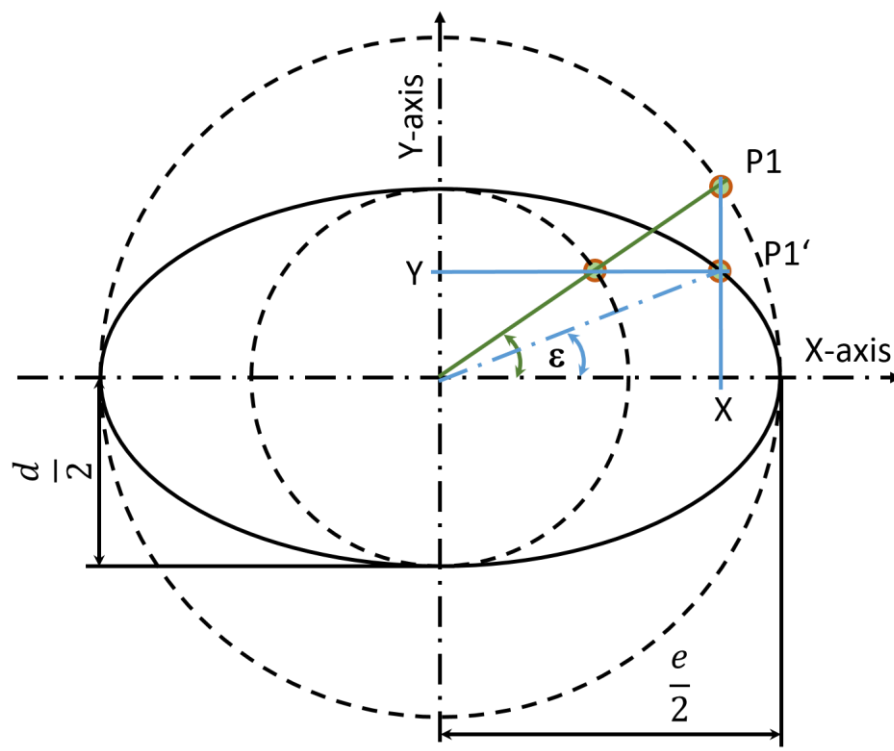


Figure 26: Conversion circle to an ellipse. Comparable to a tilted wristwatch, a tilted circle becomes elliptical in the top- and side view. With the application of trigonometric functions, the position of points on the circle can be projected on the ellipse.

The scheme presented in Figure 26, displays the transformation of the point P1 into P1' and the transformation of the C-axis angle  $\gamma$  into the projected C-axis angle  $\varepsilon$ . The point P1' is located on a circle with the diameter "e". Since the minor axis "d" is perspective foreshortened, the correct length has to be calculated. The length of the major axis "e" is the diameter of the circle, drawn by the sensing unit. Equation 11 presents the corresponding formula that includes the exact angle  $\alpha$ , taken on the fly from the A-axis encoder.

$$d = \cos(\alpha) * e \quad (11)$$

$$f = \sin(\alpha) * e \quad (12)$$

Where:

$d$  = Length of the elliptical minor axis in the top view

$\alpha$  = Angle of the A-axis

$e$  = Length of the elliptical major axis in the side view and top view

$f$  = Length of the elliptical minor axis in the side view

The final calculations of the X and Y coordinates are shown in Equation 13 and Equation 14.

$$X = \frac{e}{2} * \cos(\gamma) \quad (13)$$

$$Y = \frac{\cos(\alpha) * e}{2} * \sin(\gamma) \quad (14)$$

Where:

$X$  = Cartesian coordinate in X-direction

$Y$  = Cartesian coordinate in Y-direction

$e$  = Length of the elliptical major axis

$\gamma$  = Turning angle of the C-axis

$\alpha$  = Angle of the A-axis

The X and Y components of the measured point were calculated by using the top view of the model. The side view may be taken to calculate the Z coordinate of each point. It may be noted that the Y component in the side view represents the Z component of the mathematical model. Following this model, the Z component may be calculated by using the following Equation 15 and Equation 16.

$$\varepsilon = \tan^{-1}\left(\frac{X}{Z}\right) \quad (15)$$

$$Z = \tan(\alpha) * Y \quad (16)$$

Where:

$\varepsilon$  = Angle Epsilon, the projection of angle  $\gamma$

$Z$  = Cartesian coordinate in Z-direction

$X$  = Cartesian coordinate in X-direction

$e$  = Length of the elliptical major axis

$\gamma$  = Turning angle of the C-axis

$\alpha$  = Angle of the A-axis

The used research method requires verifying the gained results. Therefore, a Matlab™ (M2010a) model and a CREO3™ (M100) model were developed. The result of the verification is published in Figure 27 and Figure 28.



Figure 27: XYZ verification with Matlab™ (M2010a). Comparable to the verification of the A-axis angle  $\alpha$ , the verification of Equation 11 to Equation 16 was performed with Matlab™ (M2010a) and Creo™. Both software tools calculated with the same presented input parameters.

The code of the Matlab™ (M2010a) model is depicted in Appendix A.14. The result of the CREO3™ (M100) verification is illustrated in a screenshot presented in Figure 28. The comparison of both results shows significant compliance. Table 4 lists the obtained results; the differences are underlined. The presented Equation 11 to Equation 16 enables a transformation of the axis encoder values into Cartesian XYZ coordinates with an accuracy correct to eleven decimal places.

*Table 4: XYZ verification by CREO3™ (M100) and Matlab™ (M2010a). Both software packages performed the verification calculation with the same input parameters, presented in Figure 27.*

	Creo3™ (M100)	Matlab™ (M2010a)
X	64.27876096865 mm	64.27876096865 <u>39</u> mm
Y	69.4272044014 <u>9</u> mm	69.42720440148 <u>84</u> mm
Z	32.3744370967 <u>1</u> mm	32.37443709670 <u>65</u> mm
$\epsilon$	26.7324226999 <u>1</u> °	26.7324226999 <u>08</u> °

The CREO3™ (M100) model allows showing the values for each dimension. REF is a CREO3™ (M100) shortcut for “Reference dimension”. Figure 28 illustrates the computed dimensions of the sketch for one example point P1.

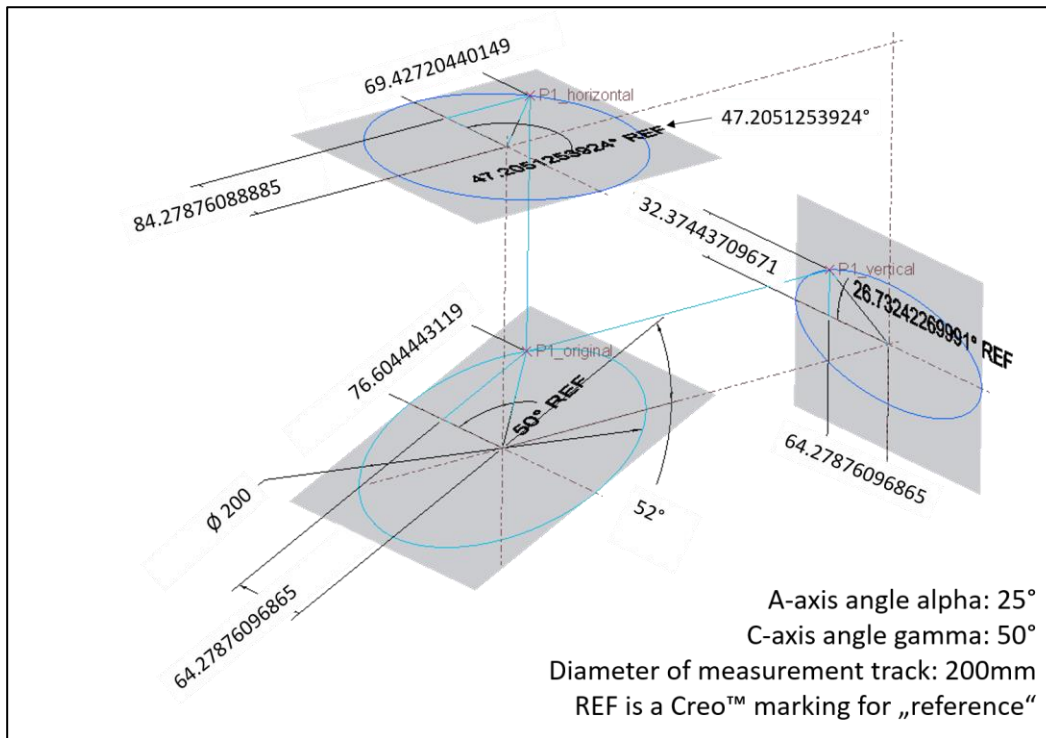


Figure 28: XYZ verification with Creo™. The CAD software suite CREO3™ (M100) has the feature of a 2D sketcher. This tool allows to draw sketches and to compute required values such as a length or an angle. The expression “REF” is a CREO3™ (M100) marker for “reference value”.

When necessary, a simple coordinate transformation enables us to move the calculated origin to other positions, for example, in the centre of the bottom of the specimen. However, the calculated XYZ coordinates include possible misalignments of the A-axis since this value is part of the calculation. The presented equations include the compensation of the bow-shaped path of the sensing unit and misalignments of the A-axis. Comparable to the planar operation mode, the alignment is a crucial factor in the measurement process.

Figure 29 shows some examples of misalignments and the corresponding measurement result.

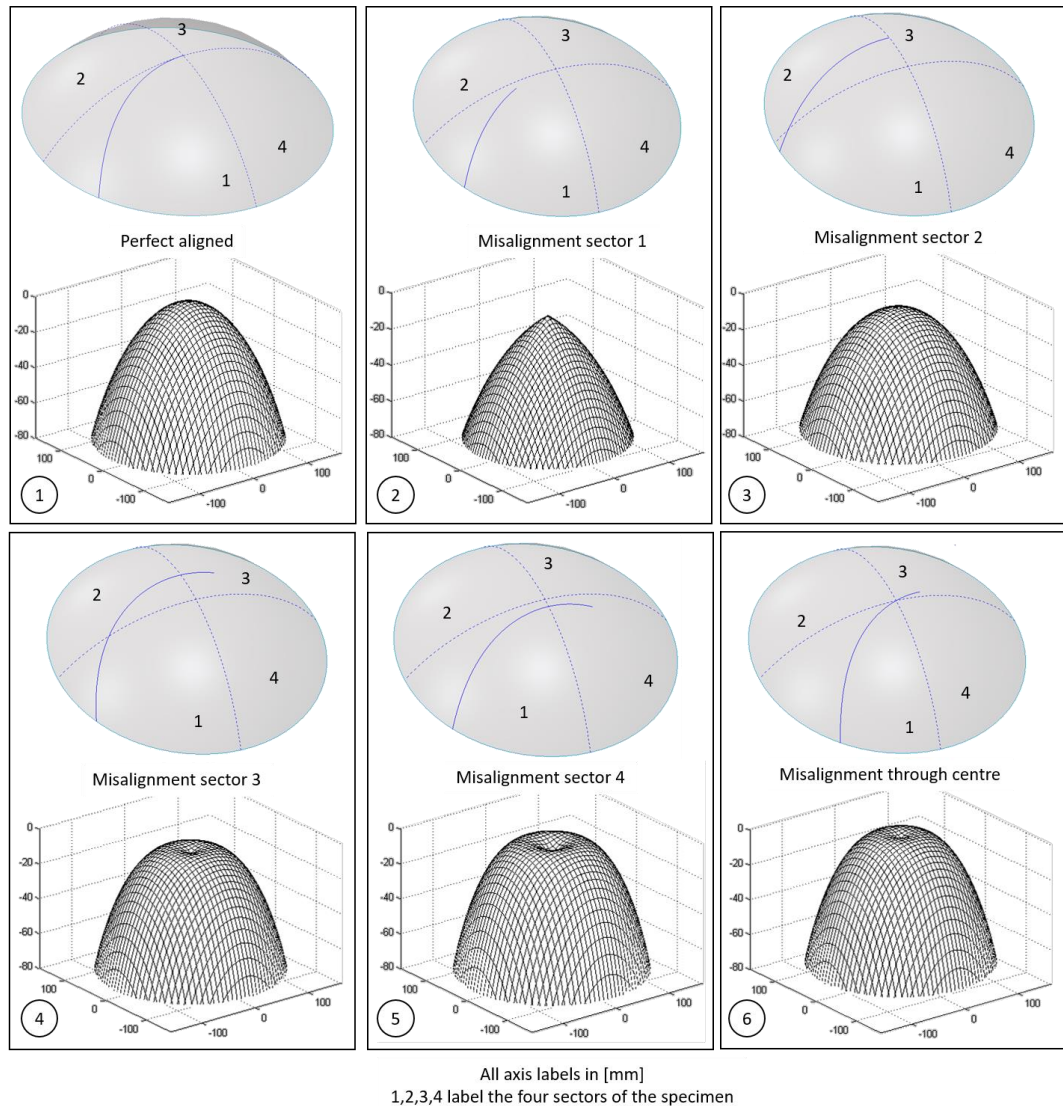


Figure 29: Examples misalignment 3D

It is essential that the sensing unit meets the centre of the specimen. The six depictions in Figure 29 illustrate a selection of possible misalignments in all four sectors of the specimen. In the picture (1), perfect axis alignment is depicted. Depictions (2-5) show misalignments in each sector of the specimen. The last picture (6) presents a faulty alignment through the centre.

With respect to these misalignments, the development of a proper alignment process is essential.



## 5.2 The Centre-search process

The axes of the presented spherical coordinate measurement machine need to be aligned. The principle of operation of the SCMM requires that the central axis of the specimen and therefore of the B-axis are aligned with the central axis of the probe. Chapter 2.4 presents solutions of international research groups to align the axes by the application of external systems, such as a laser tracker.

One of the significant developments to reach the main objective of this research is a proper alignment process. This process is operated with standard tools of the SCMM and without the need for external or additional devices. Therefore, research was performed to overcome the alignment issue of the SCMM, and a new alignment process was developed.

The proposed alignment process is using the geometrical characteristics of a rotating planar object as depicted graphically in Figure 30.

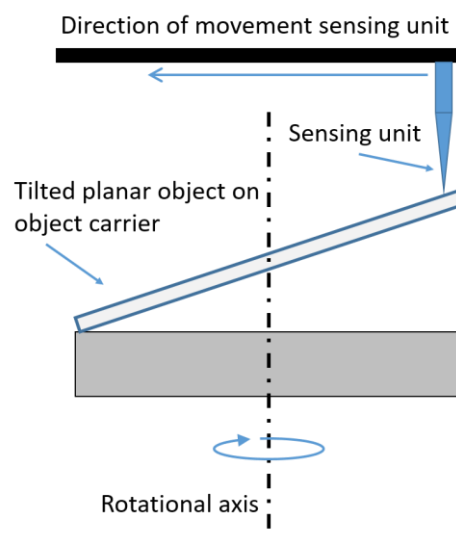


Figure 30: Centre search approach

The planar specimen is fixed on an object carrier and therefore rotating around the rotational axis. Movable probe points toward the rotating specimen and the signal provided by the sensing unit are recorded. The lateral movement of the sensing unit across the rotating specimen results is depicted in Figure 31. The signal represents the distance between the sensing unit and the surface of the specimen.

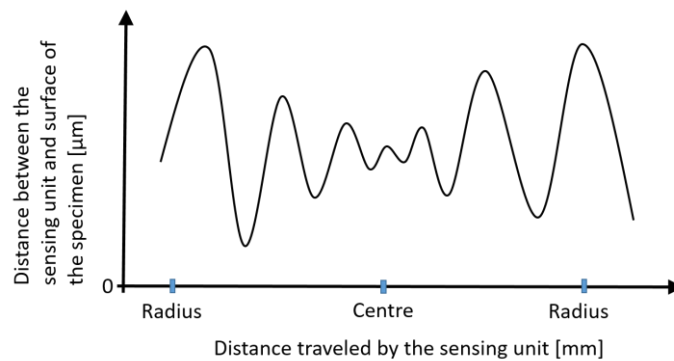


Figure 31: Expected signal of the sensing unit

In the region close to the edges of the rotating specimen, the signal of the probe is expected to show the highest range. While crossing the centre region of the rotation specimen, the amplitude of the signal is expected to show the lowest range.

A data processing of the sensor signal enables to compute the corresponding equation of the plot. With this equation, the calculation of the signals maxima can be performed. The concatenation of all maxima results in a curve with new minima. This minimum is expected to meet with the rotational axis of the specimen.

This novel approach can be associated with the presented SCMM. The sensing unit is assembled on the C-axis and the specimen on the B-axis. Therefore, the presented approach can be adapted to align the C-axis with the B-axis.

Figure 5 illustrates the concept of an SCMM and shows that two sets of axes must be aligned. The B-axis and the C-axis encompass the first set; the Y-axis and the B-axis encompass the second set. Therefore, the presented centre search concept has to be expanded, and further research has to be performed.

The goal of the concept expansion is to research a solution to align the linear Y-axis with the central axis of the specimen and consequently, with the B-axis.

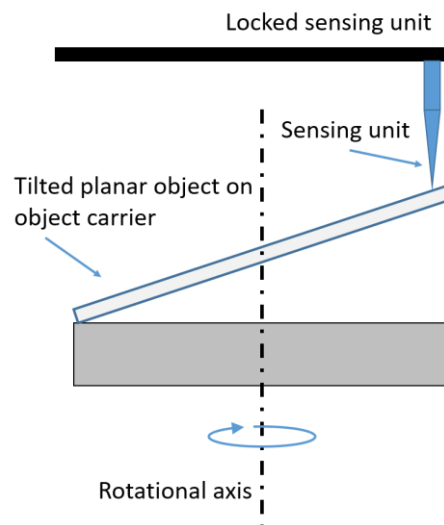


Figure 32: Y-axis alignment

Figure 32 depicts the procedure of the Y-axis alignment. The sensing unit is locked in any position between the expected centre of the specimen and the edge of the planar object while the B-axis rotates. The sensing unit generates a signal, as presented in Figure 33.

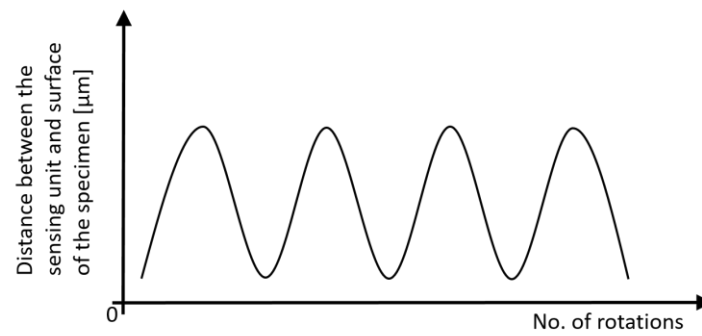


Figure 33: Sensor signal Y-axis

The height of the expected signal represents the distance between the sensing unit and the surface of the specimen. By increasing the distance to the expected centre of the planar surface, the amplitude rises. In a second step, the same procedure repeats at any other position, different from the first position and between the expected centre of the specimen and the edge. Both signals enable the computation of the corresponding maxima.

However, the entire procedure is detailed published in Chapter A.9 and the corresponding test series and verification in Section 7.2.2.

### 5.3 The 3D-scale

The analysis and the compensation of errors is an essential task in the development process of measurement machines. With respect to the design of the SCMM, research was necessary to aid the influence of the radial, axial and tilt errors of the used rotational axes. A similar reason was the objective to develop a metrology solution for the shop floor. Therefore, the price of a metrology machine is a significant factor. However, the undertaken research showed that the novel 3D-Scale is expected to be a generic and useful device to detect and to compensate for errors related to rotational axes and the used bearings such as rolling-element bearings or air bearings. The rotational axes are subject to the influence of errors. In addition to the overall accuracy of the bearing, other factors such as the installation position or even the load distribution are critical factors.

However, the 3D-Scale is a mechatronic device designed to detect and to compensate the movements in all degrees of freedom of the corresponding rotation axis.

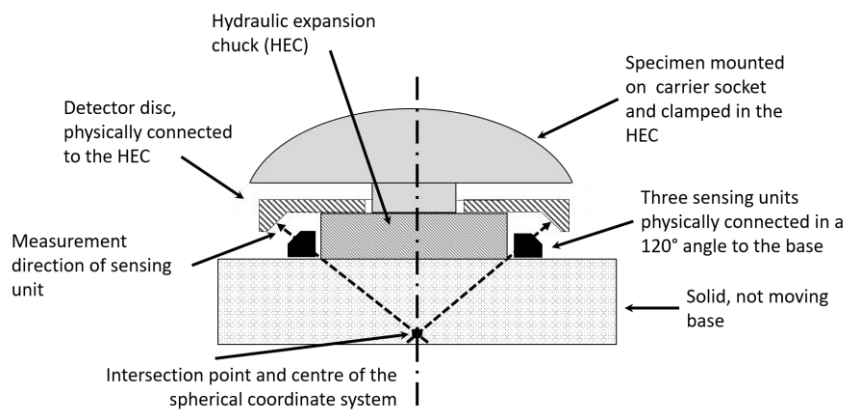


Figure 34: 3D-Scale schematic sketch

The 3D-Scale consists of four parts - three sensing units and one detector disc. The components are arranged according to Figure 34. The detector disc is mounted on the moving part of the rotational axis, for instance, a chuck. The three sensing units are mounted on the base of the rotational axis in a 120° distribution around the central axis. The system operates using a spherical coordinate system. Both angles are defined, and the length of the vector varies about the measured length.

Further details about the 3D-Scale can be found in Chapter A.8 and the result of the test series in Section 7.3.

## 5.4 Software packages

One of the main objectives of this research was to develop a metrology solution with an open software suite. This contains the NC control of the machine, the graphical user interface (GUI) and the data analysis software. All three parts of the SCMM software suite are designed to operate with open interfaces.

The NC control software controls the SPS (Siemens™ S7™), the pressurised air and the vacuum system. With the goal to develop a metrology system for the shop floor, the decision was made to develop the NC control system with an industrial SPS. All electronic components are freely available in the market and can be replaced by the user easily. However, the NC control software is written as a function block diagram (FBD). All control parameters are stored in either a software database or a synchronised

hardware interface module. This is the transfer point to the second software package, the graphical user interface, or GUI.

User indicated errors are prevalent in metrology science. Small mistakes such as a faulty alignment or unfavourable point distribution can have significant impacts on the measurement result. Therefore, the objective of this thesis was to create a software package requiring minimal user interaction. Most of the critical processes are running automatically in the background, and the user is only allowed to modify non-critical parameters such as the density of the point distribution or the measurement mode in general. However, Chapter A.12.1 illustrates the GUI software package in detail.

The third software package is the data analysis tool. This tool was necessary because the presented SCMM is not a regular metrology machine and does not directly provide a set of XYZ coordinates. Therefore, this piece of software was developed to translate the encoder information of the rotational axes, linear axes, and the sensing unit into Cartesian XYZ coordinates.

Comparable to the GUI, the data analysis software provides only limited access for the user. The data analysis software is designed to provide the raw data of the measurement process. In the context of this PhD research, raw data means that the measurement result is available as clear text and that there was no data manipulation despite the SCMM error compensation (repeatable errors, touch ball compensation, and temperature compensation). Details about the reference measurement principle, the data analysis process, and the resulting measurement files can be found in Chapter A.12.2.

## 5.5 Measurement strategies

The measurement process of a specimen requires some preparation. The user has to decide about the best sensing unit, the fixture, and the way to distribute the measurement points on the surface of the specimen. Furthermore, the ability to perform measurements at any stage of the production chain requires suitable measurement strategies.

In the context of this PhD research, the distribution of the measurement points and the resulting pattern is named measurement strategy. Chapter 2.4 presents examples of other SCMMs operating in laboratories and companies. As far as published, such systems operate by producing cross-sections. However, this PhD research has the goal to do research about a metrology device that can be used in the complete production chain. Therefore, research has been undertaken to investigate adequate measurement strategies for all stages of the production chain. A typical production chain is depicted in Figure 2.

The different stages of the production chain have different significant specifications regarding production speed, roughness, and accuracy of the resulting surface. Therefore, an adequate metrology system has to fulfil the same requirements. A presentation of modern production processes is published in Chapter A.6.

However, the first steps in the production chain, published in Figure 2, operate at high speed and produce structured surfaces with low accuracy. Therefore, the Cross-Section mode was developed. This measurement mode produces a user-defined



number of cross-sections. Contrary to the published SCMM solutions, the Cross-section mode presented in this thesis produces straight and not curved cross-sections. Depending on the number of cross-sections, the Cross-section mode is high-speed compared to other possible measurement modes. Details about the Cross-Section mode can be found in Chapter A.10.1.3 and Section 7.1.2.

The production processes in the middle of the production chain operate with medium speed and produce a medium quality regarding roughness and accuracy of the specimen's surface. However, the prospected solution is the development of the Spiral-mode. The name indicates that this measurement mode produces a spiral-shaped path on the surface of the specimen. The user can define the number of windings and therefore, the density of the measurement points. All details and test results can be found in the Chapters A.10.1.2 and 7.1.2.

The last steps in the production chain are the polishing and zonal polishing processes. Compared to earlier steps in the production chain, these processes are slow, but they produce highly accurate surfaces with a low grade of roughness. These requirements can be met with the Track-mode. This measurement mode produces a defined number of concentric rings on the surface. The user can define the number of rings and the number of measurement points per ring. Therefore, the density of the measurement points can be controlled and defined by the user. All details about the Track-mode can be found in Chapter A.10.1.1 and the test results in the Sections 7.1.1, 7.1.2, and 7.1.5.

## Chapter 6

### Uncertainty estimation of the SCMM

Each metrology machine is subject to the influence of errors. The literature describes a large variety of influencing factors. The following Chapter presents a summary of specific influencing errors and their impact on the measurement result.

#### 6.1 Environment

Depending on the accuracy level of a metrology machine, the installation location is well deliberated. The influence of the environment is variegated. The most common and critical influences are temperature drifts, radiation, vibration, and airflow.

High accurate measurement equipment is commonly operated in a separated room. Such a room usually has no window to avoid the radiation of the sunlight and therefore to avoid heating up. Furthermore, the baseplate of the entire room or better the area below the measurement machines are robust, massive, and uncoupled to other

baseplates. In combination with a shock absorber in the machine bases, this is an effective method to reduce vibrations.

The most common environmental influence is temperature drift. All materials have a thermal expansion coefficient. That means that their dimensions are addicted to variations of the temperature. Most of the materials have a positive thermal expansion coefficient, but the literature knows several materials with a coefficient of zero or even negative. Modern design procedures for metrology machines provide methods to reduce the influence of the temperature drift, for instance, a symmetrical design.

However, the most efficient method to reduce the variation of the temperature is to operate the metrology equipment in a measurement room with a climate control system. The standard temperature in measurement science is 20°C. Therefore, most of the measurement rooms are tempered at 20°C with minimal variation. Further details about the environmental influences and especially temperature variations can be found in Chapter A.7.1 and in Section A.7.5.2.

## 6.2 Specimen

The specimen is the most variable component of a measurement process. It is essential to perform an analysis of the object to evaluate the basic settings of the measurement device. Examples are the choice of an adequate sensing unit, cleanness, or temperate. However, the specimen has physical properties; for instance, the weight and the centre of gravitation. Primarily the SCMM operates with air bearing supported

rotational axes that are subject to the load distribution. Other significant properties, such as the global shape and structure of the surface, are essential for the correct setup of the metrology device. Therefore, research was undertaken to investigate the influence of the specimen related to the measurement result. Chapter A.7.2 publishes the analysis in detail.

### 6.3 Operator

The user or operator is a significant factor in the metrology process. His influence is not directly predictable but substantial. The user indicated errors could be split into two categories:

- Errors caused by user application errors.
- Errors caused by preparatory work.

Both categories comprise avoidable error sources. Therefore, in the context of this PhD research, a number of behaviour rules are published. The detailed discussion of the effects and solutions can be found in Chapter A.7.3.

## 6.4 The accuracy of the SCMM

The prior presented effects, published in Chapters 6.1 - Environment, have a partial influence on the measurement result. Effects such as the variation of the temperature or mechanical inaccuracies are measurable and therefore compensatable. Other aspects, for example, the influence of the specimen or the operator has to be considered carefully, and proper operating cycles have to be defined to avoid negative influences.

However, this Chapter presents the two most significant and controllable effects and their contribution to the error budget of the presented SCMM. Both are the influence of the mechanical inaccuracies of the rotational axes and the influence of temperature variations.

### 6.4.1 Tolerance of the air bearings

The concept of the SCMM requires the usage of two rotational axes to realise 3D measurements. This PhD research presents an SCMM applying rotational axes with air bearings. Each rotational axis is subject to tolerances. The manufacturer provides information about the preferred installation position and the tolerances to be expected. The preferred installation position is related to a Cartesian coordinate system. The central axis of the rotational axis rotates parallel to the Z-axis, and the base of the rotational axis is in the XY-plane. Furthermore, the manufacturer provides information

about the tolerances; these are the radial and axial runout and the tilt. These three parameters describe the accuracy of the axis.

With respect to the presented SCMM, the vertical B-axis and the tiltable C-axis are equipped with an air bearing. The B-axis air bearing is operated as recommended by the manufacturer. The C-axis air bearing is mainly operated in a tilted position. Only in the planar mode does the actual position correspond with the recommended installation position.

The manufacturer published the technical data sheet of the used air bearings. Therefore research was necessary to investigate the tolerance situation in non-conform installation situations. The given tolerances are depicted in Table 5.

*Table 5: Technical data of the used air bearings*

Axial runout:	< 50 nanometres in total
Radial runout:	< 50 nanometres in total
Tilt (3D):	< 0.5 $\mu$ rad

Both rotational axes are identically constructed and have the same datasheet.

The datasheet reveals that both air bearings are highly accurate.

The C-axis of the SCMM is designed to be operated in a tilted position, the best-fit mode (ref. Chapter 5.1.3). The tilt angle is dependent on the A-axis angle  $\alpha$  with a theoretical range of  $\pm 80^\circ$ . The zero degree position represents the planar mode where the C-axis central axis is rectangular and therefore parallel to the B-axis central axis.

However, for a detailed analysis of the expected error, the B-axis and C-axis have to be investigated together in essential positions. Table 6 presents the result of the analysis.

*Table 6: Combined error in Z-direction. The combined errors of the B-, and C-axis caused by the axial and radial runout (arr) of both axes (BC).*

<i>arr<sub>CZ</sub> as function of alpha (-80° to 80°)</i>
<i>arr<sub>BCZ</sub> = 215.84 nm (alpha = -80°)</i>
<i>arr<sub>BCZ</sub> = 215.84 nm (alpha = +80°)</i>
<i>arr<sub>BCZ</sub> = 200 nm (alpha = 0°)</i>

*Table 7: Combined error in Y- direction. The combined errors of the B-, and C-axis caused by the axial and radial runout (arr) of both axes (BC).*

<i>arr<sub>CY</sub> as function of alpha (-80° to 80°)</i>
<i>arr<sub>BCY</sub> = 215.84 nm (alpha = -80°)</i>
<i>arr<sub>BCY</sub> = 215.84 nm (alpha = +80°)</i>
<i>arr<sub>BCY</sub> = 200 nm (alpha = 0°)</i>

Therefore, the expected combined positioning error shows only a low variance over the entire positioning range. The expected error is predicted in a range of 200 nanometres. Experiments verified the theoretical analysis and confirmed an error of 214 nanometres. The entire analysis and the corresponding test series are published in Chapter A.7.5 and A.7.5.1.

### 6.4.2 The temperature variations

The other influencing effect is the variation of the temperature. The presented SCMM operates in an air-conditioned measurement room. According to the standard rules in metrology science, the temperature is set to 20°C.

The components of the SCMM have different thermal expansion coefficients. Therefore, variations in the temperature cause a variation of the component dimensions. Research has been conducted to analyse and describe the change of the physical dimensions of all relevant components of the SCMM. Some of the used components, for instance, the linear axes (Y-axis and Z-axis) are variable in length. Therefore, the maximum length of each SCMM component was taken to calculate the predicted total length variation in Y- and Z-direction of the entire metrology machine. The result is presented in Table 8 and Table 9.

*Table 8: Results thermal expansion prediction. This table presents the normal length variation per 1K in Y- and Z-direction.*

*The setup of the SCMM knows three critical positions of the A-axis, +80°/0°/-80°, therefore, all three positions have to be considered in the analysis*

Length variation per 1K
$\Delta Y_{tot} = 12.843 \frac{\mu m}{K}$ at $alpha\ 0^\circ$
$\Delta Z_{tot} = 8.2 \frac{\mu m}{K}$ at $alpha\ \pm 80^\circ$



*Table 9: Predicted temperature influence . This table presents the normal length variation per 0,15K in Y- and Z-direction. The setup of the SCMM knows three critical positions of the A-axis, +80°/0°/-80°, therefore, all three positions have to be considered in the analysis*

Length variation per 0.15K
$\Delta Y_{tot\ 0.15} = 1.93 \frac{\mu m}{0.15K}$ at alpha 0°
$\Delta Z_{tot\ 0.15} = 2.23 \frac{\mu m}{0.15K}$ at alpha ± 80°

The complete analysis of the frame and of the used components can be found in Chapter A.7.5.2.

## Chapter 7

### Experimental validation of the system

The validation of a developed component or a complete system is an essential step in the development process. This section reports the experiments and test series conducted to investigate the performance of the theoretical approach.

#### 7.1 Test series test carrier

The presented approach needs to be verified. Since there is no comparable machine in the market, the decision had been made to design an own system, especially for verification purpose.

##### 7.1.1 Test series verification of the function

The verification test was a comparative test series. Two test series were performed, one with the SCMM, the second with a Fisba™ interferometer.

The first test series contained 25 measurement runs with the SCMM, equipped with a contactless Micro-Epsilon™ confocal sensing unit (uncertainty better than 50 nanometres [29]) and a standard interferometer from Fisba™ with an accuracy of  $\lambda/20^{16}$ . A planar lens from Melles Griot™ [28] had been used as a specimen. The SCMM was adjusted in the Track-mode (concentric rings). The Fisba™ interferometer had been adjusted according to the manufacturer's guidelines. All tests were performed in the temperature stabilised measurement chamber at 20°C. Figure 35 depicts the setup of the SCMM, including the covered Micro-Epsilon™ probe and the Melles Griot™ specimen.

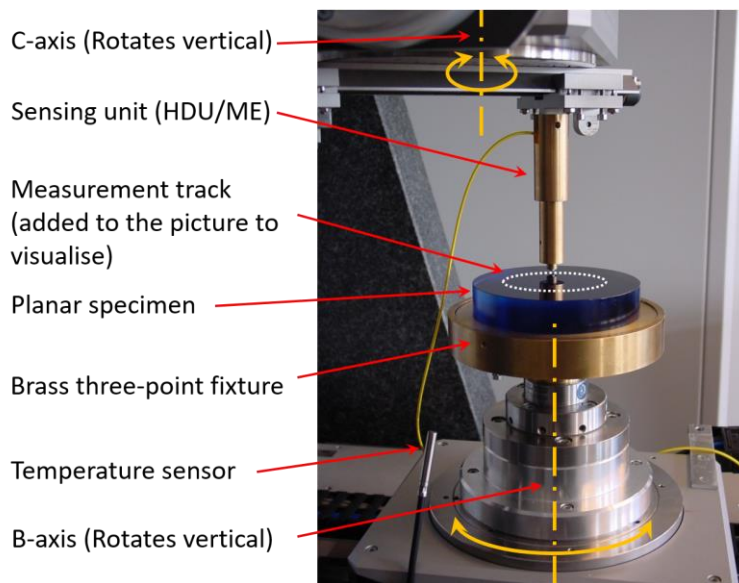


Figure 35: Setup for the general function verification. The test series was performed in the planar setup. The B-axis carries a brass three-point fixture to adjust the tilt of the planar specimen. The sensing unit was a contactless sensing unit, as presented in Chapter A.5.5. The test series was performed in the temperature stabilised measurement room of the LOE in the Track-mode.

<sup>16</sup>  $\lambda/20 - \lambda$  represents the wavelength of a He Ne Laser (red) with a wavelength of 632.816 nanometre.  $\rightarrow \lambda/20 = 31.6408$  nanometre

An SCMM measurement result is published in Figure 36. The SCMM measured a PV<sup>17</sup> of 309 nanometres. It has to be noted that the measurement was not treated with any data modification or smoothing filters. The result published in Figure 36 depicts the raw measurements.

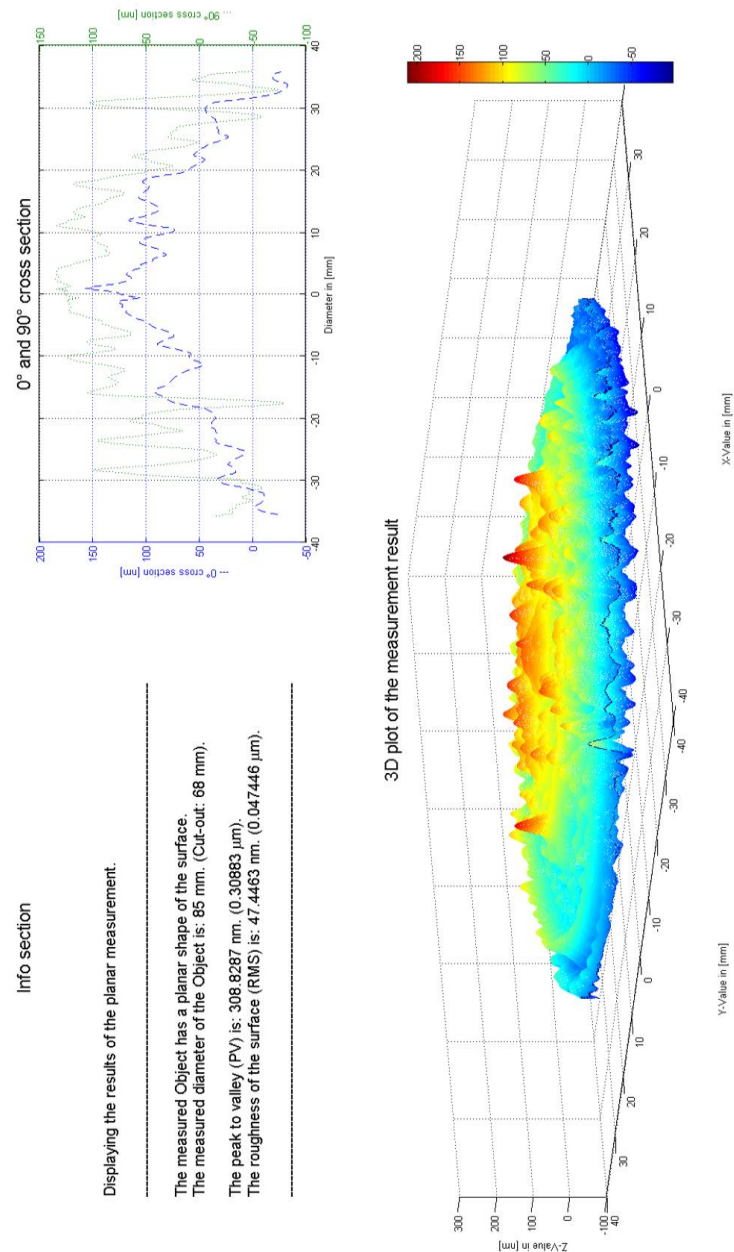


Figure 36: Measurement result SCMM. The planar specimen was measured with the presented SCMM, and the measurement was performed with a Fisba™ interferometer. The result was a concave and bowl-shaped structure

<sup>17</sup> PV – Peak to Valley. Distance between the highest and lowest point of a measurement result.

Figure 37 illustrates the result of the interferometer measurement. The used Fisba™ interferometer uses error compensation methods such as compensation of mechanical inaccuracies and correction of optical effects caused by the used lens arrays. The result of the interferometer measurement showed a PV of 23 nanometres.

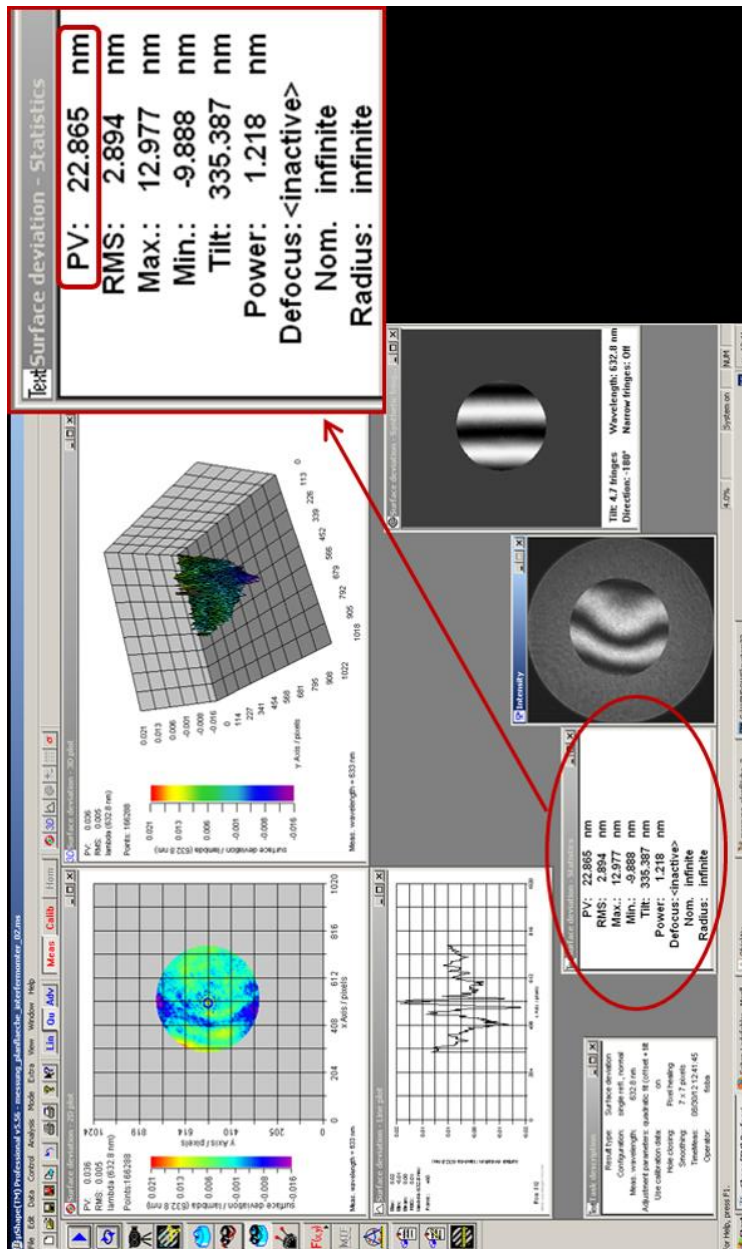


Figure 37: Measurement result interferometer. The Fisba™ interferometer verification measurement obtained a heavily structured area in the middle region of the specimen.

### 7.1.2 Test series Measurement modes

The SCMM concept requires different measurement strategies. The need for the measurement strategies is based on the widespread of the measurement tasks in a production chain. Not all measurement tasks require the maximum achievable accuracy. The majority of the measurements performed during the production cycle of a product require lower accuracy but a higher measurement speed. Grinding processes, for example, require many measurements to ensure that the overall geometry meets the given requirements. Mostly the final measurement steps need high accuracy, for example, polished products. Therefore, different measurement strategies were developed. The details of the measurement modes are presented in Chapter A.9. The following test series were conducted to determine the best appropriate settings for each measurement mode and the related measurement accuracy.

The specimen had been a polished planar specimen with accuracy, at the diameter of 100 millimetres, better than  $\lambda/20$ <sup>18</sup>. The total diameter of the object was 110 millimetres. As a probe, a Heidenhain™ Certo™ sensing unit with an accuracy better than 30 nanometres was used. The complete test sequence was controlled by the NC control system and by the user interface. The test procedure was programmed by the application of the Job queue feature (ref. Chapter A.12.1). This feature enables measurements without the presence of a user. Once programmed, the system proceeds automatically. As may be seen in Figure 38, the SCMM is equipped with an HD resolution camera. This camera, in combination with remote control, enables to monitor the status

---

<sup>18</sup>  $\lambda/20 - \lambda$  represents the wavelength of a He Ne Laser (red) with a wavelength of 632.816 nanometre.  $\rightarrow \lambda/20 = 31.6408$  nanometre

of the system over a network or even the internet. Therefore, all tests were performed in a stable temperature room at  $20^{\circ}\text{C} \pm 0.15\text{K}$ . During all tests, no person attended or interrupted the test series. Since the test series took several hours, the tests started on Friday evening hours and were finished in the early morning hours of the next day. During this period, the LOE was closed. Figure 38 shows the entire setup, and Figure 39 depicts a detailed view of the specimen.

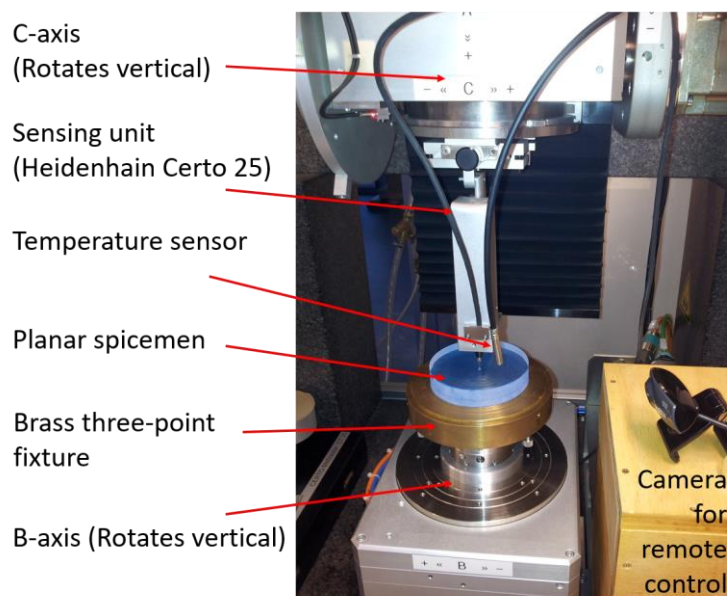


Figure 38: Setup of the test series Track-mode. The setup was adjusted to the planar mode. The sensing unit was a tactile Heidenhain sensing unit, as depicted in Chapter A.5.1. The test series was performed in the temperature stabilised measurement room of the LOE at  $20^{\circ}\text{C} \pm 0.15\text{K}$ . The complete test series was performed in the queue mode, therefore was no user in the measurement mode during the complete test cycle.

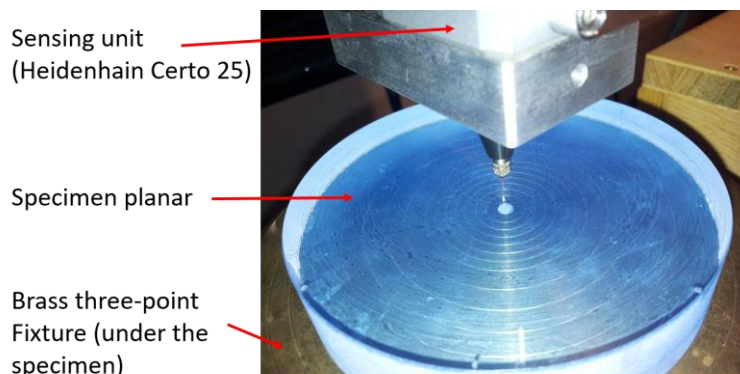


Figure 39: Details of the test series. This picture presents a detailed view of the specimen on the three-point fixture and the sapphire ball tip of the sensing unit.

The measurement strategy was the Track-mode that produces concentric rings on top of the surface of the specimen. The queue file editor was programmed with a set of different measurements, each one with a different number of rings, as may be seen in Figure 40. All of the results were compared to a Fisba™ interferometer reference measurement.

The test series conducted in the Track-mode consisted of ten single measurements, including one comparison measurement performed with a standard interferometer from Fisba™ [19] (Figure 40, number (10)). The test sequence started with a minimum of 50 tracks, one track per one millimetre radius of the specimen. All tests started with 1000 measurement points at the first track and reduced stepwise towards the centre. For the next test runs, the number of tracks increased progressively (50 – 500 tracks). Since the primary parameters, especially the turning speed of the axes, have not been changed during the complete test run, the measurement time increase in the same way as the number of tracks did. In Figure 40 is the results of all nine Track-mode measurements and the corresponding interferometer measurement published.

---

<sup>19</sup> <http://www.fisba.ch>



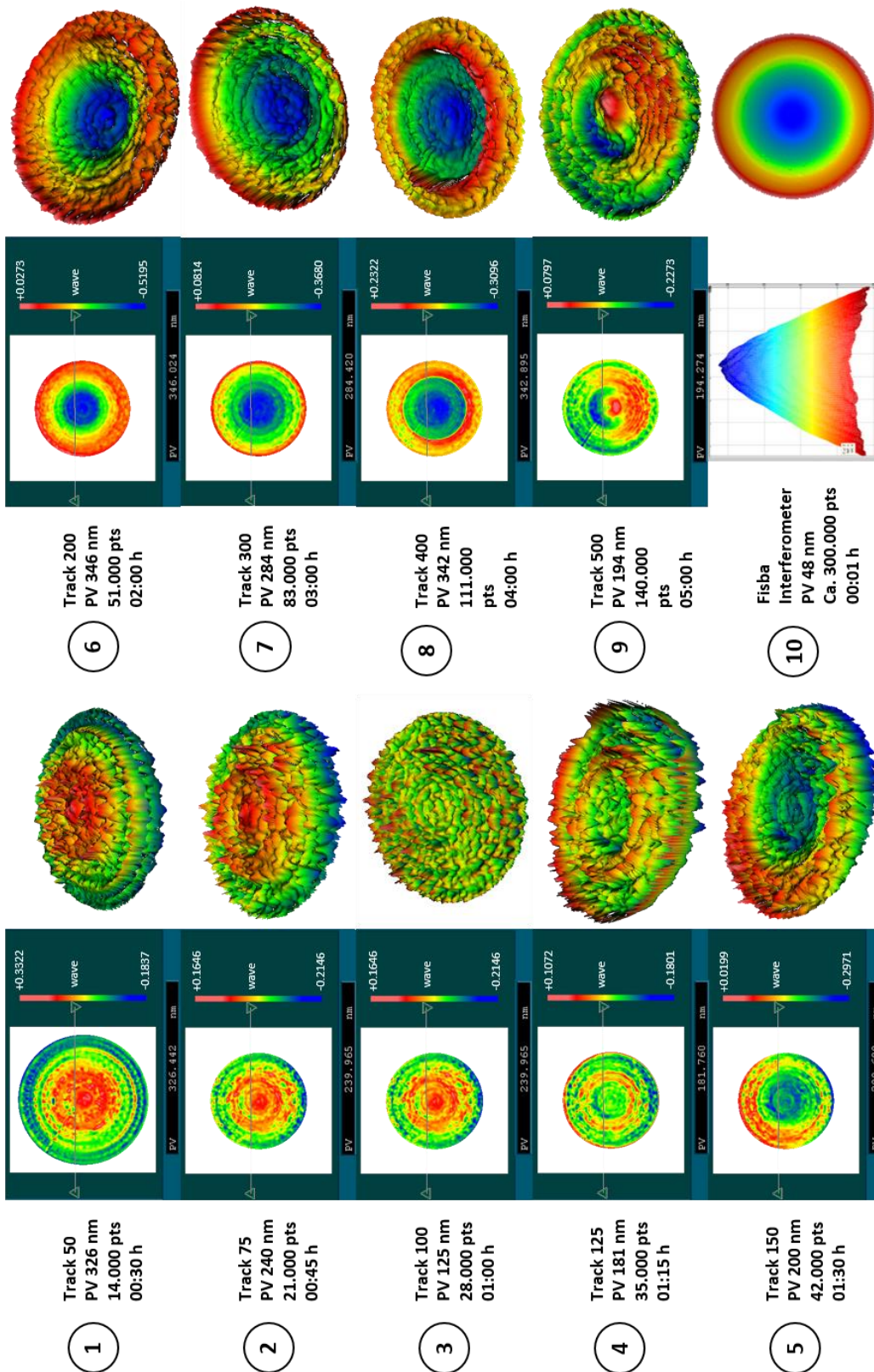


Figure 40: Results of the Track-mode measurements . The depicted test series consisted of ten measurements. Nine performed with the SCMM and one with a Fisba™ interferometer. Each measurement started with 1000 measurement points on the first track.

A general view on the measurement results, pictured in Figure 40, shows that the shape of the measurement result turns from a convex shape (between 50 and 125 tracks) to a concave shape (between 150 and 500 tracks). The turning point is the measurement result with the lowest  $PV^{20}$ , measurement result number (3) recorded with 100 tracks. The PV has the same characteristic as the variation of the surface shape; it decreases from 308 nanometres down to 125 nanometres (3) and turns upwards in the area of approximately 300 nanometers.

All measurements show the same characteristic structure with four concentric rings in the outer area of the object and a clean area in the middle. The raising of the number of measured tracks comes along with an extension of the measurement time from 30 minutes to five hours. As mentioned in the data analysis Chapter, the software package did no smoothing or cleaning. The presented illustrations are error corrected raw data.

In addition to the Track-mode measurements, a test series with measurements in the Spiral-mode had been performed. The interferometer measurement, presented in Figure 41 number (10), is the same measurement as presented in Figure 40 number (10). Compared to the Track-mode measurement, the test sequence started with a minimum of 50 windings, one winding per one-millimetre radius of the specimen. For the next test runs, the number of windings increased progressively from 50 to 500.

---

<sup>20</sup> Peak to valley value (PV) represents the range between the lowest and the highest point in the measurement result.

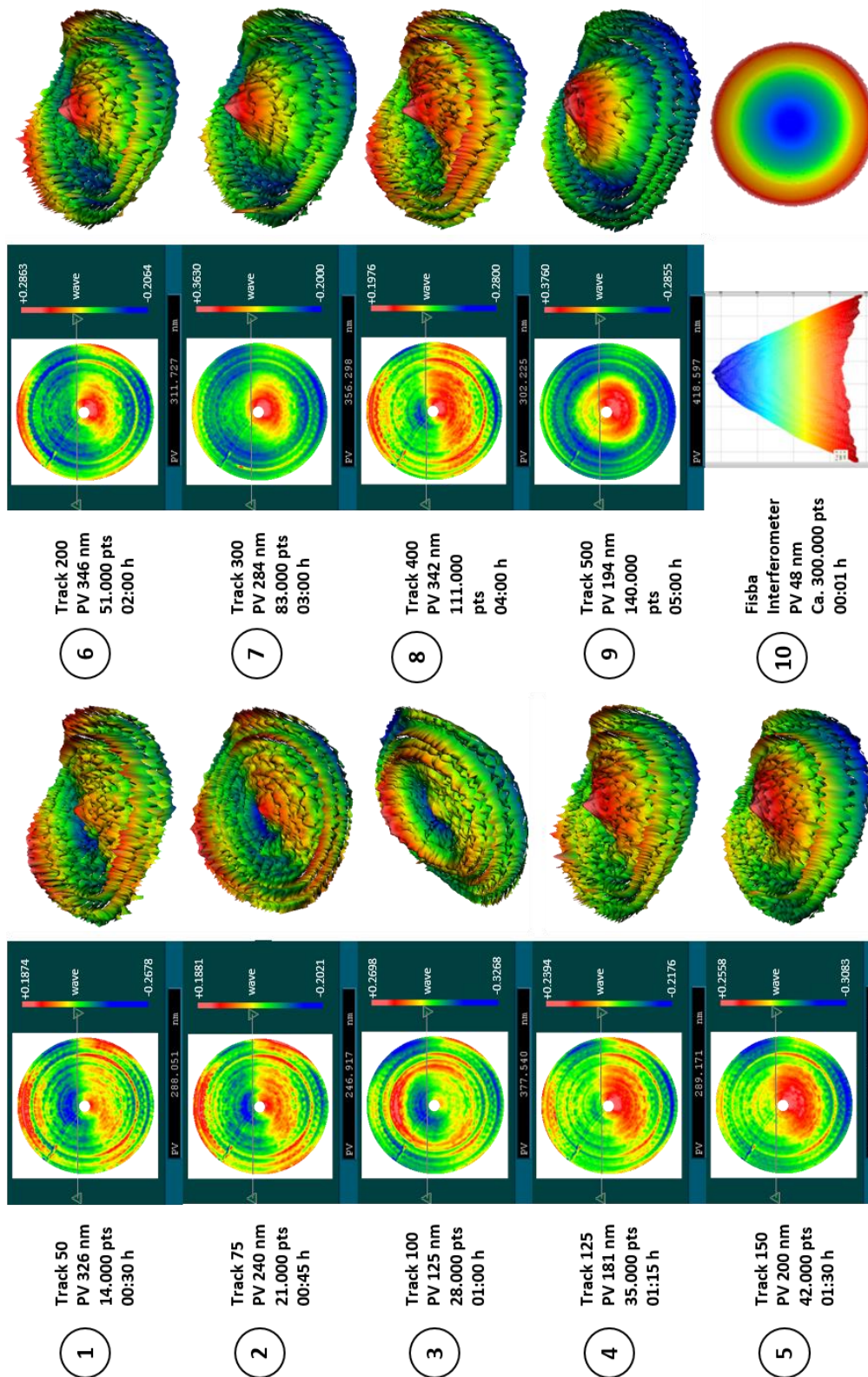


Figure 41: Results of the Spiral-mode measurements . The depicted test series consisted of ten measurements. Nine performed with the SCMM and one with a Fisba™ interferometer. The sensing unit was set to maximum detection speed.

All measurement results posted in Figure 41 show no variation in the basic shape. In general, all nine results look quite similar within the limits of the SCMM system accuracy. The concentric rings are evident to see, and the ratio between the outer edge and the area in the middle is comparable. All PV of the measurement results alternates roughly around the average PV of all nine measurements, which is 302 nanometres. A very distinctive characteristic of all measurement results is the coma structure.

The Cross Section-Mode is the newest measurement mode of the SCMM measurement machine. This mode enables the user to define an arbitrary number of cross-sections. In the case of the measurement results depicted in Figure 42, the test series started with 82 cross sections and ended with only two. Since the developed algorithms are more stable with more measurement results, the test series started with 82 measurements and reduced their number steadily.

Figure 42 illustrates the process of computing three-dimensional measurement results from an arbitrary number of cross-sections. It may be noted that the Cross-section-mode is only used for single cross-section measurements at the moment. Further research has to overcome this measurement mode and enhance it to a full 3D mode.

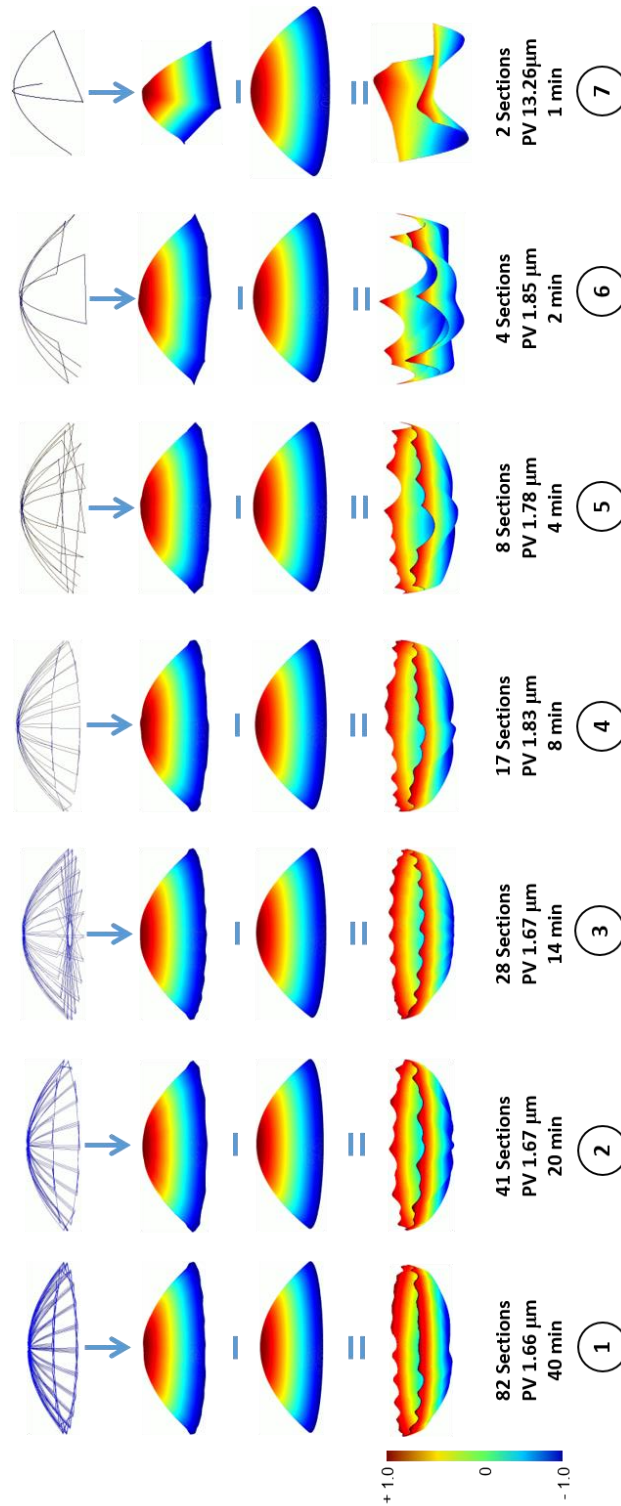
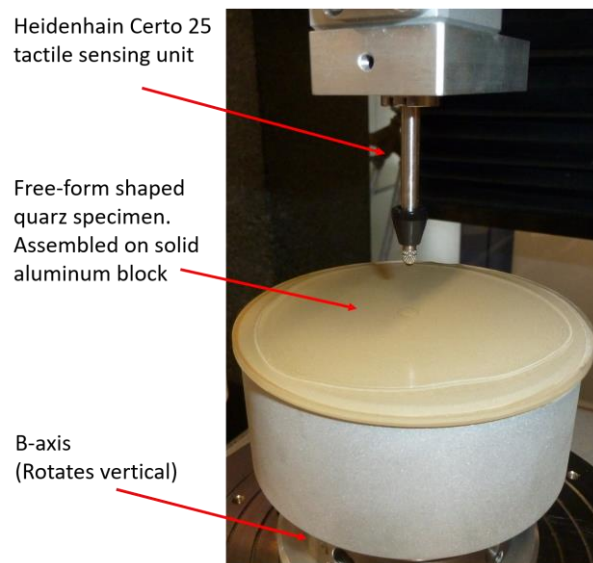


Figure 42: The Cross-section-mode measurements . The depicted test series consisted of eight measurements. Seven were performed with the SCMM and one with a Fisba™ interferometer. During the Cross-Section mode, the applied sensing unit operates with the maximum speed.

### 7.1.3 Test series free-form mode

A full 3D measurement of a free-form shaped element is one of the challenging goals of this PhD research. The used test object is a real free-form shaped surface employing a sinus shape. At the edge of the lens, the target-shape applies a sinewave with three oscillations and with an amplitude of 0.6 millimetres. The sine waves are converging in the middle of the lens (ref. Figure 44 and Figure 45). The used sensing unit was a Heidenhain™ tactile sensor of the Certo™ series (see Figure 43). The sensing unit itself has a repeatability of approximately 25 nanometres [71, 72]. Since short measurement times are an essential factor for the industry, the Spiral-mode had been used. Approximately  $20 \times 10^4$  measuring points in only 45 minutes had been measured.



*Figure 43: Setup free-form test series . The free-form capability was tested with an individually designed specimen, as depicted in Figure 45. The sensing unit was a Heidenhain Certo sensing unit, as presented in Chapter A.5.1. The test series was performed in the temperature stabilised measurement room of the LOE at  $20^{\circ}\text{C} \pm 0.15\text{K}$  in the Track-mode.*

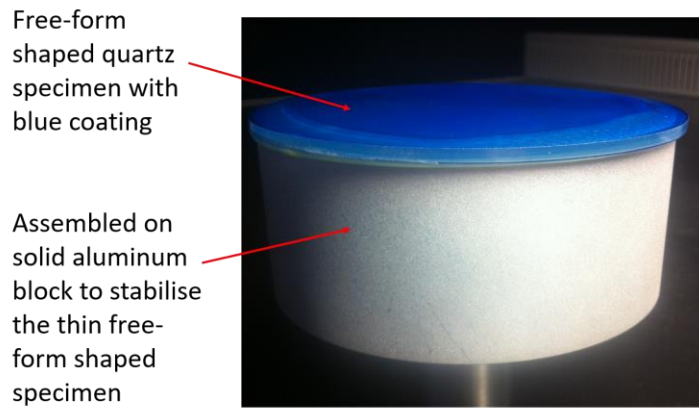


Figure 44: Free-form shaped demonstrator. The quartz demonstrator was joined on a solid aluminium block to avoid damages and deformations due to the thin design of the specimen.

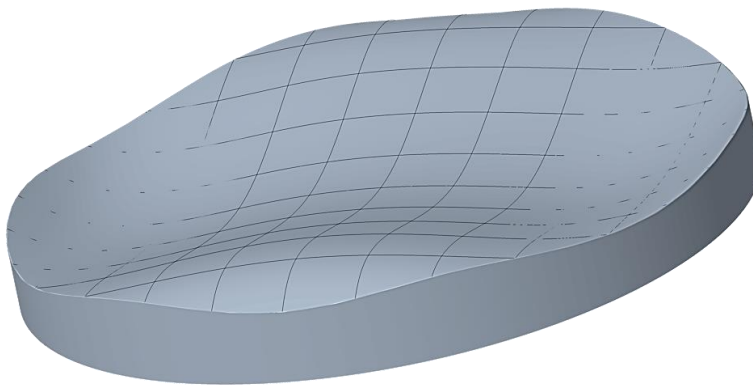
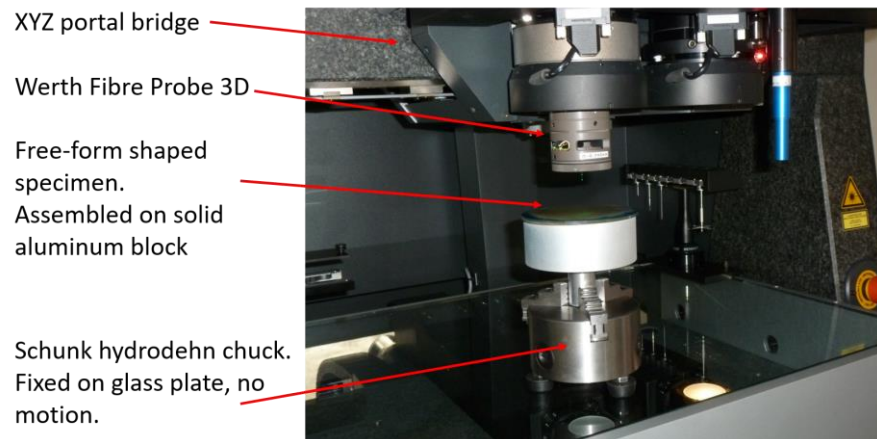


Figure 45: 3D sketch of the free-form specimen. The goal of the design was to create a free-form shaped structure combining convex and concave areas.

The long shaft of the Heidenhain™ sensing unit in combination with the high slope gradients of the specimen causes the risk of displacing the sensing unit. This disadvantage does not occur with the quasi-contactless, tactile-optical Werth™ Fibre-Probe. The used measurement machine for the test was the Werth™ Video Check UA™. The test setup is depicted in Figure 46.

In the first step, the sensor was used in the single point-probing mode with approximately  $11 \times 10^3$  sampling points. The repeatability of the sensor is approximately

150 nanometres. The measured sampling points served as input data for two evaluation software tools, the Werth™ analysis software and a self-developed Matlab™ (M2010a) tool for the SCMM.



*Figure 46: Werth-Video-Check-UA™ measurement of the free-form shaped specimen. The measurement was performed in a temperature-stabilised room at  $20^{\circ}\text{C}\pm 0.25\text{K}$ . The measurement was performed in concentrically distributed circles with a Werth™ fibre probe tactile sensing unit.*

The results from the two software tools are very similar [22, 23]. Consequently, it may be stated at this point, that the LOE has successfully implemented a trustable analysis software for the measurement of real freeform surfaces. Further, the Werth™ Fiber-Probe sensor may also be used in the scanning mode, the repeatability is sufficient for the precision optics, the contact force is negligible, and the bending of the probing element does not influence the measuring result. As a consequence, it has the potential to be the sensor of choice for the development of the needed measurement system for all types of test objects. The next milestone is to include the new sensor technology into the physical test carrier of the spherical-coordinate-measurement-machine.



### 7.1.4 Test series thermal influence

The influence of temperature is a critical effect. The following test series had been performed at the LOE in a temperature-stabilised chamber at  $20^{\circ}\text{C} \pm 1$  Kelvin. The specimen was a Melles Griot™ planar object with an accuracy of PV 2.613 lambda (with 632.8 nanometres). The result of the Fisba™  $\mu$ shape™ measurement is depicted in Figure 47. The result shows a bowl-shaped structure.

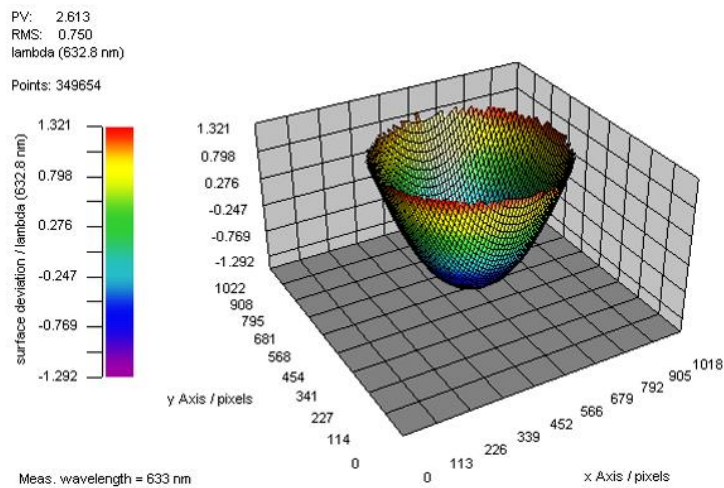


Figure 47: Interferometer measurement result. The Fisba™ interferometer measurement result was taken as a reference for the test series.

The SCMM was aligned by the application of the Centre-search procedure, presented in Chapter 5.2. With this alignment procedure, the axes had been aligned better than 0.5 micrometres. The specimen was fixed on a three-point fixture and adjusted until the radial, and the axial runout was lower than 0.5 micrometre. The used sensing unit was a Micro-Epsilon™ confocal sensing unit with an accuracy of 50 nanometres. The setup is illustrated in Figure 48.

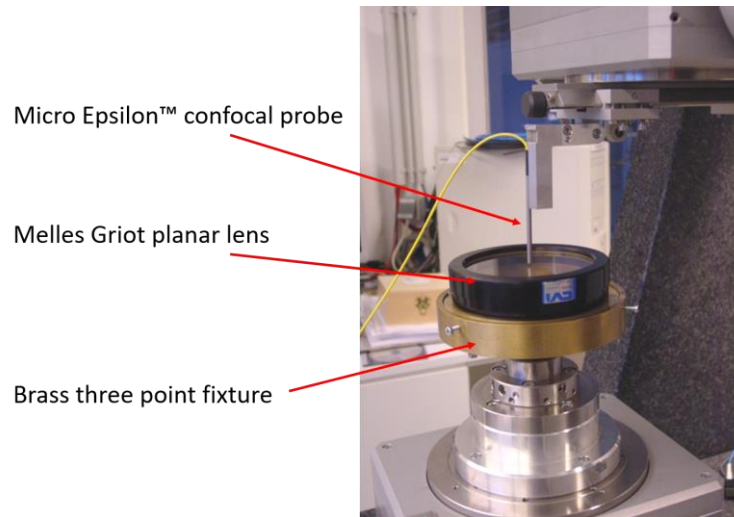


Figure 48: Setup temperature influence test series. The planar specimen was placed on a brass three-point fixture to compensate the tilt. The measurement was performed in a temperature stabilised measurement room at  $20^{\circ}\text{C} \pm 1\text{K}$  in the Track-mode.

For all measurements, the Track-mode with 100 tracks and 1000 points on the track was used. The measurement time was 45 minutes per measurement. The measurement chamber was closed for staff.

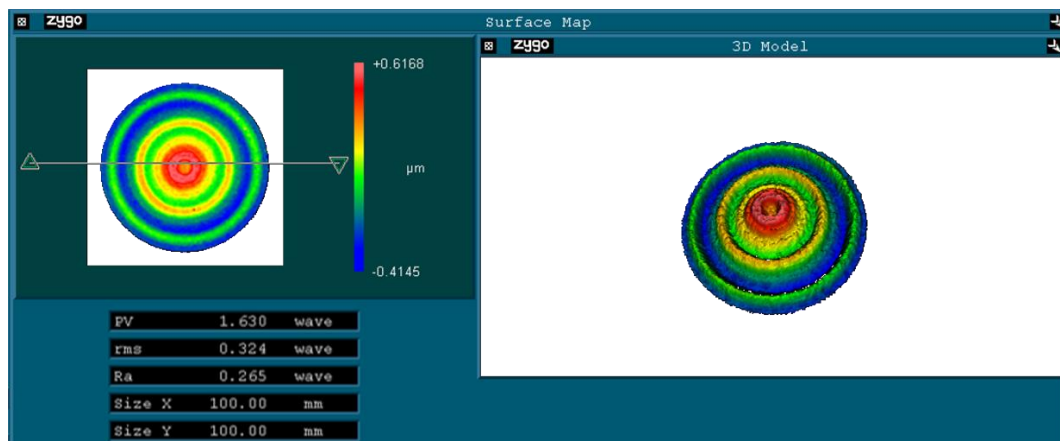


Figure 49: 1<sup>st</sup> result of temperature influence test. The result shows a structure with three dominant circular waves and a generally convex shape.

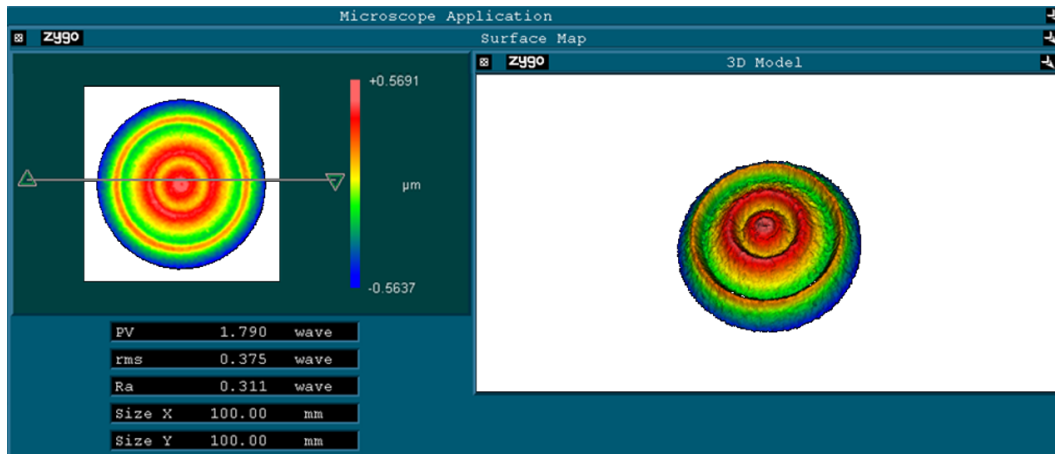


Figure 50: 2<sup>nd</sup> result of temperature influence test. The result shows a structure with three dominant circular waves and a generally convex shape.

Two measurements had been performed. The results are depicted in Figure 49 and Figure 50. Both measurement results show a different shape as expected. While the interferometer measurement results in Figure 48 depicts a bowl-shaped structure, the two SCMM measurement results show a peak-shaped structure with concentric rings. The PV of both measurements is between 1.6 and 1.8 lambdas, compared to a PV of 2.6 lambdas of the interferometer measurement.

Before the third test run had been performed, some modifications of the test setup had been done.

- Change of the hysteresis of the climate control to 300 seconds (instead of 600 seconds)
- Change of the hysteresis of the climate control to  $\pm 0.25$  Kelvin (instead of 1 Kelvin)
- Cover the complete SCMM with foil
- Break during the night to acclimatise the SCMM (machine switched on)

Figure 51 shows the covered SCMM. The complete test setup of the SCMM had not been changed. The specimen and the sensing unit had been untouched.



*Figure 51: Foil covered SCMM. In a first attempt, the SCMM was covered with a simple foil. This primitive cover had the goal to minimise the volume around the measurement area of the SCMM and to protect against turbulence. Furthermore, the parameters of the climate control had been changed from  $\pm 1K$  temperature tolerance to  $\pm 0.25K$  and the hysteresis of the climate control system from 600 seconds to 300 seconds*

With the application of the modifications of the climate control system and the covering of the SCMM, the third test run of the test series was performed. The settings of the SCMM stayed untouched; the system operated in the Track-mode with 100 tracks and 1000 measurement points at the first track. Figure 52 presents the 3D plot of the performed measurement.

Additionally, a plot of climate control is depicted. The measurement result of the third test run has the same appearance as test-run 1 and 2 with the difference that the number of concentric rings has increased. A consolidated view on the climate control plot shows that each of the concentric rings of the measurement result belongs to one peak of the climate control chart. 45 minutes of measurement time and 300 seconds

hysteresis resulted in nine concentric rings on the surface of the specimen. Figure 52 illustrates the expected nine rings on top of the measured surface.

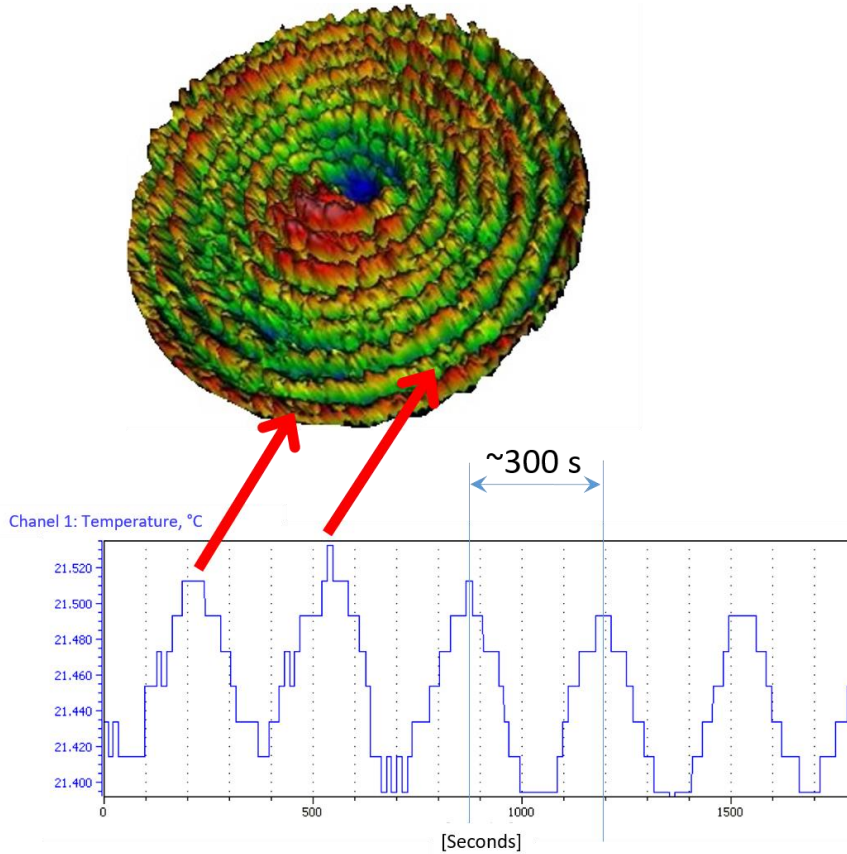


Figure 52: 3<sup>rd</sup> result of temperature influence test. In the upper area of the figure is the 3D plot depicted. The 3D plot of the measurement shows nine characteristic circular waves on the topside. In the lower area of the figure is the corresponding plot of the climate control published.

The modifications of climate control had a tremendous impact on the measurement result. A consolidated view on the measurement result reveals that the surface appears flat. The influence of the temperature drifts is better visible than in test run 1 and 2.

The next step of the test series was to modify the SCMM. The temporary foil covering was changed into a robust housing with better protection against movements

of the air and temperature drifts. Furthermore, since the Micro-Epsilon™ sensor has only a thin aluminium housing, the sensing unit was covered with additional, stable housing.

Figure 53 shows the latest housing of the SCMM. Please note that the picture was taken from another test series with a sizeable aspherical specimen. However, the housing fits around the SCMM without touching it in any position. It is completely closed from all sides. Figure 54 illustrates the covering of the Micro-Epsilon™ (ME) confocal sensing unit. The housing consists of a massive bronze metal housing that shields the actual sensing unit from the environmental influences.



*Figure 53: Housing of the SCMM. The stable housing with Plexiglas™ replaces the first simple foil cover.*

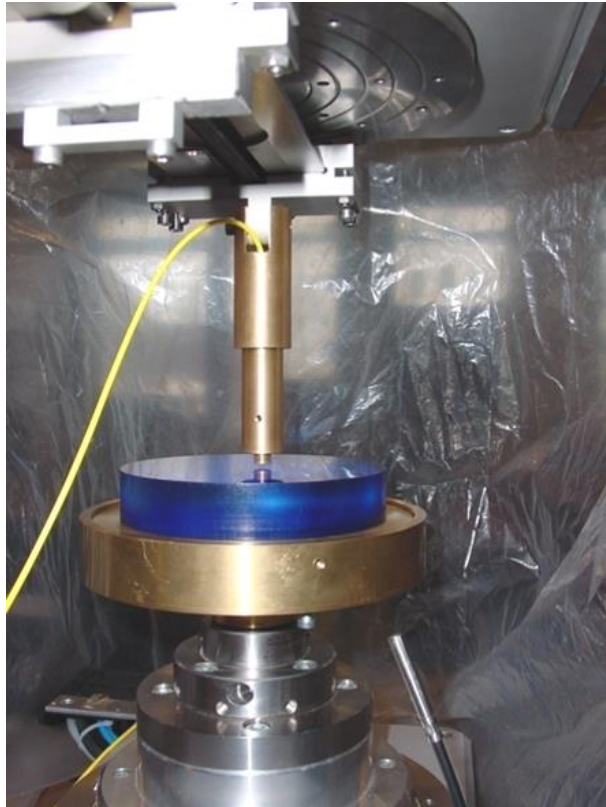


Figure 54: Housing of the sensing unit. Another step in the chain of improvements was the covering of the Micro-Epsilon™ sensing unit, as presented in Chapter A.5.4 and A.5.5.

The changes of the SCMM, especially the changes of the sensing unit requires a new calibration of the SCMM. Therefore, the Centre-search was performed, and the sensing unit was aligned with the axes. The specimen was not moved and remained in the previous position. The test series was performed with the application of the Track-mode with 100 tracks and 1000 points on the first track. The result of the fourth test run of the temperature-influence test series is depicted in Figure 56.

The result of the interferometer measurement is repetitively presented in Figure 55. The interferometer software showed a PV result of 1.653 microns (2.56 lambda) and the SCMM a PV of 1.619 microns (2.61 lambdas), a difference of 34 nanometres in shape.

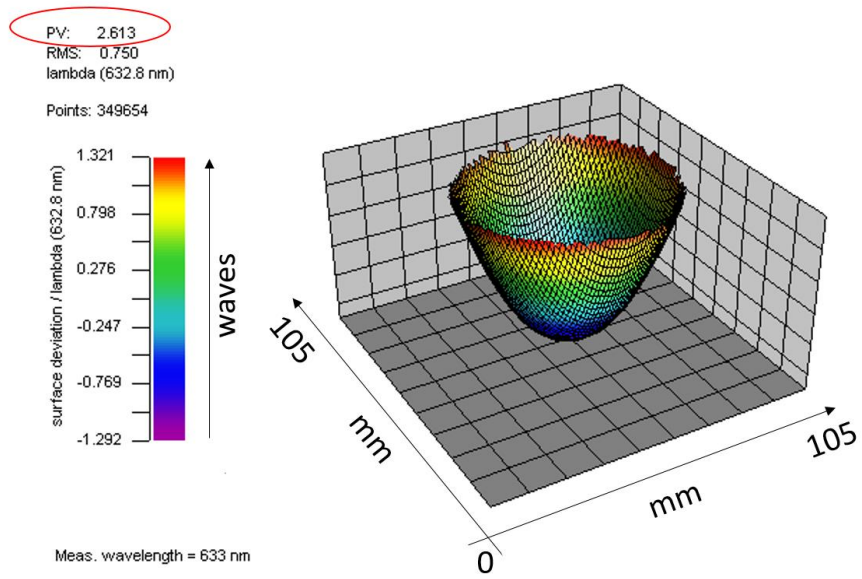


Figure 55: Interferometer measurement to verify the temperature influence

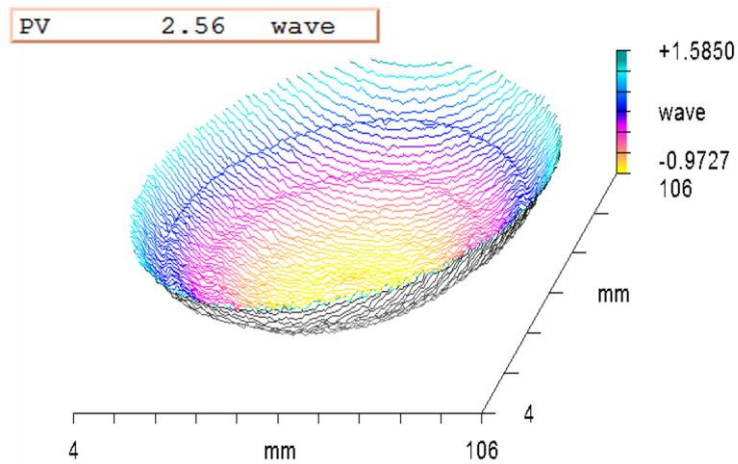


Figure 56: 4<sup>th</sup> result of temperature influence test. The modifications of the climate control system and the housing of the SCMM and the sensing unit resulted in a significant improvement of the measurement result.



### 7.1.5 Test series repeatability

The adequate method to verify the quality and accuracy of the metrology system is to perform a set of repeated measurements, all under the same conditions. The differences between the measurement results provide evidence about the quality of both the reference object and of the repeatability quality of the SCMM.

Therefore, a set of measurements was conducted to prove repeatability. The test series was performed in the Track-mode with the application of the Luhos™ sensing unit. All measurements were performed with 100 tracks and 1000 measurement points on the first track. The processing time for one measurement was 1 hour. The specimen was a planar shaped Melles Griot™ object with a form error of 1.6 microns on the surface measured with a Fisba™ interferometer, Figure 57.

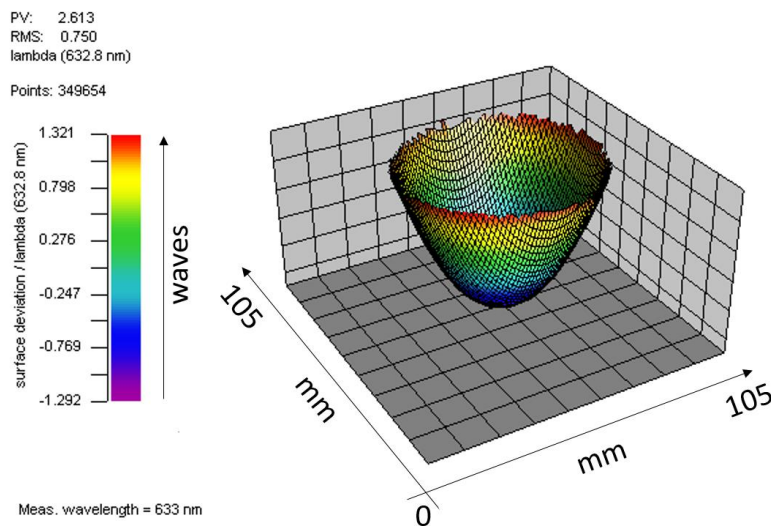


Figure 57: Measurement of the reference surface with a Fisba™ interferometer.

Figure 58 illustrates the results of the test series in one plot. The SCMM was operated in the queue mode. That mode enables the SCMM to operate autonomously according to a defined job list. This feature enables the SCMM system to operate during the night or at weekends. This test series had an operation time of 100 hours, performed during a long weekend with public holidays.

Therefore, environmental effects, such as traffic or people moving, had been minimal. Furthermore, the remote control of the SCMM enables to monitor the machine without entering the measurement room.

The result of the complete test series showed the following results.

- The repeatability of the SCMM is better than 160 nanometres.
- The Fisba™ interferometer measured a PV of 2.6 waves ( $632.8 \text{ nm} \times 2.613 = 1.654 \text{ microns}$ ).
- The SCMM measured an average of 1.543 microns - a difference of fewer than 100 nanometres.
- The influencing errors are mostly repeatable or lower than the SCMM resolution.

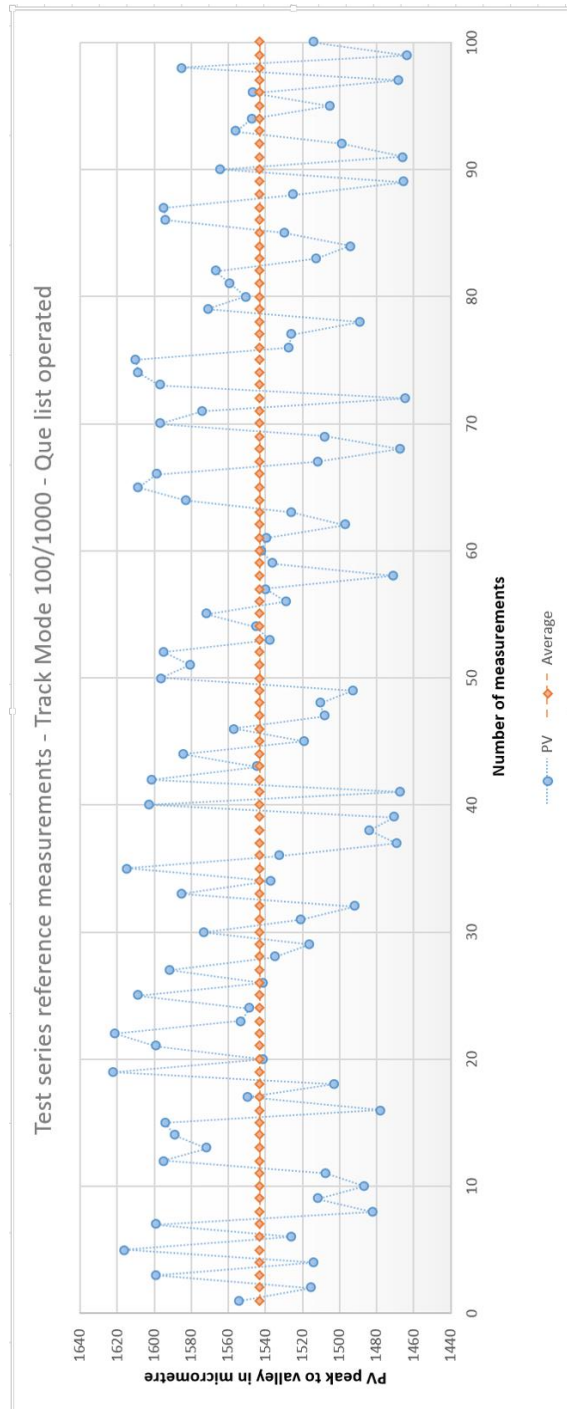


Figure 58: Result of 100 SCMM measurements of the reference surface. The Y-axis represents the PV result in microns of all measurements. The X-axis represents the number of performed measurement. All measurements have were performed subsequent in the queue mode feature. Therefore, no member of the staff was needed to supervise the measurement. The measurement was closed and locked to realise stable conditions during the complete measurement process. All measurements were performed in the Track-mode with 100 tracks and 1000 measurement points at the first track.

### 7.1.6 Summary

The test series performed with the test carrier demonstrated the reliability and the accuracy of the presented approach. Prior work has documented the importance of flexible coordinate measurement machines. Notably, the introduction of multi-sensor capabilities was a significant milestone in the development process of CMMs. This feature enhanced CMMs to become a universal and adjustable metrology solution for the modern industry. The significant disadvantage of standard CMMs is their slow measurement speed and the low accuracy of high-quality measurements. This issue is caused by the basic design of most of the CMMs. Machines operating with three orthogonal assembled linear slides are physically limited in speed. Fast accelerations and changes in the direction generate dynamic issues like vibration.

The published concept of a spherical coordinate measurement machine uses only two rotational axes during a measurement. Additionally, a collection of suitable measurement modes enables quick measurements with reduced dynamic effects. Furthermore, rotational axes have the physical advantage of a very high elemental accuracy.

The presented approach may help to avoid the disadvantages of standard coordinate measurement machines to improve the accuracy and to increase the measurement speed, but concerning the positive features such as multi-sensory and universality. A combination of all features fulfils the requirements of a modern

production chain. The use in the complete production cycle, at best for 100% inspections, may be reached.

Most notable are the mathematical models and the calculations of the geometrical issues behind the spherical coordinate measurement machine. This publication demonstrates an approach with trigonometric functions. Trigonometric functions have a couple of advantages compared to other mathematical operations such as rotation matrix operations. Trigonometry has a significant advantage that the calculations produce no rounding errors. A spherical coordinate measurement machine operates by simulating a spherical-coordinate-system. All angles given by the rotary encoders can be computed directly. The decisive advantage of the postulated approach is the fast computation of the data. This aspect supports the measurement speed and subsequent data analysis.

Further developments had been necessary to realise an accurate computation of the measurement results. The subsequent data analysis required the development of another software tool. The purpose of this analysis software is to compare the gained raw measurement data with a previously done reference measurement. Such a principle is well known in metrology science. It is used to identify and eliminate recurring axis and movement errors. The result of this computation is the result of the measurement without guiding errors.

However, such a referencing measurement takes time. It has to be updated when the environmental conditions or the measurement task changes. A metrology frame has to be developed to increase the flexibility of the measurement system. Such a metrology

frame is a separate metrology device. It monitors the complete movements of the critical machine parts and provides the necessary information to compensate for the documented errors. Metrology frames are an ideal instrument to detect and compensate deviations of the measurement machine during a measurement. Even when metrology frames are ubiquitous, the unique design of an SCMM requires the development of an individual solution, fit for an SCMM.

## 7.2 Centre search process

An axis alignment procedure is the key feature of a successful measurement with any mechanical or mechatronic measurement or production machine. The quality of the alignment process decides about the quality of the machine and therefore of the products machined with the system. In the context of this PhD research, a highly accurate alignment procedure for a highly accurate metrology device had been required. The requirement of a modern high accurate measurement system is to be able to scan the entire surface of a specimen. Therefore, research has to enable the development of a system capable of scanning the entire surface of an object under test, especially in the centre region. The literature describes research on the use of external elements, such as metrology frames or laser tracker. One of the primary goals of this PhD research was to find solutions to develop a metrology system for the shop floor. This approach makes a new approach necessary, a solution that may be included in the system and uses the existing features and capabilities of the system.

### 7.2.1 Setup of the experiments

The test series performed with the physical test carrier presented in this PhD thesis. As a sensing unit, the Heidenhain™ Certo™ CT 2502 probe was used. The specimen was a planar, black coloured optical lens with an accuracy better than  $\lambda/20$ <sup>21</sup> and a diameter of 100 millimetres. The test was conducted with the latest software version of the centre search, which had been fully implemented in the NC control. Details about the latest algorithm may be followed up in Section 5.2.

All tests had been carried out in a temperature stabilised climate chamber at  $20^{\circ}\text{C} \pm 0.1^{\circ}\text{C}$ . However, the SCMM had been arranged in the measurement position for planar objects (ref. Section 5.1.2). The alignment was done in the manual mode until the axes had been roughly aligned. A paper mask with a central cut-out of 3 millimetres in diameter had been used to position the C-, and Y-axis to ensure equal start positions. The test cycle started according to the implemented alignment procedure.

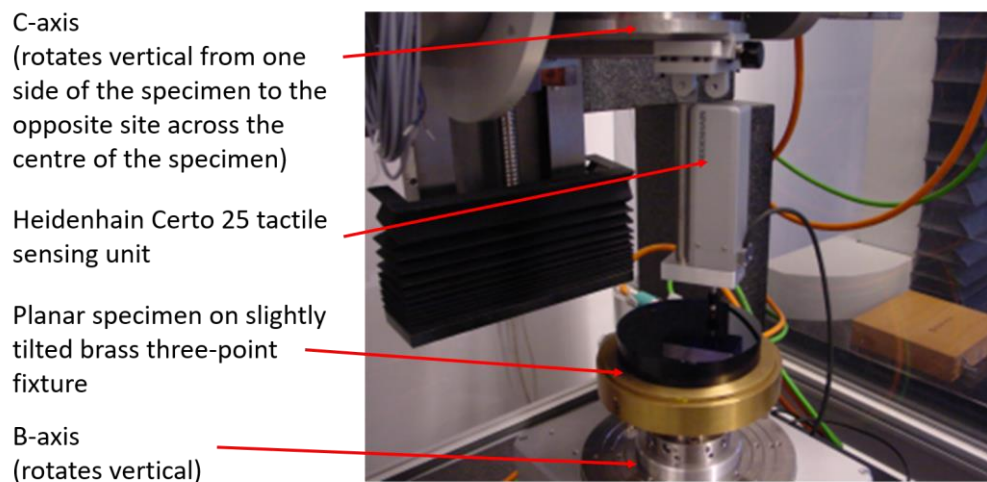
- Start at the outer boundary of the test specimen
- Scan across the surface through the centre
- (Calculate the zero degrees position of the C-axis and lock in this position)
- Drive +10 millimetre in the Y direction with the Y-axis and record five complete circles
- (Calculate the average of found maxima at the current Y-axis position)

---

<sup>21</sup>  $\lambda/20 - \lambda$  represents the wavelength of a He Ne Laser (red) with a wavelength of 632.816 nanometre.  $\rightarrow \lambda/20 = 31.6408$  nanometre

- Drive -5 millimetres from the current Y position with the Y-axis and record five complete circles
- (Calculate the average of found maxima at the current Y-axis position)
- (Calculate the mathematical Y-axis zero position and lock at this position)
- Redo the complete cycle with the new start position and verify the zero point

This test procedure had been looped 100 times to verify the reliability of the theoretical approach.



*Figure 59: Centre Search test series setup in detail. The requirement for the centre search process is slightly tilted planar specimen. For this test series, a planar lens in combination with a brass three-point fixture was used. The sensing unit was a Heidenhain Certo sensing unit, as presented in Chapter A.5.1. The test series was performed at the measurement room of the LOE at  $20^{\circ}\text{C}\pm 0.15\text{K}$  in the regular centre search mode.*



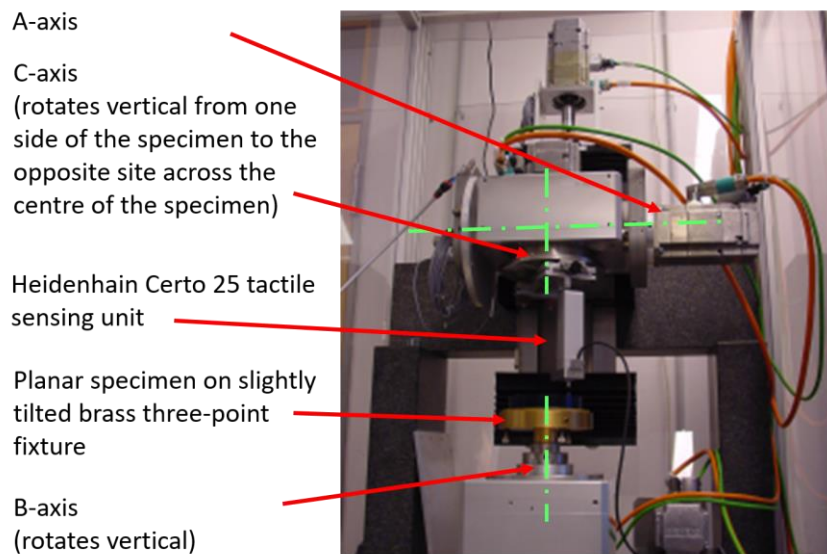


Figure 60: Centre Search test setup. This picture presents a general view on the complete setup including all axes, sensing units and the housing.

### 7.2.2 Results of the Centre search tests

For the Centre search test series, 100 cycles were performed. For this experiment, each cycle contains two centre search measurements — the first to find the correct C-axis zero position and a second to verify the result. At the beginning of each centre search process, the SCMM was positioned in the centre region of the specimen. The centre search process requires a rough first positioning of  $\pm 3$  millimetres. Another process requirement is the need for a slightly tilted planar object with no particular requirement regarding accuracy. The centre search process is automated and needs no further support of a user. After the successful centre search process, the SCMM is resetting the C- and Y-axis. The proceeding is concluded by moving to a save position enabling the change of the specimen.

After performing 100 test cycles, an average misalignment of the C-axis of  $0.52^\circ$  was documented. The SCMM C-axis moved  $16^\circ$  ( $-8^\circ$  to  $+8^\circ$ ) to cover the used specimen

with 100 millimetres in diameter. Therefore, a misalignment  $0.52^\circ$  of the C-axis corresponds to 3.25 millimetres. Figure 61 depicts the results of the 100 test cycles.

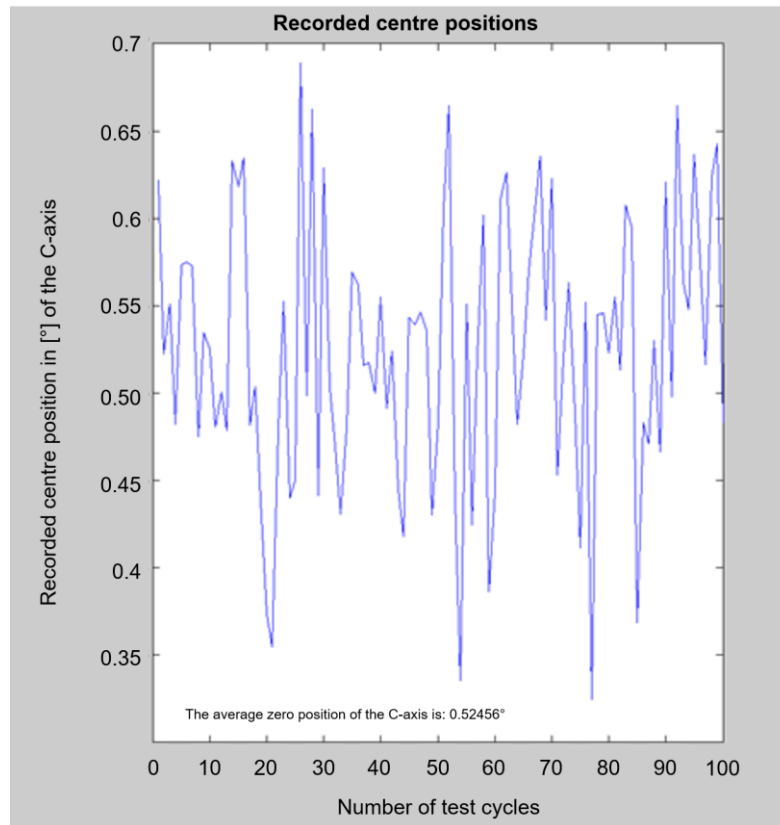


Figure 61: Result of the C-axis positioning process. The Y-axis represents the delta between the C-axis manual start position ( $0^\circ$ ) and the calculated C-axis zero degree position. The X-axis provides the number of cycles.

However, the manual centre search is only recommended to move the SCMM into a reasonable start position for the automated Centre search process. After each proper manual positioning, a complete Centre search process was performed. Therefore, 100 automated Centre-search processes were performed. The plot Figure 62 shows the corrected C-axis values. The average of the corrected centre point of the C-axis is at  $0.5 \times 10^{-3}^\circ$  or converted  $3.125 \times 10^{-3}$  millimetre off-axis alignment.

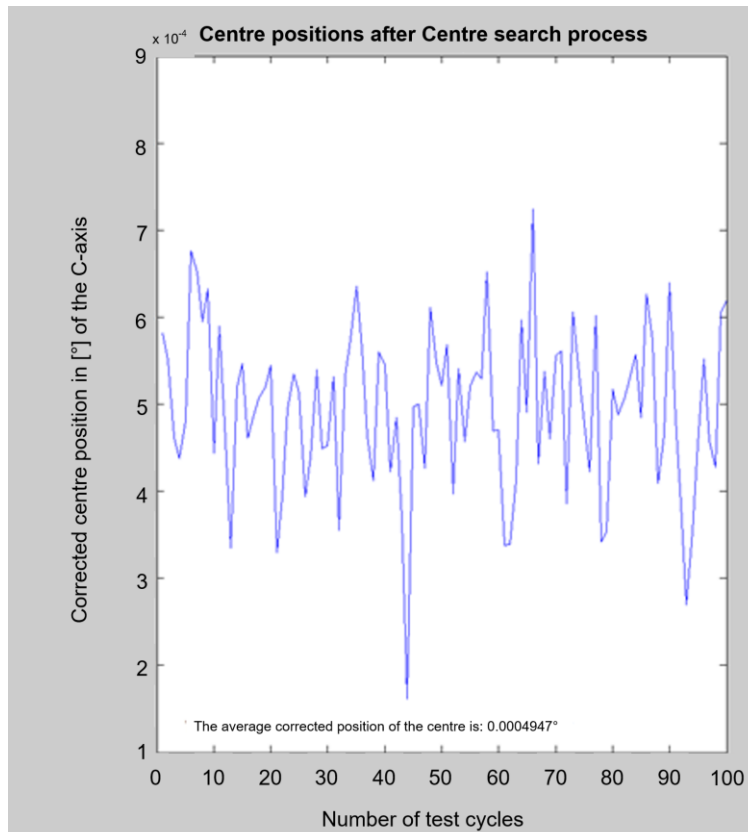


Figure 62: Corrected C-axis position in degree after performing the centre search process.

The centre search process consists of two measurement processes: the detection of the C-axis zero position and the detection of the Y-axis zero position. Therefore, 100 Y-axis alignment measurements were performed.

The Y-axis alignment process consists of two measurements, at position Y1 and Y2. Algorithms presented in Chapter A.9 enable to calculate the final Y0. Figure 63 illustrates the results of the Y0 alignment. Since the Y-axis is a linear axis, the values of the encoder are directly available in millimetres.

The average of all 100 measurements of Y0 was at  $3 \times 10^{-3}$  millimetres. This result is in the range of the resolution of the Y-axis encoder.

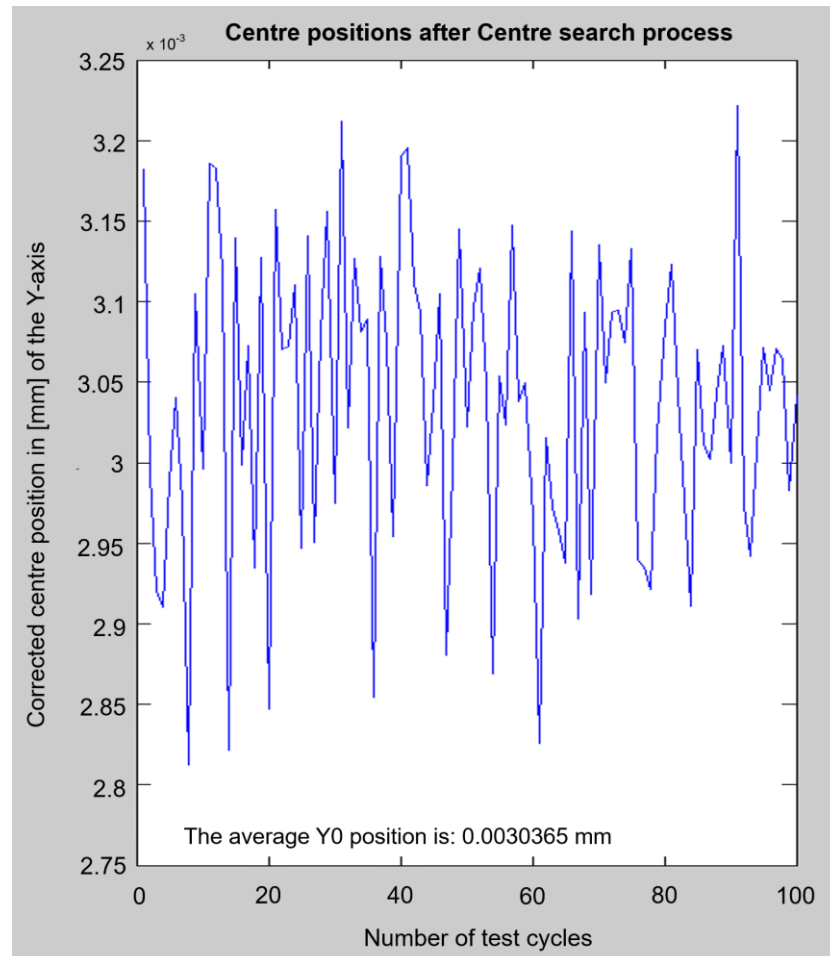


Figure 63: Y-axis alignment. The Y-axis represents the corrected zero position  $Y_0$  in millimetres. The X-axis shows the number of test cycles.

### 7.2.3 Summary

The test series had verified and validated the Centre Search procedure. The alignment test results proved that the alignment strategy is a reliable and very accurate procedure. It enables the SCMM to be aligned without the use of expensive external devices, such as laser trackers or metrology frames. However, the alignment strategy takes a couple of minutes before the actual measurement may start. Another

advantage of the presented procedure is that the alignment has to be carried out only once until the setup of the system is not changed.

### 7.3 3D-scale

The 3D-scale is a generic measurement device for rotational axes. The primary purpose of the system is to detect and correct the radial and axial runout of axes. Chapter 5.3 illustrates the mathematical background of the system and presents the developed algorithms. The primary goal of this PhD research is to replace the expensive but highly accurate air bearings with cheap ball bearings without decreasing the accuracy of the system. Since the device is a mechatronic system that needs hardware, software and electronic components, the most reasonable method to verify the function and accuracy are physical tests.

#### 7.3.1 Setup of the experiments

The test series had been carried out with a demonstrator of the 3D-scale. The system, presented in Figure 64, consists of the mainframe, the detector disc, inductive sensing units, very rough bearings with a large clearing (Type C3), and a stepper motor including the control unit and tooth belt.

Moveable ball bearing with large clearance (Type C3)

Displacement direction marked with double arrows.

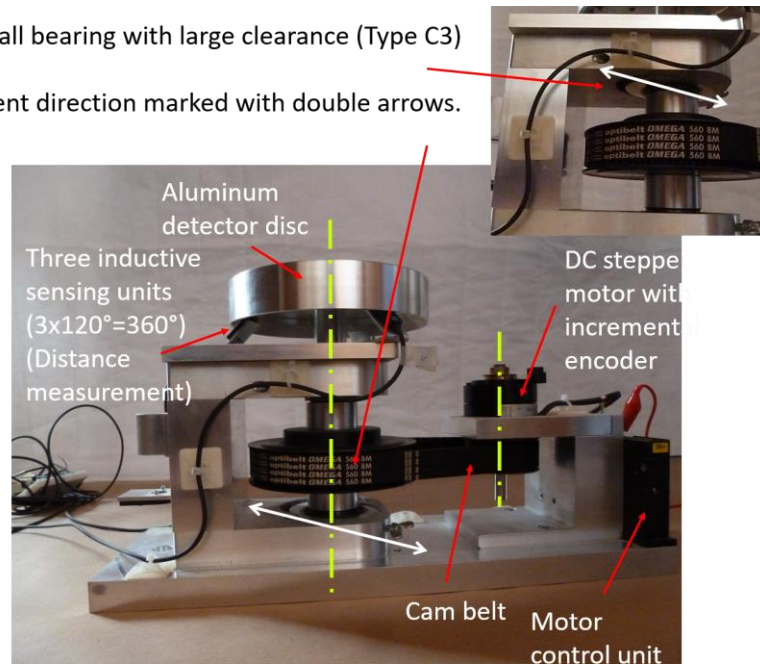


Figure 64: 3D-scale demonstrator This demonstrator was built to verify the theoretical assumptions of the 3D-scale principle.

The two ball bearings can be displaced and therefore create radial and axial runout. A belt to reduce the influence on the measurement result had decoupled the stepper motor. The rotation speed had been 30 rotations per minute, measured on the detector disc. All tests took place in a climate chamber at  $20^{\circ}\text{C} \pm 0.1^{\circ}\text{C}$ .

The measurement of the device was realised with three Balluff™ BAW R03K-UAE40B-BP00.3 inductive sensing units operating at 100 Hertz. The repeatability of the sensing units is  $\pm 35$  microns. The polished aluminium detector disc was produced with a tested axial- and radial-runout tolerance of 5 microns with a digital dial gauge in the production machine. The deviation of the assembly had been in the range of  $\pm 0.5$  millimetres in all directions, measured with a Micro-Epsilon™ confocal sensing unit with an accuracy better than 100 nanometres.

However, the software used for this experimental setup had been developed with Matlab™ (M2010a). All sensing units, Balluff™ and Micro-Epsilon™ were recorded with 100 Hz in four separate channels. This feature ensures a parallel readout of the sensing units with a 40 MHz microcontroller, which converts the analogue signal into digital signals. The test series consisted of 100 iterations with ten rotations during each test run. The obtained data were computed with the mathematical models presented in Chapter 5.3.

### 7.3.2 Experimental results

The recorded results are depicted in Figure 65, graphically. The point distribution is evident to see. It might be noted that there are a significant number of data points in the upper and in the lower area of the axial measured range. The distribution in the axial direction (Z-axis) is spread over a range of 300 microns. The radial distribution (XY-plane) of the measured points is in a range smaller than 100 microns. This result corresponds with the expectations of the C3 clearance of the used ball bearings.

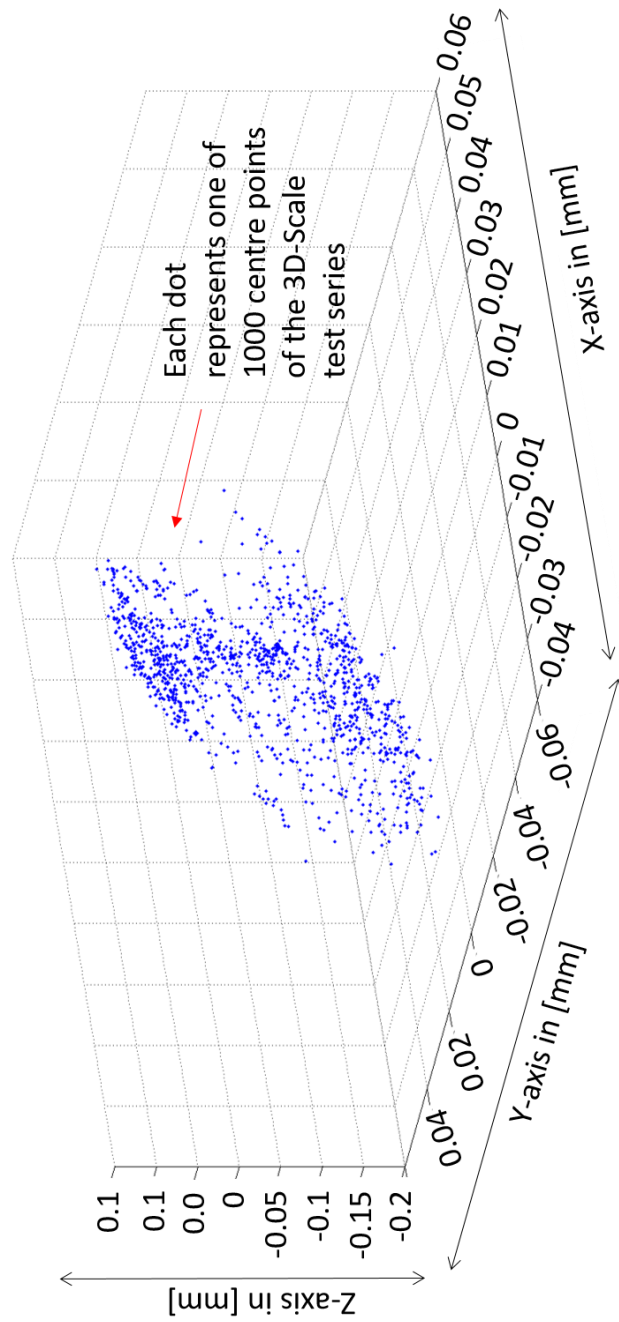


Figure 65: Result 3D-scale test series. The X-, Y-, and Z-axis represent the Cartesian component of the calculated centre points in millimetres.



### 7.3.3 Summary

The 3D-scale can detect the radial and axial runout of ball bearings. The limitation of the system is the accuracy of the used three sensing units in combination with the production accuracy of the detector disc. In this experimental setup, all data had been recorded, and the computation of the results had been done after finishing the test series.

This new device may help to reduce the costs of devices employing rotational axes. The 3D-scale offers opportunities for the modern industry. On the first hand, the accuracy of existing machine configurations may be increased only by adding the 3D-scale. On the other hand, the manufacturers may use cheaper and less accurate bearings and still keep the original system accuracy.

Since this new device comprises a very generic solution, it can be included in a large number of different machines. The novel and reliable mechanical design in combination with the stable and efficient mathematical models lead to a very competitive and advanced metrology solution. The application of this generic device enables older machines to be updated without changing components or machine parts.

However, a first prototype had been developed to investigate and verify the theoretical approach. This physical prototype might be very useful to investigate the limitation of the design. In particular, two issues need further development and investigations. All metrology systems need a necessary calibration. Since this device and the design are unique, there is no existing approach to calibrate the 3D-scale. The

second issue is the production of the detector disc. The ideal materials for the detector disc might have a low thermal expansion coefficient, such as Zerodur [22], Invar [23] or similar materials. The disadvantage of such materials is that they are challenging to handle and to machine. Therefore, the first prototype was made out of aluminium. This compromise enables verification of the function but does not provide the best reachable accuracy.

For future prototypes, especially for the detector disc, the application of materials with low thermal coefficients is essential. This task requires the expertise of advanced manufacturers concerning the high accurate grinding and polishing of Zerodur or Invar. Furthermore, the development of a calibration method is a significant milestone on the way to a successful product.

---

<sup>22</sup> Zerodur – A lithium aluminosilicate glass-ceramic and a registered trademark of Schott AG

<sup>23</sup> Invar – A nickel–iron alloy (64FeNi)

## Chapter 8

### Discussion of the results

#### 8.1 Analysis of repeatability and accuracy

The repeatability is one of the three significant classifications of a metrology system. The repeatability tests have to be performed under the same conditions and under the same specifications:

- The same SCMM setup. Except for the B-, and C-axis, all axes are locked.
- The same specimen. A Melles Griot™ planar lens was used.
- The same sensing unit. For this test series, the Lumphos™ MWLI™ sensing unit was used.
- The same operator. The test series was performed in the queue mode (automatic).
- The same climate conditions. The air condition operated with 20° and tolerance of 0.15K.

- No persons allowed. The test was performed during a long weekend with public holidays.
- All measurements were performed successively.
- A reference measurement of the same specimen was required.
- A comparative measurement with another metrology machine was required.
- Use of the same measurement mode - track mode with 100 tracks and 1000 measurement points.

All measurements were compared with the reference measurement. The reference measurement was performed with the same specimen. Therefore, the typical measurement result of each of the 100 measurements should be zero. The difference between the reference measurement and the actual measurement is a good indicator for the repeatability of the system.

Chapter 7.1.5 presents the test results. The specimen was measured with a Fisba™  $\mu$ shape™ interferometer. The documented result of the measurement is a PV of 2.6 waves. Converted into SI units: (632.8 nanometres interferometer-wavelength x PV 2.613 = 1.654 microns).

However, the statistical analysis of the test series showed the following result, depicted in Table 10.

*Table 10: Statistical average and standard deviation of the SCMM. The data had been obtained in Chapter 7.1.5*

Statistical average	Standard deviation
1,54 microns	0.454 microns

A standard deviation indicates the spread of results compared with the statistical average. The literature employs the term Sigma ( $\delta$ ) to specify the number of measurements within a defined limit.

- + 1 Sigma contains 68% of all data
- + 2 Sigma contains 95% of all data
- + 3 Sigma contains 99.73% of all data

Figure 66 shows the histogram of the repeatability test series. The tolerance range was set to 150 nanometres, which is the expected accuracy level in the Track-mode for planar measurements.

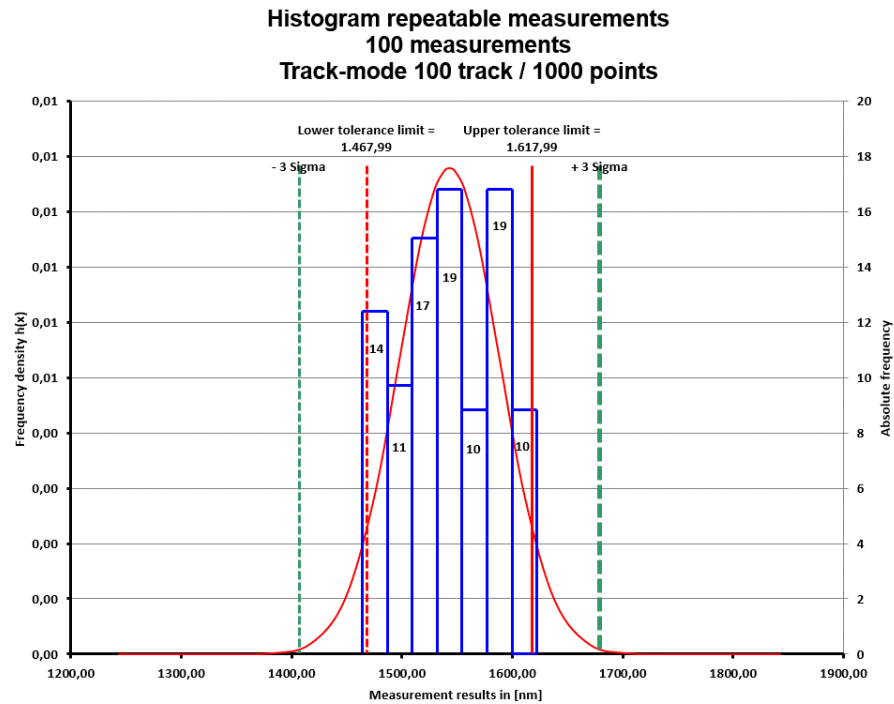


Figure 66: Histogram of the repeatability test series. For the calculation of the histogram, Microsoft™ Excel™ was used. The data basis was taken from the test series presented in Chapter 7.1.5.

The diagram shows that 95% of all measurements are within the tolerance range. The most (19) measurements are within +1 Sigma, and 76 measurements are within the +2 Sigma band.

Furthermore, the statistical analysis shows that 4.94% of all measurements are not inside the tolerance range.

However, the result of the test series demonstrates that most of the errors of the SCMM are repeatable errors and can be removed with a reference measurement.

## 8.2 Reliability of the SCMM

The reliability of a measurement system is a significant challenge. One of the critical milestones in the development process was to develop a reliable metrology machine. All components of the SCMM were developed according to the latest industrial standards. For example, the usage of state of the art Siemens™ SPS system is a significant feature. Furthermore, all mathematical models were validated with virtual 3D models by the application of the CAD software CREO3™ (M100), including the motion analysis tool. Furthermore, the SCMM is equipped with software and hardware limit switches on each axis. This feature reduces the probability of a crash. The system is designed to freeze when one of the limit switches activates.

However, the development of the queue list feature was another significant milestone to prove the reliability of the SCMM. The queue list feature enables the user to define a certain number of test series with different measurement modes. All measurements are performed successively without interactions of the user. For example, during the repeatability test series, the SCMM operated approximately 100 hours without a break and performed 100 measurements.

Two further developments assist the user in monitoring the SCMM during the operation. The “error log-file” documents all commands and responses of the GUI and the SPS. The second feature is the two-way remote control. The NC control system and the GUI can be controlled from any verified computer in the same network. In the case of a system error, the system stops and informs the operator immediately.

### 8.3 Discussion of the experimental results

The multi-axis framework has to be considered carefully to be able to interpret the results presented in Chapter 6.4. The test series of this PhD research consisted of three primary test series that were performed to verify all features of the SCMM.

The test series presented in Section 7.1.1 had the fundamental goal to verify the functions of the machine regarding the settings and the correct axes movements. Furthermore, the test series was used to verify some features of the metrology device, for example, the readout of the axes, the implementation of the sensing units and the function of the data analysis software. All primary functions of the test series had been successfully verified by the conducted test series.

In detail, the test series showed that the result of the measurement might be comparable to the result measured by the Fisba™ interferometer. The SCMM test carrier measured a PV of 309 nanometres and the Fisba™ interferometer of 23 nanometres (ref. Chapter 7.1.1). It may be noted that, contrary to the interferometer, the test carrier does not use any filter or smoothing algorithms. The obtained SCMM measurement result meets the accuracy limits of the presented SCMM system at that time. Further improvements, for example, the Lumphos™ sensing unit and a housing of the SCMM, improved the accuracy level of the SCMM.

However, the second test series conducted with the SCMM test carrier investigated the measurement modes in detail (Chapter 7.1.2). It may be noted that the SCMM prototype had not been equipped with a temperature compensation feature at



that time. The multi-axis framework and the specimen have to be considered carefully to interpret the results obtained with the test series.

A detailed analysis of the measurement results, presented in Figure 40, identify two distinct findings. Firstly, the error correction of the SCMM data analysis software operates comparable with MetroPro™ and delivers comparable results. All measurement results show none of the predicted errors, especially the tilt, axial displacements, and geometric machining errors.

Secondly, the measurement series uncovers a temperature drift. The numbers (1) – (9) in Figure 40 show a significant change in the overall shape of the specimen. At the beginning of the test series, it had a convex shape; the geometry changed slowly and turned into a concave bowl shape. The cooling down phase after the blocking process explains this effect. The specimen is cemented on a massive block (ref. A.6.3). Therefore, there is an area of material accumulation in the centre of the specimen. This area can store more thermal energy than the rest of the blocked specimen (ref. Figure 40(1)).

During the progress of the test series, the area cooled down, and the temperature smoothly aligned with the environment temperature in the measurement chamber. The interferometer measurement, printed in Figure 40(10), proves that the overall shape of the specimen is correct.

The second part of the test series was performed by employing the Spiral-mode. The test series identified a second tilt in addition to the tilt of the specimen. The multi-

direction movement of the sensor unit during the Spiral-mode measurement has to be analysed to investigate the origin of this second tilt. In opposite to the Track-mode measurement, where the C-axis is locked while recording the data, the Spiral-mode uses the B-, and C-axis to move the sensing unit in a spiral-shaped path over the surface of the specimen. This second movement causes a second tilt; that effect can be seen in Figure 41 (5).

A further aspect that appeared in Figure 41 is the coma-shaped 3D structure in every single measurement. S-shaped errors with this appearance are named coma. The removal of the coma error is the next step in the development stage of the Spiral-mode feature of the analysis software tool.

In summary, the Spiral-mode measurement confronts the data analysis software with more complex and detailed errors than the Track-mode does. However, the latest version of the Spiral-mode enables two-times quicker measurements than the Track-mode. The reduction of the measurement time comes along with more and multiple errors caused by the synchronic movement of the B-, and C-axis. The measurement result is not as accurate as of the measurement result obtained with the Track-mode; the PV value is approximately two times higher.

The third measurement mode is Cross-Section-mode. This measurement mode is the latest strategy, and the development process is in the first test stage while publishing this PhD thesis. As explained in Section A.10.1.3, this is a mode where the user can choose the number of cross-sections, starting with one. The data analysis software differentiates between the numbers of uploaded cross-sections; if a user wants

to load less than ten measurement files, the software shows the result of all ten cross-sections as individual two-dimensional plots (Figure 139). If the software detects more than ten measurement files, it computes a three-dimensional measurement result. Figure 138 presents an arbitrary selection of cross-sections measurement results with a decreasing number of cross-sections. In Figure 138, the pictures in the row marked with a Roman (II) show the fitted surface that covers the single cross-sections. The test series indicates that the used algorithms need a suitable number of sampling points and therefore of cross-sections. The result of the surface generation process reminds on an umbrella. The used algorithms are insufficient and have to be improved. The latest version of the data analysis software allows measurements with a resolution between one and two micrometres. Further developments have to be carried out to improve the algorithms for surface creation.

The third test series, published in Section 7.1.3, presented the measurement of a free-form shaped object. Two measurement machines had been applied, the SCMM test carrier in the latest version, and a Werth™ Video Check UA™. The Video Check™ is one of the most accurate and expensive series metrology system available in the market. The SCMM test carrier provided a comparable measurement result of the specimen. The length of the used sensing unit and the corresponding lateral displacement may explain the differences between both measurement results by moving across slopes. Furthermore, the measurements had not been carried out subsequently. It was necessary to send the specimen to another facility with different environmental

conditions. However, the test series demonstrated the performance of the free-form capability of the test carrier.

#### 8.4 Advantages and limitations

Summarising the test results gained in Section 6.4, the test carrier in detail and the SCMM concept, in general, is a reliable and high accurate metrology system. The primary goals of this PhD research had been met, and the result aroused the interest of a significant manufacturer in the metrology market. The advantages of the system reflect the original goals of the PhD research, to create a modern, flexible, and high accurate metrology system with the capability to operate on free-form shaped surfaces.

The developed test carrier provides several interfaces for all kinds of modern sensing units. The user interface supports the implementation of different sensing units by the use of the sensor list, presented in Section A.5 in Figure 127. This feature enables the user to implement and use all kinds of a modern sensing unit according to the measurement task requirements. Furthermore, the employment of a significant amount of sensing units enables the user to operate on all common surface types, from very rough surfaces to high-grade polished surfaces.

Other advantages of the system are unique measurement modes. The user may decide what is more important, the measurement accuracy or the measurement speed. For that purpose, three measurement modes had been developed and implemented. Beginning with the Cross-section-mode, this enables the user to check the geometrical

relations of the specimen with only one cross-section. This feature is beneficial in the first steps of the production chain, especially on rough, ground objects. Further research may improve this feature to a reliable, full 3D capable measurement mode. The second mode, the Spiral-mode, may be seen as mixed mode. The reachable accuracy is much higher than by the application of the Cross-section-mode, and it delivers a full 3D scan of the test specimen. Another advantage of the Spiral-mode is the measurement speed and density of the measured data points. The GUI of the developed software package provides the most accurate settings as default parameters. The test series employing these parameters are presented in Section 7.1.2. The third and most accurate measurement mode is named Track-mode. This mode produces a user-defined number of concentric rings on top of the surface. This measurement mode is designed to be used for the measurement of highly accurate measurements, especially for polished optical elements.

Other very distinctive advantages presented in this PhD thesis are the developments of the Centre Search procedure and the 3D-scale device.

The integrated Centre Search procedure enables the system to align the axes automatically. There is no need for further external or expensive metrology systems such as measurement frames or laser tracker. The procedure is fully integrated into the NC control and the user interface. One of the goals of the PhD research was to develop a user-friendly system with a minor influence of user indicated errors. This feature has a significant impact to reach that goal. The user is not allowed to perform measurements

when the axes are not aligned. Therefore, errors caused by misalignments or even damages on the system due to wrong positions of the axes are most widely impossible.

The 3D-scale is a newly developed device. The system monitors the movement of a rotational axis and detects all deviations regarding the radial and axial runout. The significant feature of this development is the simplicity. Contrary to a measurement frame solution, this device does not need expensive sensing units with an extensive measurement range. However, the system provides a complete error map of the movement of a rotational axis during a measurement. The corresponding correction data may be used to increase the accuracy of cheap ball bearings up to the level of costly air bearings.

The limitations of the systems are still the measurement speed and the reachable accuracy compared to modern interferometers. Since interferometers may take a dozen pictures in one second, the SCMM test carrier needs at least a couple of second for only one cross-section scan. Furthermore, the reachable accuracy is still not as high as provided by modern interferometers. The application of a multi-axis framework increases the influence of measurement errors. Another fundamental reason is the number of measurement points. An interferometer analyses the picture of wavefronts, while a CMM has to move to each point physically. Stitching interferometers need to be positioned in different positions as well. The measurement speed of such systems is comparable to the presented test carrier.

## 8.5 Application of the SCMM

The presented approach aroused the interest of a famous significant player in the metrology market. Therefore, the application of the developments may be leading towards a mass production metrology machine. Other aspects are the developments made during this PhD research. Several components and procedures are unique and generic. For example, the 3D-scale is a very generic solution that may be used for any device using rotational axes.

## 8.6 Summary and reflection

This PhD research presented new knowledge, generic approaches, and new developments in metrology science. The presented PhD research may aid the demand for a modern, flexible, and modular metrology system for the shop floor of production facilities. The combination of the completed research and the new and generic developments may support another researcher in appropriate fields.

A consolidated view of this PhD research project revealed some things that I may should have done differently. The most crucial point is that I left the laboratory after finishing most of the practical work. A university environment is essential for a successful PhD research; the access to knowledge, publications, and assistance is essential. Furthermore, this research touched many different and exciting areas, and it was challenging to stay focused on the original research topic and the related research questions. Summarising, the initial research opened many new research questions. Only

the constructive advice of my supervisors and of course the proper research methodology enabled me to finish this extensive research project in a successful way.



## Chapter 9

### Conclusions

#### 9.1 Conclusions

The primary goal of this PhD research was to conduct research about a flexible and modular metrology solution in order to aid the demand for highly accurate measurements on the specimen with different surface shapes and surface structures - at any stage of the production chain. As a physical result of this PhD research, an efficient metrology device was created.

The literature review of other spherical coordinate measurement machines revealed that they are mainly used in the last stage of the production process and mostly for large objects, greater than 500 millimetres in diameter. Furthermore, the existence of different measurement modes and of multi-sensor interfaces is not documented. Papers proof that research regarding the axes alignment was performed, but all publications describe only external solutions or the application of two sensing units. Furthermore, these machines are specialised, and the used operating system is

designed for experienced operators. Therefore, one of the objectives of this PhD research is research about a proper user interface.

The presented PhD research investigates the following areas with respect to spherical coordinate measurement machines.

- a) Axes alignment strategy applicable with onboard tools
- b) Measurement modes to operate at any stage of the production chain
- c) Implementation of an interface to enable multi-sensor operations
- d) Design of a proper user interface (GUI)

Physical test series revealed that the alignment of the axes is a critical factor for successful measurements (a). The basic design of the SCMM requires an accurate and reliable axes alignment solution to ensure that the sensing unit scans the entire surface of the specimen. Furthermore, correct alignment is necessary to keep the sensing unit normal to the surface of the specimen. Therefore, successful research had been performed to develop a novel and generic alignment process that can operate without the need for additional sensing elements (internally or externally). Furthermore, the test series verified the accuracy of the axes alignment. The presented procedure fulfils the given requirements to be a reliable, accurate, and generic axes alignment system. An updated and modified version of the alignment method may be found in Chapter 10.2.

The second (b) objective of this research was to perform research to enable the presented SCMM to operate at any stage of the production chain. Each stage in the

production process has different requirements regarding the expected accuracy and the production or measurement speed. In the early stages of the production chain, the production processes are fast and not accurate. The last stages in the production chain are slow but highly accurate. Therefore, research was performed to investigate and to develop measurement strategies beneficial for any stage of a production chain. The thriving research revealed three measurement modes - a quick and less accurate Cross-Section mode, a slow but highly accurate Track-mode and the Spiral-mode for between. Test series proof the potential of the three measurement modes at any stage of the production chain and on any style of the specimen's surface.

The usage of the SCMM at any stage of the production chain requires the application of different sensing units (c). Depending on the roughness grade of the surface of the specimen, different sensing units are necessary. Rough, structured, and non-reflective surfaces are commonly measured with tactile sensing units. Clean, smooth, and reflective surfaces are suitable for contactless sensing units such as confocal or interferometrical sensing units. Therefore, it is essential to provide an interface to change the sensing units depending on the stage of the production chain. The significant feature of the interface is the communication with the NC control of the SCMM. The specific parameters of all sensing units must be known by the NC control system to grant a proper data exchange and to avoid damages and errors because of wrong settings. Successful research had been applied to develop a reliable interface and a suitable NC control system, including a proper software package.

The last significant objective of this PhD research was to develop the control software of the SCMM (GUI) (d). The application at any stage of the production chain requires a stable and straightforward user interface. Therefore, successful research was performed to investigate the influence of the user control interface. The general usability at any stage of the production chain requires a simple concept. A user can make mistakes. Therefore, the entire positioning process, the measurement modes, and the alignment procedure have been automated. The user only has to define the general data of a specimen, such as a diameter and a curvature; all other machine settings are performed by the NC control system. This procedure reduces user indicated errors.

Most notably, the presented PhD research illustrates novel and generic approaches to enable the use of spherical coordinate measurement machines in the complete production chain of the optical industry. This research obtained significant results: The application of three measurement strategies, a new alignment procedure, a novel and patented 3D-Scale, the integration of a multi-sensor interface and a unique graphical user interface.

The presented approaches and processes are generic. This research can be adopted for other industry than the optical industry as well. The 3D-Scale is a generic device, detecting and compensating rotational errors. This device may be used in many different fields, applying rotating components. The novel centre-search-process may be used to locate the centre of rotating components, for instance, positioning systems, lathes, or milling machines. The application of pre-defined measurement strategies

and a minimised graphical user interface may find their way into several different metrology machine types.

The presented SCMM has some limitations. Since the system operates like a spherical coordinate system, the sensing unit describes a best-fit sphere. Therefore, the SCMM is recommended for symmetrical rotational specimens, especially when using tactile sensing units.

The broad scope of this PhD research revealed further fields for future research. Chapter 10 illustrates some of the most specific and exciting fields.

## 9.2 Differences to the initial PhD roadmap

The presented research has enormous scope and touches many aspects associated with metrology sciences in the optical industry. The initial goal to perform research about a metrology system useable during the entire production chain made some further sub-projects necessary. It was not possible to reach a satisfying result of this PhD research without performing research in the sub-projects. Therefore, it was necessary to change and to adjust the initial roadmap of this PhD research.

For instance, it was necessary to develop a proper research methodology designed for large research projects. The original intention was to follow Montgomery's engineering and scientific method as a guideline through this thesis. During the verification process of the developed algorithms, some reasonable questions became apparent. For example, the transfer of the theoretical mathematical

models into a functional physical prototype was a challenging task. Therefore, it became necessary to use the CAD models for the verification of the geometric relations and not only for the design of the prototype. This process enabled the qualitative and cost-efficient design of the hardware, software, and electrical components of the prototype.

Form the technical point of view, the performed research revealed the need for further processes and solutions that had not been planned. For example, the need for an alignment strategy is an essential feature. In theory, the multi-axis framework of the presented metrology system is correctly aligned, but not in reality. Therefore, research was performed to develop a proper procedure without the need for external devices. Another example is the tolerance of the used air bearings and other mechanical components including the positioning errors of all axes. Theoretically, all axes stop in the exact position. In reality, there is always a difference between the expected position and the actual position. This effect is caused by tolerances of the used components and the resolution of the used encoders and actors.

However, the development of a generic measurement device became necessary. It is named 3D Scale and enables to detect, monitor and to compensate the motion errors of rotational axes.

Concluding, a PhD is a challenging task, and maybe such research will never be finished. It teaches humility and patience towards science.

## Chapter 10

### Suggestions for future work

The results and the conclusion of this PhD research indicate that there is a demand for further research. Radial and axial runouts of the rotational B- and C-axis have a tremendous influence on the measurement result. The research was performed to monitor and to remove both effects. As a result, the 3D-scale device was developed. Furthermore, this device has a high potential to become a generic device for all kinds of rotational axes. Chapter 10.1 presents a summary of different milestones in order to develop a system ready for the market.

Another important conclusion of this PhD research had been the influence of the alignment procedure. The first version of the alignment procedure had been used during this PhD research, and it is published in Chapter A.9. A new and generic enhancement of the alignment strategy is the Centre Search 3D V3, illustrated in Chapter 10.2. This Chapter provides a short project description including a list of reasonable milestones with the goal to develop a ready for the market system.

Concerning the initial objectives of this PhD research, price sensitivity had been a goal. The sensing unit is one of the most expensive and elaborate systems in a metrology system. Therefore, research had been undertaken to develop a new and generic sensing system. Chapter 10.3 illustrates the first prototype of the new system. It had been primarily designed to operate on rough and heavily structured surfaces employing a considerable working distance.

The last suggestion for future work is a software project. The presented research showed the need for a rapid measurement mode, mainly to classify the general shape of an unknown surface or to check the progress of rough production processes such as grinding. Chapter 10.4 presents such a software solution. The essential features of the process had been included in the presented SCMM software suite, but there is still a tremendous opportunity for further research.

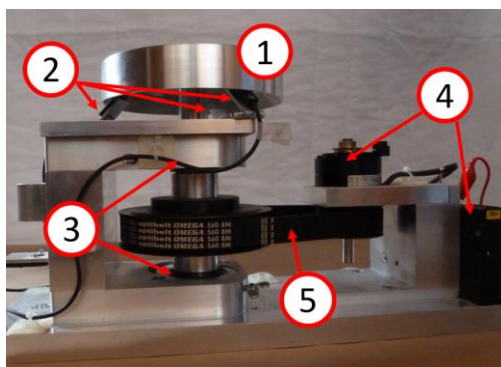
The following subchapters present and discuss the basic ideas, the latest state in the research and some ideas about the next milestones.



## 10.1 3D-scale

The 3D-scale, initially presented in Chapter 5.3, is a mechatronic device developed to improve the accuracy of rotational axes. All rotational axes are subject to the influence of axial and radial runout. Usually, radial axes are designed to operate in only one assembling position, for example, horizontal or vertical. The bearings of the rotational axes are designed to operate primarily in a given position. Measurement or production machines mostly require the 3D movement of rotational axes, for example, the SCMM or a modern turning machine.

Concerning this issue, the first version of the 3D-scale had been developed and assembled in the SCMM presented in this PhD research. The system operates only with one detector disc combined with three sensing units. The first prototype is depicted in Figure 67.



- 1: Detector disc
- 2: Sensing units
- 3: Ball bearings (C3)
- 4: Motor + controller
- 5: Teeth belt

Figure 67: 3D-scale prototype The goal of the future work is a compact and generically useable device for rotational axes.

The basic concept of the 3D-scale consists of two design features. The first feature is the usage of three sensing units in a 120° setup. The second design feature is the shape of the detector disc. The disc has a 45° chamfer close to the outer edge, as may be seen in Figure 68.

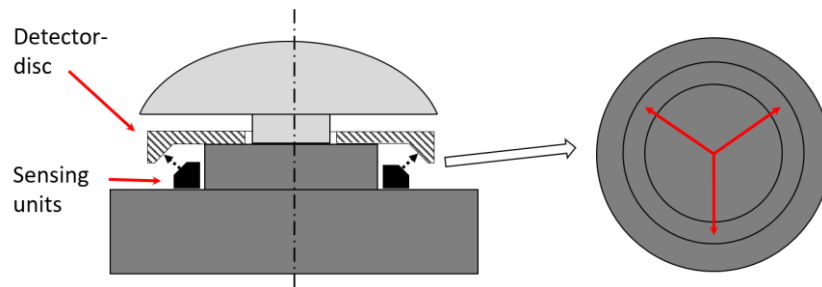


Figure 68: 3D-scale sketch The basic design and the principle are verified.

Each of the three sensing units is assembled in such a manner that the working distance is halved. That means the sensing unit can detect variations of the detector disc in both directions, towards the sensing unit and away from the sensing unit.

However, the following milestones may define the goal of the future task:

- ***Design and produce a detector disc by the application of a material with a minimum temperature coefficient.***
- ***Research concerning the interaction of needed sensing units and the new material of the detector disc.***
- ***Research regarding the influence of the geometrical dimension of the detector disc on the accuracy of the system.***
- ***Research concerning the influence of the production process on the system accuracy.***

- *Research concerning the influence of the assembling about system accuracy.*

The combination of the stated milestones may finally lead to a generic device, increasing the accuracy of rotational axes in many branches. Further details may be found in a publication of the author of this PhD thesis.

## 10.2 Centre Search 3D V2

There is an increasing demand for devices to improve the accuracy of machines. During the last years, the quality and accuracy of the axis encoder system have improved. For instance, incremental encoders have been replaced by absolute encoder systems. The Centre Search 3D V2 may present a solution of the next generation of rotational encoding systems that combines the centre search feature with a linear scale feature.

The detection of the centre of a rotating device is an essential task. This suggestion for future work combines both tasks. It may measure the distance to an object, the tilt in all direction, and it detects the deviation to the expected centre point.

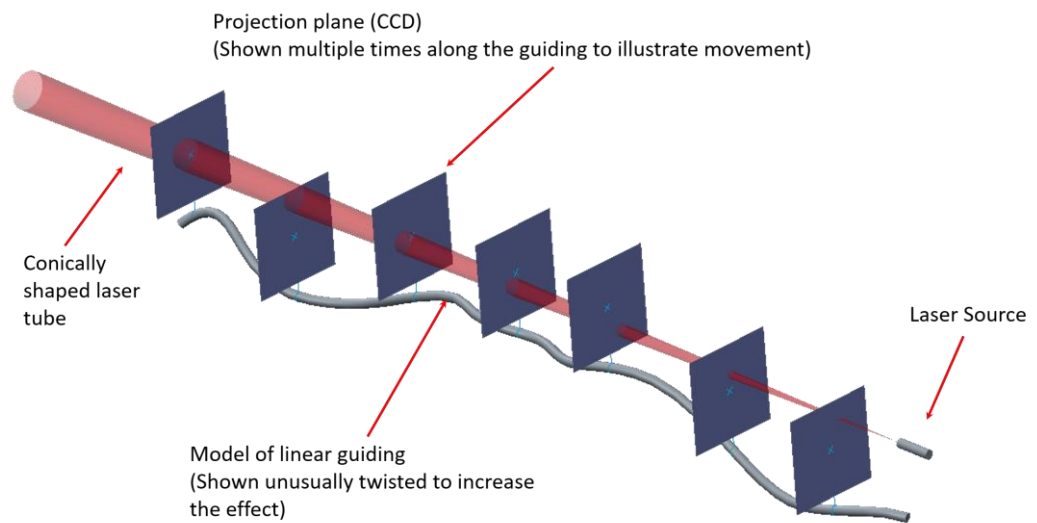


Figure 69: Concept of Centre Search 3D. The conically shaped laser beam hits the CCD sensor chip. Depending on the diameter, roundness, and lateral position of the projection of the beam on the chip, the position can be calculated in three dimensions. Furthermore, the roundness of the projection can be used to calculate the tilt with respect to the central axis of the beam.

Figure 69 illustrates the concept of the Centre Search 3D V2. It mainly consists of a conic laser beam and a high-resolution CCD sensor. The essential principle of the system uses the geometric relations of a conic-shaped laser beam. By increasing the distance between the laser source and CCD sensor, which may be used as the projection plane, the cross-section diameter of the conic-shaped beam increases. Furthermore, any tilt of the projection plane in relation to the axis of the laser beam results in an elliptical projection of the laser beam on the projection plane. Additionally, the lateral displacement of the laser beam with respect to the centre of the projection plane may be detected in a secure manner. Therefore, the distance, the tilt, and the lateral displacement of the projection plane in relation to the laser source may be detected. The natural limit of the system is the combination of the dot pitch of the CCD sensor and the angle of the conic laser beam. Future research has to overcome this issue.

However, the initial motivation for the development of this system and the reason for the name of the device had been the need for an improved centre search. Section 5.2 describes the first concept of a centre search, which had been used for the SCMM test carrier. The Centre Search 3D V2 had been designed to be the successor of the solution described in Chapter 5.2. Therefore, the detection of the centre of a rotating axis had been the initial goal.

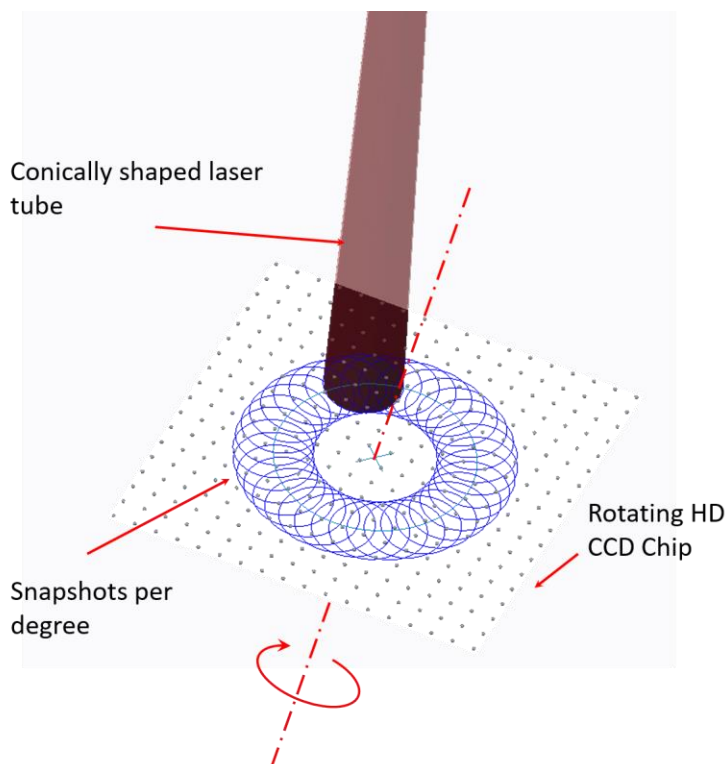


Figure 70: Centre of rotating devices detection. A conically shaped laser beam hits the detector disc in an arbitrary position. The rotation of the CCD chip transforms the projection into a circle around the central axis of the rotational axis.

Figure 70 illustrates the process of the centre-detection. The CCD sensor is fixed on rotational axes, for example, a turning machine. In an ideal setup, the laser beam creates a perfect circle in the centre of the CDD sensor. A misaligned system may cause a result, as depicted in Figure 70. The projected diameter of the conically shaped laser

beam rotates around the centre. A simple calculation of the centre point of the projected diameter leads to the radial runout of the rotational axes.

However, the combination of the presented features leads to a robust and generic device to monitor and to calibrate rotational axes as well as to use the system as axes scale for rotational axes and linear axes.

The following milestones are suggested to be carried out for future work:

- ***Rework the existing 3D model regarding state of the art CCD sensors.***
- ***Design and create a test carrier for the system to research all features***
- ***Carry out measurement series for all features***

Further details about the Centre Search 3D V3 may be found in a publication of the author of this PhD thesis.

### 10.3 The new tactile sensing unit

The comprehensive test series conducted with the prototype of the SCMM reveals a need for cheap but accurate tactile sensing units. The rough surfaces of ground or cut surfaces cannot be served with contactless sensing units due to physical reasons (ref. Chapter 2.3.1). However, the test series had mostly been carried out on brittle and harsh surfaces, such as different types of glass and ceramics (ref.2.1.1). Because of the test series, the sensing units had worn out quickly. Especially during measurement, in particular at long-term measurements, this effect negatively influences the

measurement result. As the main reason for the wear out, the energetic vibrations had been detected. However, sensing units are usually costly, and mainly research laboratories and small companies do not have a variety of sensing units to compensate for the outage time until the service centre finished the maintenance and recalibration.

Therefore research has been carried out to find a suitable solution for the test series with the SCMM prototype.

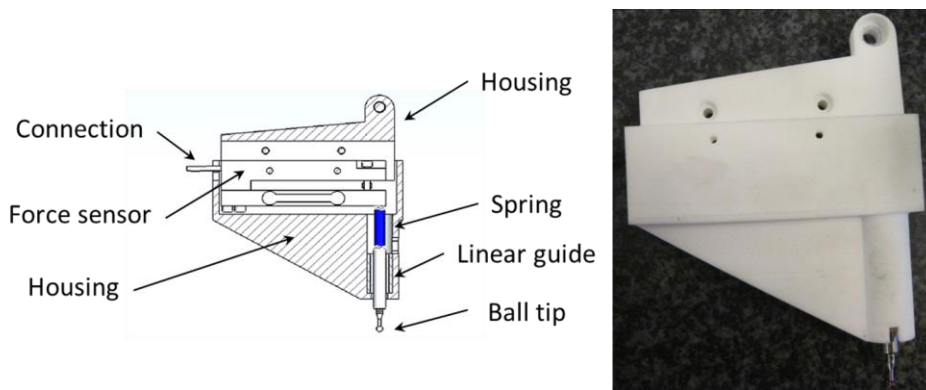


Figure 71: Prototype of a new tactile sensing unit. The sensing unit consists of a ball tip that compresses a spring against a force sensor.

Figure 71 illustrates the prototype of the new tactile sensing unit. This sensing unit operates according to the well-known principle of a bending beam. The sensing tip is fixed on the bending beam and slides through a linear guide. The axial movement of the tip interacts with the force sensor. All parts of the sensor device are assembled in a closed housing to reduce the influence of the environment. The presented prototype had been tested successfully in several testing series. The results may be found detailed in another publication of the author of this PhD thesis. Furthermore, a second prototype had been created; this prototype may be the base for future research.

The next milestones of this suggestion of future work are:

- ***Carry out test series with the second prototype and generate test results for deformation analysis.***
- ***Create a compensation tool and compensation strategy to calibrate the sensing unit.***
- ***Design the pre-series version of the sensing unit and design the production process.***

#### 10.4 Full 3D Cross-section-mode

To generate a full three-dimensional surface just by calculating the results given by a set of cross-sections is the primary goal of the fourth suggestion of future work. There are already measurement systems in the market operating with cross-sections. For example, the Mahr™ Tallysurf™ series is a metrology device operating with cross-sections.

However, the SCMM design allows for operation in cross-sections as well. This measurement-mode claims to be very quick, and it seems to be the best option for rough surfaces, especially in the early steps of the production chain. In contrast to the current metrology devices, the spherical coordinate measurement device is not limited to only one operation mode. This Cross-section-mode completes the range of available measurement modes of the spherical coordinate measurement machine. Therefore, research has to overcome the issues regarding the 3D Cross-section-mode. The main



task of the future work is to develop algorithms and methods to enable a reliable and accurate surface generation.

The essential milestones of a future project in the field of the 3D Cross-section-mode are:

- ***Design algorithms to reduce the number of needed cross-sections without losing accuracy.***
- ***Carry out test series and compare the results with a different number of cross-sections and measurement points.***
- ***Compile the software tool into a generic software tool with a connection to the spherical coordinate measurement machine.***

## References

- [1] J. Bliedtner and G. Graefe, *Optiktechnologie [Technology of optics]*. Grundlagen, Verfahren, Anwendungen, Beispiele [Basics, methods, applications, examples], 2nd ed. Munich, Germany: Carl Hanser Fachbuchverlag, 2010.
- [2] E. Brinksmeier, O. Riemer, and R. M. Glaebe, Eds., *Fabrication of Complex Optical Components*. Berlin, Heidelberg, Germany: Springer Berlin Heidelberg, 2013.
- [3] M. Schinhaerl, F. R. Schneider, R. Rascher, C. Vogt, and P. Sperber, "Relationship between influence function accuracy and polishing quality in magnetorheological finishing," in *Advanced optical manufacturing technologies: 5th International Symposium on Advanced Optical Manufacturing and Testing Technologies, [AOMATT] ; 26 - 29 April 2010, Dalian, China, 2010*.
- [4] OSA Publishing, Ed., *Optical fabrication and testing: [part of] International Optical Design Conference and Optical fabrication and testing ; 13 - 17 June 2010, Jackson Hole, Wyoming, United States*. Washington, DC: OSA The Optical Society, 2010.
- [5] M. Schinhaerl, C. Vogt, F. R. Schneider, P. Sperber, and R. Rascher, "Investigations on Magnetorheological Finishing of High-Quality Optical Surfaces with Varying Influence Function," in *Optical fabrication and testing: [part of] International*

*Optical Design Conference and Optical fabrication and testing ; 13 - 17 June 2010, Jackson Hole, Wyoming, United States, 2010.*

- [6] C. Vogt, M. Schinhaerl, F. R. Schneider, P. Sperber, and R. Rascher, "Investigations on Grinding Tools for Silicon Carbide Based Advanced Materials," in *Optical fabrication and testing: [part of] International Optical Design Conference and Optical fabrication and testing ; 13 - 17 June 2010, Jackson Hole, Wyoming, United States, 2010.*
- [7] O. W. Faehnle, R. Williamson, and D. W. Kim, Eds., *SPIE Optical Engineering + Applications*: SPIE, 2013.
- [8] C. Vogt *et al.*, "An Experimental Study on a Flexible Grinding Tool," in *ADVANCED MATERIALS RESEARCH*, vol. 325, *ADVANCED MATERIALS RESEARCH: Advances in Abrasive Technology XIV*, Tawakoli T, Ed.: Scientific.net, 2011, pp. 91–96.
- [9] Tawakoli T, Ed., *ADVANCED MATERIALS RESEARCH: Advances in Abrasive Technology XIV*: Scientific.net, 2011.
- [10] F. R. Schneider, R. Maurer, R. Rascher, R. Stamp, and G. Smith, "Analysis of three different measurement strategies carried out with the TII-3D coordinate measurement system," in *SPIE Optical Engineering + Applications*, San Diego, California, United States, 2013.
- [11] A. F. Kunz, "Aspheric Freedoms of Glass," *Optik & Photonik*, vol. 4, pp. 46–48, 2009.
- [12] M. J. Digonnet and S. Jiang, Eds., *OPTICAL COMPONENTS AND MATERIALS XV*: SPIE PRESS, 2018.

- [13] *Melles Griot*. [Online] Available: <http://mellesgriot.com/>. Accessed on: Nov. 19 2015.
- [14] R. W. Tustison, Ed., *Defense and Security*: SPIE, 2005.
- [15] H. P. Stahl, "Aspheric surface testing techniques," in *San Diego - DL Tentative*, San Diego, CA, 1991, pp. 66–76.
- [16] P. E. Murphy, J. Fleig, G. Forbes, and M. Tricard, "High precision metrology of domes and aspheric optics," in *Defense and Security*, Orlando, FL, 2005, pp. 112–121.
- [17] P. H. Lehmann, Ed., *SPIE Europe Optical Metrology*: SPIE, 2009.
- [18] M. F. Kuechel, "Interferometric measurement of rotationally symmetric aspheric surfaces," in *SPIE Europe Optical Metrology*, Munich, Germany, 2009.
- [19] C. P. Grover, Ed., *San Diego - DL Tentative*: SPIE, 1991.
- [20] R. Huang *et al.*, "Measuring aspheric surfaces with reflection deflectometry," *SPIE Newsroom*, 2013.
- [21] Coord3 Industries, *Coordinate Measuring Machine History – Fifty Years of CMM History leading up to a Measuring Revolution*. [Online] Available: <https://tinyurl.com/y6tdlrre>. Accessed on: Aug. 19 2015.
- [22] F. R. Schneider, R. Rascher, and C. Wuensche, "Measurement of a freeform object with the TII-3D measurement system," in *Freeform Optics 2013: Topics in Freeform Surfaces (FW2B)*, Tucson, Arizona United States, 2013, p. 6.
- [23] F. R. Schneider, R. Rascher, R. Stamp, and G. Smith, "A simple procedure to include a free-form measurement capability to standard coordinate measurement machines," in *SPIE Optifab*, Rochester, New York, USA, 2013.

- [24] Fraunhofer Institute for production technologies IPT, Ed., *CAX Technologies – Ultra precision optics machining*. 52074 Aachen, Germany: Fraunhofer Institute for Production Technology IPT.
- [25] A. Weckenmann, J. Hoffmann, and P. Kraemer, “Manufacturing Metrology - State of the Art and Prospects,” in *Proceedings of the 9th International Symposium on Measurement and Quality Control in Production: November 21 - 24, 2007, Chennai, India*, Chennai: Manufacturing Engineering Section Dep. of Mechanical Engineering Indian Inst. of Techn. Madras, 2007, pp. 1–8.
- [26] WENZEL Praezision GmbH, *CMM RAplus*. [Online] Available: <https://tinyurl.com/y5c5y7sf>. Accessed on: Mar. 01 2016.
- [27] Werth Messtechnik, *Werth ProbeCheck - Werth Messtechnik*. [Online] Available: <https://tinyurl.com/y58rzkah>. Accessed on: Mar. 01 2016.
- [28] R. Christoph and H. J. Neumann, *Multisensor-Koordinatenmesstechnik [Multisensor coordinate metrology]*. Maß-, Form- Lage- und Rauheitsmessung ; optisch, taktil und röntgentomografisch [Dimensional Measurement Using Optics, Probes, and X-ray Tomography], 3rd ed. Landsberg/Lech: Verl. Moderne Industrie, 2006.
- [29] R. K. Leach, “Coordinate metrology,” in *Micro and nanotechnologies, Fundamental principles of engineering nanometrology*, R. K. Leach, Ed., 1st ed., Amsterdam: Elsevier William Andrew, 2010, pp. 263–288.
- [30] C. Bond, *Photonics Applied: Metrology:: Stitching interferometers: Direct imaging aids asphere metrology*. [Online] Available: <https://tinyurl.com/y3mc5uxy>. Accessed on: Sep. 12 2015.

- [31] International Measurement Confederation; International Symposium on Measurement and Quality Control in Production; ISMQC, *Proceedings of the 9th International Symposium on Measurement and Quality Control in Production: November 21 - 24, 2007, Chennai, India*. Chennai: Manufacturing Engineering Section Dep. of Mechanical Engineering Indian Inst. of Techn. Madras, 2007.
- [32] F. Z. Fang, X. D. Zhang, A. Weckenmann, G. X. Zhang, and C. Evans, "Manufacturing and measurement of freeform optics," *CIRP Annals - Manufacturing Technology*, vol. 62, no. 2, pp. 823–846, 2013.
- [33] K.-C. Fan, "A non-contact automatic measurement for free-form surface profiles," *Computer Integrated Manufacturing Systems*, vol. 10, no. 4, pp. 277–285, 1997.
- [34] precizika, *CMM TIGO SF: TIGO SF versatile, air-free high performance Coordinate Measuring Machine*. [Online] Available: <https://tinyurl.com/y5lcr74t>. Accessed on: Mar. 01 2016.
- [35] J. A. Bosch, P. H. Pereira, and R. J. Hocken, Eds., *Coordinate measuring machines and systems*, 2nd ed. Boca Raton, FL: CRC/Taylor & Francis, 2012.
- [36] J. M. Bennett and H. Vogeley Gourley, Eds., *Surface Measurement And Characterization*, 1009th ed.: SPIE, 1989.
- [37] W. B. Ribbens, "Interferometric Surface Roughness Measurement," *Appl. Opt.*, vol. 8, no. 11, p. 2173, 1969.
- [38] M. Stedman, "Limits Of Surface Measurement By Optical Probes," in *Surface Measurement And Characterization*, Hamburg, Germany, 1989, pp. 62–67.

- [39] Donald Golini, "A brief history of QED Technologies: Chapter VII," in *A jewel in the crown: Essays in honor of the 75th anniversary of the Institute of Optics*, C. Stroud, Ed., Rochester, NY: Meliora Press, 2004, pp. 313–318.
- [40] W.-H. Lee, "III Computer-Generated Holograms: Techniques and Applications," in *Progress in Optics, Progress in optics*, E. Wolf, Ed., Amsterdam, Oxford: North-Holland Publishing Co, 1978, pp. 119–232.
- [41] *DIN EN ISO 10360-2:2010-06, Standard - Beuth.eu*, DIN EN ISO 10360-2:2010-06, 2010.
- [42] D. S. Anderson and J. H. Burge, "Swing-arm profilometry of aspherics," in *Advanced Technology Optical Telescopes I: PROCEEDINGS VOLUME 0332*, 1982, pp. 169–179.
- [43] Anderson, D.S., Parks, R.E., Shao, T., "A versatile profilometer for the measurement of aspherics," in *Proceeding of OF&T, Volume 11, Workshop Technical Digest, Optical fabrication and testing (OF&T)*, Ed., pp. 119–122.
- [44] J. R. P. Angel and R. E. Parks, "Generation Of Off-Axis Aspherics," in *Advanced Technology Optical Telescopes I: PROCEEDINGS VOLUME 0332*, 1982, pp. 316–327.
- [45] P. Su, Y. Wang, C. J. Oh, R. E. Parks, and J. H. Burge, "Swing arm optical CMM: Self calibration with dual probe shear test," in *SPIE Optical Engineering + Applications*, San Diego, California, USA, 2011.
- [46] P. Su, C. J. Oh, R. E. Parks, and J. H. Burge, "Swing arm optical CMM for aspherics," in *Proceedings of SPIE - The International Society for Optical Engineering: Introduction*, San Diego, CA, 2009.

- [47] P. Su, "Swing-arm optical coordinate measuring machine: Modal estimation of systematic errors from dual probe shear measurements," *Opt. Eng.*, vol. 51, no. 4, 2012.
- [48] H. Jing, C. King, and D. Walker, "Measurement of influence function using swing arm profilometer and laser tracker," (eng), *Optics express*, vol. 18, no. 5, pp. 5271–5281, 2010.
- [49] H. Jing, C. King, and D. Walker, "Simulation and validation of a prototype swing arm profilometer for measuring extremely large telescope mirror-segments," (eng), *Optics express*, vol. 18, no. 3, pp. 2036–2048, 2010.
- [50] G. T. Smith, *Machine tool metrology: An industrial handbook*. [Cham], Switzerland: Springer, 2016.
- [51] H. Liang, H. Hong, and J. Svoboda, "A Combined 3D Linear and Circular Interpolation Technique for Multi-Axis CNC Machining," *J. Manuf. Sci. Eng.*, vol. 124, no. 2, p. 305, 2002.
- [52] S. Ekinovic, E. Begović, I. Plančić, and E. Ekinovic, *CHECKING THE GEOMETRICAL ACCURACY OF MACHINE TOOLS*, 2015.
- [53] M. Schinhaerl and F. R. Schneider, "Procedure and device to detect and the movements of a rotating device," P-500725-DE, Germany 10 2010 000 655.6.
- [54] R. Maurer *et al.*, "Physical marker based stitching process of circular and non-circular interferograms," in *Modeling aspects in optical metrology III: 23 - 24 May 2011, Munich, Germany ; [part of the SPIE Optical Metrology Symposium]*, 2011.
- [55] M. Bray, "Stitching interferometry: how and why it works," in *Singapore*, Singapore, 1991, pp. 259–273.



- [56] S. DeFisher, "Advancements in non-contact metrology of asphere and diffractive optics," in *Optifab 2017*, Rochester, United States, 2017, p. 50.
- [57] S. DeFisher, E. Fess, and G. Matthews, "Form, figure, and thickness measurement of freeform and conformal optics with non-contact sensors," in *SPIE Window and Dome Technologies 2015*.
- [58] S. DeFisher, G. Matthews, and E. Fess, "Validation of accuracy and repeatability of UltraSurf metrology on common optical shapes," in *Optifab 2015*.
- [59] S. DeFisher, G. Matthews, and J. Ross, "New advancements in freeform optical metrology," in *SPIE Defense + Security Window 2017*.
- [60] Werth Messtechnik, *Werth VideoCheck Fixed-Bridge - Werth Messtechnik*. [Online] Available: <https://tinyurl.com/y5hcnqtp>. Accessed on: Mar. 01 2016.
- [61] D. C. Montgomery, G. C. Runger, and N. F. Hubele, *Engineering statistics*, 5th ed. Hoboken, NJ: John Wiley, 2011.
- [62] Florian Richard Schneider, "Topographische Koordinatenmessmaschine TII-3D [Topographical coordinate measurement machine TII 3D]: Topographical coordinate measurement machine TII-3D," *Untertitel - Das Magazin der Hochschule Deggendorf*, vol. 2013, p. 52, 2013.
- [63] Y. Wang, "Swing arm optical coordinate-measuring machine: High precision measuring ground aspheric surfaces using a laser triangulation probe," *Opt. Eng.*, vol. 51, no. 7, p. 73603, 2012.
- [64] R. Maurer, F. R. Schneider, C. Wuensche, and R. Rascher, "Calculation of the reference surface error by analyzing a multiple set of sub-measurements," in

*Optical Manufacturing and Testing X*, San Diego, California, United States, 2013, 88380E.

- [65] F. R. Schneider *et al.*, “Effects of mechanical inaccuracies on the measurement result in metrology systems,” in *Advanced optical manufacturing technologies: 5th International Symposium on Advanced Optical Manufacturing and Testing Technologies, [AOMATT] ; 26 - 29 April 2010, Dalian, China*, 2010.
- [66] W. Gautschi, “Orthogonal polynomials (in Matlab),” *Journal of Computational and Applied Mathematics*, vol. 178, no. 1-2, pp. 215–234, 2005.
- [67] C. B. Moler, *Numerical computing with MATLAB*. Philadelphia, Pa.: Society for Industrial & Applied Mathematics, 2011.
- [68] C. Vilau, Balc, N., Leordean, D., and C. Cosma, “STATIC ANALYSIS TO REDESIGN THE GRIPPER, USING CREO PARAMETRIC SOFTWARE TOOLS,” in *Academic Journal of Manufacturing Engineering 2015*, pp. 77–82.
- [69] G. He, L. Guo, S. Li, and D. Zhang, “Simulation and analysis for accuracy predication and adjustment for machine tool assembly process,” *Advances in Mechanical Engineering*, vol. 9, no. 11, 2017.
- [70] FULAN OPTICS MACHINE CO., LTD, *Spherical generator, Lens Curve Generator, Spherical Grinding Machine - precision optics machine, electronic material machine, ophthalmic machine, optical equipment, ophthalmic instrument*. [Online] Available: <https://tinyurl.com/y5o3sre4>. Accessed on: Dec. 08 2017.
- [71] DR. JOHANNES HEIDENHAIN GmbH, *HEIDENHAIN-CERTO: Heidenhain Certo CT 2502*. [Online] Available: [https://www.heidenhain.de/de\\_EN/products/length-gauges/product-overview/certo/](https://www.heidenhain.de/de_EN/products/length-gauges/product-overview/certo/). Accessed on: Aug. 15 2018.

- [72] Heidenhain, *HEIDENHAIN-CERTO*. [Online] Available:  
<https://tinyurl.com/y52bvw9f>.
- [73] Wikipedia, *Michelson–Morley experiment - Wikipedia, the free encyclopedia*.  
[Online] Available: <https://en.wikipedia.org/w/index.php?oldid=674732764>.  
Accessed on: Aug. 19 2015.
- [74] D. Malacara, *Optical shop testing*, 3rd ed. Hoboken, NJ: Wiley; Wiley-Interscience,  
2007.
- [75] Organización Internacional de Normalización, *ISO 10110-11: Optics and optical  
instruments : preparation of drawings for optical elements and systems*, 1st ed.  
Genève: ISO, 1996.
- [76] Juergen Petter, Ed., *OP4 - Multi Wavelength Interferometry for High Precision  
Distance Measurement*. AMA Service GmbH, P.O. Box 2352, 31506 Wunstorf,  
Germany, 2009.
- [77] Dr. Gernot Berger, *Laserbased distance measurement system MWLI*. Technical  
datasheet.
- [78] Dr. Gernot Berger, *MWLI Sensorkopf-Abmessungen (MWLI sensing unit head  
dimensioning)*. Technical data sheet.
- [79] Micro-Epsilon Messtechnik GmbH & Co. KG, *confocalDT Confocal chromatic  
measuring system*. [Online] Available: <https://tinyurl.com/y2uzx8ye>. Accessed on:  
Aug. 15 2018.
- [80] Micro-Epsilon Messtechnik GmbH & Co. KG, *Confocal miniature sensors for  
displacement*. [Online] Available: <https://tinyurl.com/y6lf73mv>. Accessed on: Nov.  
19 2015.

- [81] L. Zhang and W. Liu, "Precision glass molding: Toward an optimal fabrication of optical lenses," *Front. Mech. Eng.*, vol. 12, no. 1, pp. 3–17, 2017.
- [82] A.-T. Vu, H. Kreilkamp, O. Dambon, and F. Klocke, "Nonisothermal glass molding for the cost-efficient production of precision freeform optics," *Opt. Eng.*, vol. 55, no. 7, 2016.
- [83] H. Kreilkamp, O. Dambon, F. Klocke, and T. Grunwald, "Analysis of form deviation in non-isothermal glass molding," in *OPTICAL COMPONENTS AND MATERIALS XV*, San Francisco, United States, 2018, p. 25.
- [84] O. Dambon *et al.*, "Efficient mold manufacturing for precision glass molding," *J. Vac. Sci. Technol. B*, vol. 27, no. 3, p. 1445, 2009.
- [85] T. Zhou, J. Yan, and T. Kuriyagawa, "High-Efficiency and Ultra-precision Glass Molding of Aspherical Lens and Microstructures: Report from Proceedings of ISUPEN 2011," *Proceedings of ISUPEN 2011*, vol. 2011, <https://tinyurl.com/y4otl2j6>, 2011.
- [86] *DIN 8580:2003-09: Manufacturing processes - Terms and definitions, division*. Beuth Verlag GmbH: Beuth Verlag GmbH, 2003.
- [87] L. Yang, Ed., *Advanced optical manufacturing technologies: 5th International Symposium on Advanced Optical Manufacturing and Testing Technologies, [AOMATT]; 26 - 29 April 2010, Dalian, China*. Bellingham, Wash.: SPIE, 2010.
- [88] R. E. Fischer and B. Tadic-Galeb, *Optical system design: Chapter 17 Optical Design Considerations for Optics Fabrication*. New York: McGraw-Hill, 2000.
- [89] Deutsches Institut für Normung, *Grundlagen der Meßtechnik: DIN 1319 = Fundamentals of metrology*. Berlin: Beuth, 1995.

- [90] *DIN 1319-1:1995-01: Fundamentals of metrology - Part 1: Basic terminology*. Berlin: Beuth, 1995.
- [91] *DIN 1319-2:2005-10: Fundamentals of metrology - Part 2: Terminology related to measuring equipment*, 2005th ed. Berlin: Beuth, 2005.
- [92] *DIN 1319-3:1996-05: Fundamentals of metrology - Part 3: Evaluation of measurements of a single measurand, measurement uncertainty*. Berlin: Beuth, 1996.
- [93] Deutsches Institut für Normung e.V., *DIN 1319-4:1999-02: Fundamentals of metrology - Part 4: Evaluation of measurements; uncertainty of measurement*.
- [94] *DIN V ENV 13005:1999-06: Guide to the expression of uncertainty in measurement; German version ENV 13005:1999*. Berlin: Beuth, 1999.
- [95] *DIN 8593-0:2003-09 Manufacturing processes joining - Part 0: General; Classification, subdivision, terms and definitions*, 9, 2003.
- [96] Renishaw plc, *Incremental optical linear and rotary encoders*. [Online] Available: <https://tinyurl.com/yyack95g>. Accessed on: Aug. 28 2018.851Z.
- [97] J. F. Cuttinoa, D. E. Schinstock, and M. J. Prather, "Three-dimensional metrology frame for precision applications," *Precision Engineering*, vol. 23, no. 2, pp. 103–112, 1999.
- [98] H. D. Young, R. A. Freedman, A. L. Ford, M. W. Zemansky, and F. W. Sears, *Sears and Zemansky's university physics*, 12th ed. San Francisco [Calif.]: Pearson Addison-Wesley, 2008.
- [99] I. N. Bronštejn *et al.*, *Handbook of mathematics*, 9th ed. Haan-Gruiten: Verl. Europa-Lehrmittel; Deutsch, 2013 // 1985.

- [100] L. Papula, *Mathematik für Ingenieure und Naturwissenschaftler [Mathematics for engineers and scientists]*, 10th ed. Braunschweig: Vieweg, 2001.
- [101] L. Papula, *Mathematische Formelsammlung für Ingenieure und Naturwissenschaftler [Mathematical formulaic collection for engineers and scientists]*, 11th ed. Wiesbaden: Springer Vieweg, 2014.
- [102] C. B. Markwardt, "Non-linear Least Squares Fitting in IDL with MPFIT," *Proc. ADASS XVIII*, <http://arxiv.org/pdf/0902.2850v1>.
- [103] G. H. Golub and C. F. van Loan, *Matrix computations*, 3rd ed. Baltimore: Johns Hopkins Univ. Press, 1996.
- [104] Trioptics GmbH, "μPhase® & μShape," <https://tinyurl.com/yy7a52np>.

## Appendix A

### Index of appendices

A.01 Project EMMA.....	188
A.02 Designs of metrology systems .....	190
A.03 Commonly used materials for optical elements.....	200
A.04 Common optical shapes and elements .....	202
A.05 Sensing units implemented in the SCMM .....	219
A.06 Manufacturing machines and processes in the optical industry.....	227
A.07 Uncertainty estimation of the SCMM.....	237
A.08 The 3D-Scale .....	273
A.09 Centre Search process .....	285
A.10 Measurement strategies.....	297
A.11 Methodology and approach .....	312
A.12 The SCMM software tools .....	318
A.13 Matlab™ source code for XYZ coordinate transformation verification.....	349
A.14 Matlab™ source code for A-axis angle alpha verification .....	351
A.15 Publication 01	
Relationship between influence function accuracy and polishing quality in magnetorheological finishing.....	353
A.16 Publication 02	
Effects of mechanical inaccuracies on the measurement result in metrology systems .....	354

---

A.17 Publication 03	
Investigations on Grinding Tools for Silicon Carbide Based Advanced Materials.....	355
A.18 Publication 04	
Investigations on Magnetorheological Finishing of High-Quality Optical Surfaces with Varying Influence Function .....	356
A.19 Publication 05	
Physical marker based stitching process of circular and non-circular interferograms.....	357
A.20 Publication 06	
An Experimental Study on a Flexible Grinding Tool .....	358
A.21 Publication 07	
Calculation of the reference surface error by analysing a multiple set of sub-measurements.....	359
A.22 Publication 08	
Analysis of three different measurement strategies carried out with the TII-3D coordinate measurement system .....	361
A.23 Publication 09	
A simple procedure to include a free-form measurement capability to standard coordinate measurement machines.....	363
A.24 Publication 10	
Measurement of a freeform object with the TII-3D measurement system.....	365
A.25 Publication 11	
Tactile and contactless measurement of an optical surface.....	366



## A.1 Project EMMA

In 2009, the University of Applied Sciences Deggendorf started a BMBF<sup>24</sup> funded project named EMMA. EMMA is the acronym for the German sentence “Entwicklung einer flexiblen, modularen Messtechnik für die Fertigung von hochpräzisen Asphären und Freiformen“. Translated into the English language “Development of a modular and flexible metrology system to aid the demand for aspherical and free-form shaped objects”.

This project may be seen as the foundation and inspiration for this thesis. The project EMMA, completed at the Deggendorf Institute of Technology<sup>25</sup>, started to develop such a multi-sensor metrology solution for planar, spherical, aspherical, and free-form shaped objects. This Chapter provides a brief description of the primary goals of the project EMMA and its influence regarding this thesis. The objective was to develop a suitable metrology solution to cover the complete production process performed in the optical industry. This goal may be reached by developing a multi-axis coordinate measurement machine based on the mathematical spherical coordinate system. Up to now, there is no known mass-produced coordinate measurement machine in the optical industry, which uses this kind of design. The significant benefit of the spherical coordinate measurement system is that the number of axes needed for the measurement of an object under test can be reduced to 1.5 rotational axes. The first

---

<sup>24</sup> BMBF: Bundesministerium für Bildung und Forschung – Federal Ministry of Education and Research

<sup>25</sup> TH Deg; Technische Hochschule Deggendorf – Deggendorf Institute of Technology

axes carry and move the object under test, the second axis moves the sensing unit across the surface, but it is locked during the actual measurement process.

#### A.1.1 History:

The primary goal of the project EMMA was to develop a suitable measurement solution to measure aspherical and free-formed optical devices. This goal should be reached by upgrading and enhancing an old measurement system named TII-3D. The University of Applied Sciences Deggendorf owns two of these measurement systems. In the early beginning of the project, it transpired that both systems could not operate as required, have critical malfunctions, and finally, both systems suffered a total system breakdown. To keep the project running, the University of Applied Sciences Deggendorf decided to rebuild and redesign the complete measurement system. Since both systems had been old-fashioned prototypes without any support of the original manufacturer, it was necessary to develop an entirely new state of the art numeric control system, replace and redesign all electrical and electronic components and finally to develop utterly new control and analysis software. All efforts finally lead to the successful completion of the project EMMA.

## A.2 Designs of metrology systems

The metrology science in the optical industry mostly operates by employing two different main groups of measurement machines – Interferometers and coordinate measurement machines.

### A.2.1 Interferometer concepts

This section presents the four main categories of interferometer concepts.

#### A.2.1.1 Michelson interferometer

The Michelson interferometer is the reference design for interferometers used in the optical industry. Albert Abraham Michelson invented this measurement device, based on the famous Michelson-Morley experiment from 1887 [73].

The basic setup is straightforward and illustrated in Figure 72. A laser source emits a laser beam towards a partially reflective mirror fixed at 45° to the emitted laser beam. The beam is divided into two parts, one part travels towards the object to be measured, and the second part travels towards a high-quality planar reference mirror. Both beams are supposed to be reflected from their targets back to the partially reflective mirror that reflects the beams to the CCD chip.

Both beams interference together and the well-known Newton's rings appear and can be analysed by a computer system by using analysis software.

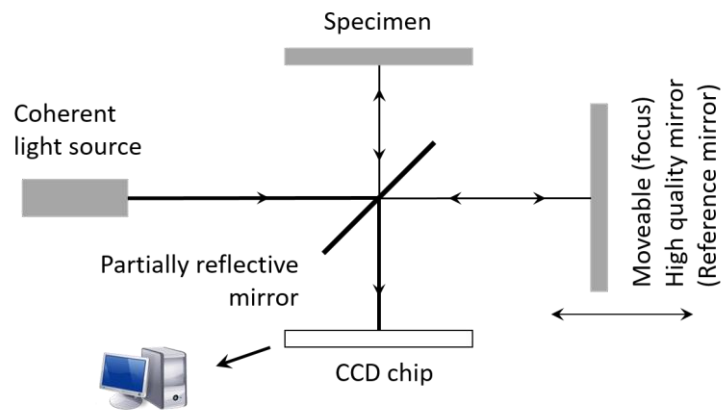


Figure 72: Michelson interferometer

### A.2.1.2 Twyman-Green interferometer

Twyman and Green 1916 developed the Twyman-Green interferometer. Both the Michelson and the Twyman-Green interferometer are nearly identical. There are only two significant differences in the setup. The coherent light source of the Michelson interferometer changed to a monochrome laser source, and the Twyman-Green interferometer uses some collimating lenses to expand the laser beam. Figure 73 shows a simple interferometer setup according to Twyman-Green to operate on a spherical object [74, pp. 46-48].

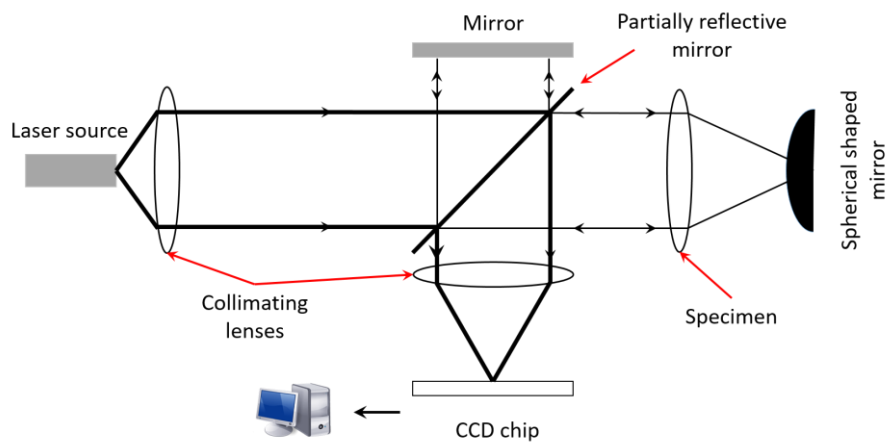


Figure 73: A Twyman-Green interferometer

A.2.1.3 Fizeau interferometer

The Fizeau interferometer is the standard interferometer used in the optical industry. The exclusive benefit of this interferometer design is that the reference and measurement beam follow the same path. This benefit enables a very compact design. In this design, the laser source emits the laser that is filtered and expanded by the spatial filter. The beam travels through the partially reflective mirror towards a collimator lens. The collimator collimates the light into a parallel beam. After that modification, the beam passes the first mirror, the reference mirror, almost unhindered, and is reflecting on the object under test. In the optical path backwards, both beams are deflected by the semipermeable mirror and guided to the CCD chip [74, pp. 17-20]. A computer system does the analysis of the superimposed signal with an appropriate software tool.

Figure 74 illustrates a schematic sketch of the Fizeau-interferometer.

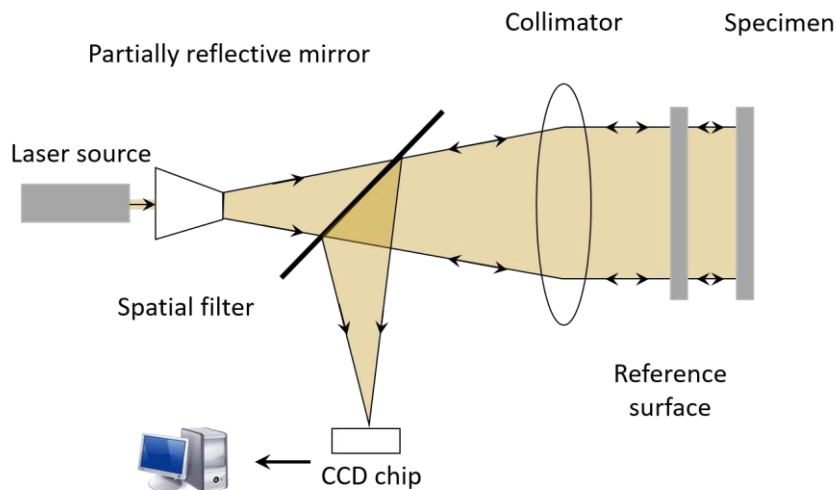


Figure 74: Fizeau interferometer

#### A.2.1.4 Stitching Interferometer – SSI

The stitching technology for planar and spherical elements was developed by a company named QED™<sup>26</sup> in 2004 [39]. Later developments published in 2007 and 2009 presented a feature to measure aspheres.

This technology can be used to measure objects that are bigger than the aperture of the used interferometer. The fundamental principle behind the stitching technology is depicted in Figure 75. The object under test and the interferometer move in defined positions. It is essential that the interferometer is aligned with the normal of the spot to be measured and that the sub-apertures overlap. After all single measurements have been carried out and recorded, all measurement results are sewed, or stitched, together to one pre-final measurement result that includes all single measurements. Some error calculations are applied to the pre-measurement result [55] to finalise the measurement result. Figure 75 presents the working principle of the stitching interferometry.

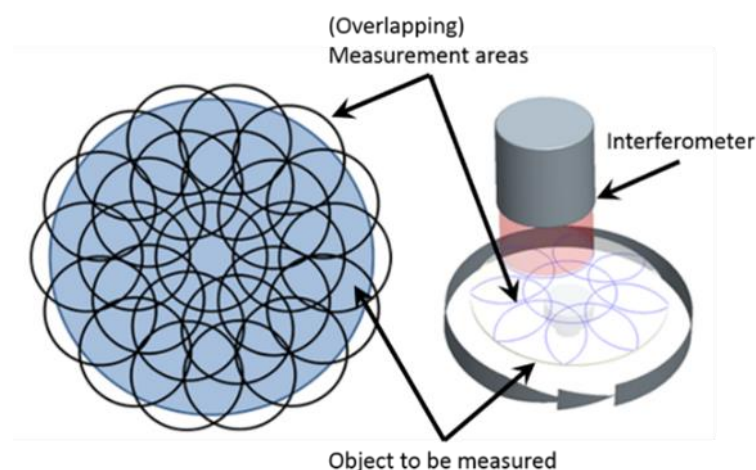


Figure 75: Stitching Interferometry

<sup>26</sup> QED™: QED™ TECHNOLOGIES, a CMC Company; 1040 University Avenue, Rochester, NY 14607 USA

## A.2.2 Coordinate measurement machine concepts

The four main categories of coordinate measurement machines are presented in this Chapter.

### A.2.2.1 Cantilever design

The cantilever design consists of a ridged and in Z-direction moveable cantilever that carries the sensing unit. The Z-axis construction with the cantilever and the sensing unit can be moved along the Y-axis that is assembled on the main table. The object under test is mostly fixed on a table construction with travels along the X-axis. The movement of all three rectangular to each other mounted axes allows the measurement system to reach each unique point on the object under except the bottom.

This design is commonly used for smaller measurement systems, often used in the Quality Management and audit rooms of the automobile industry. In the optical industry, such a design is often used for profilometers in the medium accuracy level in the lower micrometre range.

Due to the large cantilever that is only fixed on one side, this design is very addictive to environmental influences like vibration and thermal issues. Further, if used in combination with tactile sensing units, it is liable to the forces caused by the measurement process itself.

The significant advantage of this system is the cost-efficient design with only three standard linear guidings and some granite blocks. Figure 76 presents a sketch of a cantilever design.

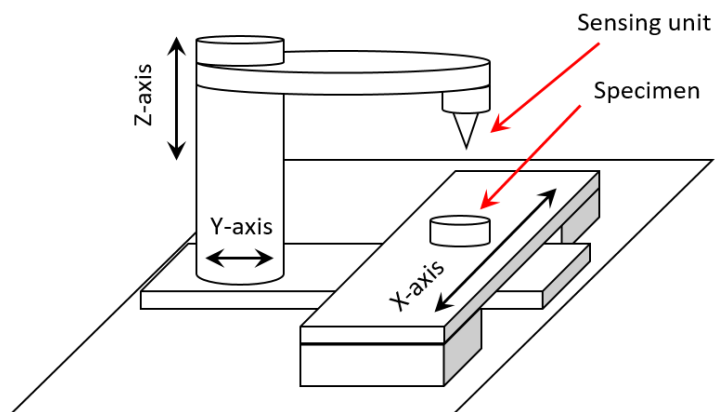


Figure 76: 3D sketch of the CMM cantilever design



### A.2.2.2 Bridge design

The bridge design is very often used for measurements of large objects, for example, sheet metal parts of the automotive and aircraft industry.

The feature of this design is that the system is divided into two primary assemblies. The first assembly represents the bridge construction, including the Y-axis, and the Z-axis carries the sensing unit. The sensing unit can be moved from one side of the bridge to the other by travelling along the Y-axis, and it can move up and down by using the Z-axis. The complete bridge assembly can travel along the X-axis from the front to the back.

The second assembly consists of the fixing elements for the object under test. It can be installed somewhere on the ground under the reachable area of the bridge. This setup enables us to operate in a large volume. The measurement accuracy depending on the size of the design to be measured. Equipped with high-quality air-guiding it is still possible to reach an accuracy in the micrometre range. However, such significant machines are expensive and very subject to environmental influences. This design is not very often used in the optical industry; it is only used for vast lens arrays for telescopes. Figure 77 depicts a sketch of the bridge design.

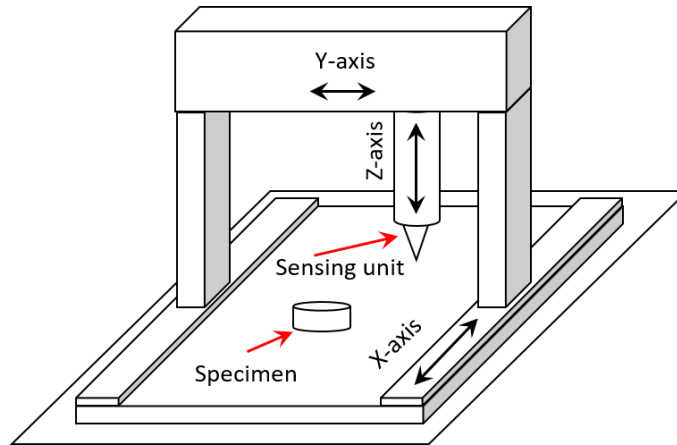


Figure 77: 3D sketch of the CMM bridge design

### A.2.2.3 Portal design

The portal design is the most common and traditional used design in the coordinate measurement technology. The primary design feature is the portal construction that consists of some ridged and massive granite blocks forming the U-shaped portal. Identical to the bridge construction is the sensing unit vertical moveable fixed on the Z-axis, whereas this construction can travel along the horizontal part of the portal on the Y-axis. The portal is fixed with both feet on two X-axes that are fixed on a mutual basis. All axes are rectangular to each other and form a Cartesian coordinate system.

Due to the large design is this setup not very subject to environmental influences. The excellent relationship between reachable accuracy, measurement space, and manufacturing costs make this machine concept to the first choice in the optical industry. Reaching a low three-digit nanometre accuracy level is possible. The average size of this design is one cubic metre. Figure 78 shows a sketch of the portal design.

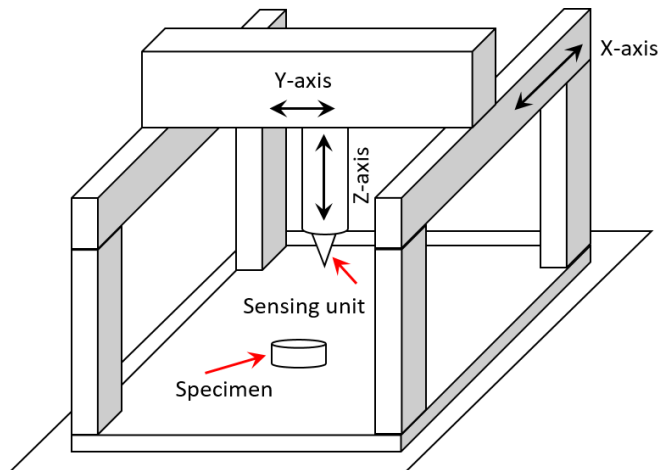


Figure 78: 3D sketch of the CMM portal design

#### A.2.2.4 Gantry design

The gantry design is very close to the cantilever design. The significant difference is that all movements are carried out by one column construction.

The sensing unit is assembled on a horizontal movable Y-axis that in turn is vertical moveable mounted on the column. The complete column assembly can travel along an X-axis in the Cartesian coordinate system. The object under test is fixed in a fixture mounted on a table. This table can be part of the same platform where the X-axis is fixed or on a separate unit.

Comparable to the cantilever design is this design subject to environmental influences like dynamic effects and thermal issues. Next to the combination of all movements, in the column construction is the size the significant difference to the cantilever design. While the cantilever design is mostly used in small machines, often for the use of measurement tables, the gantry design is commonly known from the

automotive industry. This design grants excellent access from three directions and depending on the size of a significant measurement volume.

The accuracy known from the automotive industry is located in the lower micrometre range. Use in the optical industry is not documented. Figure 79 presents a sketch of the gantry design.

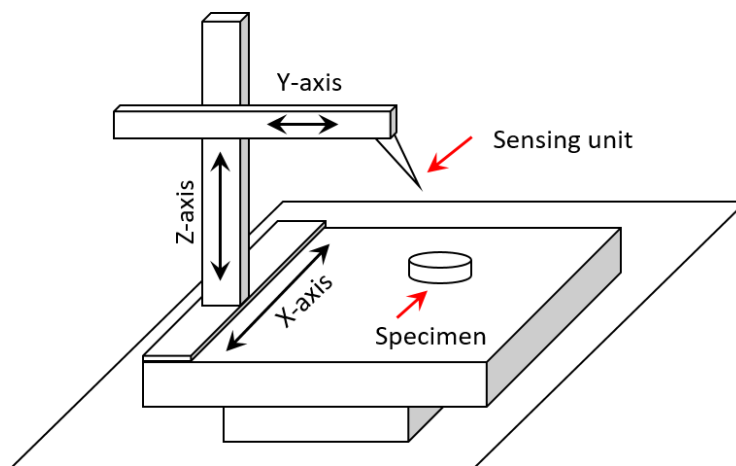


Figure 79: 3D sketch of the CMM gantry design

### A.3 Commonly used materials for optical elements

Optical elements are ubiquitous in our environment. With the technological progress in many different industrial branches, for example, hand-held devices such as mobile phones and digital cameras, the use cases for optical elements increased. Starting with the traditional types, planar or plano, spherical, aspherical, and ending modern free-form shaped objects. Furthermore, chemists created a wide range of new materials to improve and to optimise the characteristics of the optical elements. The following Chapter provides a brief contribution to commonly used materials.

*Table 11: Common materials for optical elements*

Material	Use case
Zinc Sulphide – ZnS (Cleartran™)	Infrared (IR) windows, lenses, domes, laser optics and other IR optical elements, night vision systems.
Germanium (Geo2)	Infrared (IR) windows, wide-angle camera lenses, microscopy, and the core part of optical fibres, night vision systems.
Glass (Fused silica, BK7, etc.)	A wide range of optical elements, lenses, windows, prisms, camera systems, lens arrays, telescopes.

Table 11: Common materials for optical elements (continued)

Sapphire	Scratch-resistant surfaces and windows, lenses, screens for devices, glasses for watches, LED production.
Silicon glass	Laser fusion optics, waver, windows, lenses, LED production, cover, and lenses for light, free-form shaped lenses.
Zinc selenide (ZnSe)	Aerospace, reference lenses, reference disc, laser fusion optics, medical equipment (filter).
LAS system ceramics (Cerodur™, Ceran™, etc.)	A material with an ultra-low temperature expansion coefficient and high-stress resistance. Cooktops, mirrors, focus lenses, heat resistant covers for light, scratch resistance, and objectives for devices.

## A.4 Common optical shapes and elements

Optical elements are produced in many different styles and variations. The use of different materials enables the optical industry to produce elements for a wide range of applications - for example, very hot or cold environments, for aerospace and handheld devices. Optical elements do have to be transparent for visible light, they can be reflective, or they filter different wavelengths.

However, the demand for the global industry is steadily growing. Optical elements are part of our modern life.

### A.4.1 Planar shaped objects

Planar shaped objects are one of three traditional surface types. Despite the misbelief, planar objects are more complicated to produce than spherically shaped parts. In ancient times craftsman took two pieces of hard material, pressed them together, and turned both pieces by hand. The result is a convex and a concave-shaped part. However, planar shaped parts are still a significant optical element in the modern optical industry.

#### A.4.1.1 Surface description

Planar shaped optical elements are usually described with one of two mathematical methods. Figure 80 illustrates a general sketch of a cylindrical coordinate

system. Since the height of a planar object is always defined with the value  $H$  for the height in  $Z$ -direction, only the  $XY$ -position is of interest.

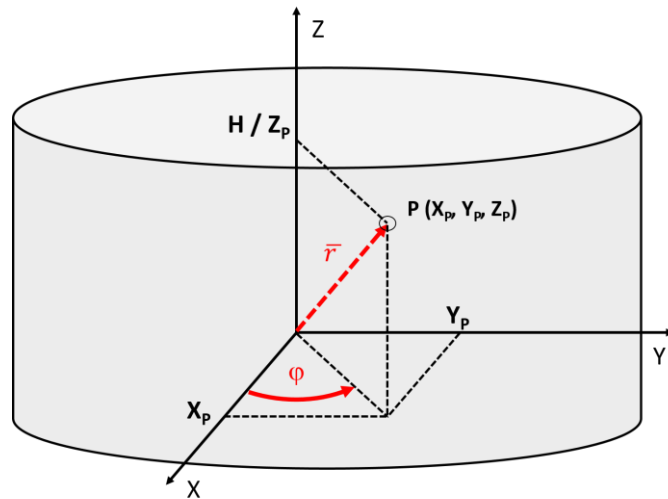


Figure 80: Cylindrical coordinate system

The vector  $\vec{r}$  is the shortest distance between the origin of the cylindrical coordinate system and the point  $P$ . The inclination angle  $\varphi$ , or polar angle, is the angle between the zenith direction and the projection of  $\vec{r}$  in the  $XY$  plane.

Most of the machines involved in the production process of optical elements can be programmed with cylindrical coordinates directly. For the case that the coordinates of a specimen are given in Cartesian coordinates, they can be transformed into cylindrical coordinates by the application of Equation 17 and Equation 18. The coordinate in  $Z$ -direction is fixed to one value across the entire surface of the specimen.



$$\vec{r} = \sqrt{X^2 + Y^2} \quad (17)$$

$$\varphi = \tan^{-1} \left( \frac{Y}{X} \right) \quad (18)$$

For the case that the specimen is defined in cylindrical coordinates, they can be transformed into Cartesian coordinates by the application of Equation 19 to Equation 21.

$$X = \vec{r} * \cos \varphi \quad (19)$$

$$Y = \vec{r} * \sin \varphi \quad (20)$$

$$Z = Z \quad (21)$$

Where:

$\vec{r}$  = Is the shortest distance between the origin of the cylindrical coordinate system and point P.

$\varphi$  = inclination angle, the angle between zenith direction and the projection of  $\vec{r}$  in the XY plane.

X = Cartesian X-coordinate.

Y = Cartesian Y-coordinate.

Z = Cartesian Z-coordinate.

#### A.4.1.2 Manufacturing processes

The manufacturing of planar optical elements changed over the last 20 years. Before the development of numeric control systems (NC), conventional lever arm grinding and polishing machines had been used. Meanwhile, such machines are only used in small shops for the production of the individual specimen or small series. The name of the used process is averaging. A grinding or polishing tool is moved across the surface of a rotating specimen. Depending on the required material removal rate (grinding or polishing), the tool is equipped with diamond plates or a polyurethane foam pad. Between the tool and the specimen is a thin film of the slurry. This traditional technique is still used today; only the conventional machines are updated with NC controlled machines. A detailed overview of the different production processes can be found in Chapter A.6.

- Grinding, conventional lever arm machines
- Lapping, conventional lever arm machines

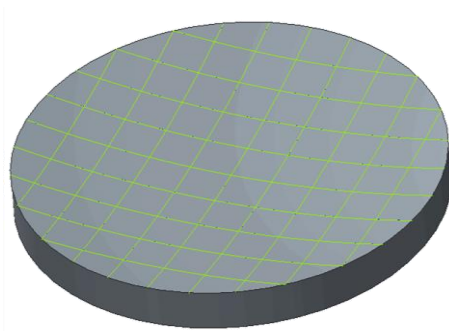
#### A.4.1.3 Application examples

Spherical components are used in many products. To reduce the effect of optical aberration, spherical lenses are often assembled in arrays. Most important applications are:

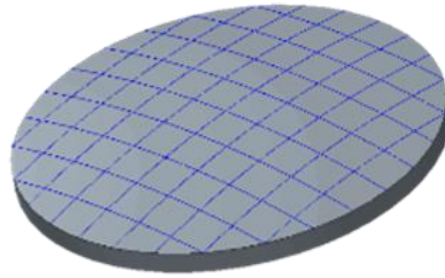
- Imaging systems
  - o Telescopes, especially mirrors
  - o Cameras
  - o Prisms
  - o Laser systems
  - o Glass-fibre connections (telecommunication)
  - o Windows (IR, UV, etc.)
  - o Etc.

#### A.4.2 Spherically shaped objects

The significant feature of a spherical-shaped object is the radial curvature of the surface. This surface can be either concave or convex. Figure 81 and Figure 82 illustrate both cases. The mesh on top of the surface is an optical effect for better visualisation of the curvature.



*Figure 81: Concave spherical surface*



*Figure 82: Convex spherical surface*

The main feature of spherical elements is to focus rays. The main disadvantage of spherical lenses is that the rays do not meet precisely at one point. This effect is called a spherical aberration. To reduce this effect, optical designers take a combination of different materials and spherical shapes. Such assemblies are well known from old telescopes and goggles.

#### A.4.2.1 Surface description

Spherical objects can be designed by the application of a spherical coordinate system or by the application of a Cartesian coordinate system. A plot of combining a spherical coordinate system and a Cartesian coordinate system is depicted in Figure 83.

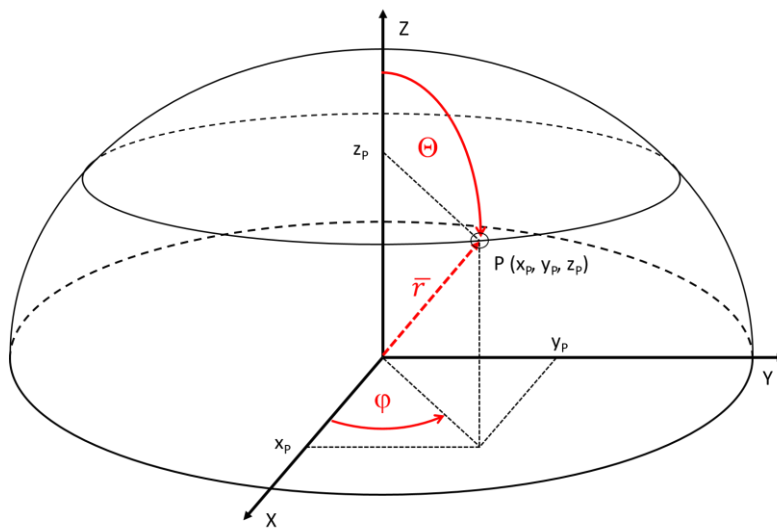


Figure 83: Spherical coordinate system

An arbitrary point  $P$  is defined with two angles and one vector. The vector  $\vec{r}$  is the shortest distance between the origin of the spherical coordinate system and the point  $P$ . The inclination angle  $\varphi$ , or polar angle, is the angle between the zenith direction and the projection of  $\vec{r}$  in the  $XY$  plane. The azimuth angle  $\theta$  is the angle between the  $Z$ -axis and the vector  $\vec{r}$ .

The correlations between the spherical coordinate system and the Cartesian coordinate system are well known in the literature. The spherical coordinates can be translated into Cartesian coordinates and backwards by the application of Equation 22 to Equation 27.

$$\vec{r} = \sqrt{X^2 + Y^2 + Z^2} \quad (22)$$

$$\theta = \cos^{-1} \left( \frac{Z}{\vec{r}} \right) \quad (23)$$

$$\varphi = \tan^{-1} \left( \frac{Y}{X} \right) \quad (24)$$

$$X = \vec{r} \sin \theta \cos \varphi \quad (25)$$

$$Y = \vec{r} \sin \theta \sin \varphi \quad (26)$$

$$Z = \vec{r} \cos \theta \quad (27)$$

Where:

$\vec{r}$  = Is the shortest distance between the origin of the spherical coordinate system and the point P.

$\theta$  = Azimuth angle, the angle between the Z-axis and the vector  $\vec{r}$ .

$\varphi$  = inclination angle, the angle between the zenith direction and the projection of  $\vec{r}$  in the XY plane.

X = Cartesian X-coordinate.

Y = Cartesian Y-coordinate.

Z = Cartesian Z-coordinate.

#### A.4.2.2 Manufacturing processes

A detailed overview of the different production processes can be found in Chapter A.6. The manufacturing process of spherical objects changed over the years. At the beginning of the optical industry, very time consuming and craftsman-intensive production processes were used. Such processes are:

- Grinding
- Lapping

With the development of NC controlled machines, the two traditional procedures were complemented with modern technologies such as:

- NC grinding
- NC lapping
- NC polishing
- Moulding
- NC controlled zonal polishing processes (e.g. MRF, AFM, etc.)

#### A.4.2.3 Application examples

Spherical components are used in many products. To reduce the effect of optical aberration, spherical lenses are often assembled in arrays. Most important applications are:

- Imaging systems
  - o Telescopes
  - o Cameras
  - o Smart devices (handheld devices)
  - o Laser systems
  - o Glass-fibre connections (telecommunication)
  - o Medical devices (endoscopes)
  - o Light (LED)
  - o Many more

#### A.4.3 Aspherical shaped objects

Spherical optical elements cannot focus on one point. This effect is called spherical aberration or optical aberration. Therefore, aspherical elements fulfil the need for focusing rays at one point. This effect is beneficial in areas with low space for lens arrays. Figure 84 illustrates the effect of the optical aberration. While aberration limits spherical objects, aspherical objects can focus even the outer rays' perfect.

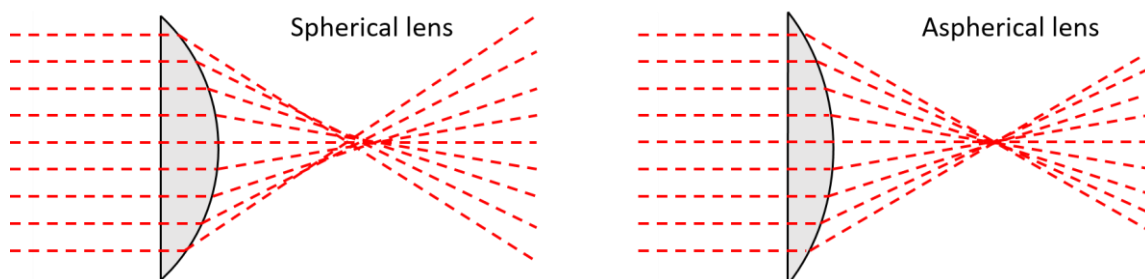


Figure 84: Optical aberration



The trend towards the minimisation of devices pushes the development of aspheres. However, the production and the measurement of aspherical objects are very complicated, compared with planar or spherical objects. The current production process, including CAD<sup>27</sup>, CAD/CAM<sup>28</sup>, CNC<sup>29</sup> technology, and advanced metrology, enables the industry to adopt aspherical shaped objects of sufficient quality.

#### A.4.3.1 Surface description

Without the deployment of NC<sup>30</sup> machines, it was much more challenging to generate the shape that follows the aspherical equation, printed in Equation 28, according to DIN ISO 10110 [75].

$$Z = \frac{\frac{1}{R_0} * (X^2 + Y^2)}{1 + \sqrt{1 - (k + 1) * \left(\frac{1}{R_0}\right)^2 * (X^2 + Y^2)}} + \sum_{n=2}^m B_{2n} * \sqrt{(X^2 + Y^2)}^{2n} \quad (28)$$

<sup>27</sup> CAD – Computer aided design.

<sup>28</sup> CAM – Computer aided manufacturing.

<sup>29</sup> CNC – Computerised numerical control.

<sup>30</sup> NC – Numeric control.

Table 12: Conic coefficients

<b>k</b>	<b>Conic section</b>
$k < -1$	Hyperbola
$K = -1$	Parabola
$-1 < k < 0$	Prolate rotational ellipsoid
$k = 0$	Sphere
$k > 0$	Oblate rotational ellipsoid

The equation consists of the following components:

Z = Sag of the surface parallel to the optical axis

$R_0$  = Curvature, the inverse of the radius

k = Conic constant (for options, see Table 12)

X = Position of Z on X-axis

Y = Position of Z on Y-axis

B4, B6, B8 = 4<sup>th</sup>, 6<sup>th</sup>, eigh<sup>th</sup>... order aspheric terms

#### A.4.3.2 Application examples

Aspherical optical elements are essential parts of modern optical systems. Since aspherical objects focus all rays, even close to the edges, into one focal point, they are fascinating for many applications:

- Optical data storage (CD, DVD, Blu-ray, etc.)
- Camera system (Especially in zoom arrays)
- Projection system (Beamer)
- Medical systems (Endoscopes and cameras)
- Telecommunication (Glass-fibre connection and signal repeating)
- Light (LED, headlights in cars and aircraft)

Aspherical shaped lenses are not subject to spherical aberration. That means that an aspherical shaped object focuses incoming rays in one point. Therefore, aspherical shaped lenses are beneficial for use in the optical industry. The use cases are rampant, everywhere where rays have to be focused, aspherical shaped objects are involved. However, the production process of aspherical shaped objects requires the application of modern CNC production machines.

#### A.4.3.3 Manufacturing processes

Aspherical shaped optical elements are complex structures with changing slope gradients of the curvature. The modern manufacturing industry knows four possibilities to produce aspheres. The newest possibility is diamond turning. This procedure allows combining the generating and grinding process in step. Diamond turning machines can remove material quick and accurate. The main problem with the process is the quality of the resulting surface. This technology still requires a subsequent polishing process.

Another manufacturing process is moulding. Moulding is a suitable process for bulk production. Eastman Kodak produced the first aspheres with this technology in the early 1970s. The production of the first Polaroid™ cameras boosted this technology to increase the production speed of the required aspherical lenses.

The third technology is the traditional process chain for generating, grinding and polishing with conventional production machines. These type of machines do not have an NC control system. Therefore, special tools are required. The tools are negatives of the required shape of the aspherical element. The main disadvantage of this process

chain is a unique set of tools. Each toolset can only be used for one type of aspherical object. Even small modifications require the production of a new set of machining tools.

However, since the development of NC controlled production machines, the machines are not limited to one design of the specimen. Modern machines and their tools are designed to produce all kinds of optical elements. The market even knows complex grinding machines (grinding centres) with the additional metrology system to measure the specimen. This measurement task is done in-line. That means that there is no need to remove the specimen from the production machine and insert it into a separate measurement machine; the specimen can be measured directly in the production machine. The development of sub-aperture polishing technologies is the crucial factor for high precision aspherical shaped optical elements.

#### A.4.4 Free-form shaped objects

The next trend in optical design is free-form shaped objects. In contrast to planar, spherical, or aspherical objects there is no unified surface description available. Lacking a discrete description of whether a shape is a free-form structure or not, the optical industry calls the following optical elements free-form shaped:

- Off-axis sections of rotationally symmetric parts
- Rotationally symmetric shapes which are not planar, spherical or aspherical
- Conformal optics (shaped to fit into products)
- Other free-form geometries

#### A.4.4.1 Application examples

Free-form shaped optical elements can be designed to fulfil a large variety of requirements. For example, such objects eliminate projection errors such as coma or optical aberration. Free-form shaped optical elements enable product designer to include the optical elements into the design of the products. Some examples of applications are:

- Optical data storage (CD, DVD, Blu-ray, etc.)
- Camera system (Especially in zoom arrays)
- Projection system (Beamer)
- Medical systems (Endoscopes and cameras)
- Telecommunication (Glass-fibre connection and signal repeating)
- Light (LED, headlights in cars and aircraft, head-up displays)
- Consumer products (Google-glass™, smart mobile devices, action cameras, spy cameras)

#### A.4.4.2 Surface description

The description of a free-form surface is a mathematical task. Modern mathematics knows several methods to describe free-form shaped surfaces. However, the optical industry still has no agreement about the usage of only one mathematical description. Therefore, many computational methods are standard:

- Phi-polynomial descriptions (for example Zernike polynomials)

- Radial based functions (RBFs)
- Control point surfaces (Nurbs)
- Etc.

With the introduction of free-form shaped optical elements and their related mathematical models, 3D computer models became more critical. However, most of the available optical software suites or ray-tracing software packages can compute Zernike polynomials. Therefore, the optical designer has to decide about the preferred or required mathematical description method. It is essential to find a method appropriate for all parts of the individual production chain, starting from the design, to the manufacturing machines and finally to the metrology system. The integration of data is a crucial factor in the optical industry.

#### A.4.4.3 Manufacturing processes

The manufacturing process of free-form shaped optical elements is a challenge. There are two significant issues regarding the manufacturing process.

The first issue to be discussed is the tool path generation. Physically, most of the NC controlled manufacturing machines can produce free-form shaped optical elements. Practically, many are not. A manufacturing machine needs to know the geometry of the planned product and of the blank. With both information, it is possible to generate the tool path and to define the process parameters. However, not all machines have an interface to insert mathematical equations, or they cannot compute the given parameters. For such a case, it is essential to have an additional software package that

can generate the tool path and translates the information into the correct machine language.

The second issue is subject to the alignment and referencing procedure. Free-form shaped optical elements mostly have no reference plane or any other alignment feature. This issue is not a problematic unit the specimen is locked in the fixture. However, most of the production machines do not have an inline (onboard) metrology system. Therefore, the specimen must be transferred into the measurement machine and backwards. At this time, it is crucial to find the original orientation of the specimen. This is very important for non-rotational symmetric elements. During a normal production process, this issue can be solved with a suitable blocking system. The main problem is the correct orientation of the specimen after de-blocking it. In that case, the customer of the specimen needs a marking or alignment feature to reproduce the original orientation with respect to the result of the final measurement, and the final position in the customer's assembly.

Concluding, to produce free-form shaped optical products, advanced NC controlled production machines, and software packages are required.

- Interface to compute a mathematical description of free-forms (Nurbs, etc.)
- Tool path generation tool for free-form shaped optical elements
- Available tools to produce all geometries of the specimen
- At least three moveable axes (Cartesian XYZ)
- Fixture with a distinctive orientation

## A.5 Sensing units implemented in the SCMM

The system has been designed to operate with different sensing units to realise a multi-sensor coordinate measurement machine.

The significant advantage of a multi-sensor coordinate measurement machine is that the user can choose the best fitting sensing unit for his measurement task. The following list shows some necessary information about the sensing units. The detailed information may be found in the references and the appendix.

### A.5.1 Heidenhain™ Certo™ CT 2502

The Heidenhain™ Certo™ CT 2502 is a tactile sensing unit. The length gauges of the Heidenhain™ Certo™ program with a measuring range of 25 millimetres with  $\pm 0.03$  microns accuracy are exceptionally well suited for this system [71]. The unique advantage of these sensing units is their ability to be implemented as an additional axis to the NC control system. Therefore, data read of all axes includes the information provided by the Certo™ sensing unit with no time shift.

Furthermore, the NC control system provides temperature compensation for all axis encoders, including the Certo™ sensing unit. The measurement accuracy is  $\pm 0.1$  micrometre under natural conditions and with linear error and temperature compensation up to  $\pm 0.03$  microns. Both the linear and the thermal compensation have been included in the SCMM control system.



The critical feature of this sensing unit is the extremely long measuring distance of 25 millimetres. Despite this feature, the sensing unit has a repeatability of 0.02 microns. Detailed information about the Heidenhain™ Certo™ sensing unit and the official data sheet may be found at the corresponding website of the manufacturer.

#### A.5.1.1 Application:

The Heidenhain™ Certo™ tactile sensing unit has been used as one of two universal SCMM sensing units. It performs well on all tested surface shapes, such as planar, spherical, aspherical, and free-form shaped surfaces. Furthermore, the sensing unit is able to operate even on rough surfaces created by rough production processes such as grinding. The full working range enables the sensing unit to operate on objects with distinct embossed areas, such as sinus-shaped areas or areas with sharp gradients.

The disadvantage of this sensing unit is the weight of the sensor head, including the touch ball. Especially on very rough surfaces with thin spikes on the surface, the sensing unit may cause damage to the structure.

#### A.5.2 Luhos™ MWLI™

The Luhos™ MWLI™ is a very highly accurate, contact-less, sensor system. The accuracy of the sensor system is in the low nanometre range [76–78]. According to the datasheet, the resolution is 0.1 nanometres and the accuracy 2 nanometres. The system is interferometer based and operates by superposition of four wavelengths. However, the disadvantage of the system is the required software package. The software tools are

needed by the sensing system and need their own computer. Therefore, it is not possible to implement the sensor system directly in the NC control. The system is equipped with a trigger input. Therefore, the measurement process can be started and stopped by receiving a signal from the NC control. The data are saved in a file on the computer and have to be added to the measurement result after finishing the complete measurement. The system comes with a complete temperature compensation feature and an own error compensation feature. Figure 85 publishes the Luphos™ sensing system assembled in the SCMM.

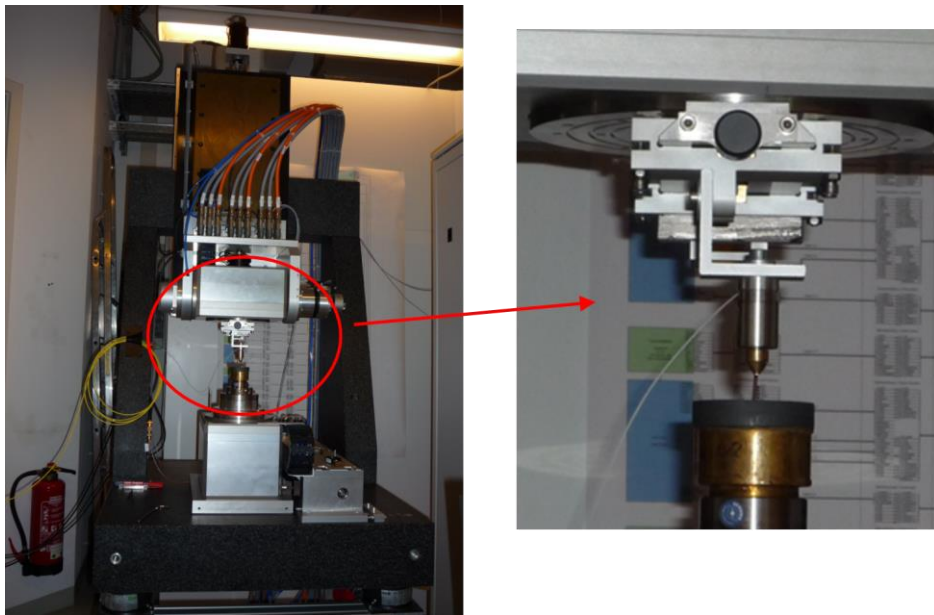


Figure 85: Luphos™ sensing unit in SCMM

#### A.5.2.1 Application:

The Luphos™ MWLI™ contactless sensing unit has been used as one of two universal SCMM sensing units. It performs well on all tested surface shapes, such as planar, spherical, aspherical, and free-form shaped surfaces. Furthermore, the sensing unit is able to operate even on rough surfaces created by rough production processes

such as grinding. The full working range enables the sensing unit to operate on objects with distinct embossed areas, such as sinus-shaped areas or areas with sharp gradients.

The disadvantage of the system is the sensing unit control system. This black box does not provide an interface for data communication with other systems. This circumstance is caused by the design of the system. All data are computed and prepared internal first. This process takes time, therefore is no direct data communication possible. The only interface is a trigger input. This feature enables the NC control system to send a start and stop signal to the MWLI™.

### A.5.3 Sios™ TII-3D sensor

The Sios™ sensing unit is a mixture of a micro-interferometer and a tactile needle. The system had been developed exclusively for Satisloh™. The system is not available on the market. The needle is equipped with a sapphire ball, the bottom side with a mirror. The interferometer measures against that mirror. Therefore, this sensing unit is very accurate. An RS232 interface handles the implementation into the NC control, including temperature compensation. Since this sensing unit had never reached a series production stage, there is no reference or description available. Figure 86 presents the Sios™ sensing unit in a use-case situation at the SCMM.

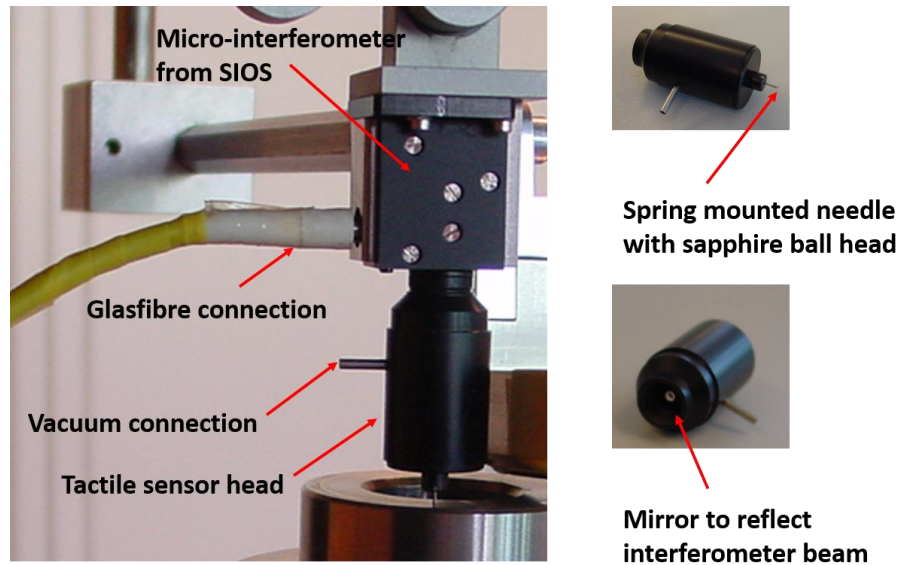


Figure 86: Sios™ sensing unit

#### A.5.3.1 Application

Since the SIOS™ sensing unit is a reliable mixture between an interferometer and a tactile sensing unit. It can be used on all common surface types, but with limitations to the roughness grade of the surface. The connection between the sapphire ball the end of the scanning needle is not very strong. Therefore, it is possible that the ball gets lost during a measurement. Because of this reason, the LOE decided to use the SIOS™ sensing unit only for polished surfaces. The measuring range of approximately 2 millimetres would theoretically allow operating on embossed structures or free-form shaped structures, but the risk to lose the sapphire ball is high.

#### A.5.4 Micro-Epsilon™ confocal sensors

Micro-Epsilon™ confocal sensing units are widespread in the field of metrology. The company offers a wide range of different sensing units for different applications. The SCMM features several different confocal chromatic sensor systems with different accuracy and measurement distances. A representative picture of the probe is shown in Figure 87. The implementation of the sensing unit is realised with USB or with RS 232 [79, 80]. Furthermore, the sensing unit needs an electronic device for operation. This box provides temperature compensation as well.



Figure 87: MicroEpsilon™ Confocal chromatic sensor [79]

##### A.5.4.1 Application:

The Micro-Epsilon™ confocal chromatic sensing unit can be used on all polished, reflective surfaces where the sensing unit can be aligned normal to the surface. The acceptance angle of these sensing units is very narrow; the test showed a required alignment better than  $3^\circ$ . However, for that reason, these sensing units can only be used

for planar shaped objects and spheres in combination with the SCMM. Another issue is the physical length of the body of the sensing unit. Including the stiffness cover for the fibre cable, the length is 75 millimetres.

#### A.5.5 Self-developed tactile sensing unit I

Based on the Micro-Epsilon™ confocal chromatic sensing units, a new type of sensing unit was developed. Related to the SIOS™ micro interferometer with tactile head, a system with a confocal chromatic sensing unit and tactile head were developed. Base of the ME LOE I sensing unit is an IFS2402-4 with the beam in an axial direction. The beam is reflected on the mirror of the SIOS™ tactile head. Figure 88 depicts the complete ME LOE I sensing unit in a disassembled situation. The technical data of the system corresponds with the technical data of the Micro-Epsilon™ confocal chromatic sensing units. Furthermore, the ME LOE I sensing unit has the same interface connection as the Micro-Epsilon™ confocal chromatic sensing units. To avoid the issue to lose the sapphire ball head, the connection was reworked with a micro drill in the ball and particular type of resin (replaceable with heat).

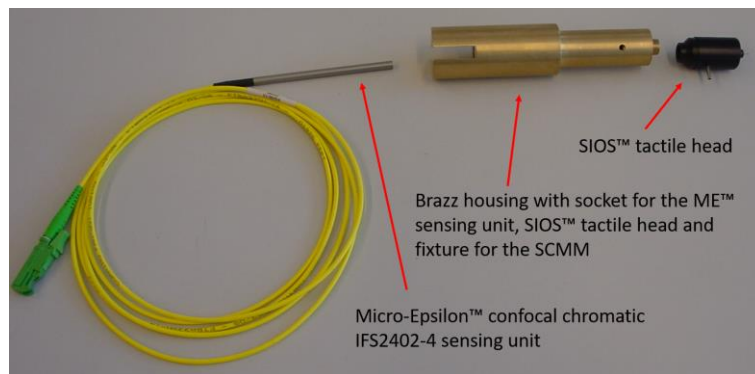


Figure 88: ME/LOE sensing unit

### A.5.5.1 Application:

The ME LOE I sensing unit is a combination of a confocal chromatic sensing unit and with a tactile head. Therefore, it does not have the limitation to the narrow acceptance angle like the confocal chromatic sensing units. This feature enables to use the sensing unit even on rough surfaces. The improvement of the sapphire ball fixture enables the sensing unit to operate on all familiar surface shapes, and on either, rough, and smooth surfaces.

### A.5.6 Self-developed tactile sensing unit II

The last development is a particular type of tactile sensing unit. The basic idea behind the sensing system is to create a very inexpensive tactile solution, especially for ground objects with a rough surface. Surfaces with a rough structure are hazardous for tactile sensing units since their touch heads may be damaged. Details about the development may be found in Section 10.2.3. Figure 89 presents a schematic sketch and a picture of the first prototype during test measurement.

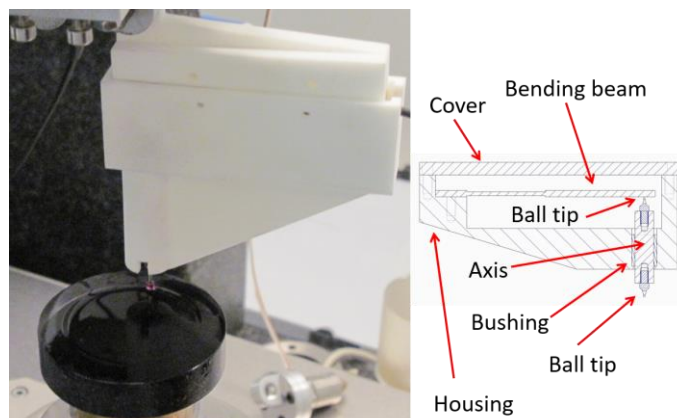


Figure 89: LOE sensing unit II

## A.6 Manufacturing machines and processes in the optical industry

Advanced numeric controlled production machines can commonly produce objects with a diameter of approximately 250 millimetres and with nearly each surface shape. The only limitations are, next to the accuracy, the process, the material, the used tools and the number of iterations. In general, the optical industry distinguishes between four essential processes and machine types:

### A.6.1 Pre-production process

The first step in the production chain of optical elements is the pre-production process. The industry produces blanks can be purchased or produced in a large variety of shapes. Commonly the best fitting design is taken to reduce the amount of material waste and the tool wear and finally to reduce the production time. Commonly produced designs are:

- Blocks
- Rods
- Prisms
- Plates/windows
- Precision glass moulded elements
  - o Spheres
  - o Aspheres
  - o Free-forms



Usually, such blanks are produced in large quantity, in many cases for direct orders of customers. Therefore, the elements can be produced with less than one millimetre oversize or even better to reach the customer's requirements firmly, and to reduce the customers machining time in the production chain.

#### A.6.2 Moulding – moulding machines

Since the boom of aspherical elements in modern consumer electronics started, the industry developed new techniques to produce large quantities of these elements. The essential production process is moulding technology. Eastman Kodak invented the precision moulding technology in the early 1970s. This process forms small and hot, but stable, glass blanks by shaping with a moulding tool in only one process. With this method, it is easily possible to produce many elements in one process step. After the moulding process, the elements are finished and ready to use. The significant advantage of this technique is the freedom of shape. Many different shapes can be produced, as long as there is no undercut. The only limitation is the amount of moulded material; up to now, this technology is only usable for lenses with less a few grams. The same effects knew from the plastic moulding/injecting technology, such as to cause this limitation:

- Flow lines
- Sink marks
- Surface delamination

Further information about precision moulding technology can be found in the literature [11, 12, 81–84].

The process follows this scheme: After positioning the glass blanks in the cavities, the oxygen around the tool is replaced with nitrogen to avoid chemical reactions between the hot glass and the oxygen. In a third step, the tool and the glass blank is heated up, mostly with IR or halogen lamps. After reaching the correct process temperature (depending on the type of glass and shape of the specimen), the mould closes and presses the glass blank into the cavities and therefore into the final shape of the specimen. In the fifth step, after a short pre-cool-down phase, the mould opens again, and the nitrogen is extracted from the process area. Finally, the complete specimen can be withdrawn from the mould for the final cooling down phase.

The process of glass moulding changed over the last ten years. The technology split up into two technologies. The traditional glass moulding process delivers glass blanks for the optical industry, for example, for the traditional manufacturing of lenses with abrasive technologies. The second technology is named precision glass moulding. This technology is able to produce optical elements, for example, aspheres, with consistent quality and without the need for additional machining processes. Recent research [12, 81, 85] documented results of precision glass moulding technologies with a forming error of 0.63 microns with respect to the ideal shape.

### A.6.3 Blocking / cementing / supporting

In a production machine, for example, a grinding machine, high forces interact with a specimen. Therefore, it is a critical step to support the specimen because of two significant reasons. The first is to provide a connection between the specimen and the

production machine. All of the modern machines are equipped with a universal hydrodehn chuck or a manufacturer-specific solution. The term blocking means to fix one or more specimen on a block. The second reason for a proper blocking is that some specimens need physical support to avoid, for example, bending or damages caused by the applied forces of the machining process. However, the process of blocking requires a lot of knowledge, especially regarding the target shapes of the specimen, the applied forces, the used abrasive fluid (slurry) and the used locking agent (cement) for the connection between the specimen and the block. Some of the commonly used types of cement are, for example:

- Epoxies (one or two components, heat or UV light activated)
- RTV's (Room Temperature Vulcanizing, silicone-based glue)
- Pitch
- Wax
- Hot resin (melts at approximately 80 °C)

Figure 90 presents a not transparent, planar specimen blocked on a brass block with resin. The combination of brass, resin and not the transparent specimen is ubiquitous in the optical industry. All components are heated up to 80°C. After the resin melted on the brass block, the specimen is centred and pressed into the resin. The complete package has to cool down very slowly to avoid tensions and damages caused by a rapid temperature change.

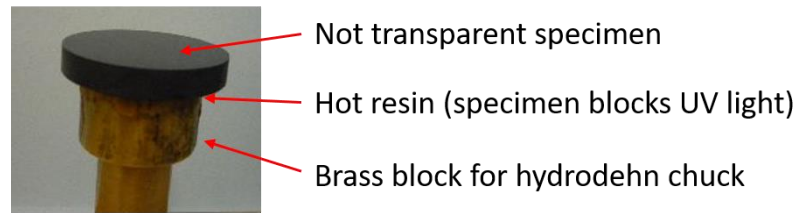


Figure 90: Specimen on a brass block, blocked with resin

#### A.6.4 Grinding processes – grinding machines

According to DIN 8580 [86], grinding is an abrasive production process that uses grinding tools with an undefined geometrical edge. Usually, the grinding tools consist of robust grains bound by a particular type of a bonding agent (e.g. glue or rosin). The size and amount of the grain are called knurling and defines the quality of the resulting surface; more grains mean a smoother result. The result of a grinding process is an opaque surface with an accuracy in the region of a few micrometres [6, 87]. Depending on the used block-design (ref. A.6.3), grinding machines can operate on more than one specimen at the same time.

Furthermore, the development of NC-controlled machines influenced optical grinding machines as well. Modern CNC grinding machines have precision axes and position encoders with high resolution. Therefore it is possible to produce very smooth surfaces with excellent repeatability [88].

The grinding process in the optical industry can be divided into two sub-categories - generation (shaping) and precision grinding. Both processes are known with two different methods, operating with slurry or tools with diamond cutting edges. A

slurry is a mixture of water, emulsion, and loose grit with a size of 200 microns down to 5 microns, depending on the required material removing rate and process time.

However, generation is a rough process with the goal to remove a lot of material in a short period to 'generate' the general shape and dimensions of the specimen out of the blank. The generation causes damages to the surface and to the sub-surface. Sub-surface-damages (SSD) are very thin cracks and scratches in the surface. Since the resulting surface is not smooth enough to start a successful and efficient polishing process, a second grinding step is necessary - the precision grinding. This second step operates with a slurry with smaller grids, down to 5 microns or very smooth diamond-edged grinding tools. In addition, the driving forces and the removal rate are reduced. The result of the second grinding process is a specimen with a smooth and partially reflective surface, ready for the polishing process.

#### A.6.5 Polishing process – polishing machines

DIN 8589 tells us that polishing is not an own production process. It is always in association with other processes, in the case of optics, it is a subprocess of grinding and precision grinding. The difference is the size of the used grains, the bounding force of the bonding agent and the density of the grains in the knurling. The result of a simple polishing process is a very smooth and reflecting surface. Advanced polishing machines

used in the optical industry can produce objects with an accuracy better than  $\lambda/20$ <sup>31</sup> [5, 65].

Similar to the grinding process, the polishing process operates with two different methods - the application of slurry and diamond tools. The usage of the slurry is still the preferred method. The tool is coated with soft, foamed pads.

The polishing pads, in combination with the slurry, ensure an even and steady abrasion of the surface of the specimen. Polishing is a time-consuming process with low forces.

The disadvantage of a traditional polishing technology is the even removal of material all about the surface of the specimen. That means that embossed areas become flattened. A zonal polishing, especially in small areas, is very difficult. For that purpose, the sub-aperture polishing technology was invented by QED™.

#### A.6.6 sub-aperture polishing – sub-aperture polishing machines

Aperture is the technical term for the usable area of an optical device, for example, the opening of a camera objective. A sub-aperture is a defined segment of an aperture. The technique of sub-aperture polishing is also known as zonal polishing. This method enables the user to operate only in regions on the surface where polishing is necessary. In contrast to conventional polishing processes where large areas up to the entire surface are machined. This advantage allows a very controlled correction of

---

<sup>31</sup>  $\lambda/20 - \lambda$  represents the wavelength of a He Ne Laser (red) with a wavelength of 632.816 nanometre.  $\rightarrow \lambda/20 = 31.6408$  nanometre

defined error regions to improve the quality of the whole object. Two of the most well known sub-aperture polishing processes are the magnetorheological finishing (MRF™) by QED™ and the active fluid jet polishing (A-FJP™) by Optotech™. With such technologies, and the appropriate pre-machining, is it possible to produce objects better than  $\lambda/40$ <sup>32</sup> [3, 5].

The MRF™ performs a polishing process with a unique technique. It requires a particular type of slurry. This slurry is a mixture of magnetic particles, loose grit, and a fluid medium. That slurry is a liquid unit it comes in touch with a strong magnetic field. Then it changes the viscosity from a liquid to rubbery. Even tiny changes in the magnetic field result in a viscosity variation of the slurry.

However, the liquid slurry is pumped on a wheel with a durable and adjustable electromagnet inside. The slurry forms a kind of rubbery worm on the wheel inside the magnetic field. On the opposite side of the wheel, the slurry is withdrawn by suction after leaving the magnetic field. This effect, in combination with a modern NC control system, allows working in defined areas of the specimen (depending on the size of the wheel). A stronger magnetic field and more rotations of the wheel result in a higher removal rate of the process. A specially developed algorithm analyses a pre-measurement of the specimen and defines a removal matrix. This removal matrix is translated into variations of the magnetic field in the defined areas. The result is a zonal or sub-aperture polishing process.

---

<sup>32</sup>  $\lambda/40 - \lambda$  represents the wavelength of a He Ne Laser (red) with a wavelength of 632.816 nanometre.  $\rightarrow \lambda/40 = 15,8204$  nanometre

Another solution is A-FJP™ from Optotech™. This process operates with a regular slurry mixture (water, coolant, and loose grit). This mixture is pressed through a nozzle, passing a pin and is ejected perpendicular on the surface of the specimen. The design of the nozzle and of the pin creates a circular rotation and axial movement of the pin. On top of the pin, pointing towards the specimen is a soft pad installed. However, by increasing the pressure of the slurry, the pin is rotating faster, and it is pressed stronger against the surface of the specimen. This effect causes a higher removal rate in the process. In combination with a modern NC control system and pre-measurement, a removal map can be created. In areas where more material must be removed, the pressure increases.

#### A.6.7 Application

The trend in the optical industry is tending towards complex aspheres, free-form and large optics. The most popular products for free-form shaped optics are one lens cameras (Smartphones) and head-up displays. The most important use cases for large optical objects are telescope mirrors.

Free-formed objects become more and more critical due to the miniaturisation of consumer products. The use of free-formed objects may aid this demand in the future. Analysts predict that the number of vehicles equipped with head-up displays will increase tremendously. Exemplary the latest developments like Google Glass need a free-formed shaped element in large quantities.



Further challenges are large objects, greater than 250 millimetres up to 2000 millimetres. These elements, especially mirrors, are needed for large telescopes like those used at the European Southern Observatory (ESO) located in Chile. Such very large telescopes (VLT) are mostly designed by combining some individual mirrors into one large mirror. The process of reliable production and measurement of large mirrors are one of the new challenges in the optical industry.

## A.7 Uncertainty estimation of the SCMM

Each machine is subject to the influence of errors, especially metrology systems. To be able to reduce or even compensate for the error influence, it is essential to know and to understand the different types of errors. The German DIN<sup>33</sup> 1319 [89] - Fundamentals of metrology - from the 1940s is the primary standard for Metrology. Its European equivalent is the DIN V ENV<sup>34</sup>13005 - Guide to the expression of uncertainty in measurement (GUM). Since the demand for standards in the metrology raised continuously, the standard had been extended step by step. The most significant change had been in the 1960s, where the DIN 1319 had been split into four parts.

- DIN 1319-1: Basic terminology (valid copy from 1995) [90]
- DIN 1319-2: Terminology related to measuring equipment (valid copy from 2005) [91]
- DIN 1319-3: Evaluation of measurements of a single measurand, measurement uncertainty (valid copy from 1996) [92]
- DIN 1319-4: Evaluation of measurements; the uncertainty of measurement (valid copy from 1999) [93]

The complete DIN V ENV<sup>35</sup> 13005 will be replaced by the coming ENV 13005 [94] from 1999 - when finally released. This section discusses the influence of different groups of errors to the measurement result. To be able to realise a proper error

---

<sup>33</sup> DIN: Deutsches Institut für Normung e.V. - German Institute for Standardisation

<sup>34</sup> EN: Europäische Norm – European Standard

<sup>35</sup> ENV: Europäischer Normvorschlag – European pre-standard

estimation and compensation, detailed knowledge of all possible influences is necessary. Figure 91 illustrates the most critical influences.

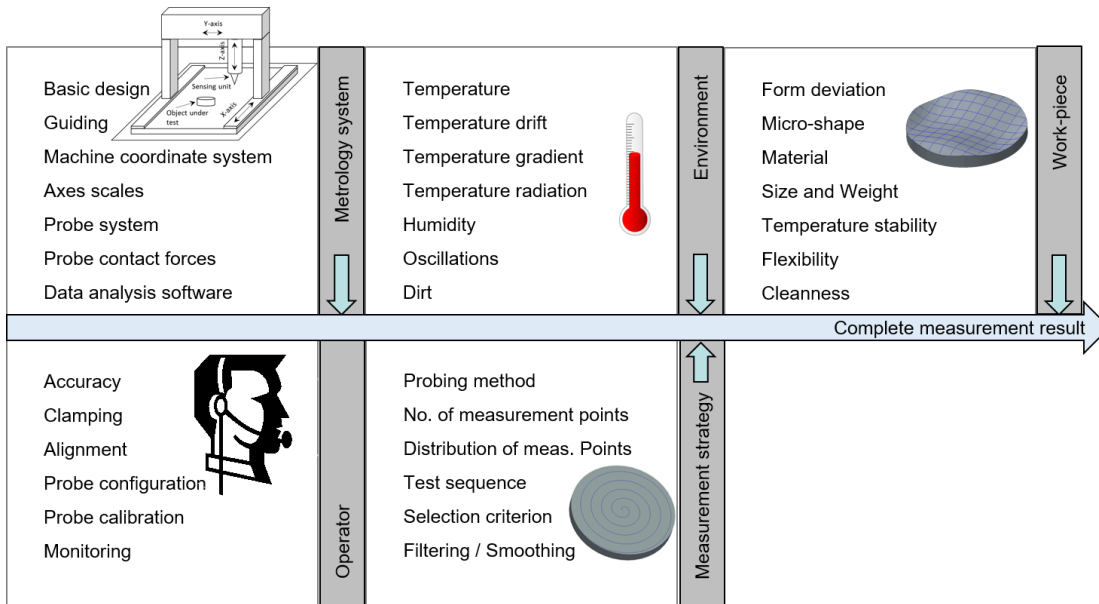


Figure 91: Influences on the measurement result. A measurement process is subject to a considerable variety of influences. This figure presents the most significant influences in five categories

The five most significant error sources are:

- Environment
- Work-piece / specimen
- Operator
- Metrology system
- Measurement strategy

The following sub-Chapters publish their impact in relation to the presented SCMM.

### A.7.1 Environment

The environment is a critical influence factor for operating metrology systems. Metrology and enclosures often come together to reduce or maybe even to avoid the influence of the environment. The most popular environmental influences are according to Figure 91:

- Temperature
- Temperature drift
- Temperature gradient
- Temperature radiation
- Humidity
- Oscillations
- Dirt

Temperature influences cause a thermal expansion of the machine components. This thermal expansion of the components leads to a displacement of the position between the target alignment of the specimen / sensing unit and their actual position because all metrology systems are usually designed with a mixture of different materials such as granite, steel, or aluminium. Therefore, the final thermal expansion is not linear.

A further important factor is the design of the metrology machine itself. By using a symmetrical design, the influence of the thermal expansion can be reduced. However, modern materials like carbon fibre mixtures have a thermal expansion coefficient of approximately zero or even negative thermal coefficient such as Cubic Zirconium

Tungstate ( $ZrW_2O_8$ ). Recent research demonstrated that a material mix with Cubic Zirconium Tungstate, that it is possible to create designs with a combined thermal expansion factor of zero. This achievement might be a significant step in the design of temperature critical machines and devices.

However, the development of a metrology system thermal expansion of zero is impossible or at least very expensive and uneconomic.

Therefore, modern metrology machines are enclosed and mostly placed in a windowless measurement room or chamber. The measurement rooms are mostly fully air-conditioned and have further features such as solid and uncoupled concrete floors. The air conditions are usually designed to keep the temperature and humidity very stable. Furthermore, they remove all particles out of the air.

However, the enclosures and the measurement chambers are the key features to reduce or even to avoid errors caused by the environment.

The LOE at the Deggendorf Institute of Technology is designed to keep the temperature stable. Measurement documented that the temperature variation does not exceed 0.15 Kelvin for 24 hours. The documentation in Figure 92 shows the documentation from 16<sup>th</sup> of December 2015 as an example. At this time, the long-term and repeatability measurements presented in 7.1.5 were performed.

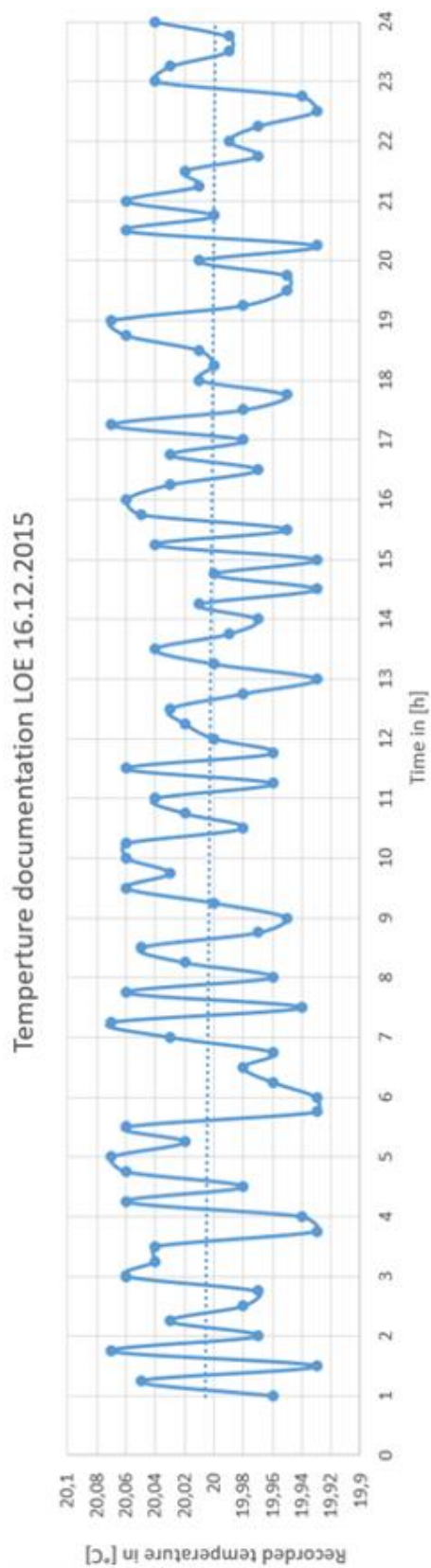


Figure 92: Temperature documentation at the laboratory of optical engineering (LOE), 16.12.2015. The temperature measurement had been performed in the main measurement room of the LOE. This room is equipped with a powerful air conditioning and cleaning system. The recorded temperature variation is lower than 0.15K/24h

The LOE, for example, uses a temperature-stabilised room with a thermal drift of only 0.15 Kelvin per day. To be able to reach such low-temperature drifts, it is necessary to take care of some fundamental rules, such as:

- Never switch off the measurement machines
- Limitation of the human workers inside of the metrology room
- Installation of a double door system
- Well-designed air condition with defined air in- and out-takes
- Sizeable changing volume to reduce turbulence and grant a slow flow
- Dirt protection in the air condition
- Humid control
- No windows to avoid thermal radiation

However, the thermal influences are only one part of the environmental influences. Further aspects are the protection against dirt and vibrations. Since the advanced optical metrology operates in the nanometre range, cleanliness is essential, because even ultra-fine dust particles have a size of a few hundreds of nanometres.

The last critical influence is vibration. It is just not possible to avoid environmental vibrations. For example, a simple gust of wind can set buildings into tiny vibrations that may influence the measurement result. The traffic on the streets near a metrology facility may also have a critical influence on the measurement result. Next, by the mentioned dampers in the machines, it is a standard way to create solid foundations for measurement facilities. The Technology Campus Teisnach, a subsidiary of the Deggendorf Institute of Technology, for example, is located in the back roads of

the Bavarian Forrester where no heavy traffic is. Further, the mentioned metrology room has been built on a one metre thick, elastic founded concrete block that has no direct connection to the rest of the facility. All these efforts, excellent insulation, well-designed air control and a massive foundation leads to an excellent environment for ultra-precision measurements.

### A.7.2 Specimen

The specimen has a particular influence on the measurement result. The most significant influences are according to Figure 91:

- Form deviation
- Micro shape
- Material
- Size and weight
- Temperature stability
- Flexibility
- Cleanness

Form deviation and micro shape are issues related to the sensing unit. As stated in Section A.4, the surface design of objects produced by the optical industry is tending from simple planar and spherical shapes towards aspherical, off-axis aspherical and free-formed surfaces. This change leads to challenges for the used sensing units. Either, non-tactile and tactile sensing units, have to challenge the new requirements. The sensing units implemented in the presented SCMM are documented in Chapter A.5.



Non-tactile sensing units work mostly by computing the reflected rays from the surface. The restrictive criterion for the proper use is that the ray reflects at a narrow-angle. Depending on the used optic of the sensing unit, the acceptance angle is minimal, often less than two degrees. By scanning an arched structure, the non-tactile sensing unit has to be always normal to the sub-aperture of the measurement area.

However, tactile sensing units do not require being normal to the surface of the specimen. Usually, these sensing elements are equipped with a ball tip that keeps the contact to the surface. Depending on the translation and displacement concerning the expected slope of the object under test, the exact position of the ball tip can be recalculated. Nevertheless, there is still an error caused by the bent shaft and the twisted chassis of the probe itself. The contact force between the sensing unit and the surface displaces not only the position of the ball tip; it bends the complete sensing unit.

The structure (roughness) of the surface of the specimen has influence as well. The standard production process used in the optical industry consists of grinding and polishing processes. Especially the grinding process causes damages to the surface.

A typical grinding process causes a rough structure on top of the object under test. This rough structure is the reason why most of the non-contact sensing units cannot operate on rough surfaces. Most of the incoming light is reflected and dispersed. However, tactile sensing units can physically operate on rough surfaces, because they physically touch the surface, independent of the surface structure. It is challenging to operate with tactile sensing units on rough surfaces. The ball tip is pressed on the surface; this cause damages to the surface, especially rough surfaces with peaks get

damages. The thin and fragile peaks break off, which leads to a visible track on the object under test. This effect is well known, and the optical industry developed two strategies to avoid this effect. The first strategy is to hone the surface before the measurement process. The honing process removes all sharp peaks smooth the surface before the measurement. This process is well known in technical grinding processes, even in the metalworking industry. The second strategy is to use lubrication during the measurement process. For this thesis, many test series with different types of lubrication had been carried out, with satisfactory results. The limitation of this strategy is the compatibility of the used material and the lubricant. Some types of glass are porous, and the lubricant infiltrates the specimen and undesirably changes the optical properties.

The following four significant characteristics are the material, the size and weight, the temperature stability and the flexibility. All of these characteristics belong to the material specifications, and they are related to the material of the specimen. Some commonly used materials are published in Chapter A.2.

However, the physical, chemical and mechanical characteristics of the used material of the specimen have a significant impact on the measurement process. It is essential not to overload a metrology system. Much, or even too much weight can cause significant damage to the measurement machine, especially to the bearing and guides. Furthermore, oversized dimensions of the specimen can cause collisions with the frame, sensing unit or other components of the metrology system.

Deformations of the specimen are a critical aspect, too. Temperature caused deformations are well known and manageable, especially in temperature-controlled measurement chambers. The flexibility of a specimen is a more critical issue. When the specimen is not blocked correctly, (ref. Chapter A.6.3), it is possible that a thin and fragile specimen is damaged during a tactile measurement. The Heidenhain™ Certo™ sensing units have a massive ball head (6 grams). Another issue is the damaging of the surface during tactile measurements, especially with rough surfaces and coated elements. A rough surface has little peaks on the surface whose easily can be damaged. The coating can be scratched.

The last point related to the specimen is cleanness. Optical production processes are dirty. All production processes are performed with a slurry or a coolant fluid. The loose grits in the slurry have a size of a few microns (ref. Chapter A.6), therefore is the cleaning process fundamental.

### A.7.3 Operator

The influence of the operator regarding a measurement has mostly unnoticed effects on the measurement process. For a better understanding of this influence, it has to be noted that this influence has to be grouped into two sub-categories.

- Errors caused by user application errors
  - o Faulty operation
  - o Low user skills
  - o Wrong planning and no proper strategy

- o False choose of sensing unit
- Errors caused by preparatory work
  - o Faulty preparation of the object under test
  - o Wrong handling of the object under test
  - o Causing damages to the measurement system
  - o Causing damages to the object under test

An excellent user interface and well-designed user guide in combination with a suitable qualification of the user are the keys to a successful measurement. The software packages can provide a significant contribution to reducing user skills. The software packages presented in Section A.12 are designed to reduce the number of user inputs down to a minimum. Validations and tests with other machines, especially metrology machines available at the LOE<sup>36</sup> showed clearly that most of the machines need much knowledge about the internal processes of the metrology systems. One of the goals of this thesis is to provide a metrology system that can be used in the complete production process, by the people working in the production process - not only by well-trained and educated professionals in the metrology laboratory.

One significant step in a user-friendly environment is to reduce the number of measurement strategies and functions. The metrology system published in this thesis provides only three strategies that are explained in Section A.10. The user has only to decide whether he needs a quick or accurate measurement result. Furthermore, to assist the user in deciding which sensing unit may be the best sensor for the planned

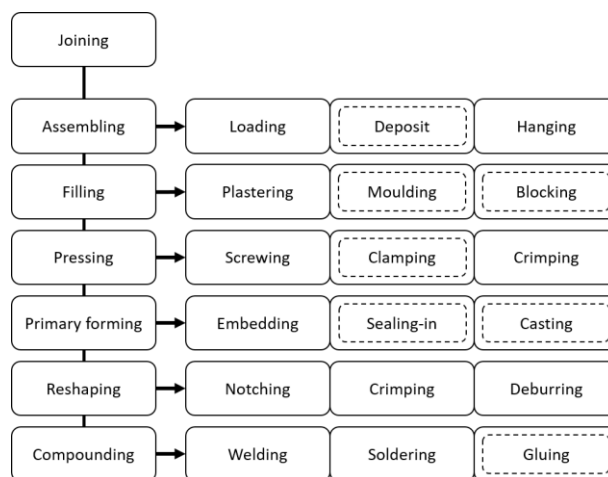
---

<sup>36</sup> LOE, Laboratory of Optical Engineering, Deggendorf Institute of Technology, Germany

measurement, a further goal is to reduce the number of used sensing units. The introduced measurement machine can operate with a significant number of sensing units, but it can be used with only one tactile sensing unit and one non-tactile sensor. Both sensing units can operate on all roughness grades produced by the production process chain. All sensing available sensing units are documented in Appendix A.5. Commonly used production processes are published in Chapter A.6.

However, incorrect handling of the measurement machine is not the only error influence caused by the user. The second group of user-caused errors deal with the preparation of the measurement and the object to be measured. The optical industry knows several techniques to prepare the object to be measured. The goal is to prepare the object under test in the best way to be measured. The DIN ISO 8593 - Manufacturing processes joining – provides a broad scope of joining strategies [95].

*Table 13: Joining technologies. Fabrication science knows many different methods to join parts. The high requirements regarding accuracy, the ductility of the material and cleanness in the optical industry excludes most of the technologies.*



Only a few of these joining techniques are suitable for usage in the optical industry. The actually used techniques are marked with a dashed line. Two joining technologies are dominating, the simple deposition in the metrology machine and a particular type of glue, called resin cementing. For this process, a metal carrier (mostly bronze), the resin, and the object under test are going to be heated up. After reaching a stable temperature, all parts come together and cool down slowly in the oven.

This process is very critical because it has more disadvantages than benefits, especially the heating process may damage the shape and causes tensions in the object under test. However, many production machines require a fixing element for their hydraulic extension chuck, so the metrology system has to fulfil the requirements.

A.7.4 Metrology system

The metrology system is responsible for some uncertainties. The most significant influences of the metrology system and of the measurement strategy are presented in

Table 14:

*Table 14: Sources of uncertainties related to different influences*

Related to machine design	Related to the sensing unit	Related to the software
Basic design	Probe system	Data analysis software
Guiding	Probe contact forces	Number of measurement points
Machine coordinate system	Probing method	Distribution of measurement points
Axes scales		Test sequence / Alignment process
		Selection criteria / Reference measurement
		Filtering / smoothing

Figure 93 presents the structure of the main four groups of coordinate measurement machines.

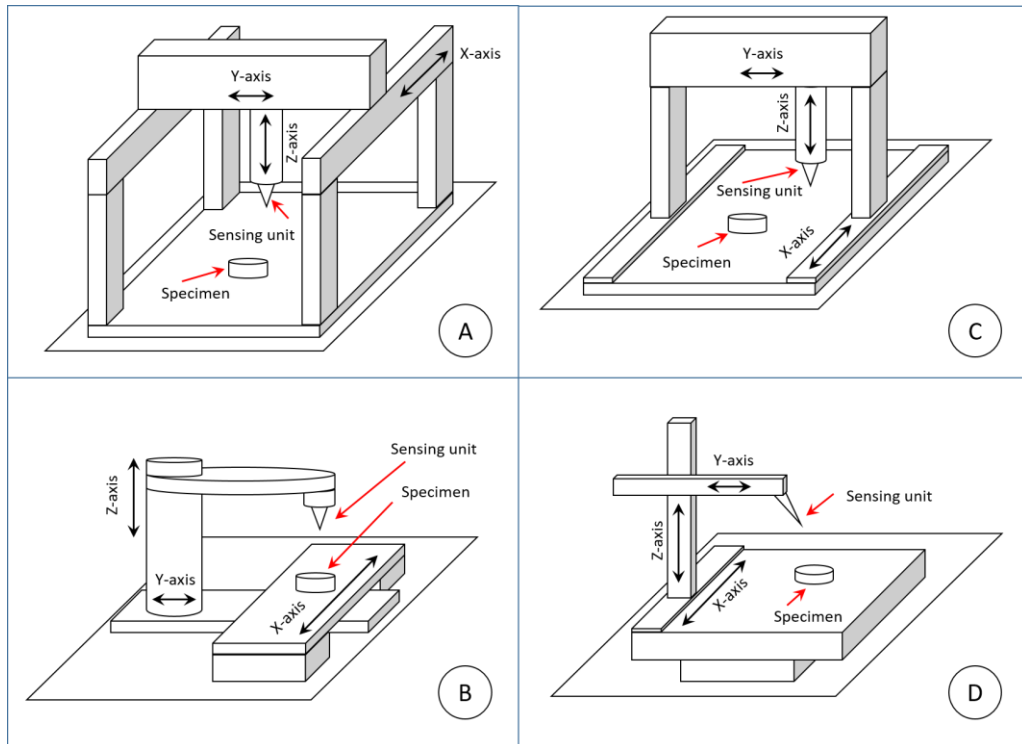


Figure 93: Examples of different CMM designs  
A: Portal design | B: Cantilever design | C: Bridge design | D: Gantry design

The significant issues can be sorted into three groups, machine design, sensing unit, and software. The mechanical aspects of the machine design are essential. During the design phase of a metrology system, many future problems can be avoided. For example, the symmetrical design is suitable for measurement machines. Since all common materials are subject to thermal expansion, symmetry is an advantageous feature. The presented SCMM is designed symmetrically with the Y-axis as a symmetrical axis. Furthermore, the used materials are used symmetrically on each side of the machine.



Another topic is related to the guiding of all moveable components. The literature knows a wide range of different solutions since metrology machines are commonly high accurate machines, the manufacturer's assembly mostly high accurate and expensive air-bearings in the linear and rotational axes. However, a system like the 3D-scale (ref. Chapter 5.3) may help to reduce the costs and step back to the cheaper roller or ball bearings. However, all axes are equipped with encoders. Modern absolute encoders can detect the position in the nanometre range [96]. The presented SCMM is equipped with highly accurate rotational encoders from Heidenhain™. The rotational axes, A, B, and C, are equipped with an ERO785 rotational encoder with 36,000 increments what is equal to 36 arc seconds. The Heidenhain™ LF481C linear encoders of the Y and Z-axis have a resolution of 4 microns.

However, the SCMM operates analogously to a spherical coordinate system. This advantage enables the use of rotational axes for the measurement process. The measurement process is published in Chapter 5.

Another group of influencing factors are related to the probe system. The presented SCMM is equipped with a modern and open NC control system (Siemens™ S7™). The S7 offers a wide range of interfaces. Therefore many different sensing units can be implemented. The list of available sensing units is presented in Chapter A.5.

The opportunity to decide between different sensing units allows the user to take care of the characteristic of the specimen. The presented SCMM is equipped with sensing units for each step in the production chain. However, the crucial factor for the decision which probing system is the material and the step in the production chain of

the specimen. The early steps in the production chain, for example, generating and grinding, are usually performed with tactile probes. Polished surfaces are measured with a contactless sensing unit.

The last group of influencing factors are related to the software package of the measurement machine. The presented SCMM is designed with three different software packages. The NC control system (SPS), the graphical user interface (GUI) and the data analysis software tool. Detailed explanations about the three packages can be found in Chapter A.12.

Simulations had verified the data analysis software of the SCMM in the CAD system and experimental validations (ref. Chapter 5 and Chapter 7). The reference software was MetroPro™. The data distribution is controlled by the NC control. The user can decide between the Track-, Spiral- or Cross-Section-mode. All measurement modes are published in Chapter A.9.

The alignment process of the presented SCMM required the development of a new process. The Centre search procedure of the SCMM does not need external devices; the complete alignment process can be performed with the available sensing units. The complete process is illustrated in Chapter A.9.

### A.7.5 The accuracy of the SCMM

The system-accuracy of the SCMM bases on the used components and their combination. Chapter 5.1 presents the kinematic correlations of an SCMM. Furthermore, Figure 5 depicts a basic sketch of a commonly designed SCMM. However, the critical components, physical aspects, and mechanical issues are illustrated in the following list:

- Air bearings of the B-, and C-axis
- The temperature of the SCMM and environment
- The probe path (related to the air bearings and the temperature variation)

Each of the listed has a different influence on the measurement result and has to be considered in detail. The following sub-Chapters present the analysis of the essential components and physical effects.

#### A.7.5.1 Analysis of the used air bearings

The used air bearings are high-quality air bearings from Physik Instrumente<sup>TM37</sup> (PI). This manufacturer is famous for its highly accurate and highly precise products. The datasheet of the used air bearings presents the following data:

- Axial runout: < 50 nanometres in total
- Radial runout: < 50 nanometres in total
- Tilt (3D): < 0.5  $\mu$ rad

---

<sup>37</sup> Physik Instrumente (PI) GmbH & Co. KG, Auf der Roemerstrasse 1, 76228 Karlsruhe. [www.physikinstrumente.com](http://www.physikinstrumente.com)

The given tolerance of the axial and radial runout of <50 nanometres in total describes the maximally allowed variation of both runouts. During one rotation of the air bearing a measurement, the gauge must not show more than <50 nanometres. The radial runout is measured perpendicular (radial) to the rotating axis, the axial runout, therefore axial to the rotational axis. All tolerances are related to the actual diameter of the air bearing, in the case of the SCMM air bearings 300 millimetres. The presented SCMM is designed to operate a specimen with a diameter of maximal 250 millimetres. The maximal length of the cantilever ( $c_p$ ) of the C-axis is 150 millimetres and therefore inside the tolerance.

The SCMM operates with two rotational axes, applying similar air bearings as presented above. The B-axis carries the chuck for the specimen. The centre axis of the B-axis is always rotating vertical, and the load does not change during measurement. Therefore, the radial runout causes a movement in the horizontal XY-plane. The second relevant error of the air bearing is the axial runout. The resulting movement goes directly into the Cartesian Z-direction of the SCMM.

The situation of the C-axis is different. The A-axis can tilt the C-axis in a range of  $\pm 80^\circ$ . Therefore, the axial and radial runouts are split into their horizontal and vertical components. Figure 94 depicts the situation of the radial and axial runout. According to the definition of the runouts, a tolerance field is defined.

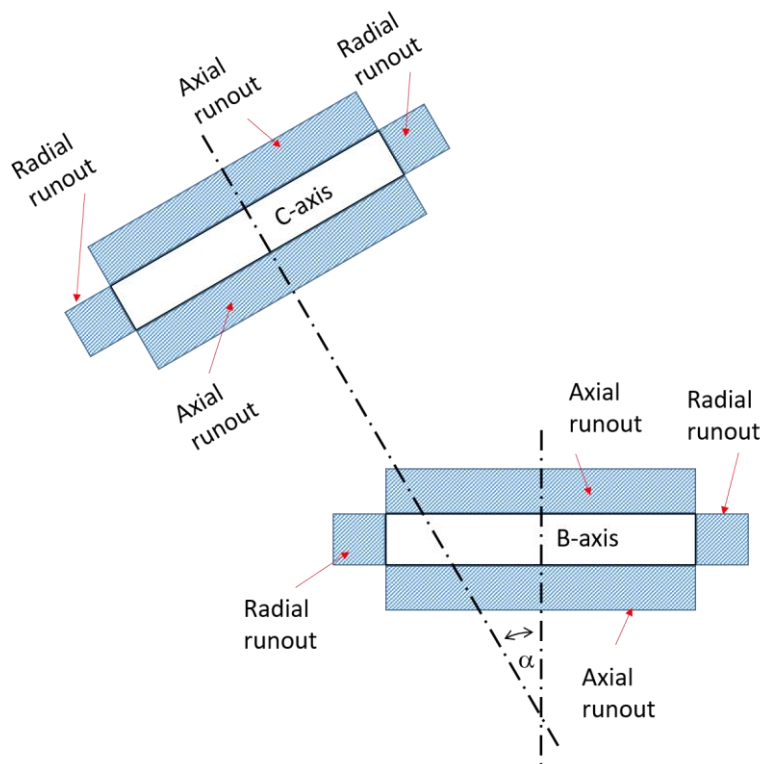


Figure 94: Radial and axial runout of the SCMM in a tilted configuration. Manufacturers provide the data of the axial and radial runout of a rotational axis for the original assembly position. In the case of the SCMM is one of the two applied rotational axes tilt-able. Therefore, the tolerances caused by the axial and radial runout related to the XYZ coordinate system have to be re-calculated.

Figure 95 illustrates the fields of tolerance of the B-axis and the C-axis. The C-axis can be tilted with the A-axis.

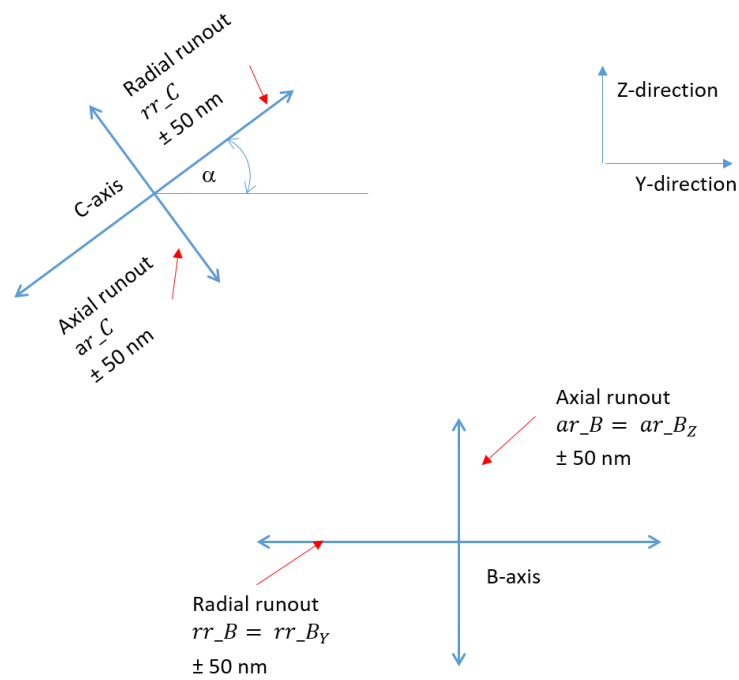


Figure 95: Tolerance analysis B-axis and C-axis. This sketch shows the situation of the axial and radial runout regarding the tilt of the A-axis.

The A-axis can be tilted in the range of  $\pm 80^\circ$ . Therefore, the radial and axial runout error of the C-axis split into a horizontal (Y-direction) and a vertical (Z-direction) component. However, both tolerance fields can be defined. The tolerance field of the B-axis is not subject to the A-axis tilt and can be noted as presented in Table 15:

Table 15: Tolerance field of the B-axis. The B-axis operates according to the manufacturer assembly instructions. Therefore, the tolerances can be considered without any further treatment

$$ar_{B_Z} = \pm ar_B \Rightarrow ar_{B_Z} = \pm 50 \text{ nm}$$

$$rr_{B_Z} = \pm rr_B \Rightarrow rr_{B_Z} = \pm 50 \text{ nm}$$

The tolerance field of the C-axis can be tilted. Therefore the tilt angle alpha of the A-axis has to be considered. With respect to the A-axis angle alpha, the tolerance field of the C-axis can be calculated with Equation 29 and Equation 30:

$$ar_{C_Z} = \pm (\cos(\alpha) * ar_C) \quad (29)$$

$$ar_{C_Y} = \pm (\sin(\alpha) * ar_C) \quad (30)$$

$$rr_{C_Z} = \pm (\sin(\alpha) * rr_C) \quad (31)$$

$$rr_{C_Y} = \pm (\cos(\alpha) * rr_C) \quad (32)$$

Where:

$ar_{C_Z}$  = Axial runout error of the C-axis in Z-direction

$ar_{C_Y}$  = Axial runout error of the C-axis in Y-direction

$\alpha$  = A-axis angle alpha

$ar_C$  = Axial runout error of the C-axis, manufacturer datasheet

Since the A-axis is allowed to operate between 80° and -80°, the significant results are noted in Table 16 -Table 19.

Table 16: C-axis axial error ( $ar_C$ ) in Z-direction as a function of A-axis angle  $\alpha$ 

$ar_{C_Z}$ as function of $\alpha$ ( $-80^\circ$ to $80^\circ$ )
$ar_{C_Z} = \pm 8,68 \text{ nm}$ ( $\alpha = -80^\circ$ )
$ar_{C_Z} = \pm 8,68 \text{ nm}$ ( $\alpha = +80^\circ$ )
$ar_{C_Z} = \pm 50 \text{ nm}$ ( $\alpha = 0^\circ$ )

Table 17: C-axis axial error ( $ar_C$ ) in Y-direction as a function of A-axis angle  $\alpha$ 

$ar_{C_Y}$ as function of $\alpha$ ( $-80^\circ$ to $80^\circ$ )
$ar_{C_Y} = \pm 49.24 \text{ nm}$ ( $\alpha = -80^\circ$ )
$ar_{C_Y} = \pm 49.24 \text{ nm}$ ( $\alpha = +80^\circ$ )
$ar_{C_Y} = 0 \text{ nm}$ ( $\alpha = 0^\circ$ )

Table 18: C-axis radial error ( $rr_C$ ) in Z-direction as a function of A-axis angle  $\alpha$ 

$rr_{C_Z}$ as function of $\alpha$ ( $-80^\circ$ to $80^\circ$ )
$rr_{C_Z} = \pm 49.24 \text{ nm}$ ( $\alpha = -80^\circ$ )
$rr_{C_Z} = \pm 49.24 \text{ nm}$ ( $\alpha = +80^\circ$ )
$rr_{C_Z} = 0 \text{ nm}$ ( $\alpha = 0^\circ$ )



Table 19: C-axis radial error ( $rr_C$ ) in Y- direction as a function of A-axis angle  $\alpha$ 

$rr_{C_Y}$ as function of $\alpha$ ( $-80^\circ$ to $80^\circ$ )
$rr_{C_Y} = \pm 8,68 \text{ nm}$ ( $\alpha = -80^\circ$ )
$rr_{C_Y} = \pm 8,68 \text{ nm}$ ( $\alpha = +80^\circ$ )
$rr_{C_Y} = \pm 50 \text{ nm}$ ( $\alpha = 0^\circ$ )

The final errors in Y- / Z-direction of the B- and C-axis are presented in Table 20:

Table 20: Combined error in Z-direction. The combined errors of the B- and C-axis caused by the radial and axial runout of both axes

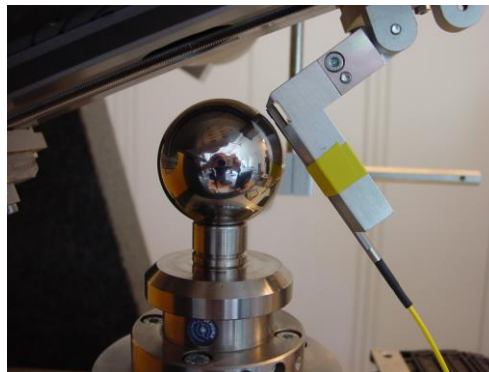
$arr_{C_Z}$ as function of $\alpha$ ( $-80^\circ$ to $80^\circ$ )
$arr_{BC_Z} = 215.84 \text{ nm}$ ( $\alpha = -80^\circ$ )
$arr_{BC_Z} = 215.84 \text{ nm}$ ( $\alpha = +80^\circ$ )
$arr_{BC_Z} = 200 \text{ nm}$ ( $\alpha = 0^\circ$ )

Table 21: Combined error in Y- direction. The combined errors of the B- and C-axis caused by the radial and axial runout of both axes

$arr_{C_Y}$ as function of $\alpha$ ( $-80^\circ$ to $80^\circ$ )
$arr_{BC_Y} = 215.84 \text{ nm}$ ( $\alpha = -80^\circ$ )
$arr_{BC_Y} = 215.84 \text{ nm}$ ( $\alpha = +80^\circ$ )
$arr_{BC_Y} = 200 \text{ nm}$ ( $\alpha = 0^\circ$ )

The results presented in Table 20 and Table 21 show that the combined errors of the axial and radial runout of the B-axis and C-axis are in a range of 200 nanometres. Therefore, it can be postulated that the maximum accuracy of the SCMM with the used air bearings is 200 nanometres. This theoretical value represents the basic accuracy of the SCMM. Furthermore, additional errors, such as presented in Chapter 6, reduce the basic accuracy of the SCMM.

However, a test series was performed to verify the result of the theoretical analysis of the radial and axial runout of the SCMM. The test series was performed in the measurement chamber of the LOE within a temperature range of 20°C and a maximal temperature variation of 0.15°C/24h. The test series was performed in 40 seconds to keep the influence of the temperature variation small. The setup of the tests is depicted graphically in Figure 96.



*Figure 96: Test setup radial and axial runout of the SCMM. The test series was performed with a measurement ball and a Micro-Epsilon™ confocal sensing unit.*

The used sensing unit was a Micro Epsilon™ confocal sensing unit, as presented in Chapter A.5.4. Figure 97 depicts the result of the interferometer measurement of the used specimen.

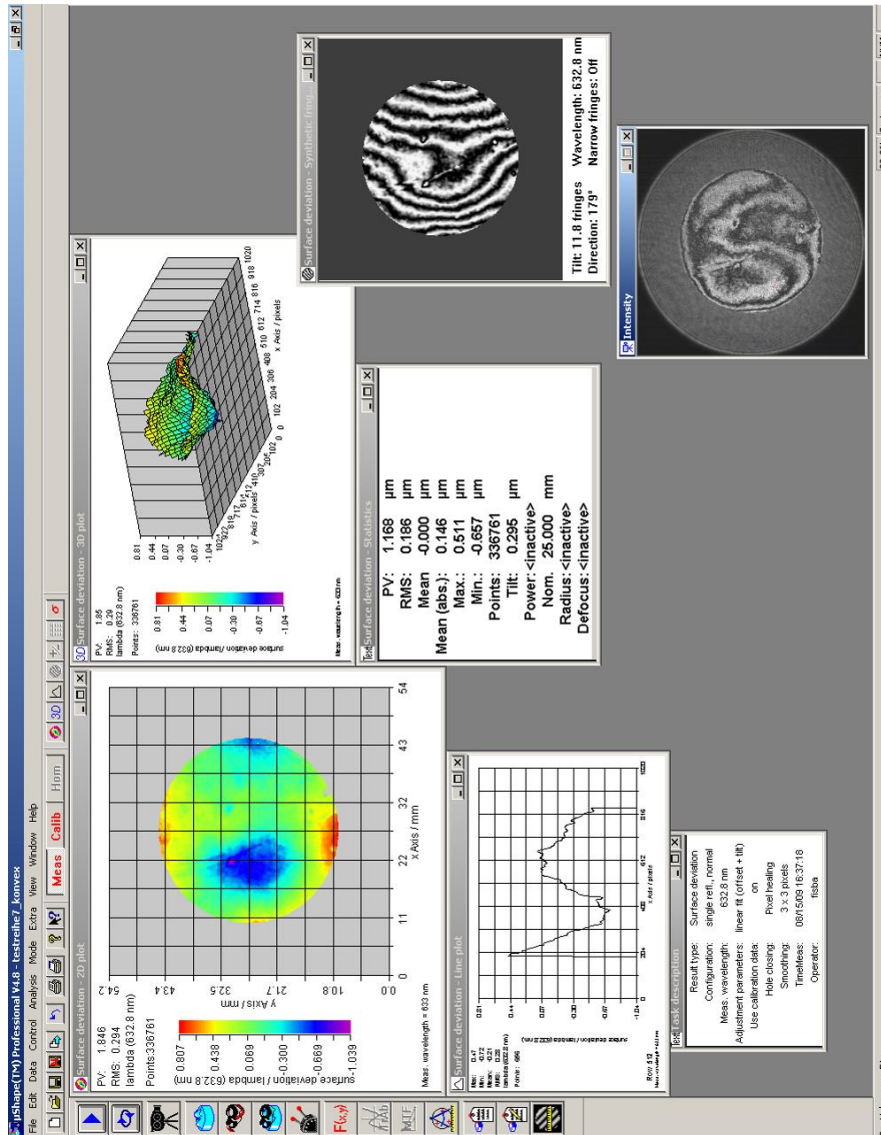


Figure 97: Resulting interferometer measurement performed with a Fisba™ interferometer.

The used specimen was a polished steel ball with an accuracy of 1.168 microns. For the test series, the A-axis was tilted to an angle of 45°, and the B-axis was rotating with 15 rounds per minute. With the total measurement time of 40 seconds, 10 rotations of the B-axis were recorded.

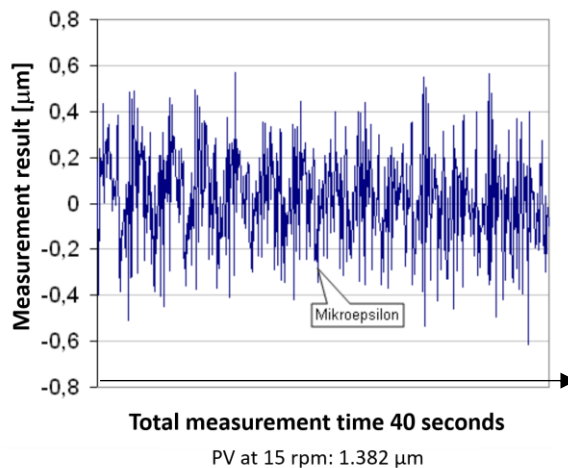


Figure 98: Result of radial and axial measurement. Of the SCMM. The Y-axis represents the value of the sensing unit converted into microns. The X-axis represents the measurement time in seconds.

The result of the performed test series confirms the theoretical analysis. The test series delivered a PV of 1.382 microns. The interferometer measurement showed a PV of 1.168 microns. Therefore, the difference between the measurement results is 214 nanometres, which verify the presented analysis.

However, there are three possibilities to compensate for the error caused by the air bearings.

- 1) Record the movement of the air bearing in all possible situations and positions.

This method requires a very comprehensive set of test series. The radial and axial runout and the tilt of the air bearing may vary in different conditions, such as:

- o Temperature drifts
- o Humidity drifts
- o Dynamic effects such as vibration
- o Variation of the turning speed
- o Variation of the load

Because of this procedure, a broad set of error maps can be recorded. Each of the error maps fits for a unique working condition of the SCMM. Therefore, this method predicts errors depending on the recorded working conditions. With an increasing number of error maps, the prediction becomes more accurate. A suitable solution to monitor rotational axes, the 3D-scale [53], can be found in Chapter A.8. The 3D-scale can be interpreted as a permanent reference measurement system.

## 2) Installation of a metrology frame

Literature knows examples of metrology frames [97]. Metrology frames are a system of sensing units tracing the movement of all critical parts and assemblies. Compared to method 1, the metrology frame covers the complete metrology device.

Depending on the accuracy, the number, and type of the used sensing units, a metrology frame may be a high accuracy, but a costly solution. One of the primary design goals of the presented SCMM was to develop a suitable metrology solution for workshops for small and medium-sized companies.

## 3) Reference measurements

The principle of a reference measurement is presented in Chapter A.12.2.1. Concerning the costs of a metrology frame and the missing flexibility of an error map solution, the presented SCMM had been designed to operate with reference measurements.

A reference measurement records all repeatable errors, very close to the time of the measurement of the specimen. The combination with a temperature drift compensation represents the chosen error compensation method for the presented SCMM.

#### A.7.5.2 Analysis of the temperature variation

The frame of the SCMM consists of different components produced out of different materials. Engineers always try to use the best suitable material for each component of a machine. The correct choice of the material is based on the purpose of the component, and some initial defined imitates, such as price, weight, or mechanical aspects.

In the case of the SCMM, thermal aspects and weight had been critical aspects. Thermal expansion falsifies test results and has to be compensated. Since it is very complicated to reduce the thermal drift around metrology equipment, the reduction of the temperature indicated errors is essential. The modern engineering science knows many different materials, natural and artificial, with a very low thermal expansion coefficient. Another method, next to material science, is the way of the product design. Current metrology systems are often designed in a symmetrical manner.

During the design phase of the presented SCMM, the following calculation had been carried out to predict the temperature indicated errors, Figure 99.

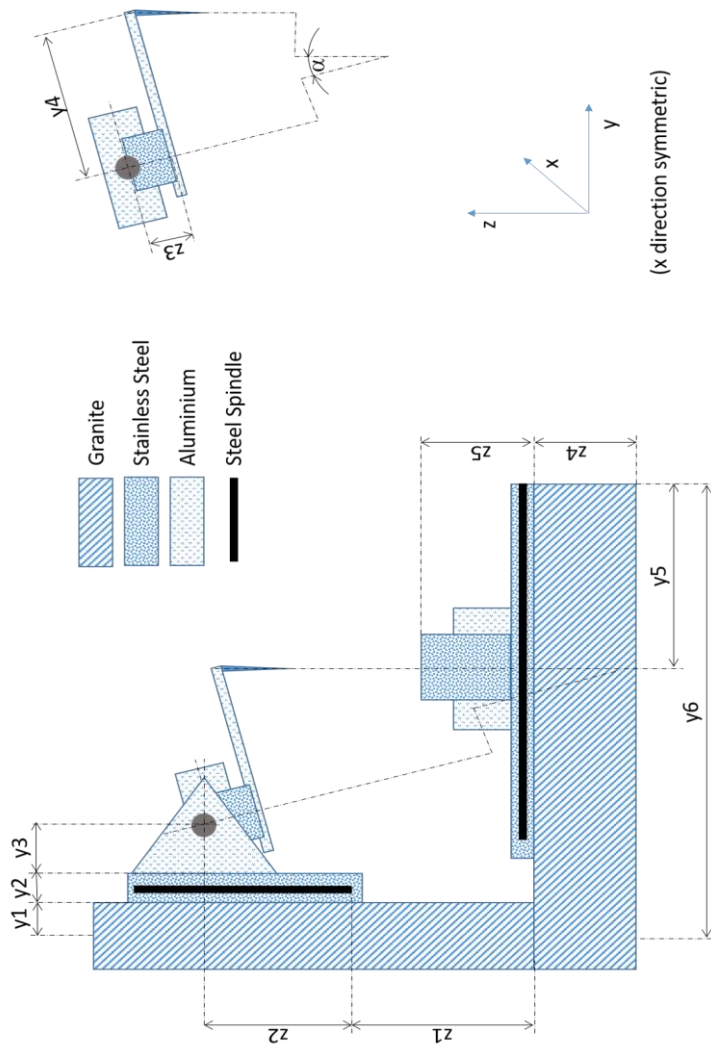


Figure 99: Geometric relations for thermal drift compensation. The SCMM was designed with different materials such as granite, stainless steel, and aluminium. All materials are subject to different thermal expansion factors. Therefore, the influence of temperature variations has to be considered entirely. This drawing illustrates the main machine components and the used materials.

The base for the calculation had been the technical data of the used materials that are depicted in Table 22. The dimensions of the SCMM are presented in Table 23.

Table 22: Thermal expansion coefficients of the used materials

Granite [1/K]	Stainless steel (V2A) [1/K]	Aluminium [1/K]	Tool steel (spindles) [1/K]
$3.0 \times 10^{-6}$	$10.25 \times 10^{-6}$	$23.8 \times 10^{-6}$	$12.5 \times 10^{-6}$

*Table 23: Dimensions and materials of the SCMM. The technical drawings of the SCMM provide the required information about the dimensions and the materials*

	Material	Dimension
Y1	Granite	100 millimetres
Y2	Stainless steel (V2A)	60 millimetres
Y3	Aluminium	130 millimetres
Y4	Aluminium	120 millimetres
Y5	Tool steel (spindles)	500 millimetres
Y6	Granite	800 millimetres
Z1	Granite	425 millimetres
Z2	Tool steel (spindles)	375 millimetres
Z3	Stainless steel (V2A)	125 millimetres
Z4	Granite	250 millimetres
Z5	Stainless steel (V2A)	200 millimetres

Concerning the design and the technical data sheets of the used components, the thermal expansion of the SCMM can be calculated. The design consists of three assembly groups, the base, the column, and the tilt axis. With the commonly known Equation 33, the change of the length as a function of the temperature can be calculated.



$$\Delta l = l_0 * \alpha_T * \Delta t \quad (33)$$

Where:

$\Delta l$  = The temperature indicated variation in length

$l_0$  = the original length

$\alpha_T$  = The thermal expansion coefficient

$\Delta t$  = The change of the temperature

With respect to the schematic sketch, presented in Figure 99, all components in the same direction can be summed up. The following Equation 33 and Equation 34 illustrate the final equations for the summed up variations in the Z and in the Y direction.

$$\Delta z_{tot} = z_4 + z_1 + z_2 - (\sin \alpha * z_3) + z_5 \quad (34)$$

Where:

$\Delta z_{tot}$  = Sum of all length variation in Z-direction

$z_1$  = Length variation of  $z_1$ , calculated with Equation 33

$z_2$  = Length variation of  $z_2$ , calculated with Equation 33

$z_3$  = Length variation of  $z_3$ , calculated with Equation 33

$z_4$  = Length variation of  $z_4$ , calculated with Equation 33

$z_5$  = Length variation of  $z_5$ , calculated with Equation 33

$\alpha$  = A-axis angle alpha

$$\Delta y_{tot} = y_1 + y_2 + y_3 + (\cos \alpha * y_3) - (y_6 - y_5) \quad (35)$$

Where:

$\Delta y_{tot}$  = Sum of all length variation in Y-direction

$y_1$  = Length variation of  $y_1$ , calculated with Equation 33

$y_2$  = Length variation of  $y_2$ , calculated with Equation 33

$y_3$  = Length variation of  $y_3$ , calculated with Equation 33

$y_5$  = Length variation of  $y_5$ , calculated with Equation 33

$y_6$  = Length variation of  $y_6$ , calculated with Equation 33

$\alpha$  = A-axis angle alpha

With the given thermal expansion coefficients of the different used materials, published in Table 22, the theoretical thermal expansion of the system can be calculated.

*Table 24: Results of thermal expansion prediction. This table presents the normal length variation per 1K in Y- and Z-direction. The setup of the SCMM knows three critical positions of the A-axis, +80°/0°/-80°, therefore, all three positions have to be considered in the analysis*

Length variation per 1K
$\Delta y_{tot} = 12.843 \frac{\mu m}{K}$ at alpha 0°
$\Delta z_{tot} = 8.2 \frac{\mu m}{K}$ at alpha ± 80°

Table 24 shows the results of the uncertainty estimation of the SCMM structure. The presented results show two critical values for the thermal expansion in the Y and in the Z direction. The values  $\Delta z_{tot}$  and  $\Delta y_{tot}$  are calculated with the maximal length of the employed axes. Since this setup is possible but not often used, the second set of values is presented.  $\Delta z_{tot}$  and  $\Delta y_{tot}$  depicts the regular setup of the SCMM as very frequently used in the laboratory. Another important aspect is the actual temperature drift of the measurement chamber where the SCMM is located. Test series proofed that the actual variation of the temperature is less than 0.15 Kelvin per hour. A regular measurement in the Track-mode takes precisely one hour. All other measurement modes are faster. Therefore, the predicted thermal expansion of the presented SCMM can be found in Table 25.

*Table 25: Predicted temperature influence. This table presents the normal length variation per 0,15K in Y- and Z-direction. The setup of the SCMM knows three critical positions of the A-axis, +80°/0°/-80°, therefore, all three positions have to be considered in the analysis*

Length variation per 0.15K
$\Delta y_{tot\ 0.15} = 1.93 \frac{\mu m}{0.15K} \text{ at } \alpha 0^\circ$
$\Delta z_{tot\ 0.15} = 2.23 \frac{\mu m}{0.15K} \text{ at } \alpha \pm 80^\circ$

Figure 100 illustrates the result of the uncertainty estimation of the SCMM frame. The simulation was performed with the dimensions and thermal coefficients presented in Table 23 and Table 24. As a function of the A-angle alpha, the error in Y-

direction reaches the maximum at 0°. Therefore, primarily planar measurements are subject to errors caused by thermal expansion.

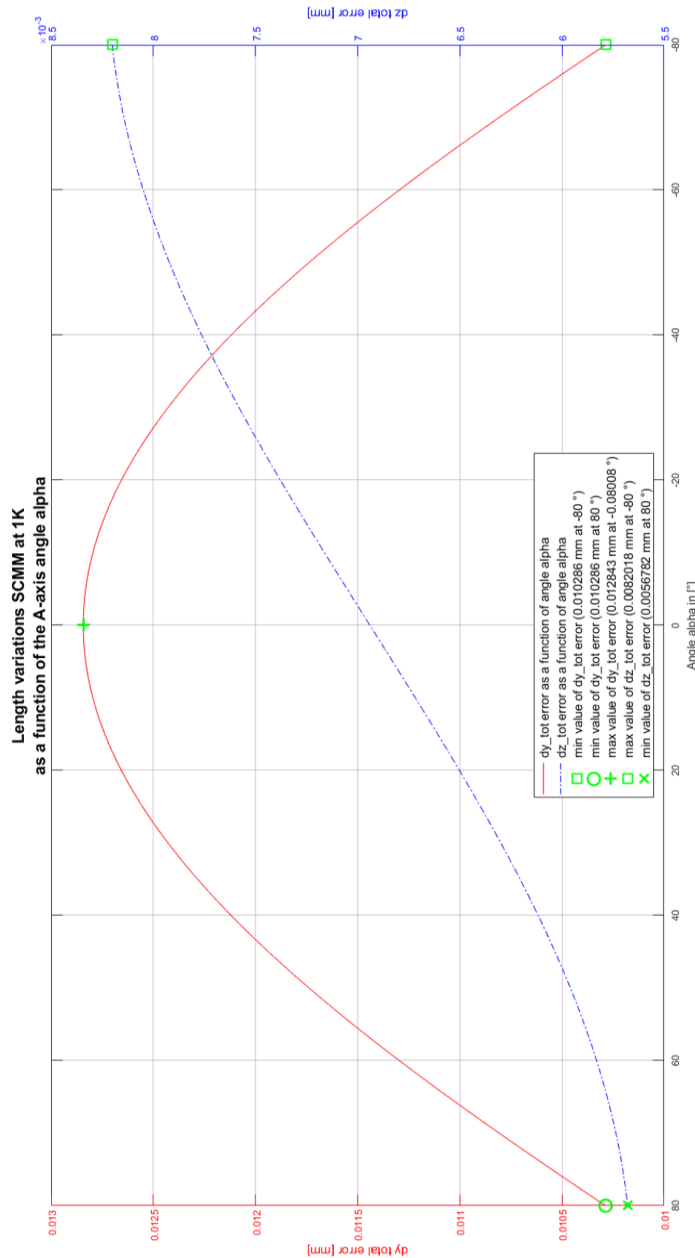


Figure 100: Length variations SCMM at 1K. The left side of the Y-axis represents the error in Y-direction in millimetres; the right side of the Y-axis represents the error in Z-direction in millimetres. The X-axis displays the A-axis angle alpha. The error in Y-direction reaches the most significant value at alpha=0°, therefore is the error in the Y-error in the planar mode greatest. The error in Z-direction is represented by the blue dashed line and reaches the most significant value at alpha=-80° what is equal to a concave setup of the SCMM.

Figure 101 shows the corresponding simulation with a temperature variation of 0.15K. This is the range where the LOE measurement chamber can be temperature controlled.

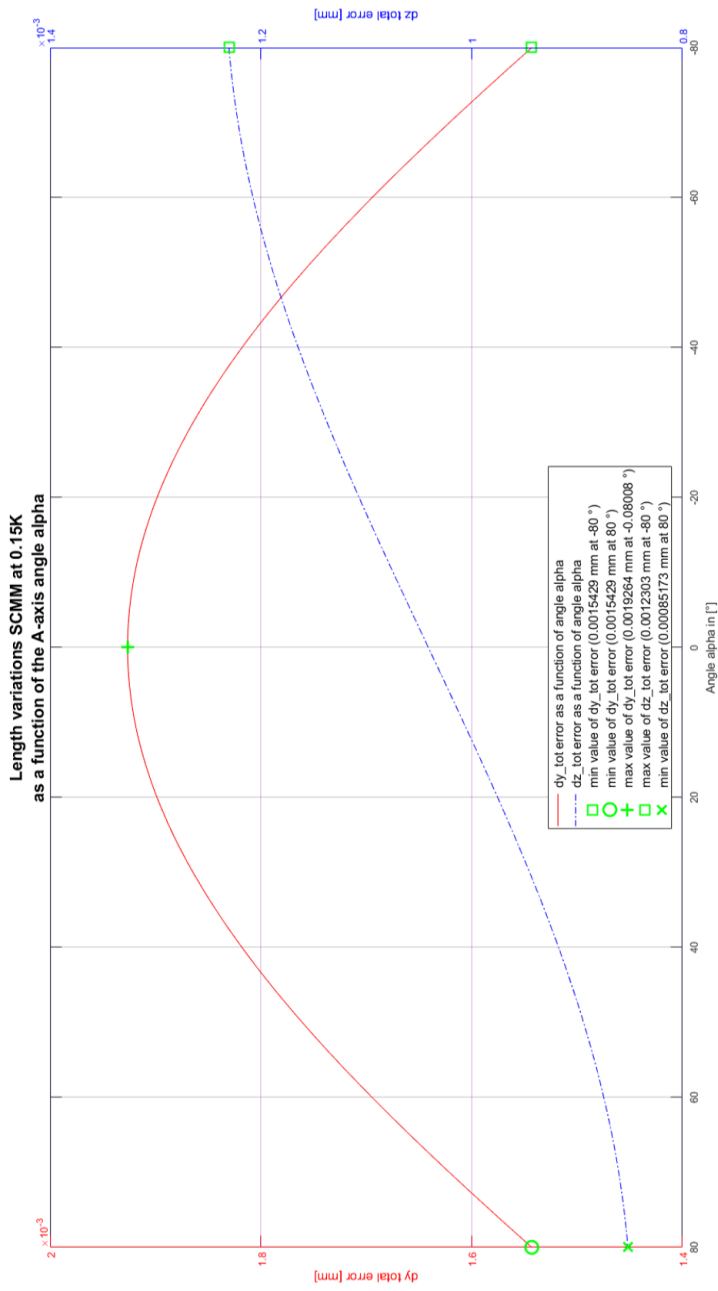


Figure 101: Length variations SCMM at 0.15K . The left side of the Y-axis represents the error in Y-direction in millimetres; the right side of the Y-axis represents the error in Z-direction in millimetres. The X-axis displays the A-axis angle alpha. The error in Y-direction reaches the most significant value at alpha=0°, therefore is the error in the Y-error in the planar mode greatest. The error in Z-direction is represented by the blue dashed line and reaches the most significant value at alpha=-80° what is equal to a concave setup of the SCMM.

## A.8 The 3D-Scale

High precise bearings, especially air bearings, are expensive. Cheaper ball or roller bearings mostly have a lower quality and lower accuracy. A solution had been required to bring the developed metrology system to the market. The replacement of the costly air bearings with cheaper ball or cylinder bearings was one of the essential goals. In the first step, the high accurate air bearings of the SCMM had not been replaced. The development of an entirely new prototype with the standard ball or roller bearings is planned as future work.

However, the 3D-scale is a mechatronic device, detecting and compensating the movement errors of rotational axes in a reliable and very accurate manner. In advance of Section 5.3, Figure 102 illustrates the essential function of the system.

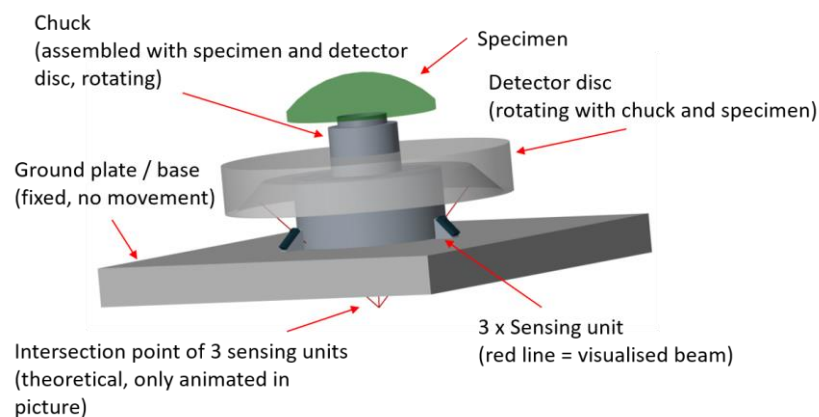


Figure 102: CREO3™ (M100) 3D sketch of the 3D-scale system.

*The illustrated 3D sketch presents the general concept of the 3D-scale. The specimen is secured in a chuck that is assembled on a rotational axis. The rotational axis is assembled on a solid basement. Three sensing units are mounted in a 120° distribution around the chuck on the solid basement. A detector disc is assembled on the rotating chuck. The three sensing unit measures the distance to the detector disc.*

The 3D-scale consist of four elements - three sensing units and one detector disc. The detector disc is designed with a  $45^\circ$  angle on the inner edge, and it is assembled on the rotating chuck. The three sensing units are pointing towards this  $45^\circ$  surface. The three sensing units are assembled on a solid base, usually the base of the machine. The lengthening of the sensor beams intersects at one point, the centre of a spherical coordinate system. The sensing units are assembled in  $3 \times 120^\circ (=360^\circ)$  around the central axis (rotational axis) of the chuck. A spherical coordinate system describes one point with two angles and one vector. Both angles are defined already,  $120^\circ$  and  $45^\circ$ . The length of the required vector is variable. The vector consists of two parts; the lengthening of the sensor beam and the distance between the sensing unit and the  $45^\circ$  slope of the detector disc measured by the sensing unit. Therefore, are all three required values fixed. Since the 3D-scale operates with three sensing units, three points (P1, P2, P3) can be calculated, one for each sensing unit.

The three points can be used to calculate a circle with its normal axis. Therefore, it is possible to calculate the movement of the disc in all six degrees of freedom (XYZ and pitch, tilt, yaw). Further details about the 3D-scale and the test series may be found in Section 5.3.

For the verification of the device, the radial and the axial runout had been measured with two Micro-Epsilon™ confocal sensing units. The axis equipped with the 3D-scale had been rotating with 30 rounds per minute. The Micro-Epsilon™ sensing units documented the radial and the axial runout with 100 Hz during the complete test cycle of 100 rotations. The data obtained from the 3D-scale had been saved in one

complete measurement file. After finishing the test cycle, the correction file from the 3D-scale had been computed with the Micro-Epsilon™ sensing unit files. The test cycle had been taken place in a climate chamber at 20°C ( $\pm 0.1^\circ\text{C}$ ).

#### A.8.1 Development of the 3D-Scale

The 3D-scale is a mechatronic device developed in the context of this PhD thesis. This device allows monitoring of rotational axes according to their radial-, and axial-runout. A spherical coordinate measurement machine employs three rotational axes, whereas two rotational axes are used during a measurement process.

Most of the production and metrology equipment is designed with highly accurate and expensive air bearings. One of the goals of this thesis is to develop a metrology system for workshops, therefore is the price of the final system a significant factor. The presented 3D-scale allows the use of cheap roller bearings. The radial and axial runout may be monitored and documented during the movement of a rotational axis. The gathered information may be used to compensate for the recorded deviations.

The 3D-Scale is a patented metrology solution [53] which can improve the accuracy of rotational axes. The system, presented in Figure 103, consists of three sensing units and an exclusively designed detector disc.

Figure 103 presents the design of the 3D-Scale. It consists of three sensing unit and a specially designed detector disc. The system is designed to be added to existing



rotational axes. The detector disc is assembled on the chuck. The three sensing units are assembled on the frame of the axis that does not rotate.

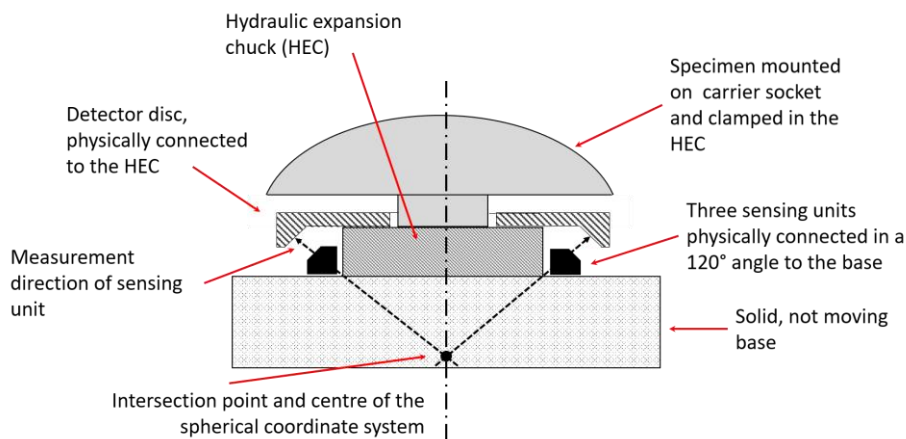


Figure 103: 3D-Scale schematic sketch. The 3D-Scale consists of two main components. The three sensing units and the detector disc. The sensing units are assembled in a 120° angle concentrically around the central axis of the rotational axis. The detector disc is assembled on the chuck of the axis.

The 3D-Scale is designed to operate according to a spherical coordinate system. The detector disc has a 45° angle on the inside. Three sensing units are homogeneously distributed (120°,φ) around the rotational axis. The sensor signal perpendicularly incidents on the 45° slope. The virtual lengthening of the sensor signal intersects with the rotation axis of the detector disc in the angle  $\Theta$ , usually 45°. Figure 104 depicts the coherencies in detail.

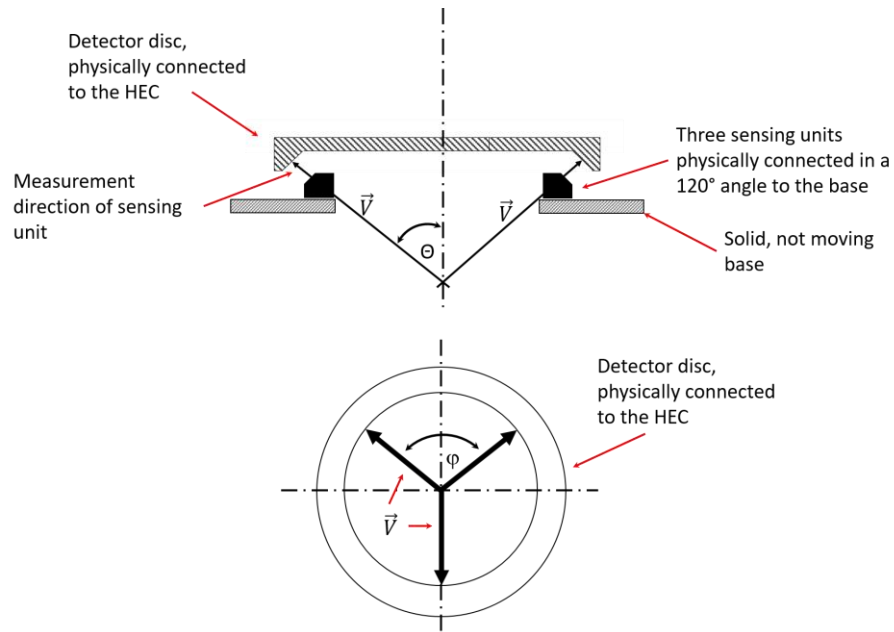


Figure 104: SCS design of the 3D-scale device. The 3D-Scale is designed analogously to a spherical coordinate system (SCS). The three sensing units have an angle  $\Theta$  of  $45^\circ$  with respect to the central axis of the rotational axis. The chamfer of the detector disc is designed to have a  $45^\circ$  angle. Therefore, the sensing units can point rectangular to the chamfer surface.

The angle  $\Theta$ , the vector  $\vec{V}$ , and the angle  $\varphi$  define the spherical coordinate systems. In the case of the 3D-Scale, the vector  $V$  is represented by the distance between the centre point of a spherical coordinate system and the sensing unit plus the length measurement by the sensing unit. Therefore, the readout of the three sensing units delivers three points.

The three points span up a defined circle. Variations of the diameter are interpreted as the axial movement of the detector disc. With the goal to detect tilts of the detector disc, the normal of the circle is calculated. Mathematical models presented in A.8.1.1 show the corresponding equations. Furthermore, the normal of the calculated circle is used to calculate the lateral movements of the detector disc.

However, the choice of the right sensing units and the best suitable materials are the critical factors for the design of the 3D-Scale. For the optical industry, materials with a minimal thermal expansion factor, such as Zerodur or Invar may be used. The sensing unit may be a highly accurate tactile sensor or an interferometer based sensing unit.

#### A.8.1.1 Mathematical model of the 3D-Scale

The 3D-Scale is designed analogously to a spherical coordinate system (ref. Figure 105). This coordinate system has the unique advantage that it operates with angles. That feature makes it predestined for systems operating with rotational axes.

The spherical coordinates can be transformed into Cartesian coordinates by using the following three Equation 36 to Equation 38 [99].

$$X = \vec{V} * \cos \Theta * \cos \varphi \quad (36)$$

$$Y = \vec{V} * \cos \Theta * \sin \varphi \quad (37)$$

$$Z = \vec{V} * \sin \Theta \quad (38)$$

Where:

$X, Y, Z$  = Cartesian coordinates

$\vec{V}$  = Vector from the centre point of a spherical coordinate system to the detector disc

$\theta$  = Polar angle

$\varphi$  = Azimuthal angle

Each measurement cycle of the three sensing units delivers three points in spherical coordinates (ref. Figure 105). The result of the transformation process is a table with Cartesian XYZ coordinates. Each row contains the XYZ information of all three sensing units. In this publication, each XYZ set of coordinates is defined as a point.

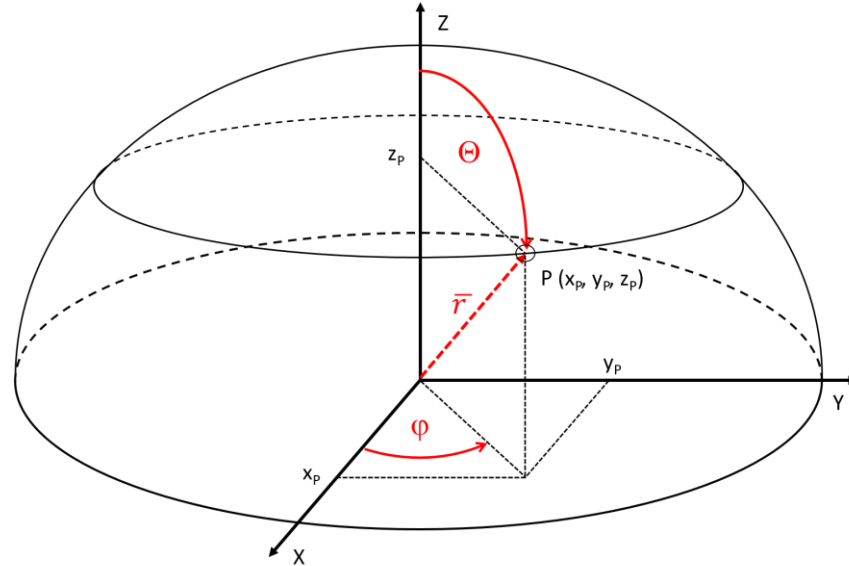


Figure 105: Spherical coordinate system. In a spherical coordinate system, the position of a point  $P$  is described with two angles and one vector. In the case of the 3D-Scale are both angles set ( $0^\circ/120^\circ/240^\circ$ ) and  $43^\circ$ . The vector is an addition of the length between the central point of the SCS and the chamfer of the detector disc.

To enable a full 3D analysis of all movements of the 3D-scale, detection of all six degrees of freedom is necessary. Three degrees of freedom for rotation (pitch, yaw, and roll) and three degrees of freedom for translation (up/down, left/right, forward/backwards). Therefore, the mathematical model has to be split into two operations, the calculation of the rotation and the calculation of the translation.

### A.8.1.2 Calculation of the tilt

Three points (A, B, and C) span up a plane. Depending on the position of the three points, the plane can be tilted in each possible direction (Figure 106).

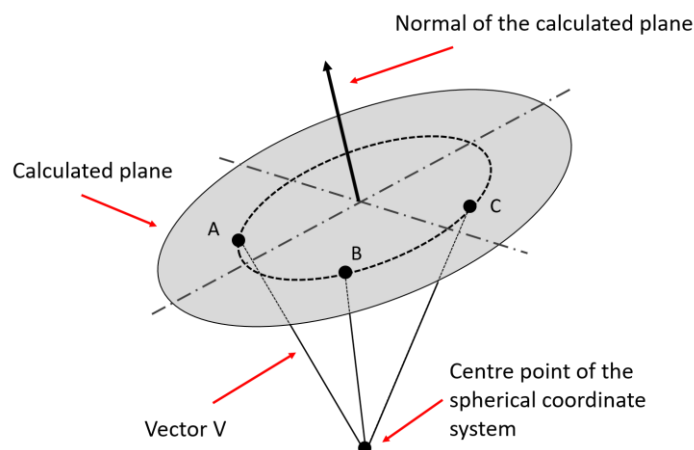


Figure 106: Calculated plane 3D-Scale. Three points are needed to create a plane. The three sensing units of the 3D-Scale deliver three independent points. Therefore, each measurement generates three points and one plane.

The points A, B and C are part of the linearly independent vectors  $\overrightarrow{AB}$  and  $\overrightarrow{AC}$ . The cross product of two linearly independent vectors is a vector that is perpendicular to both and therefore, normal to the plane between these two vectors [99, 100]. The normal vector defines the plane in its coordinate notation.

$$u \times v = \begin{vmatrix} i & j & k \\ u_1 & u_2 & u_3 \\ v_1 & v_2 & v_3 \end{vmatrix} = n \quad (39)$$

Where:

$$u = \overrightarrow{AB}$$

$$v = \overrightarrow{AC}$$

The tilt angles of the calculated plane can be computed by using Equation 40 - Equation 42 [99].

$$\cos(\alpha) = \frac{n_1}{|\vec{n}|} \quad (40)$$

$$\cos(\beta) = \frac{n_2}{|\vec{n}|} \quad (41)$$

$$\cos(\gamma) = \frac{n_3}{|\vec{n}|} \quad (42)$$

Where:

$\alpha$  = Angle for rotations with the X-axis as a central axis (Roll)

$\beta$  = Angle for rotations with the Y-axis as a central axis (Pitch)

$\gamma$  = Angle for rotations with the Z-axis as a central axis (Yaw)

$n$  = Normal of the X-, Y-, and Z-axis

The results of the computation are three angles that define the tilt angles of the plane normal in the Cartesian coordinate system. Therefore, the mathematical model delivers the tilt angles of the calculated plane, which is equal to the required result.

### A.8.1.3 Calculation of the translation

Next, to the tilt, the 3D-scale system can provide the translation in relation to the centre point of the coordinate system. The combination of the cross product and dot product allows calculating the exact radius and the Cartesian coordinates of the centre point. Concerning the points A, B, C and the angles  $\alpha, \beta, \gamma$ , the radius  $r$ , and the centre point C can be computed by using the following Equation 43 and Equation 44 [17, 18]

$$r = \frac{|A - B||B - C||C - A|}{2|A - B| \times (B - C)} \quad (43)$$

Where:

$r$  = radius of a circle containing three points ABC

$A$  = Cartesian coordinates of point A

$B$  = Cartesian coordinates of point B

$C$  = Cartesian coordinates of point C

$$CP = \alpha A + \beta B + \gamma C \quad (44)$$

Where:

$CP$  = Centre point of a circle containing three points ABC

$\alpha$  = Angle for rotations with the X-axis as a central axis (Roll)

$\beta$  = Angle for rotations with the Y-axis as a central axis (Pitch)

$\gamma$  = Angle for rotations with the Z-axis as a central axis (Yaw)

$A$  = Cartesian coordinates of point A

$B$  = Cartesian coordinates of point B

$C$  = Cartesian coordinates of point C

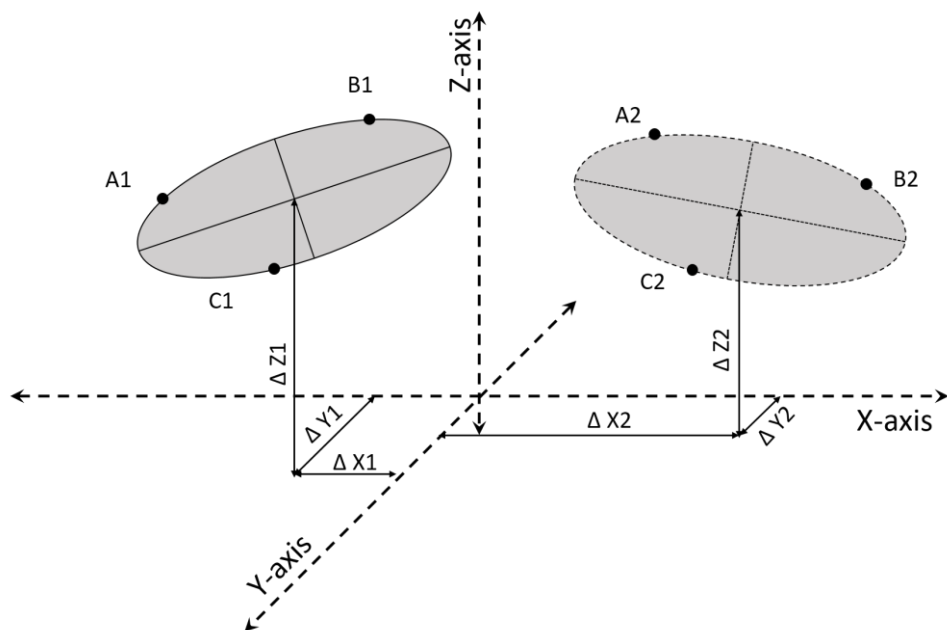


Figure 107: Two examples of planes with different centres. The 3D-Scale fetches the information of three sensing units at the same time. The three points are part of a circle. The centre point of the circle contains information about the displacement with respect to the XYZ-coordinate system.



The radius  $r$  is used as a control value to detect not useful measurements like, for example, when one or more sensing units do not meet the detector disk. The centre point of this circle provides information about the translation in relation to the coordinate system. Figure 107 presents an illustration with two examples of calculated circles and their deviations in relation to the coordinate system. Since the origin of the coordinate system has the coordinates  $(0/0/0)$ , the coordinates of the centre point can be used directly without any further mathematical treatments.

## A.9 Centre Search process

The Centre Search process is process developed for the alignment of the axes of the presented SCMM. The alignment of the axes is an essential feature to ensure accurate measurements. The presented approach does not require additional sensing units or measuring devices. The entire process can be operated with SCMM standard tools.

### A.9.1 Mathematical approach

This section presents the mathematical approach behind the generic Centre-search. The Centre-search is a procedure to aid the demand of an aligning process of machines by applying rotational axes. In the context of this PhD thesis, the presented procedure had been used to align the axes of a spherical coordinate measurement machine. The alignment process is a crucial factor in a complete and successful measurement result. The literature knows different techniques to align an SCMM or swing-arm-coordinate-measurement-machine. Commonly it is done with external measurement devices, such as laser tracker [49, 63] or additional sensing unit [45–47].

This Chapter presents a procedure to align the C-axis and the Y-axis of the SCMM without the need for external devices or additional sensing units in a very accurate manner. However, this procedure may operate with the application of any implemented sensing unit and a simple planar object with no special requirements according to

accuracy. Test series at the LOE demonstrated that a simple piece of planar float glass is sufficient. The specimen has to be blocked tilted. The only requirement for the tilt is that the used sensing unit does not leave the operation distance in any region of the specimen.

The complete centre search process consists of two essential parts, the alignment of the C-axis, and the alignment of the Y-axis.

The C-axis alignment process locates the C-axis 0° position. The correct positioning of the C-axis is a critical task. In the 0° position of the C-axis, the centre axis of the B-axis and the centre axis of the sensing should meet. For a successful C-axis alignment process, the sensing unit travels from one edge of the specimen across the centre to the opposite side of the specimen while the B-axis rotates continuously. This situation is depicted in Figure 108.

The user has to move the sensing unit roughly ( $\pm 3$  millimetres) in the centre region of the specimen (Y0) in the manual mode of the SCMM. After that manual positioning, the process starts and the sensor unit carrying cantilever moves from one edge of the specimen across the expected centre towards the opposite edge of the specimen.

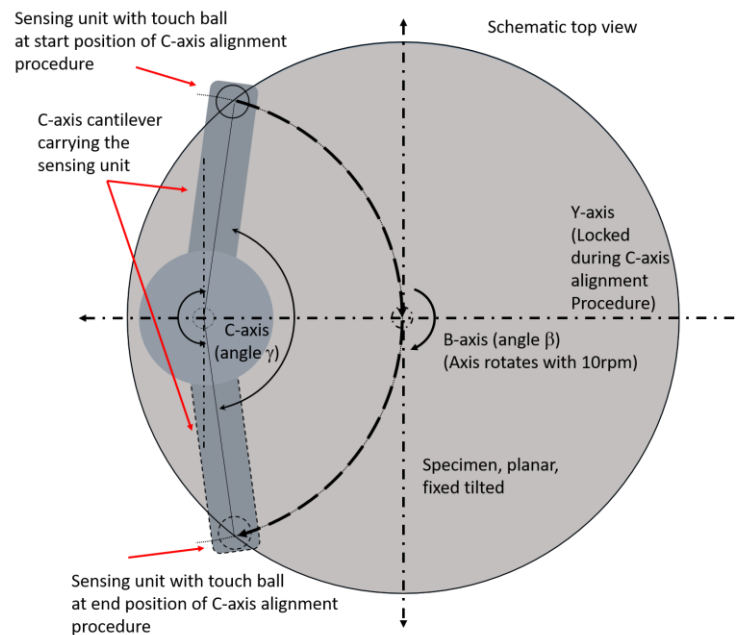


Figure 108: Centre search process – 1<sup>st</sup> step. The process starts with the alignment of the C-axis. The process requires a slightly tilted, planar specimen. The sensing unit travels across the specimen through the expected centre.

The system is designed to operate within ten seconds for the C-axis adjustment process. The B-axis rotates with one round per second. The sensing unit operates with a frame rate of 100 Hz. The resulting signal of the sensing unit is illustrated in Figure 109. In this plot, the sensing unit moves from plus 8° across the centre to the -8° position. The plot shows the signal of the sensing unit in micrometres and the turning angle of the C-axis. The plotted signal draws a sinus-shaped curve.

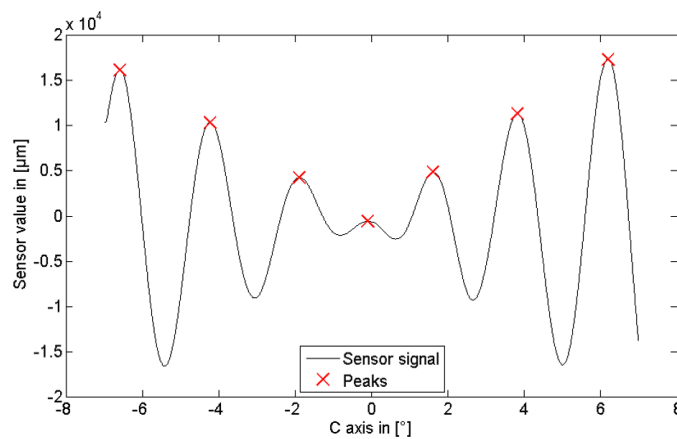


Figure 109: Sensor signal C-axis alignment. The Y-axis depicts the signal of the sensing unit, converted to microns. This is equal to the distance between the sensing unit and the surface of the specimen. The X-axis presents the position of the C-axis in degree. The sensing unit is assembled on the C-axis. The signal of the sensing unit is recorded in the maximal available speed. In the regions close to the edge of the specimen has the signal the highest amplitude, visualised on the left and right side of the plot during the movement across the expected centre of the tilted specimen, the amplitude of the signal decreases. The maxima of the signal are marked with a red X.

The C-axis alignment process requires the analysis of the measurement result.

However, the first step of the calculation is a mathematical curve fitting process. The primary function of the plotted curve is a sinus. Therefore, a nonlinear Marquardt-Levenberg [102] sum of sinus function had been used for the fit.

$$y(t) = \sum_{i=0}^{N-1} a_i * \sin(\omega_i * t + \varphi_i) \quad (45)$$

Where:

$y(t)$  = Variable Y as a function of time (t)

$N$  = Iteration variable (i = start value)

$a_i$  = Amplitudes as a function of i

$\omega_i$  = wavelength as a function of i

$\varphi_i$  = Phase shift as a function of i

The fitting algorithm operates according to the least square method. The resulting function of Equation 45 allows calculating all positive peaks (maxima) by using simple differential calculus. Figure 109 illustrates the calculated maxima (peaks) in relation to the original sensor signal.

It is essential to check the boundary conditions to eliminate adverse maxima. Such effects appear when the function starts with sinking and ends with a rising gradient. In this case, the first and/or last maximum has to be eliminated. The calculated maxima are part of a spline. The extrema of the spline represent the final 0° position of the C-axis. The graph and the calculated zero position can be seen in Figure 110.

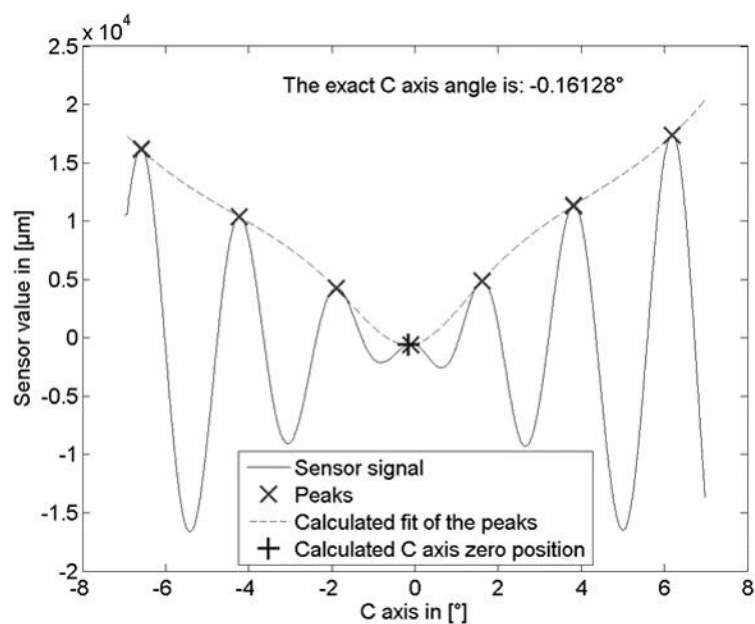


Figure 110: Result of the 1<sup>st</sup> step centre search. The Y-axis represents the sensor signal converted to microns. The X-axis represents the position of the C-axis in degrees. The application of the sum of sine fit delivered the functional equation of the signal. The analyses of the derivations deliver the maxima of the function. In the last step, a cubic spline interpolation of the obtained maxima delivers a curve with a minimum. This is the position of the C-axis zero position.

For the calculation of the graph, a cubic spline interpolation [99, 102, 103] had been used. In this example, the  $0^\circ$  position is at  $-0.16128$  degrees of the C-axis. The NC control moves the C-axis to this position and resets it to zero.

In a second step, the alignment process of the Y-axis is performed. This step includes two essential measurements. The essential setup of the Y-axis alignment requires locking the C-axis in the calculated  $0^\circ$  position obtained by the C-axis alignment process. The Y-axis moves 10 millimetres into the minus direction, starting at the manual adjusted position  $Y_0$ . This point is named  $Y_1$ . The B-axis keeps rotating with one round per second. Figure 111 presents the first step of the Y-axis alignment process.

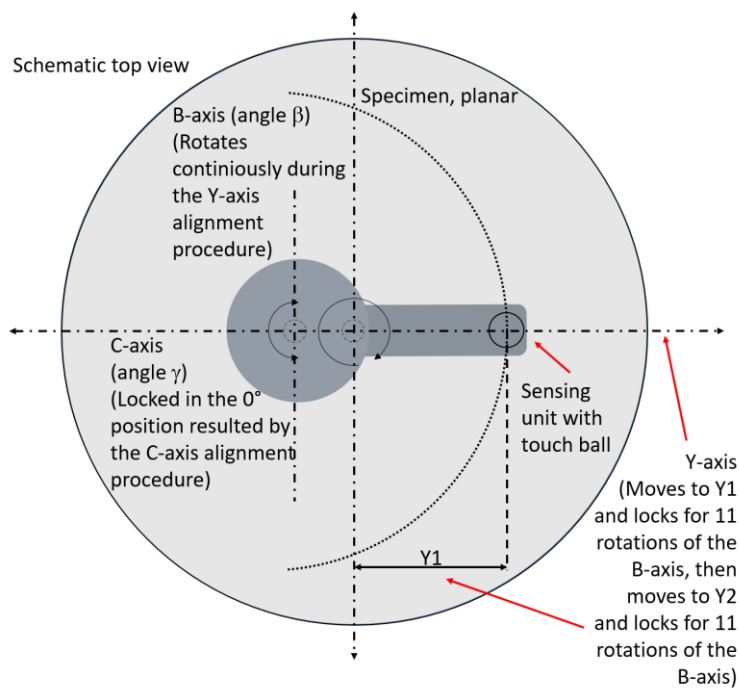


Figure 111: Centre search process – 2<sup>nd</sup> step part 1. The C-axis is locked in the obtained zero degrees position. The B-axis rotates continuously. The Y-axis is moved approximately ten millimetres in a positive direction from the expected centre of the specimen; this is position  $Y_1$ . The signal of the sensing unit is recorded during eleven rotations of the B-axis and the specimen.

The second step requires a further movement of the Y-axis. The NC control system moves the Y-axis to a position 5 millimetres into a positive direction. However, the point is located between Y0 and Y1. This point is named Y2.

The exact positioning of Y1 and Y2 is not essential; it is only relevant to read out the actual position of Y1 and Y2 by the application of the Y-axis linear encoder. Figure 112 illustrates the second step in the C-axis alignment process.

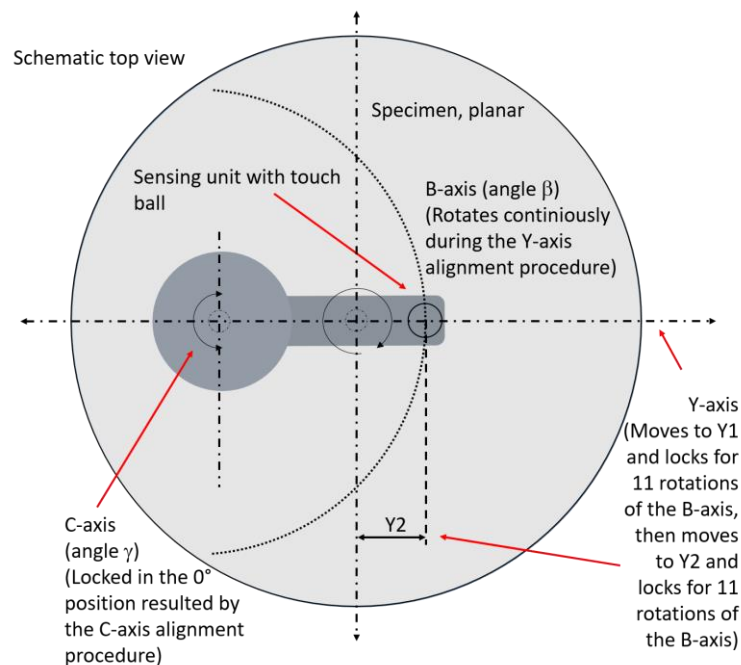


Figure 112: Centre search process – 2<sup>nd</sup> step part 2. The C-axis is locked in the obtained zero degrees position. The B-axis rotates continuously. The Y-axis is moved approximately five millimetres in a positive direction from the expected centre of the specimen; this is position Y2. The signal of the sensing unit is recorded during eleven rotations of the B-axis and the specimen.

At the position Y2, the same measurement process is performed like at Y1. The C-axis is locked in the  $0^\circ$  position, and the B-axis rotates continuously. The sensing unit tracks the complete measurement cycle.



After both measurements, at Y1 and Y2 are performed, the computation process of the obtained data starts. The results of the two initial measurement processes are depicted in Figure 113 and in Figure 114.

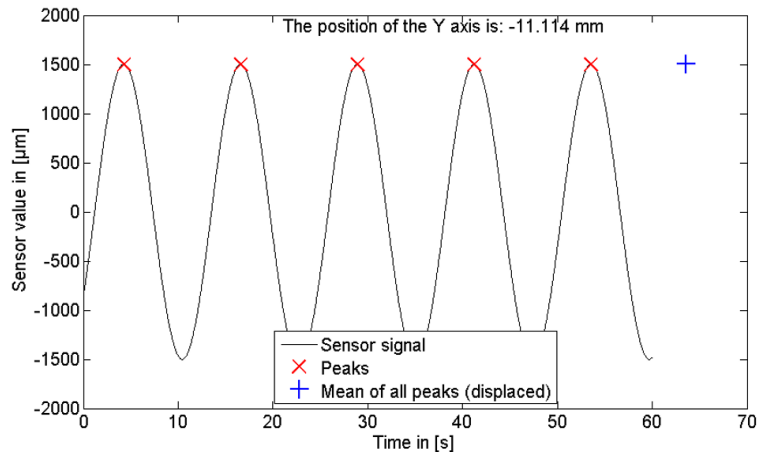


Figure 113: Result of the 2<sup>nd</sup> step centre search part 1. The Y-axis represents the sensor signal converted to microns. The X-axis represents the processing time in seconds. The application of the sum of sine fit delivered the functional equation of the signal. The analysis of the derivations deliver the maxima of the function, marked with a red X. The average of all maxima is represented with a blue +.

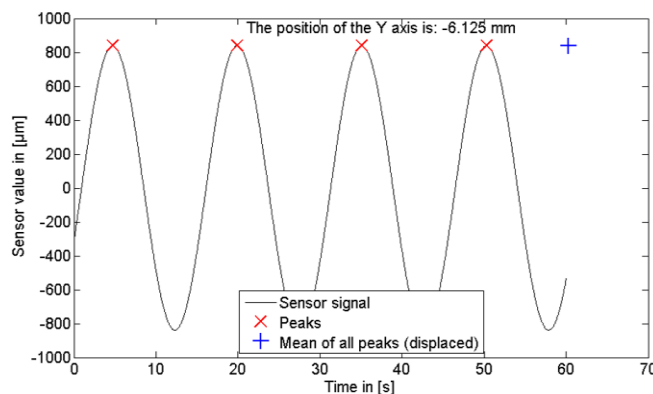


Figure 114: Result of the 2<sup>nd</sup> step centre search part 2. The Y-axis represents the sensor signal converted to microns. The X-axis represents the processing time in seconds. The application of the sum of sine fit delivered the functional equation of the signal. The analysis of the derivations deliver the maxima of the function, marked with a red X. The average of all maxima is represented with a blue +.

The plots in Figure 113 and Figure 114 illustrate the primary measurement tasks at Y1 (left picture) and Y2 (right picture). The sensing unit recorded a sinus-shaped signal in both cases. This effect comes from the tilted planar shaped specimen that rotates

with the B-axis continuously. The actual position of the Y-axis is not relevant. In this example, the Y1 position was at -11.114 millimetres and the Y2 position at -6.125 millimetres. The plots in Figure 113 and Figure 114 deliver two sinus shaped plots with different peak-to-peak values. Y1 had been measured at a distance of approximately -11 millimetres related to Y0; Y2 had been measured at -6 millimetres. Therefore, the amplitude that is closer to Y0 is smaller (Y2).

Similar to the data computation of the C-axis alignment, both signals were treated with a sum of sine fit to get a function for the calculation of the peaks (maxima). For the mathematical procedure, Equation 45 was used in both cases (Y1 and Y2). The maxima are plotted in Figure 113 and Figure 114 and marked with a cross. With the goal to reduce the influence of measurement uncertainties, a defined number of sinus waves is recorded in both positions. This method enables to compute the average maxima in Y1 and Y2. Figure 115 illustrates the two measurements along the Y-axis. In both positions, Y1 and Y2 are the obtained sensor values illustrated. Each measurement set contains ten measurements; this enables us to compute the average maxima at Y1 and Y2. For the further mathematical process, the averages for particular positions are used.

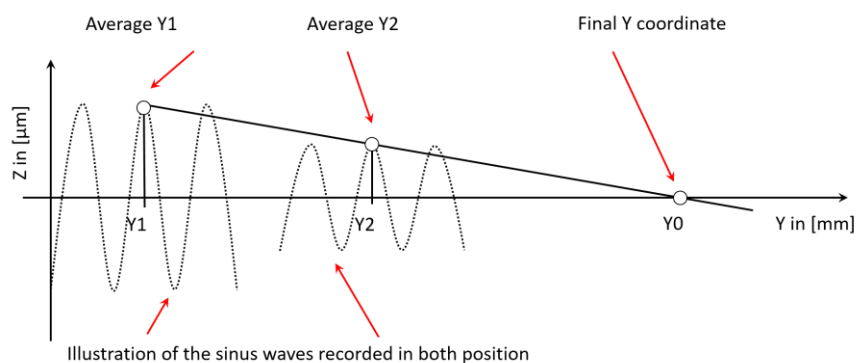


Figure 115: Scheme of the Y coordinate calculation. The obtained averages at the positions Y1 and Y2 are part of a line intersecting with the Y-axis in the diagram. The intersection point is the position Y0 and therefore part of the actual centre of the specimen at C-axis = 0° and Y-axis = 0 millimetre.

A line through the average maxima at Y1 and Y2 intersect with the Y-axis in Y0. The intersection point represents the position of the B-axis rotational axis and therefore, the target position of the Y-axis. The final coordinate Y0 can be calculated with the employment of trigonometric functions, as presented in Figure 115 and Figure 116.

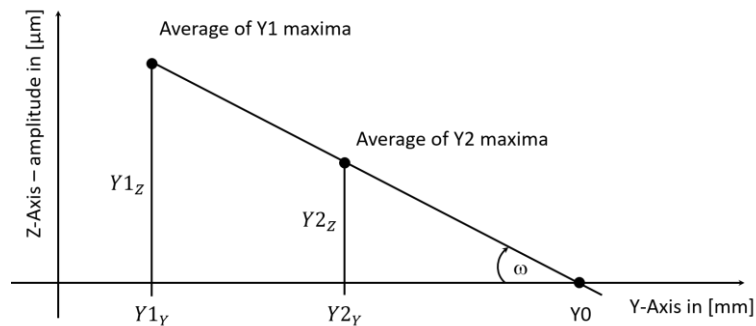


Figure 116: Calculation procedure of Y0. The average of the obtained maxima in Y1 and Y2 are part of a straight line intersecting with the Y-axis. The Z-values of the averages, the Y-axis, and the obtained straight line are part of a triangle with the angle  $\omega$ . The values of  $Y1_y$  and  $Y2_y$  are provided by the Y-axis encoder.

The Y-axis linear encoder offers the exact Y-axis positions of Y1 and Y2. The Z-value of the Y1 and Y2 average maxima can be calculated by using the function of the sinus-shaped sensor signal. This information enables the calculation of the gradient of the resulting straight line that connects both averages in Y1 and Y2. The virtual extension of this straight line intersects with the Y-axis in the searched point Y0.

Figure 116 presents the geometric relations of the trigonometric approach. The following Equation 46 and Equation 47 show the method of calculation. The triangle with the opposite  $Y1_z$  and the adjacent  $\overline{Y0Y1_y}$  create the angle  $\omega$  that can be calculated by using Equation 46.

$$\omega = \tan^{-1} \left( \frac{Y1_Z - Y2_Z}{Y1_Y - Y2_Y} \right) \quad (46)$$

Where:

$\omega$  = Angle between the Y-axis and the line segment Y0 - Y1

$Y1_Z$  = Value of the Y1 average maxima in Z-direction

$Y2_Z$  = Value of the Y2 average maxima in Z-direction

$Y1_Y$  = Position of the Y1 measurement on the Y-axis linear encoder

$Y2_Y$  = Position of the Y2 measurement on the Y-axis linear encoder

$$Y0 = \frac{Y1_Z}{\tan(\omega)} \quad (47)$$

Where:

$Y0$  = Position where the rotational axis of the specimen intersects with the Y-axis.  $Y0 =$

0.

$Y1_Z$  = Value of the Y1 average maxima in Z-direction

$\omega$  = Angle between the Y-axis and the line segment Y0 - Y1

Equation 47 depicts the equation to calculate  $Y0$ , the position on the Y-axis where the central axes of the sensing unit, B-axis and specimen intersect.

The Centre-search approach consists of three measurements. The first measurement is needed to calculate the zero position of the C-axis. The second sets of

measurements allow calculating the zero position on the Y-axis. The presented approach had been used for all test series published in this PhD thesis. Another advanced solution, but based on the presented approach, had been recently developed and is presented as a suggestion for future work in Section 10.2.

## A.10 Measurement strategies

In this thesis, a measurement strategy is defined as the manner the points to be measured are collected. In contrast to interferometer systems where the entire object can be measured with only one shot, coordinate measurement machines collect point by point on a pre-defined route. Universal XY stage coordinate measurement machines, as introduced in Section 2.3.2, operate mostly on vectors travelling from point to point or scan the complete object under test by travelling along a meander-shaped route.

The spherical coordinate design of the metrology system, introduced in this thesis, operates not with an XY stage, but instead with two rotational axes. Therefore, the preferred measurement strategies have a circular shaped tool path. A synchronisation of the two rotational axes even enable the production of straight lines

The following section presents the three implemented strategies and two further designs that are ready for release but not implemented in the latest released software package.

Along with the alignment process, the choice of the best appropriate measurement strategy is essential. In the context of this thesis is a measurement strategy, the way of moving a sensing unit about the specimen. The measurement strategies are published detailed in Section 5.4. Three strategies had been developed, the Track-mode, the Spiral-mode, and the Section-mode. The strategies differ in the number of applied axes during a measurement process. The NC control of the test carrier

is designed to offer the user the choice of the measurement mode. The procedure is implemented in the software and runs automatically in the user-defined boundaries.

The Track-mode had been tested on a planar object with 100 millimetres in diameter and accuracy of  $\lambda/20$ <sup>38</sup>. The goal of the test series had been the comparison of the three modes regarding their actual performance about the speed and accuracy. The results had been compared to the result of a  $\mu$ shape™ Fisba™ interferometer [104] measurement. All test series had been performed with a Heidenhain™ probe with a measurement distance of 25 millimetres and an accuracy better than 30 nanometres [76]. Furthermore, the physical test carrier had been located in a temperature-controlled chamber ( $20^{\circ}\text{C} \pm 0.1^{\circ}\text{C}$ ). By the application of the developed software tools, it was possible to compute all measurement points, see Section A.12.2.

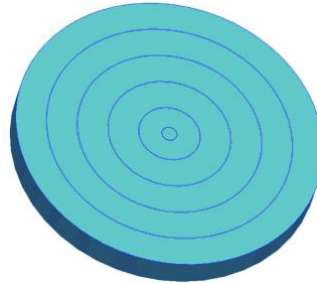
#### A.10.1.1 The Track-mode

The basic idea behind the Track-mode is to create a measurement strategy that operates with as less moving axes as possible. The Track-mode produces a user-defined number of concentric ring, so-called “tracks” on the surface (see Figure 117). The object carrying B-axis is continuously rotating while the sensor unit carrying C-axis moves only from track position to track position to create this circular-shaped pattern. The sensor unit only records when the C-axis reached the target position locked there to grant a

---

<sup>38</sup>  $\lambda/20 - \lambda$  represents the wavelength of a He Ne Laser (red) with a wavelength of 632.816 nanometre.  $\rightarrow \lambda/20 = 31.6408$  nanometre

high accuracy measurement. During the movement to the next position, the sensor unit does not record any values. All other axes are secured during the measurement.



*Figure 117: Illustration of the Track-mode. The Track-mode consists of a number of concentrically distributed rings. Each ring has a defined number of measurement points, which are automatically reduced towards the centre.*

The B-axis is rotating continuously. It is important to move the C-axis, including the sensing unit into the correct position to produce a pattern of concentrically rings with a defined number of measurement points on each track.

Each sensing unit operates with an individual sampling rate. Therefore, the turning speed of the specimen is limited. In the Track-mode, all sensing units of the SCMM are limited to 100 Hz sampling rate by the NC control software. For example, the measurement of 1000 measurement points on the first track takes 10 seconds per round with a fixed sampling rate of 100 Hz. Therefore, the maximal turning speed of the specimen is locked at six rounds per minute. The rotation speed of the B-axis is locked during the complete measurement to reduce the influence caused by a variation of the turning speed of the B-axis.

Equation 48 presents the used equation for the calculation of the spacing factor. The factor “T” can be interpreted as a divisor of the radius of the diameter to be



measured on top of the specimen. This radius is subject to the maximum angle of the C-axis, the diameter of the measurement area and the length of the cantilever  $c_p$ .

$$T = \text{ceil} \left( \frac{2 * c_p * \text{sin}d \left( \frac{2 * \text{sin}d^{-1} \left( \frac{D}{4 * c_p} \right)}{2} \right)}{SB} \right) \quad (48)$$

Where:

$T$  = Spacing factor

$\text{ceil}$  = Rounding up command, Matlab™ (M2010a)

$\text{sin}d$  = Sinus function in degrees

$\text{sin}d^{-1}$  = Arcsine function in degrees

$D$  = Diameter to be measured of the specimen ( $D \leq D(\text{specimen})$ )

$c_p$  = Length of the cantilever between the centre axes of the C-axis and of the probe

$SB$  = Distance between two concentrically rings

The spacing factor enables to define an array that includes all radius fractals representing the distance of each track to the centre of the specimen. A set of 100 concentrically rings results in an array with 100 entries. Each of the concentrically rings has the defined distance  $SB$  to both neighbours, except the centre. Equation 49 illustrates the equation, including all components, depicted in the programming language Matlab™ (M2010a).

$$\bar{s}_T = \text{linspace}(0, (2 * c_p * \text{sin}d\left(\frac{2 * \text{sin}d^{-1}\left(\frac{D}{4 * c_p}\right)}{2}\right)), T) \quad (49)$$

Where:

$\bar{s}_T$  = Array containing the spacing parameters

$c_p$  = Length of the cantilever between the centre axes of the C-axis and of the sensing unit

$\text{sin}d$  = Sinus function in degrees

$\text{sin}d^{-1}$  = Arcsine function in degrees

$D$  = Diameter to be measured of the specimen ( $D \leq D(\text{specimen})$ )

$T$  = Spacing factor

Equation 50 presents the final mathematical equation to calculate the corresponding angles of the C-axis. The resulting array contains the correct angles for all concentric rings, fulfilling the required distance SB.

$$\bar{\gamma} = 2 * \text{sin}d^{-1}\left(\frac{\bar{s}_T}{2 * c_p}\right) \quad (50)$$

Where:

$\bar{\gamma}$  = Final array with all C-axis positions

$\text{sin}d^{-1}$  = Arcsine function in degrees

$\overline{s_T}$  = Array containing the spacing parameters

$c_p$  = Length of the cantilever between the centre axes of the C-axis and of the sensing unit

Figure 118 depicts the result of a Matlab™ (M2010a) simulation applying the presented mathematical models published from Equation 48 to Equation 50. The simulation shows that the distribution of the concentric rings follows the given SB. Since the plot illustrated in Figure 130 depicts the recorded path of the sensing unit, the horizontal line shows the movement of the sensing unit between two tracks.

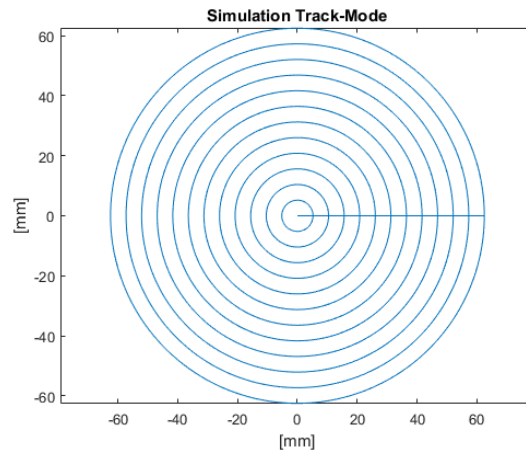


Figure 118: Simulation Track-mode. This illustration is the result of the simulation of the Track-mode measurement process in Matlab™ (M2010a). The simulation starts at the 3 o'clock position ( $B$ -axis =  $0^\circ$ ). The horizontal line in the right half of the plot illustrates the path of the sensing unit during the movement between the concentric rings.

The NC control system controls the Track-mode feature. The user can not directly influence the calculation of the axes positions, the position of the measurement point and the speed of the axes. However, the GUI allows adjusting the number of measurement tracks, the number of measurement points on the first (outer) track. The NC control does the distribution of the concentric rings and of the measurement

points. The test series had been carried out with a defined number of measurement tracks and measurement points. The complete test setup is depicted in Table 26.

*Table 26: Test setup Track-mode.* For the test series to verify the Track-mode, ten measurements had been performed. Nine measurements with a rising number of measurement tracks and one interferometer measurement as a reference measurement. The SCMM operates in the Track-mode with a stable rotation speed of the specimen, therefore is the measurement time linearly rising with the number of measurement tracks. The number of measurement points is defined in the NC control system and does not depend on the diameter of the specimen.

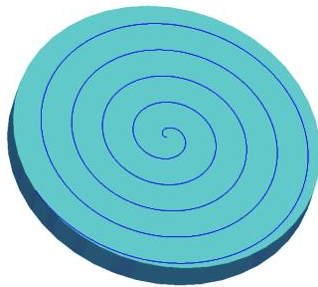
No. of tracks	50	75	100	125	150
No. of points	$14 \times 10^3$	$21 \times 10^3$	$28 \times 10^3$	$35 \times 10^3$	$42 \times 10^3$
Time [h]	00:30	00:45	01:00	01:15	01:30
No. of tracks	200	300	400	500	
No. of points	$51 \times 10^3$	$83 \times 10^3$	$111 \times 10^3$	$140 \times 10^3$	
Time [h]	02:00	03:00	04:00	05:00	

Where:

- e) No. of tracks = Number of concentric rings on the measured surface of the specimen
- f) No. of points = Total number of measurement points
- g) Time [h] = Total measurement time between the first and the last measurement point

### A.10.1.2 Spiral-mode

Another measurement method is the Spiral-mode; this mode was developed to reduce the measurement time in relation to the Track-mode. During a Spiral-mode measurement are the B- and C-axis moving constant and the sensing unit records continuously (see Figure 119). Because of the movement of two rotational axes, a more significant error is predictable.



*Figure 119: Illustration of the Spiral-mode. The Spiral-mode consists of one continuous track, starting at the outer edge of the specimen and ending at the centre of the specimen. The sensing unit operates with the maximum available speed.*

Mathematics knows several types of spirals. One essential feature of the spirally shaped path structure is that the speed of the sensing unit is constant. Therefore, the angular velocity of the sensing unit is constant. The second essential feature of the spiral-shaped path is that the gradient of the spiral is constant. That enables to create a spiral-shaped mesh grid with a constant distance between each winding. The Archimedean or arithmetic spiral fulfils these requirements.

Since the SCMM operates in a polar or spherical coordinate system, the underlying mathematical equation of the arithmetic spiral is used. The mathematical description of the Archimedean spiral is presented in Equation 51.

$$r(\phi) = a * \phi \quad (51)$$

Where:

$r(\phi)$  = Radius as a function of angle  $\phi$

$a$  = The arithmetic constant of the spiral

$\phi$  = Rotation angle

The correct calculation of the arithmetic constant  $a$  is required to create an arithmetic spiral with a defined distance between two parallel tangents. Another essential parameter is the number of degrees until the full diameter to be measured is covered. The necessary number of windings as a function of the diameter to be measured can be computed by the application of Equation 52.

$$W = \frac{D}{2 * SB} \quad (52)$$

Where:

$W$  = Number of windings

$D$  = Diameter to be measured of the specimen ( $D \leq D(\text{specimen})$ )

$SB$  = Distance between two vertical points

The number of measurement points is not essential. Since the Spiral-mode of the SCMM is designed as a quick measurement mode, all sensing units are allowed to operate with the maximum sampling rate. The rotation speed of the B-axis is locked at maximal ten rounds per minute. Therefore, for the creation of the spiral-shaped path structure, 100.000 data points are used to create a smooth path.

$$\overline{phi} = linspace(0, W * 2 * pi, 100.000) \quad (53)$$

Where:

$\overline{phi}$  = Array of the angle phi as a function of W

W = Number of windings

$pi$  = Circular constant

The calculation of the arithmetic constant “a” is essential to design a spiral-shaped path with the correct distance between the windings.

$$a = \frac{SB}{2 * pi} \quad (54)$$

Where:

a = The arithmetic constant of the spiral

SB = Distance between two vertical points

$pi$  = Circular constant

The final function of the arithmetic spiral as a function of the diameter to be measured and the distance SB is depicted in Equation 55

$$r(\overline{phi}) = \frac{SB}{2 * \pi i} * \overline{phi} \quad (55)$$

Where:

$r(\overline{phi})$  = Radius of the arithmetic spiral as a function of  $\overline{phi}$

$SB$  = Distance between two vertical points

$\pi i$  = Circular constant

$\overline{phi}$  = Array of the angle phi as a function of W

The result of the simulation of the Spiral-mode is depicted in Figure 120. The simulation showed the measurement point distribution with  $1.0 \times 10^4$  data points is sufficient to create an arithmetic spiral with the required parameters.

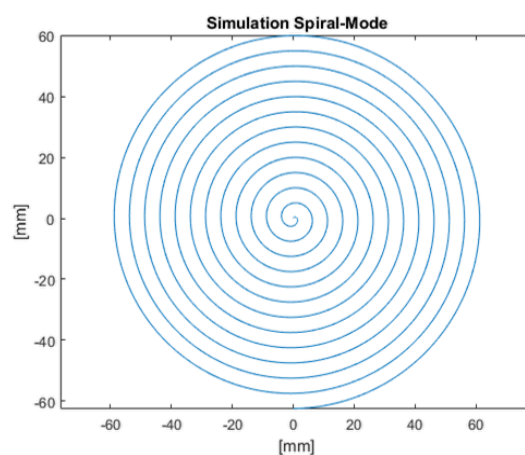


Figure 120: Simulation Spiral-mode. This illustration is the result of the simulation of the Spiral-mode measurement process in Matlab™ (M2010a). Since the B- and C-axis are applied during the measurement, a defined start position of the B-axis is not essential.



Comparable to the Track-mode, the Spiral-mode is mostly NC controlled. The GUI allows the adjustment of the number of spiral windings. The test series setup may be found in Table 27.

*Table 27: Setup of Spiral-mode.* For the test series to verify the Spiral-mode, ten measurements had been performed. Nine measurements with a rising number of windings, and one interferometer measurement as a reference measurement. The SCMM operates in the Spiral-mode with stable rotation speed, therefore is the measurement time linearly rising with the number of windings. The NC control system operates the sensing units with the maximum available detection speed.

No. windings	50	75	100	125	150
No. of points	$8 \times 10^4$	$12 \times 10^4$	$16 \times 10^4$	$20 \times 10^4$	$24 \times 10^4$
Time [h]	00:15	00:23	00:30	00:45	00:45
No. windings	200	300	400	500	
No. of points	$32 \times 10^4$	$48 \times 10^4$	$64 \times 10^4$	$80 \times 10^4$	
Time [h]	01:00	01:30	02:00	02:30	

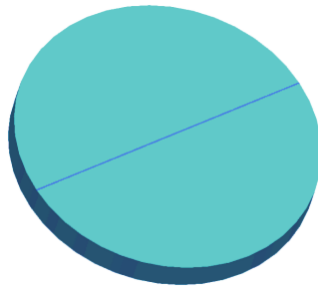
Where:

- h) No. of windings = Number of full rotations (360°) of the spiral-shaped measurement track
- i) No. of points = Total number of measurement points on the measurement track
- j) Time [h] = Total measurement time between the first and the last measurement point

Again, the results had been compared to the Fisba™ interferometer measurement result.

#### A.10.1.3 Section-mode

The Section-Mode enables the user to perform rapid measurements with the SCMM. This measurement mode produces an arbitrary number (1-99) of user-defined cross-sections that can vary in the start-angle and the diameter (see Figure 121). This measurement mode is based on the Spiral-mode. The object carrying B-axis and the sensor unit carrying C-axis are moving in a defined speed ratio to draw a straight line across the object to be measured. Depending on the number of cross-section measurement files, the data analysis software (Section A.12.2) can illustrate both a single cross-section plot or a computed 3D model.



*Figure 121: Illustration of the Cross-Section mode. The Cross-Section mode creates a straight line, starting at the outer edge of the specimen, crossing the centre and ending at the opposite side of the specimen. The sensing unit operates with the maximum available speed.*

Investigations of the essential kinematic relations of the SCMM, presented in Chapter 5.1, showed that the SCMM produces a straight line when the C-axis moves precisely with the half of rotation speed of the B-axis. Therefore, a mathematical approach is not necessary. The NC control of the SCMM is able to control the speed of the axes in a highly accurate manner since both rotation axes are equipped with highly accurate rotational encoders.

The Section-mode is a cross-section measurement mode. The NC control drives the sensing unit across a straight line on the surface of the specimen. Again, the NC control is in charge of most of the basic commands. The user interface offers the option to decide the angular position of the cross-section on top of the specimen's surface and the number of cross-sections. The computation of the gathered measurement points had been done with a very early version of the Section mode calculation tool. The complete test series are listed in Table 28.

*Table 28: Setup of the Cross-section-mode.* For the test series to verify the Cross-section-mode, nine measurements had been performed. eight measurements with a rising number of cross-sections, and one interferometer measurement as a reference measurement. The SCMM operates in the Cross-section-mode with stable rotation speed. The NC control system operates the sensing units with the maximum available detection speed. Therefore, the Cross-section-mode records more measurement points than the Track-mode.

No. cross-sections	1	2	3	6	9
No. of points	$2.5 \times 10^3$	$6.5 \times 10^3$	$8 \times 10^3$	$17 \times 10^3$	$20 \times 10^3$
Time [h]	00:01	00:01	00:01	00:01	00:03
No. cross-sections	27	41	84		
No. of points	$53 \times 10^3$	$90 \times 10^3$	$18 \times 10^4$		
Time [h]	00:05	00:08	00:15		

Where:

- k) No. of cross-sections = Number of straight lines across the complete surface through the centre
- l) No. of points = Total number of measurement points
- m) Time [h] = Total measurement time between the first and the last measurement point

## A.11 Methodology and approach

This Chapter presents the used methodology and approaches for features and processes developed during this PhD research.

### A.11.1 Centre search procedure

The developed alignment procedure is the key to a successful and accurate measurement. For the measurement process, it is essential that the normal of the best-fit sphere be aligned with the central axis of the sensing unit. The alignment procedure allows the usage of all available sensing units. The setup of the SCMM may not be adjusted after proceeding the alignment procedure. Therefore, it is essential to choose the correct sensing unit concerning the specimen before the alignment procedure starts. To reach the required accuracy of the system, the alignment procedure has to be successfully performed each time the geometry of the metrology system changes. This effect happens, for instance, by changing the setup to measure another object with a different best-fit sphere or changing the probe.

The presented test series had been carried out with the Heidenhain™ Certo™ 25 probing system [72]. This sensing unit has an extensive measurement range of 25 millimetres and an accuracy of 0.03 microns. An object under test, a planar shaped object from Melles Griot™, with a diameter of 100 millimetres and an accuracy of  $\lambda/20$ <sup>39</sup> had been used. The specimen was assembled on a three-point fixture that allows the

---

<sup>39</sup>  $\lambda/20 - \lambda$  represents the wavelength of a He Ne Laser (red) with a wavelength of 632.816 nanometre.  $\rightarrow \lambda/20 = 31.6408$  nanometre

adjustment of the tilt. The tilt of the planar object had been adjusted to an amplitude of five micrometres on the outer edge.

The test series had been performed with the developed software tools, in detail with the user interface, NC-control, data-processing-tool, and data-visualisation tool. Furthermore, all tests took place in a climate chamber at 20°C ( $\pm 0.1^\circ\text{K}$ ). The chamber has an uncoupled, solid concrete floor with a thickness of one metre. Nevertheless, the test carrier had been mounted on pneumatic vibration absorbers.

The test series, presented explicitly in Section 7.2, had been performed 100 times according to the following scheme. For this test series, the test carrier had been adjusted according to the setup for planar measurements. However, the estimated centre of the specimen had been roughly positioned under the tip of the probe by using the manual positioning mode. The alignment procedure started according to Section 5.2. The process delivers the calculated zero position of the C-axis and the Y-axis in related to the current zero position. The GUI forces the user to accept this result, and the software is resetting the axes to zero. The obtained results of the proceeded test series had been collected and visually presented in Section 7.2.

#### A.11.2 Physical test carrier

The presented research approach requires hardware equipment to test and verify the results. Since suitable hardware was not available, the decision had been made to develop, design, and build the test carrier. The basic idea to reach the goal was to create a framework of axes to simulate a spherical coordinate system instead of a

popular Cartesian coordinate system. The spherical coordinate system has a unique advantage that rotational axes may be used. Rotating axes have higher accuracy than linear axes [29, 31] naturally. Further details about the specific design may be found in Chapter 5.

### A.11.3 Accuracy measurements

Measurement machines are qualified according to their measurement accuracy. The presented spherical coordinate measurement machine can operate on all known types of surfaces, planar, spherical, aspherical, and free-form shaped surfaces. Therefore, the physical test carrier had to be verified on these surfaces. The different surface types required the application of different sensing units. The planar, spherical and aspherical test objects had been measured with the most accurate available sensing unit, the Luhos™ MWLI™ [76] with a measuring distance of 1 millimetre and an accuracy better than 1 nanometre. Due to the significant deviation to the best-fit sphere, the free-form shaped specimen had to be measured with the Heidenhain™ Certo™ probe with a measurement distance of 25 millimetre and an accuracy of 0.03 microns [72].

All tests had been carried out in a climate-controlled chamber ( $20^{\circ}\text{C} \pm 0.1^{\circ}\text{C}$ ) and the application of the Track-mode the configuration. Furthermore, the computation and the visualisation of the measurement results had been done with the developed software package.

However, the experiments applied the alignment strategy, presented in Section 7.1.2. The software tool controlling the metrology machine features a unique

automatic mode. This mode executes user-defined measurement tasks. The user may decide to measure the same object with different parameters several times in the Track-mode and again with a variety of parameters several times in the Spiral-mode. This unique and generic feature allows the automatic and computer-controlled processing of complete measurement tasks.

For that reason, it may be possible to run the complete test cycle for the accuracy measurements in only four sessions. This feature enabled to carry out the test series without the influence of the user and under stable, repeatable environmental conditions at night.

#### A.11.3.1 Planar surfaces

Planar surfaces are still an essential optical object, especially for mirrors used in laser arrangements. Therefore, a modern and flexible metrology system has to operate on planar surfaces as well as on other surface types. The test series presented in Section 7.1.2 had been carried out with different optical devices. Again, a Melles Griot™ planar N-BK7 lens with a diameter of 100 millimetres and an accuracy of  $\lambda/20$ <sup>40</sup> had been applied. Concerning the test results of the test series verifying the measurement strategies, the Track-mode had been used for this set of test series.

However, the automatic mode had been programmed to execute a Track-mode adjusted to 100 track with a total of exact t  $2.8 \times 10^4$  measurement points, repeated 60

---

<sup>40</sup>  $\lambda/20 - \lambda$  represents the wavelength of a He Ne Laser (red) with a wavelength of 632.816 nanometre.  $\rightarrow \lambda/20 = 31.6408$  nanometre



times. The test took 61 hours, including the axis alignment process in advance. It took from a Friday evening until Monday in the early morning. This period had the significant advantage of empty laboratories without any persons in the laboratory.

More information about planar shaped optical elements and the corresponding production processes are published in the Chapters A.4 and A.6.

### A.11.3.2 Spherical surfaces

Again, the test had been carried out with under the same conditions as the test series with the planar object. One hundred Tracks, exact  $2.8 \times 10^4$  measurement points and an alignment process ahead, repeated 60 times. Only the geometrical setup of the metrology machine changed from planar mode to spherical mode, and the object under test changed from the planar Melles Griot™ lens into a spherical shaped Melles Griot™ lens. The spherical N-BK7 object had a diameter of 50 millimetres, a radius of 259.4 millimetres on the surface and an accuracy of  $\lambda/2$ <sup>41</sup>.

The verification of the measurement had been done with the  $\mu$ shape™ Fisba™ interferometer again.

More information about spherical shaped optical elements and the corresponding production processes are published in the Chapters A.4 and A.6.

---

<sup>41</sup>  $\lambda/2 - \lambda$  represents the wavelength of a He Ne Laser (red) with a wavelength of 632.816 nanometre.  $\rightarrow \lambda/2 = 316.408$  nanometre

### A.11.3.3 Aspherical surfaces

Similar to the previous test series of the planar and spherical objects, the aspherical test series used the identical basic setup. The metrology machine had been adjusted in the mode to measure aspherical objects. An object under test, an aspherical Melles Griot™ object had been used. The crown glass object had a diameter of 75 millimetres and a focal length of 50 millimetres by the accuracy of  $\lambda/10^{42}$ . The verification of the measurements had been done by the application of the QED™ SSI™ available at the Laboratory of Optical Engineering.

More information about aspherical shaped optical elements and the corresponding production processes are published in the Chapters A.4 and A.6.

### A.11.3.4 Free-form shaped surfaces

The free-form shaped object taken for the measurements had a sinus-wave-shape surface with an amplitude of 0.6 millimetres at the outer boundaries and a diameter of 90 millimetres. The Heidenhain™ Certo™ sensing unit had been used to measure the object. Since the overall shape of the object resembles a planar object, the measurement mode for the planar object had been chosen. The verification measurements carried out with a highly accurate Werth™ Video Check UA™. More information about free-form shaped optical elements and the corresponding production processes are published in the Chapters A.4 and A.6.

---

<sup>42</sup>  $\lambda/10 - \lambda$  represents the wavelength of a He Ne Laser (red) with a wavelength of 632.816 nanometre.  $\rightarrow \lambda/10 = 63.2816$  nanometre

## A.12 The SCMM software tools

Advanced mechatronic devices may be designed by using standard components. The original production of mechanical parts is often not economical. High accurate air bearings, for example, are desperate to produce or to purchase. Therefore, the significant parts of the presented hardware had been taken from existing machines and standard products of well-known manufacturers. However, the critical elements of modern machines are the design and the software. The following Chapter presents the developed software solutions.

Modern machines are mostly computer-controlled. Since a metrology machine is a very complicated mechatronic device, the software is needed to realise the required functions. The basic idea behind the complete metrology device was to create a modern, flexible, and modular metrology device. Therefore, software packages have to fulfil this requirement in the same manner. Three pieces of software had been developed to achieve the following requirements:

- A reliable graphical user interface
- The numeric control software package
- The data analysis software, including the error compensation

The following Chapter presents the different tools and their characteristics.

### A.12.1 Graphical user interface

The graphical user interface (GUI) is one of the essential features of the metrology system. The first reason for the development of the GUI had been the influence of the user indicated errors in the measurement result. However, the spherical coordinate measurement machine comes with different measurement modes, different measurement strategies, and helpful features such as the alignment process. To reduce possible input errors and to increase the comfort of the SCMM, many processes had been designed to run automatically in the background.

The presented SCMM has two main modes, the manual mode, and the automatic mode. The manual mode allows the user to drive each axis individually according to his needs but limited to some safety features such as end-of-axis-sensors and collision-sensors. The manual mode is the only mode where no centre search is required before the user may start a manual measurement. This mode is mostly used for quick measurements in the shop.

Figure 122 illustrates the original graphical user interface, developed for the presented SCMM. The section marked with “1” contains the individual axis controls. Each axis may be controlled by using the following buttons:

- Power: Axis main switch; on/off button
- Home: Axis starts to calibrate itself. The new assembled absolute scales obviate this function.
- Reset: Allows rebooting the axis controls in the case of an error.

- Move: Pressing the “Move” button enables to drive the axis to the position defined in the text box on the left side of the button.
- Velocity: This slide bar controls the speed of the axis (within the defined limits).
- << >>: Direction control, left and right or up and down.

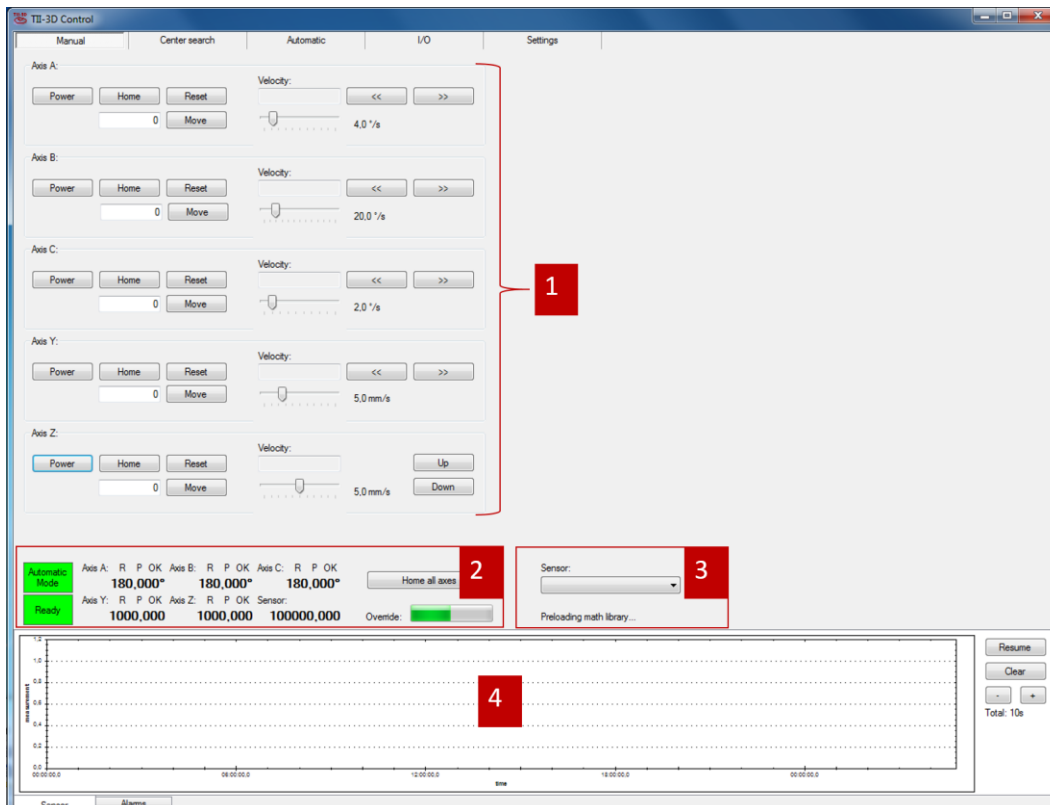


Figure 122: GUI- manual user mode. The software package of the presented SCMM enables the user to command each axis manually. Furthermore, the presented information allows the user to monitor critical operating conditions.

Section “2” is named “Axis information section”. This area provides axes with valuable information to the user. Next to the status of the axis (**R**eset, **P**ower and **O**K), the current position is visualised. Furthermore, the user gets information about the current mode of operation and the overall status of the system. The “Home all axes” button is going to be removed in the next software update. The new absolute encoders of all axes do not need to be calibrated.

Section “3” is the sensor selection section. This pull-down menu allows the user to choose the best fitting sensing unit for the measurement task. All available sensing units are listed here. The specific sensor specifications are saved in a closed settings file, which cannot be edited in this section. Further details about the sensor unit settings may be found in Figure 127.

Section “4” is the plot area. In this section is the data stream of the sensing unit depicted. This section is significant, especially in the case when the SCMM is used for non-regular measurements.

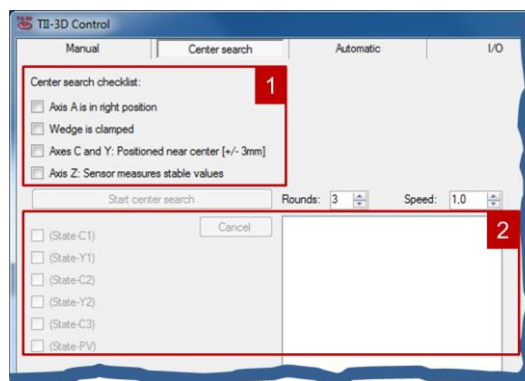


Figure 123: GUI - Centre Search. The centre search feature is fully implemented in the control software package. The user has to confirm the tasks of the checklist; the centre search process itself is fully automatic.

Figure 123 depicts a screenshot of the Centre Search feature. Measurements in the automatic mode always require an initial centre search. A standard user can not skip this procedure. The mathematical background of this feature is presented in detail in Section 5.3.

However, section “1” shows the software front end of the centre search tool. It asks the user to check some questions and maybe to adjust the default number of

rounds and the turning speed of the axes. The complete procedure is automatized, and the user cannot take any further influence.

Section “2” is the visualisation area of the centre search results. The left side provides the status and shows which part of the procedure has been completed. The right side of the section provides the results of the mathematical computation as clear text.

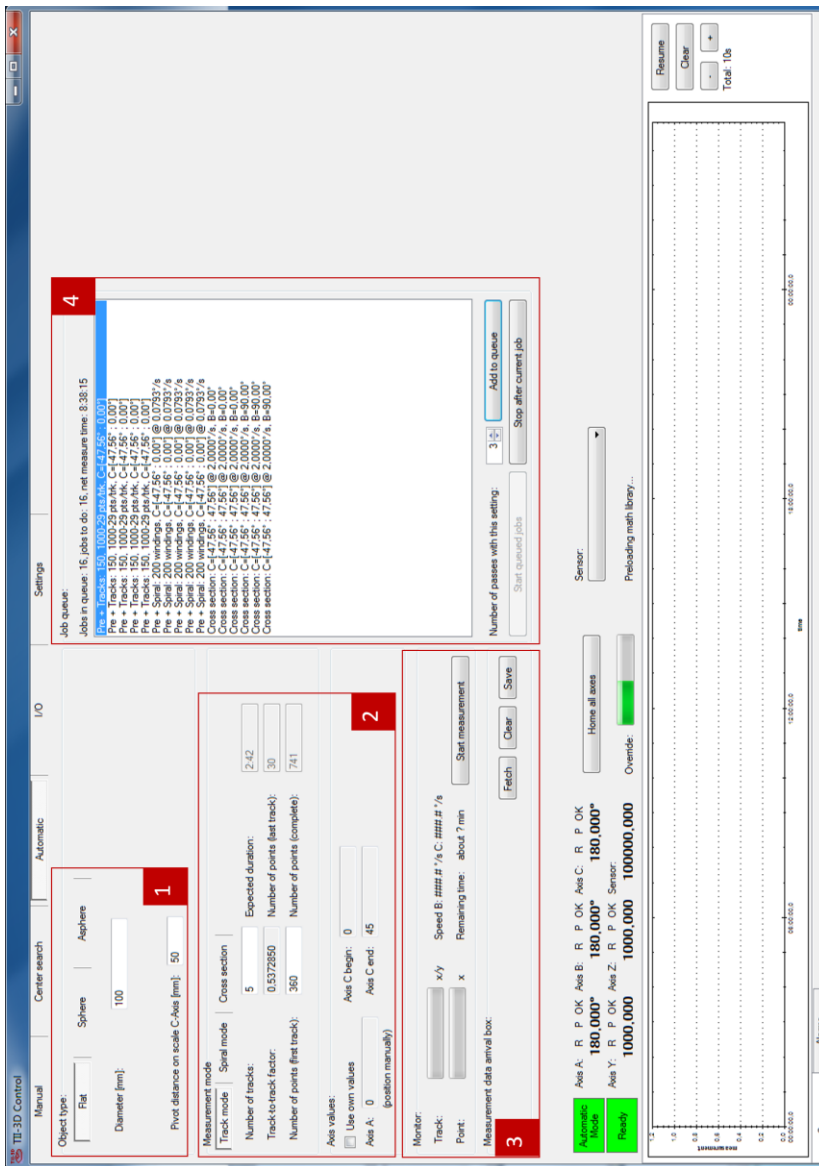


Figure 124: GUI - Automatic mode. This menu provides the control section for the automatic mode. The Track-Mode, Spiral-Mode, and Cross-Section Mode are mostly automatized to avoid user indicated measurement errors. Therefore, the user can only adjust the necessary parameters.

Figure 124 depicts the screen of the automatic mode. Section “1” provides the input fields for the different parameters of the planar, spherical, and aspherical objects. The mathematical calculation behind the front end delivers the exact position for each axis. Concerning the reduction of the user indicated errors, the number of input parameters had been reduced to the minimum.

Section “2” of the GUI provides the selection of the measurement mode. The user may decide between Track-mode, Spiral-mode, and Cross-section-mode.

The figure shows three panels of the GUI for measurement modes, all with 'Track mode' selected. The top panel shows parameters for Track mode: Number of tracks (5), Expected duration (2:42), Track-to-track factor (0.5372850), Number of points (last track) (30), Number of points (first track) (360), and Number of points (complete) (741). The middle panel shows parameters for Spiral mode: Velocity B axis (120.0000 %/s), Velocity C axis (0.3 %/s), Spiral windings (50), Points/winding (267), Expected duration (2:30), and Points/measurement (13357). The bottom panel shows parameters for Cross section mode: Velocity B axis (1.0 %/s), Position B axis (0.0000 \*), and Velocity C axis (2.0 %/s).

Figure 125: GUI - Measurement modes in detail. This detailed screenshot is part of the automatic control menu.

Figure 125 are the input variables of the three measurement modes depicted in detail. The Track-mode requires defining some concentric rings and furthermore the number of measurement points on the first ring. The measurement of the first ring starts at the given diameter (Figure 124, section “1”). Integrated algorithms reduce the number of points automatically to a maximum of 30 points at the last ring to reduce the data density towards the centre point. Furthermore, the software calculates the



expected measurement time and especially the position of all points to be measured, including the speed control of the motors.

The settings of the Spiral-mode are presented in Figure 125. It requires only the number of spiral windings on top of the specimen. In contrast to the Track-mode, both rotational axes are in operation to drive in a spiral-shaped path. Comparable to the Track-mode, the algorithms behind the software controls the position and the speed of all axes. The speciality of the Spiral-mode is that the sensing unit is allowed to measure with its maximum scanning rate. Furthermore, a slide-bar for the speed control had been added. This feature is a comfort feature for the user.

The third measurement mode is the Cross-section-mode. The user chooses the angle on top of the object under test and the algorithms behind control the speed of the two rotational axes in such a manner that a straight tool path is generated. This mode is mostly used to get a quick view of the surface shape and the structure of the specimen. The Cross-section-mode has excellent potential for further developments. Please see Chapter 10.4.

Section "3" of Figure 124 is an additional monitor area. The user may watch the current progress in detail. The area provides information about the progress of the measurement and some critical axis information. Furthermore, this area contains the start button for single measurements.

However, in the last area, the automatic-user-interface is presented in Figure 124. It is the Que list feature in the area "4". This unique feature had been beneficial for

carrying out a vast amount of test series of this PhD research. The tool is limited to the current object under test and the current sensing unit. Concerning this limitation, the user may define a set of unlimited measurement — for example, ten times Track-mode with 100 tracks and 1000 starting points, followed by 36 cross-sections in 10° steps. For data storage, all measurements are treated like single measurements. Each measurement will be saved in an own file including all axes information and the time stamp. The most extended test series by using this feature had been ten days. Furthermore, the control computer of the SCMM is equipped with an HD webcam and a remote service. This feature enables the system to operate in a closed room with stabilised environmental conditions such as temperature and humidity, without any further influence from users.

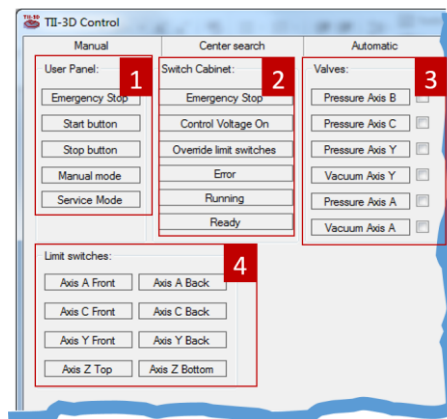


Figure 126: GUI - I/O settings. This menu fulfils two functions. For regular users, it is only a visualisation with no further function. For service staff, the menu becomes active, and the service crew can manipulate all settings.

The fourth user option, presented in Figure 126, is the input and output (I/O) settings of the complete machine. For standard users, these options are only a visualisation of the status; the user is not allowed to change any value. Area “1” displays

the controls of the handheld device, the user panel. It contains the primary controls, such as emergency stop, start-button, stop-button, and a key switch accessing the Service mode.

Area “2” presents the monitoring of the control features located in the central switch cabinet.

The pneumatic control cabinet may be monitored and controlled in section “3”. In the case of switching to the Service mode, all valves can be controlled individually. For a standard user, the status of all valves is only displayed, and the computer controls the setting. Again, the standard-user has only limited access to the control unit. Algorithms in the background, including the setting of the valves, handle all of the calculations.

However, section “4” provides an overview of the status of the axes limiting switches. Each of the indicators is used for both hardware and software limiting switches. The system is designed with three-time safety. The SCMM owns software limit switches, electrical limit switches, and mechanical limits. In the case that one system does not react, the next limit switch reacts. If the first two systems do not react, the final stop is a soft rubber bumper at the end of each axis. This feature avoids mechanical damage to the axes.

The last but significant development is illustrated in Figure 127. This area is named “Settings”, and it contains the critical data of the system. This section contains

the adjustable parameters of the SCMM. These parameters are essential for the measurement and alignment processes.

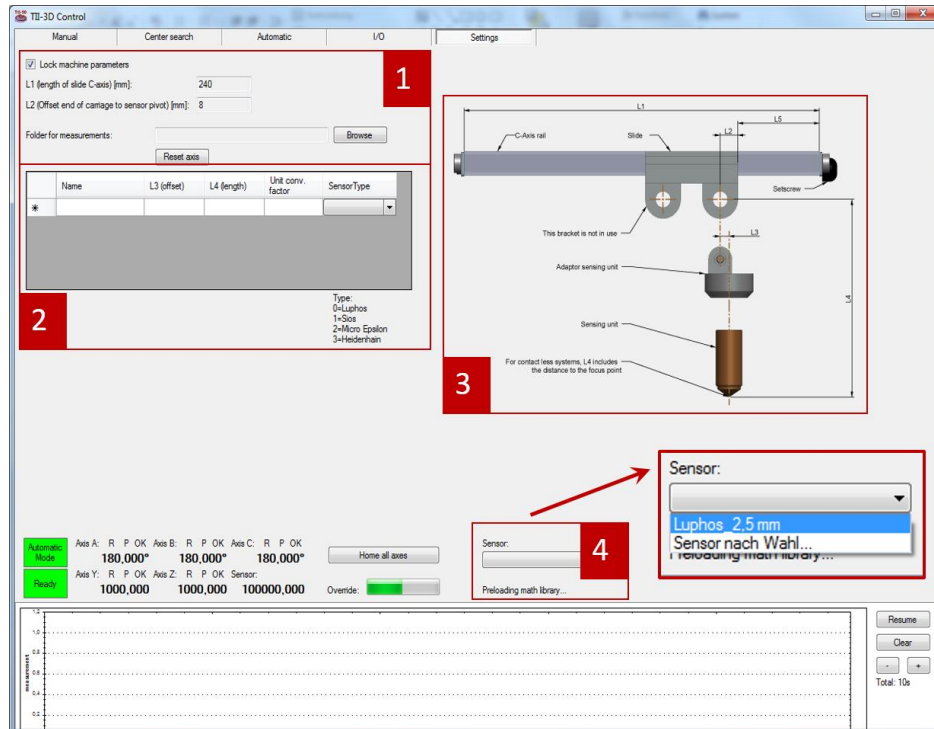


Figure 127: GUI - Settings of the SCMM. For regular users, this menu does only allow to change the sensing unit. All other parameters are locked. The change of the parameters is only allowed for service staff.

Area “1” enables the user to change the two main geometrical parameters of the measurement machine. The first is the length of the C-axis cantilever (L1). The second is the offset between the sensing unit axis and its fixture (L2). All values are depicted graphically in the area “3”.

However, another critical part of the machine is illustrated in section “2”. This list contains all parameters of the applied sensing units. The list is not limited and can be expended; therefore, all available sensing units may be stored there for later use. The critical sensor unit parameters are the offset to the centre axis (L3) and the actual length

(L4) of the sensing unit. Furthermore, there is there a unit conversion factor implemented. This factor provides the correct length unit to the software, for example, mm or even nm.

The last field is “4”; the sensor selection drops down box. This box presents all sensing units, and the user may decide which device is the best choice.

#### A.12.2 Data analysis tool

The analysis of the gained data is an essential step in the measurement process. There are some favourite software tools in the market to aid in this demand. All of these software tools have one significant disadvantage. They may be seen as a black box. The algorithms and the way of computing the results are mostly unknown. Researchers may only compare the results computed by two software packages according to similar results.

This PhD research has the goal to provide a flexible and modular metrology system that is open. In the context of this thesis, open means that other researchers may take the gained results as raw data and use them for further research. For that purpose, the decision felt to create an own, open, software package to convert and display the results by the application of published algorithms. Figure 128 presents the primary user interface of the data-analysis-software-tool. According to the principal goal to reduce possible error influences, the design and the number of features and options had been reduced to a minimum.

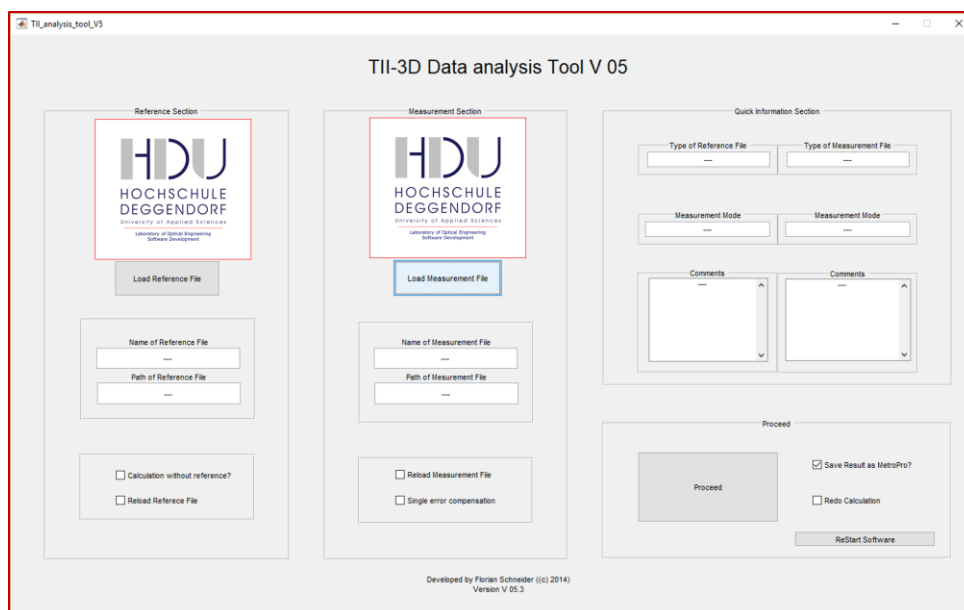


Figure 128: GUI – Data analysis software. Since the presented SCMM is self-developed, there was no software package to translate the measurement result in Cartesian coordinates and to visualise the details.

The SCMM may be operated by using a reference measurement or with a single measurement without reference. This procedure of reference measurements requires the measurement of a highly accurate specimen that may be subtracted from all the following measurements. This procedure is prevalent and has the goal that all regular machine uncertainties are documented in this highly accurate measurement result, and therefore, they will be subtracted from the actual measurement.

In the second column counted from the left side in Figure 128 is the measurement file section depicted. The input of the measurement file is the initial procedure of the data analysis process. Once loaded, the header information is analysed, and the results are shown on the right side in the Quick information section. This feature may assist the user to choose the correct file since the complete data analysis procedure takes a couple of minutes.

On the left side of the software tool presented in Figure 128 is the reference section depicted. The user has a few options to choose from. The user may decide to go ahead without a reference measurement, to load the reference template file or to load a new reference measurement file. The reference template contains statistical information, including the chosen setup and all axis positions of the measurement machine. Since all produced measurement files own a header section where vital information is saved, the data analysis software can choose the best fitting template. An example of a measurement file is illustrated in Figure 129.

Once the new file had been loaded, the load button appears. Further information such as the path and the file name appears in the corresponding box as well as in the Quick information section. At this stage, the user can decide whether all information is correct or not and cancel the procedure. The Proceed button starts the complete procedure presented in the following sub-Chapters.

```

Started: 2012-06-30 14:33:19
Saved: 2012-06-30 15:03:23
Lens:flat
Lens diameter:0
Lens radius:0
Mode:unknown
Param1:0
Param2:0
Param3:0
Param4:0
Param5:0
Sensor:Luphos-1
L1 (slide len):0
L2 (pivot offset):0
L3 (sensor offset):0
L4 (sensor len):0
L5 (pivot distance):0
Axis A (real):0
Axis Y (real):0
Axis Z (real):0
Track:Point.Sensor.AxisB.AxisC.AxisY.AxisZ.T1.T2.T3.T4.T5.T6.X.Y.Z.Luphos_ms.SPS_ms
##
1,1,-40,126165,1,062,-29,999998,0,995003999999994,50,007,0,0,0,0,0,0,0
.
.
3,100,0,356,416992,-29,999998,0,589996999999997,85,103996,0,0,0,0,0,0,0
##
1,1,-0,277529,1,047,-29,999998,0,589996999999997,85,103996,0,0,0,0,0,0,0
.
.
100,23,-0,399064,2,62,-29,999998,0,589996999999999,85,103996,0,0,0,0,0,0,82,0
    
```

```

Mode;Section
Axis B (begin);0
Axis C (begin);0
Axis C (end);0
Speed axis B (°/s);0
Speed axis C (°/s);0
    
```

Figure 129: SCMM measurement file. All measurements performed with the SCMM are documented with a measurement file in cleartext. This file locks and displays all settings and results.

Figure 129 illustrates an example of the SCMM measurement file that had been developed during this PhD research. The file contains essential information about the measurement process. The block marked with “1” contains the header information. In this block is a marked section of six entries. These entries may vary according to the used measurement mode (Track, Spiral or Cross-section). Section “2” contains the data of a new feature, the “on the fly referencing”. This feature is still under development, and further information may be found in the future work Chapter. This new feature needs further research and is not part of this PhD thesis. Finally, section “3” contains the complete dataset with a maximum resolution of the data points as provided by the encoder or sensor system.

#### A.12.2.1 Data analysis procedure

The data analysis of the measurement modes follows the principle of the reference measurement procedure. This procedure is prevalent, and many metrology systems use this kind of data analysis, especially for error compensation. In the context of the data analysis, error compensation means to compensate for repeatable and systematic errors caused by the metrology machine. Such errors may be defined as mechanical inaccuracies, production inaccuracies or even errors caused by the geometrical design of the device. The reference measurement procedure consists of one or a set of measurements with a well-known and high accurate specimen. The accuracy of this reference specimen has to be lower than the required accuracy of the following actual measurements.



Research has been undertaken to provide a set of reference measurements and archive them in the data analysis software. This procedure allows measurements without an additional measurement because the data analysis software compares the setting of the current measurement with the deposited reference measurements. However, for the design of the data analysis software, it is not essential whether the file is taken from the database or a current reference measurement. The following sub-Chapter presents the methods of data analysis used for the three different measurement modes, Track-mode, Spiral-mode, and Cross-section-mode.

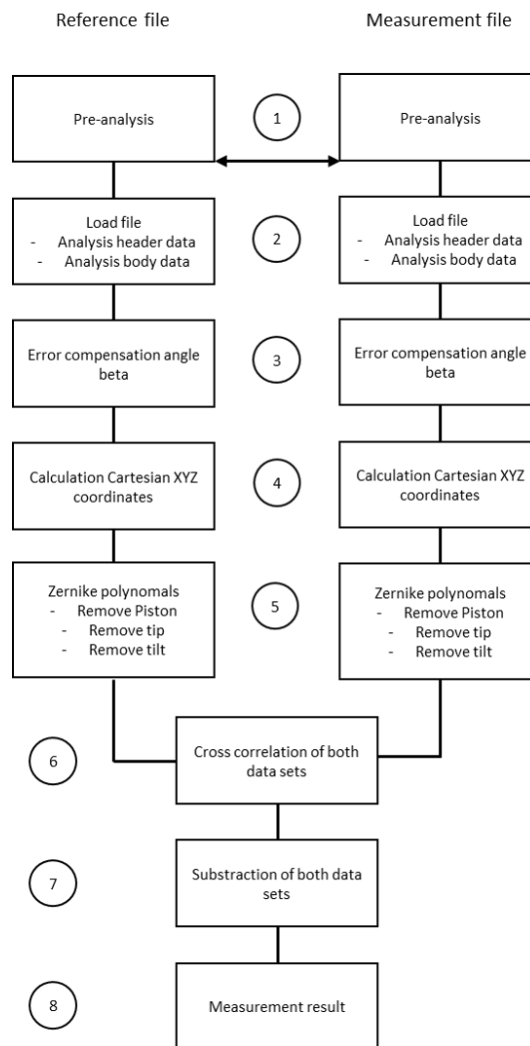


Figure 130: Process of data analysis. The data analysis process consists of eight subsequent steps. The first five steps are performed with the actual measurement and with the reference measurement. Starting with step 6, the results from the actual measurement and of the reference measurement are combined in one file.

Figure 130 illustrates the process of the data analysis of a regular measurement conducted with the SCMM. This mathematical model describes the used mathematical methods for comparative measurement. The presented process consists of eight steps, whereas the first five steps proceed parallel.

In the first step, the pre-analysis of the measurement files is executed. The goal of this step is to investigate the header information of both measurement files. The

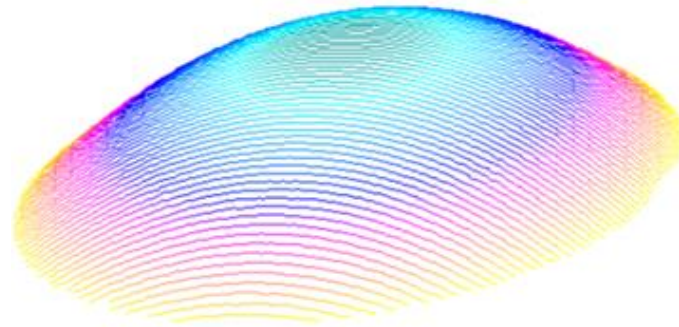
reference file and the measurement file are obliged to show the same setup information, such as the axis positions and the used sensing unit. For the case that this is not applicable, the user has to decide whether he wants to quit or to go ahead with a reference file taken from the database.

In the second step, both files are analysed. The design and content of a measurement file may be seen in Figure 129. The header contains information about the A-axis, the used sensing unit and some geometrical parameters of the SCMM. This information is used to compute an ideal reference surface according to the SCMM setup parameters and to load the correct protocols of the used sensing unit, such as tip-ball correction for tactile sensing units. The proceeded analysis of the body investigates the obtained data according to irregularities. Such irregularities may be not a number (Nan) values of the sensing unit or axis data that does not match with the expected axis positions compared with the header information. Nan values of the sensing unit are an indication that the sensing unit operated outside its working range.

During the third step, the correction of the angle beta proceeds. Since the sensing unit crosses the object under test in a bow-shaped path, a correction may be necessary. The detailed explanation of this specific geometrical issue may be found in Chapter 5.1 and Equation 7.

The calculation of the Cartesian XYZ coordinates proceeds in step number four. The detailed mathematical model may be found in Chapter 5 and the related equations.

The result can be seen in Figure 131. The result of the XYZ transformation process is tilted and displaced with an offset in Z-direction. Therefore, further mathematical treatments are necessary.



*Figure 131: XYZ transformation. The plot displays the first result of the data analysis process. All axes information of the SCMM is translated into XYZ coordinates.*

The fifth step in the calculation procedure is to convert the Cartesian XYZ coordinates into Zernike polynomials ( $Z_p$ ) as presented in Figure 132. Zernike polynomials are often used in optical science. The first three polynomials represent piston, tilt in X-direction and tilt in Y-direction.

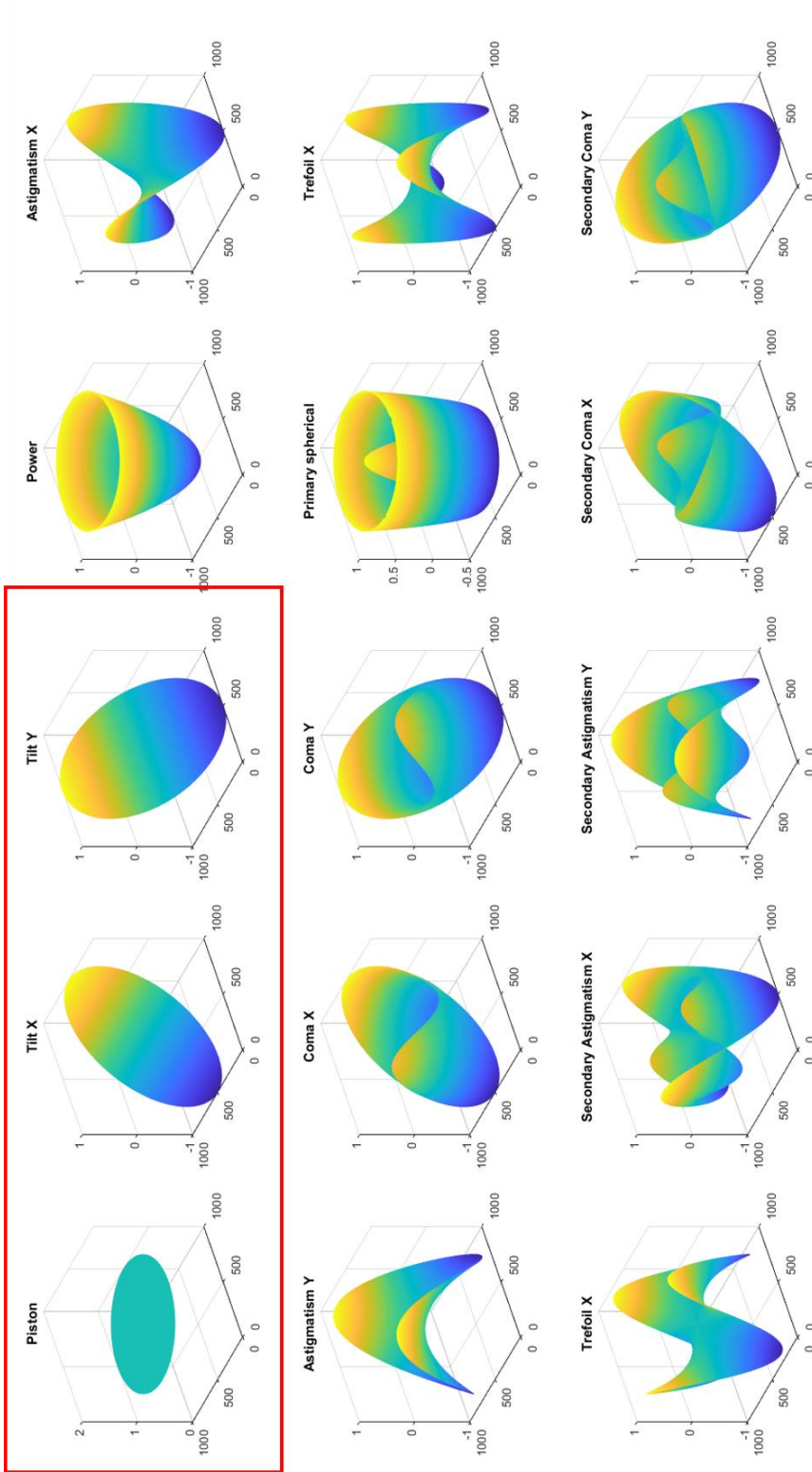


Figure 132: Zernike polynomials . A prevalent method to compensate the errors of a measurement result is the translation of the data set into Zernike polynomials. The subtraction of the first three polynomials removes the offset and the tilt in XY direction.

$$z_0 = 1 \quad (56)$$

$$z_1 = \rho * \cos[\theta] \quad (57)$$

$$z_2 = \rho * \sin[\theta] \quad (58)$$

Where:

$z_1, z_2, z_3$  = First three Zernike polynomials

$\varphi$  = Azimuthal angle

$\theta$  = Polar angle

The result of the Zernike computation is presented in Figure 133. With the application of the Zernike polynomials, it is possible to remove the piston/offset and the tilt in X- and Y-direction.

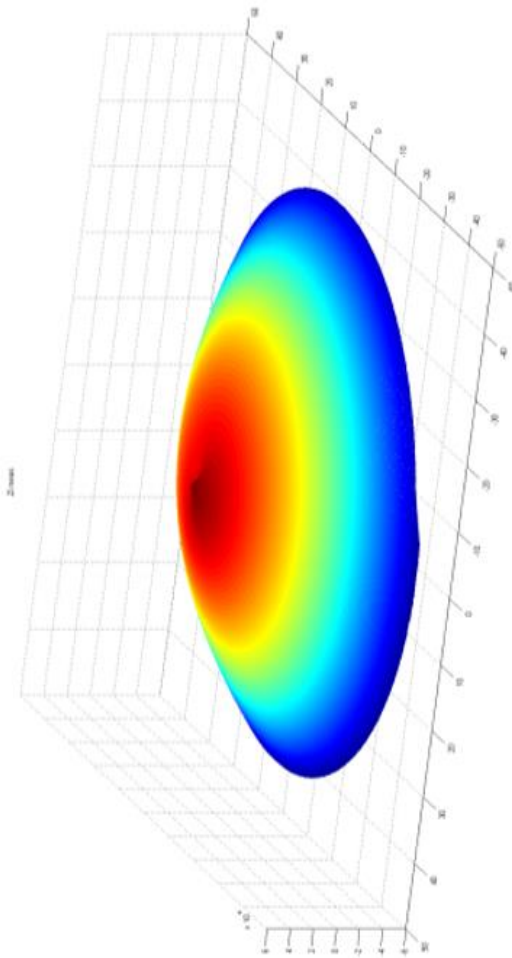


Figure 133: Surface with removed piston and XY-tilt. Compared to Figure 131, this plot has not piston and no tilt in XY direction.

The presented first six steps of the calculation process must be performed with both, the measurement file and the reference file. Since it is possible to use an achieved reference measurement file, it is possible that the dimensions of the reference file do not fit to the measured specimen. However, to ensure a proper subtraction of both files, a cross-correlation calculation is performed in advance of step seven of the calculation process scheme.

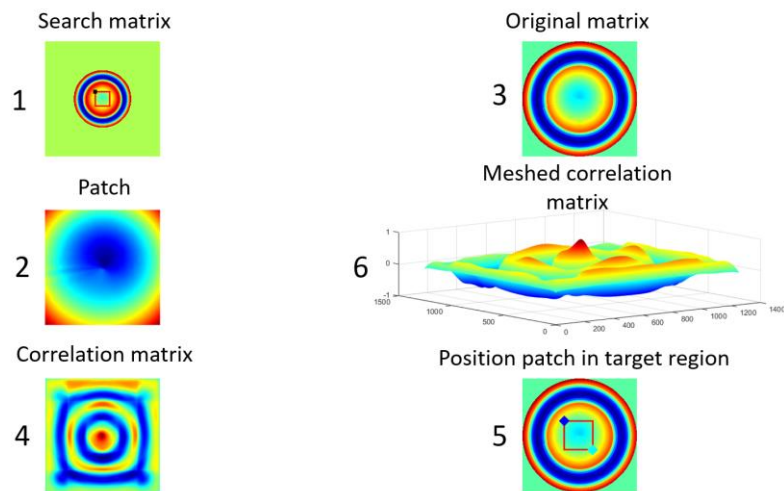


Figure 134: Cross-correlation of the measurement and the actual measurement. (1) represents the complete matrix of the actual measurement file. (2) represents the patch to search out of the centre region of (1). (3) represents the matrix of the reference measurement. (4) represents the correlation matrix of the reference measurement. (5) represents the meshed correlation matrix. Areas with the highest accordance show the highest peak. (6) represents the exact position of the patch in relation to the reference matrix.

In preparation of the cross-correlation process, a search matrix (1) must be specified. This matrix is the centre region of the actual measurement (4). This matrix will be searched in another matrix, named Patch (2). This Patch is represented by the reference measurement. The cross-correlation algorithm, presented in Equation 59, generates a correlation matrix (3/5). The correlation matrix is the result of a least-squares calculation. The highest peak of the correlation matrix represents the area with the best fit. The position of the search matrix in relation to the patch delivers the XY displacement of both measurement files. A simple matrix shifting operation finalises the cross-correlation calculation and delivers two perfect aligned measurement results.

The equation of the correlation coefficients at each position of X and Y in the input matrix is given by Equation 59.



$$r(X, Y) = \sum_{\substack{xx < NX/2 \\ XX = -NX/2}}^{\substack{YY < NY/2 \\ YY = -NY/2}} \left( \text{patch} \left[ xx + \frac{NX}{2} \right] * \left[ yy + \frac{NY}{2} \right] - \overline{\text{patch}} \right) * (\text{matrix}[X + xx] * [Y + yy - \overline{\text{matrix}}]) \quad (59)$$

Where:

$r$  = Coordinates of correlation coefficients, given in pixel

$X$  = Dimension in X-direction, given in pixel

$Y$  = Dimension in Y-direction, given in pixel

$xx$  = positions in X-direction of the patch, given in pixel

$yy$  = positions in Y-direction of the patch, given in pixel

$NX$  = Dimension in X-direction of the patch, given in pixel

$NY$  = Dimension in Y-direction of the patch, given in pixel

$\overline{\text{Patch}}$  = is the mean of the patch pixels

$\text{Patch}$  = is the matrix of the patch

$\overline{\text{Matrix}}$  = is the mean of the image pixels

$\text{Matrix}$  = is the matrix of the measured surface

The last step in the calculation process is a simple matrix subtraction. The reference file is subtracted from the measurement result. Both files are without offset, tilt in XY direction and both files are aligned.

The result of this process is the final measurement result of the SCMM, and an example is presented in Figure 135.

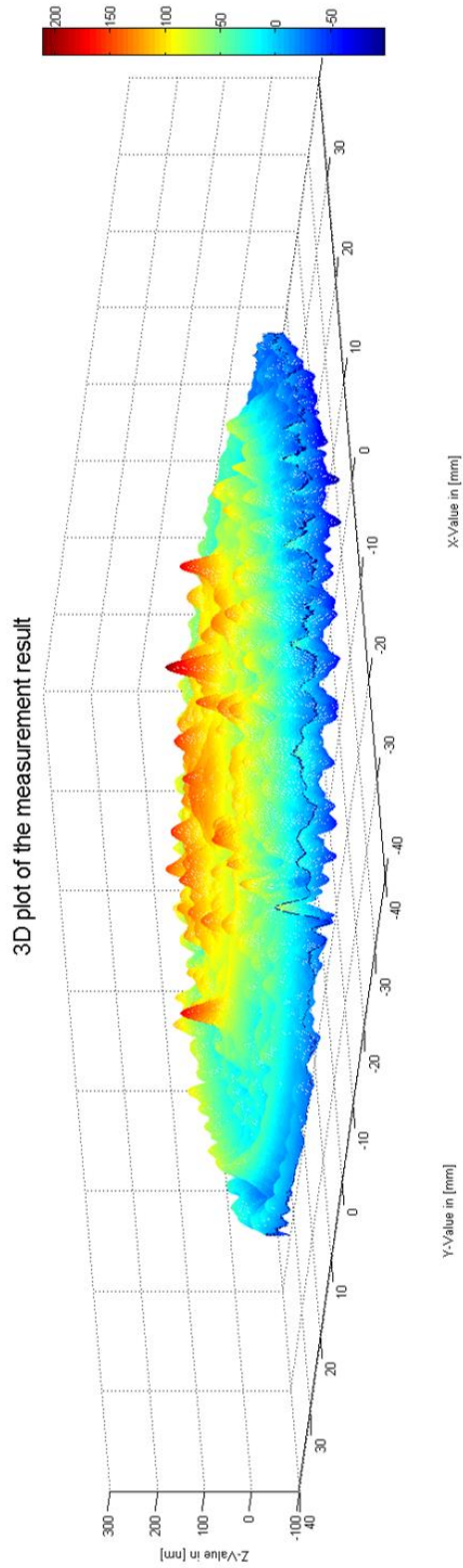
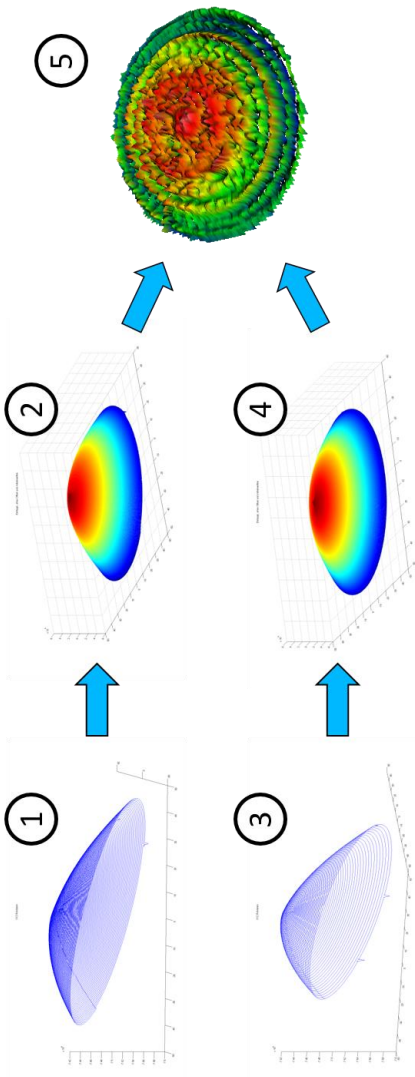


Figure 135: Final result of the data analysis. This plot illustrates the result after step seven of the data analysis process, depicted in Figure 130. Basically, this plot shows the differences between the actual measurement and the reference file. This matrix can be used as an error map for production machines to rework the specimen as well.

A.12.2.2 Track-mode and Spiral-mode

The most accurate measurement mode is the Track-mode. During a measurement with the Track-mode, only one of the two rotational axes is employed. All other axes are locked and secured.



- 1) XYZ coordinates of the reference measurement
- 2) Computed measurement matrix, with removed offset and tilt
- 3) XYZ coordinates of the actual measurement
- 4) Computed measurement matrix, with removed offset and tilt
- 5) Result of the subtraction (2) – (4)

Figure 136: Data analysis in the Track-mode. This scheme illustrates the process for Track-mode and Spiral-mode measurements. (1) is the reference measurement in XYZ coordinates. (2) depicts the reference measurement after removing the piston and XY tilt. (3) illustrates the actual measurement in XYZ coordinates. (4) shows the actual measurement after removing the piston and XY tilt. (5) illustrates the result of the subtraction after the cross-correlation of both measurements.

Figure 136 depicts the theoretical approach of the data analysis procedure used for the Track-mode and of the Spiral-mode. Both measurement modes are handled equally. The process may start with the conversion of the encoder values, provided by all axes, from the spherical coordinate system into XYZ values. Since the system operates only with the computation of the real raw data, all encoder values are saved with the maximum available amount of digits in the original format in the provided measurement file. The conversion from the provided format into XYZ coordinates is provided in Chapter 5.1.3.1.

In the second step, the first Zernike polynomials are removed, these polynomials contain the offset, tilt in all directions and the power errors. This procedure is done with both the measurement file and the reference file. All operations are carried out with matrices and floating-point values to avoid the loss of digits. However, the current measurement matrix has to be computed with two new algorithms. In the case of using a tactile sensing unit, a touch ball correction is necessary. Furthermore, the SCMM owns a set of temperature sensing units. The temperature compensation is another important feature that is applied to the measurement matrix.

The last and most crucial step is the subtraction of the two resulting matrices, the matrix of the reference measurement, and the matrix of the current measurement. Since both measurement files, reference and current measurement, may have different sizes, algorithms had been developed to equalise the size of both matrices. However, since the centre region in different areas of their matrices, a cross-correlation procedure had been developed to ensure the exact overlapping of both matrices.

The result of the process is depicted in Figure 137. As mentioned already, the data analysis software is designed to operate without any filter or smoothing algorithms. To provide data that are raw data is one of the goals of this PhD research. If required, filter and smoothing algorithms may be applied by using another, additional, software package available in the market.

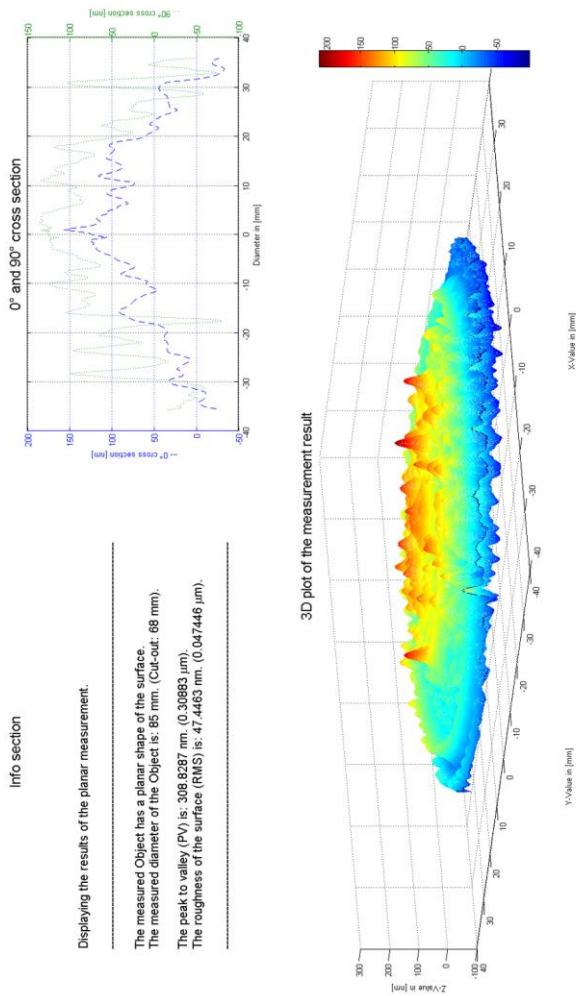


Figure 137: Result screen of the data analysis software. This figure presents the result window of the data analysis software. It provides three crucial information. The area in the upper left side presents the result of the measurement in numbers. The plot on the upper right side shows two cross-sections of the measurement result. The 3D plot in the lower area illustrates the final measurement result

The result screen provides all essential and necessary information to the user. In the upper left corner of Figure 137 is the Info section located. This section provides the necessary results of the measurement, such as PV and RMS. In the right upper corner are two cross-sections displayed ( $0^\circ$  and  $90^\circ$ ). This feature had been exposed to be very informative to the user. In the lower area is the 3D plot of the measurement result depicted. The result is marked with a colour map to monitor significant areas on top of the specimen's surface.

#### A.12.2.3 Cross-section-mode

In contrast to the Track-mode and the Spiral-mode, the Cross-section-mode requires different data handling. Since the Cross-section-mode produces only 2D values of each cross-section, a third component has to be added to create 3D data. However, this third component may be taken from the encoder of the B-axis that rotates the object under test during each measurement. There are two options to generate an even cross-section with the test carrier. The first, and most reasonable, might be to drive the Y-axis under the fixed sensing unit. This procedure would require using the Z-axis to lift the sensing unit up and move it down to follow the shape of the test specimen. Such a procedure correlates not with the basic idea of the SCMM to ensure that all possible measurements are carried out with a maximum of two rotational axes. Therefore, research had been taken to develop algorithms to control the two rotational axes (B-axis and C-axis) in such a manner to generate a straight cross-section on top of the best-fit sphere of all objects under test.

However, the developed algorithms provide the XYZ values of each measured data point in the Cross-section-mode. Figure 138 presents the procedure schematically. A set of cross-sections may be computed to a three-dimensional structure of data points.

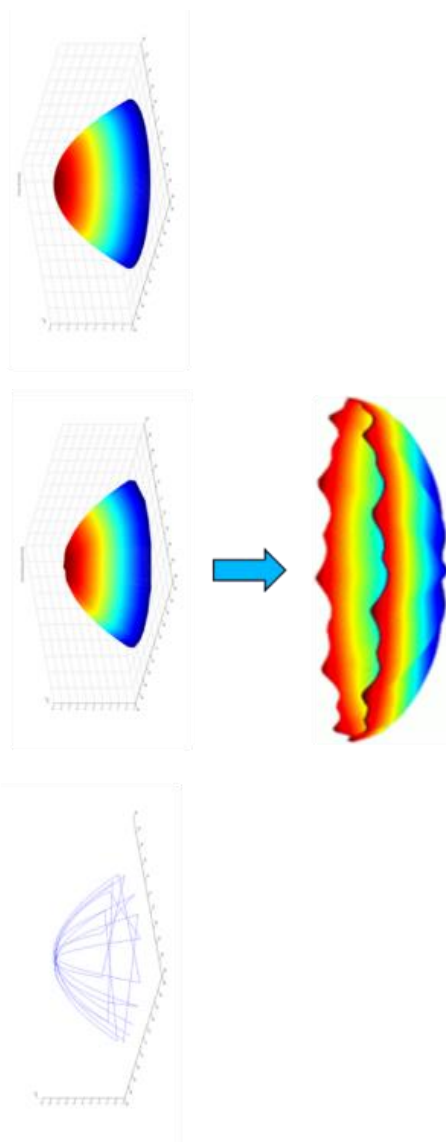


Figure 138: Computation of the Cross-section-mode. The data analysis of the Cross-Sections requires one additional step compared to the Track- and Spiral-mode. (1) illustrates the XYZ coordinates of all single Cross-sections obtained during the measurement process. An additional algorithm loads all available Cross-section measurement files in the corresponding work folder and generates one complete XYZ file. (2) shows the result after removing the piston and the XY tilt. (3) illustrates the problems of the Cross-Section mode. The latest version of the SCMM surface generator has problems with the distribution of the measurement points. Therefore, the Cross-Section mode is not verified for 3D measurements.

The major problem of this measurement mode is a massive amount of not scanned areas. In these areas, the algorithms have to interpolate the missing data

points. A particular result is not possible; only a statistical result may be provided. Therefore, research has to overcome this measurement mode and enhance the mode. In the context of this PhD research, the Cross-section-mode is only a rapid diagnostic mode for rough surfaces. Many previous production steps require quick but not as accurate measurement, especially measurement of the curvature and general shape of the object.

However, after applying the interpolation algorithms, the procedure of the Track and Spiral-mode is applied. In the following sequence, the ball correction and the temperature compensation algorithms correct the measurement file. Finally, the size adjustment and cross-correlation algorithms prepare the measurement matrix to be able to be subtracted from the reference file. The result of the process is depicted in the Cross-section-mode result screen, illustrated in Figure 139.



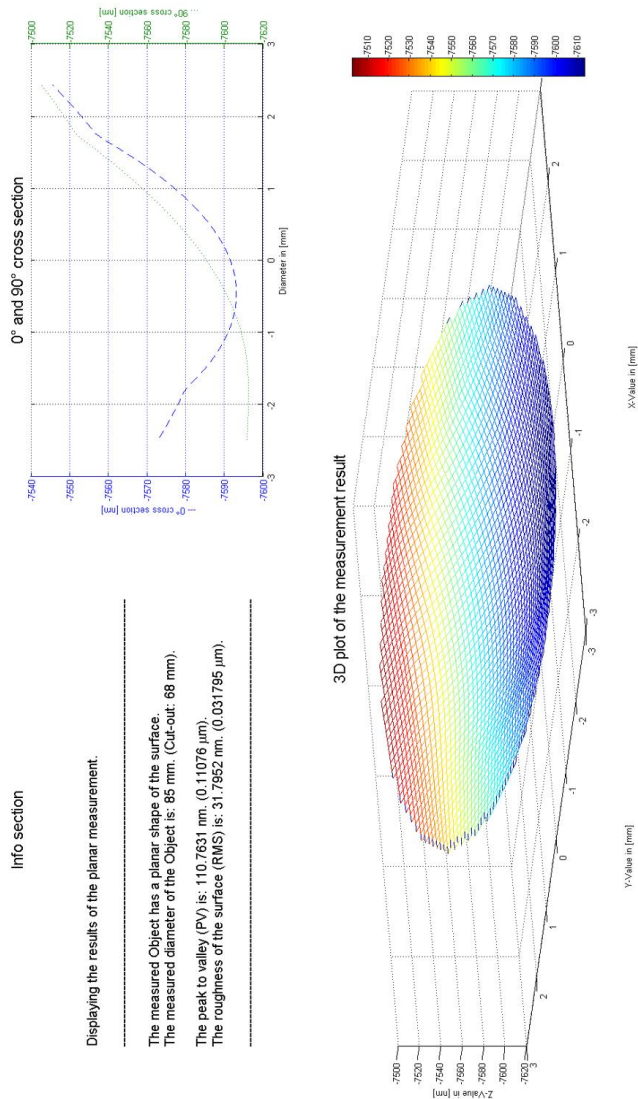


Figure 139: Cross-section-mode result screen . The result window of the Cross-section mode is identical to the Track-and Spiral-mode. In the upper left area are essential numbers and values of the measurement depicted. In the upper right area are two cross-sections shown. The result of the measurement in 3D is illustrated in the lower area.

The design of the Cross-Section result screen is similar to the result screen of the Track-mode and the Spiral-mode. The upper left corner provides essential information such as PV and RMS; the upper right corner displays two orthogonal cross-sections (0° and 90°). The lower are a full 3D plot including a colour map visualisation.

## A.13 Matlab™ (M2010a) source code for XYZ coordinate transformation verification

```

%% Verification of the SCMM coordinates transformation

clear all
close all
clc
format long g

%% Main section

% Setting parameter
e = 200;           % Diameter of Track in mm
alpha = 25;       % In deg (Angle of the A-axis)
gamma = 50;       % In deg (Angle of the C-axis)
precision = 15;   % Digits of result

% Minor axis d projected into the horizontal plane in dependence of alpha
(deg)
d = cosd(alpha) * e;           % [mm]

% Minor axis f projected into the vertical plane in dependence of alpha (in
deg)
f = sind(alpha) * e;           % [mm]

% X value of projection (gamma in deg)
X = e/2 * cosd(gamma);        % [mm]

% Y value of projection (gamma in deg)
Y = d/2 * sind(gamma);        % [mm]

% Z value of projection (alpha in deg)
Z = tand(alpha) * Y;          % [mm]

% Angle epsilon
epsilon = atand(Z/X);          % [°]

%% Popup textbox results

e = num2str(e,precision);
d = num2str(d,precision);
f = num2str(f,precision);
X = num2str(X,precision);
Y = num2str(Y,precision);
Z = num2str(Z,precision);
epsilon = num2str(epsilon,precision);

g = msgbox({'Verification of the SCMM coordinate
transformation'; []; ...
          'User settings:'; []; ...

```

```
['Diameter of the Track = ', num2str(e), ' mm']; ...
['A-axis angle alpha = ', num2str(alpha), ' °']; ...
['C-axis angle gamma = ', num2str(gamma), ' °']; [];
...
'Parameters of the ellipse:'; []; ...
['e = ', e, ' mm']; ...
['d = ', d, ' mm']; ...
['f = ', f, ' mm']; ...
['epsilon = ', epsilon, ' °']; [];...
'XYZ Coordinates:'; []; ...
['X = ', X, ' mm']; ...
['Y = ', Y, ' mm']; ...
['Z = ', Z, ' mm']}, 'Results');
```

**END OF CODE**

## A.14 Matlab™ (M2010a) source code for A-axis angle alpha verification

```
%% Verification of the SCMM coordinate transformation

clear all
close all
clc
format long g

%% Main section

% Setting parameter
CP = 100;           % Distance central axis C-axis and
                   % central axis sensing unit in mm
PS = 50;           % Length of sensing unit starting from
                   % fixture to end of housing
SB = 4;           % Distance measured by the sensing unit
R = 100;          % Radius of curvature of specimen in mm
precision = 15;   % Decimals of result

% Calculation of the angle alpha (required tilt angle of
the A-axis)

alpha = asind( (CP / (PS+SB+R) ) );

%% Popup textbox results

alpha = num2str(alpha,precision);
CP = num2str(CP,precision);
PS = num2str(PS,precision);
SB = num2str(SB,precision);
R = num2str(R,precision);

g = msgbox({'Verification of the SCMM A-axis angle alpha
calculation'; []; ...
          'User settings:'; []; ...
          ['Distance CP = ', CP, ' mm']; ...
          ['Physical sensor length PS = ', PS, ' mm']; ...
          ['Length measured by sensing unit SB = ', SB, ' mm'];
          ...
          ['Radius of curvature of specimen = ', R, ' mm'];
          [];...
          ['A-axis angle alpha = ', alpha, ' °'] }, 'Results');
END OF CODE
```

**A.15 Publication 01:**

Relationship between influence function accuracy and polishing quality in magnetorheological finishing

M. Schinhaerl, F. R. Schneider, R. Rascher, C. Vogt, P. Sperber

In 5th International Symposium on Advanced Optical Manufacturing and Testing Technologies: Advanced Optical Manufacturing Technologies, volume 7655, page 76550Y ff. SPIE, Dalian, PR China, 2010

**Abstract**

Magnetorheological finishing is a typical commercial application of a computer-controlled polishing process in the manufacturing of precision optical surfaces. Precise knowledge of the material removal characteristic of the polishing tool (influence function) is essential for controlling the material removal on the workpiece surface by the dwell time method. Results from the testing series with magnetorheological finishing have shown that a deviation of only 5% between the actual material removal characteristic of the polishing tool and that represented by the influence function caused a considerable reduction in the polishing quality. The paper discusses reasons for inaccuracies in the influence function and the effects on the polishing quality. The generic results of this research serve for the development of improved polishing strategies and may be used in alternative applications of computer-controlled polishing processes that quantify the material removal characteristic by influence functions.

**A.16 Publication 02:**

Effects of mechanical inaccuracies on the measurement result in metrology systems

F. R. Schneider, M. Schinhaerl, C. Vogt, R. Maurer, P. Sperber, R. Rascher, R. Stamp, G. Smith

In 5th International Symposium on Advanced Optical Manufacturing and Testing Technologies: Optical Test and Measurement Technology and Equipment, volume 7656, page 765611 ff. SPIE, Dalian, PR China, 2010

**Abstract**

Metrological systems commonly consist of a mechanical axial framework. However, any mechanical inaccuracies in such axial systems may cause falsifications in the measurement results. Therefore, precise knowledge of the effects of mechanical inaccuracies on measurement results is essential for measurement error compensation. This paper discusses the results of a testing series with a topographical coordinate measurement machine for the measurement of precision optical components in order to analyse and specify the different effects of mechanical inaccuracies on measurement results. The results obtained are not only beneficial for the design of new measurement machines and techniques. They may also be advantageously used for rapid measurement error compensation in metrological systems.

## A.17 Publication 03:

## Investigations on Grinding Tools for Silicon Carbide Based Advanced Materials

C. Vogt, M. Schinhaerl, F. R. Schneider, P. Sperber, R. Rascher

In Optical Fabrication and Testing on CD-ROM, page OWD2 ff. Optical Society of America, Washington, D.C., USA, 2010

**Abstract**

The results of experiments with grinding tools for carbon fibre infiltrated Silicon Carbide (C/C-SiC) materials are presented. Trials with ELID-support show improved self-sharpening. Resin bond tools improved the smoothness of the surface, whereas the form deviation increased.

**A.18 Publication 04:**

Investigations on Magnetorheological Finishing of High-Quality Optical Surfaces with Varying Influence Function

M. Schinhaerl, C. Vogt, F. R. Schneider, P. Sperber, R. Rascher

In Optical Fabrication and Testing on CD-ROM, page OWD3 ff. Optical Society of America, Washington, D.C., USA, 2010

**Abstract**

The paper reports on a testing series with a different influence function (Spot) in magnetorheological finishing. Effects on the polishing quality and recent developments in the field of varying influence functions are presented and discussed.



## A.19 Publication 05:

## Physical marker-based stitching process of circular and non-circular interferograms

R. Maurer, F. R. Schneider, C. Vogt, M. Schinhaerl, P. Sperber, R. Rascher

Proceedings of SPIE - The International Society for Optical Engineering 05/2011;

DOI:10.1117/12.889491, San Diego, USA, 2013

**Abstract**

The usage of stitching technologies in the interferometrical precision optics measurement technique becomes more and more popular. There exist already a few metrology stages providing the stitching principle, such as, for example, the well-known Sub-Aperture Stitching Interferometer for Aspheres (SSI™-A1) [1] [2] [3] from QED™ technologies. For measurements with the SSI-A™, the greatest measurable diameter of the test object is approximately 280 mm [1]. As a consequence, the University of Applied Sciences Deggendorf develops an own measuring system in order to test large telescope mirrors with a diameter of more than one meter which should be ready for application in 2012. The expected positioning accuracy of the measuring patches is significantly lower in comparison with the high-accurate SSI-A™. Therefore a cross-correlation based translation detection tool is implemented in our current software solution. Since the metrology system is currently being established the SSI-A™ and the μPhase2™ interferometer from TRIOPTICS™ are used as input data sources for the software development.

**A.20 Publication 06:****An Experimental Study on a Flexible Grinding Tool**

C. Vogt, S. Sinzinger, H. Adelsberger, R. Maurer, F. R. Schneider, R. Mandler, L. Kuepper, R. Rascher, P. Sperber

44th CIRP Conference on Manufacturing Systems, 08/2011; 325:91-96.

DOI:10.4028/www.scientific.net/AMR.325.91, Madison, Wisconsin, USA, 2011

**Abstract**

This paper reports on results of experiments on BK7 glass materials with a novel tool for fine grinding of faces for optical purposes. The ball-shaped tool comprises of a plastic wheel, several elastic layers and a polyurethane compound with diamond abrasives, which was developed and provided by OptoTech™. Removal test runs led to samples with very smooth surfaces without subsurface damages. The tool's elastic properties enable dwell time assisted grinding.

**A.21 Publication 07:**

Calculation of the reference surface error by analysing multiple sets of sub-measurements

R. Maurer, F. R. Schneider, C. Wünsche, R. Rascher

Proceedings of SPIE - The International Society for Optical Engineering 09/2013;

DOI:10.1117/12.2024003, San Diego, USA, 2013

**Abstract**

In the field of precision optics, the interferometry is the most applied measurement method to test spherical and flat objects. In principle, a standard interferometer setup is limited to these surface geometries, but interferometric systems may be modified with the aid of CGH's or the stitching technology. As a consequence, aspherical shapes and even freeform optics are measurable up to a certain extent. In an interferometric measurement, the measured variable is the optical path difference (OPD) between the reference wave and the test wave. Based on the detected OPD, the surface error of the test object is calculated by phase-shifting methods, for instance. It is evident that the error from the reference surface affects the determination of the test object surface error. One option to face this problem is the calibration of the system prior to the measurement. For this, the determination of the reference surface error may be realized with the aid of a two sphere test or a random ball test, e.g. [1]. In the well-known SSI-technology from QED™ technologies, the reference surface error is calculated on the basis of the sub-measurements. Due to the self-calibrating nature of

the QED™ stitching principle [2-4], a calibration of the system prior to the measurement is not necessary. The University of Applied Sciences Deggendorf has implemented a similar algorithm to estimate the reference wavefront error or to be exact the error of the whole optical system, based on a multiple set of sub-measurements. This paper describes the applied algorithm in detail and discusses the results. To verify the implemented tool, the results are compared to the outcomes of the QED™ stitching software. © (2013) COPYRIGHT Society of Photo-Optical Instrumentation Engineers (SPIE). Downloading of the abstract is permitted for personal use only.

**A.22 Publication 08:**

Analysis of three different measurement strategies carried out with the TII-3D coordinate measurement system

F. R. Schneider, R. Maurer, R. Rascher, R. Stamp, G. Smith

Proceedings of SPIE - The International Society for Optical Engineering 09/2013;

DOI:10.1117/12.2024001, San Diego, USA, 2013

**Abstract**

Together with the group of interferometry based systems, coordinate measurement machines are an essential part of the metrology in the modern optical industry. Coordinate measurement machines commonly consist of a multi-axis framework. They are designed to operate in a defined three-dimensional work zone, where every possible point can be reached by the measurement tooltip. This basic design principle leads to some interdependent challenges. A detailed measurement result needs a large number of measurement points to detect even minor irregularities and short-wave errors. However, a rising of the number of measurement points increases the corresponding measurement time analogous. On the other hand, the extended operation time increases the access to undesired thermal and dynamic influences, which cause multiple errors to the measurement result. Furthermore, modern production processes need rapid metrology systems to aid the machining time. This paper discusses results obtained by operating with three different measurements in order to find an agreement between speed and certainty of the coordinate

measurement machine. The topographic coordinate measurement system TII- 3D had been re-developed at the University of Applied Sciences Deggendorf in the laboratory of Optical Engineering, and it is equipped with three different measurement strategies. The first mode, the Track-mode operates in concentric circles on top of the surface of the object to be measured. The Spiral-mode measures along a dynamic moveable spiral line and the Section-Mode produces multiple cross-sections. © (2013) COPYRIGHT Society of Photo-Optical Instrumentation Engineers (SPIE). Downloading of the abstract is permitted for personal use only.

**A.23 Publication 09:**

A simple procedure to include a free-form measurement capability to standard coordinate measurement machines

F. Richard Schneider, R. Rascher, R. Stamp, G. Smith

SPIE - Optifab 2013, Rochester, New York, USA, 2013

**Abstract**

The modern optical industry requires objects with complex topographical structures. Free-form shaped objects are of large interest in many branches, especially for size reduced, modern lifestyle products like digital cameras. State of the art multi-axes-coordinate measurement machines (CMM), like the topographical measurement machine TII-3D, are by principle suitable to measure free-form shaped objects. The only limitation is the software package. This paper may illustrate a simple way to enhance coordinate measurement machines in order to add a free-form function. Next, to a coordinate measurement machine, only a state of the art CAD system and a simple piece of software are necessary. For this paper, the CAD software CREO3™ (M100) had been used. CREO3™ (M100) enables the user to develop a 3D object in two different ways. With the first method, the user might design the shape by drawing one or more 2D sketches and put an envelope around. Using the second method, the user could define one or more formulas in the editor to describe the favoured surface. Both procedures lead to the required three-dimensional shape. However, further features of CREO3™ (M100) enable the user to export the XYZ-coordinates of the created surface. A special

designed software tool, developed with Matlab™ (M2010a), converts the XYZ-file into a measurement matrix which can be used as a reference file. Finally, the result of the free-form measurement, carried out with a CMM, has to be loaded into the software tool and both files will be computed. The result is an error profile which provides the deviation between the measurement and the target-geometry.



## A.24 Publication 10:

## Measurement of a freeform object with the TII-3D measurement system

F. R. Schneider, R. Rascher, C. Wünsche

OSA - Freeform Optics, Houston Texas, USA, 2013

**Abstract**

Since interferometer based measurement systems mostly doesn't have the capability to operate on free-formed objects to be measured, coordinate measurement machines, like the TII-3D, can proof their right to exist and close this gap

## A.25 Publication 11:

## Tactile and contactless measurement of an optical surface

R. Maurer, F. R. Schneider

Symposium of Freeform technologies, The National Metrology Institute of Germany (PTB), Braunschweig, Germany, 2014

**Abstract**

The demand for high-quality optical devices is greatly increasing. Optical devices are going to be needed in many modern industrial products, it is barely imaginable to sell, e.g. mobile phones, smartphones or mobile computers without a digital camera system. The commonness of most modern consumer electronics is miniaturization. For optical systems used in such products, it is therefore very important to reduce the size and the weight of the assembly. Many larger and heavy lens arrays may be replaced by a few aspheric or sculptured refractors.